UNIVERSITÀ
DEGLI STUDI
DI PADOVA

Università degli Studi di Padova

DIPARTIMENTO DI INGEGNERIA INDUSTRIALE

Corso di Dottorato di Ricerca in
Ingegneria Industriale
Ciclo XXVII

GLASSES AND GLASS-CERAMIC

COMPONENTS FROM INORGANIC

WASTE AND NOVEL PROCESSING

Dottoranda:

Inès M.M.M. Ponsot

Supervisore:

Prof. Enrico Bernardo

Coordinatore:

Prof. Enrico Savio

Direttore della Scuola di dottorato:

Prof. Paolo Colombo

Abstract

Thanks to European environmental rules and regulations establishment, waste recycling has become a more and more relevant problematic. For manufacturing plants, especially those producing hazardous wastes, expenses linked to waste production have drastically increased over the last decades. In the proposed work, various hazardous and non-hazardous wastes, among: soda-lime and borosilicate glass cullet, cathode ray tubes glass, exhausted lime from fume abatement systems residues, sludge and slags from ferrous and non-ferrous metallurgy, and pre-stabilized municipal solid waste incinerators ashes are used to elaborate several compositions of glass-ceramics. High-temperature treatment (minimum 800 °C) associated to a Direct Sintering process (30 min) was an efficient way to stabilize chemically the final products. The impact of each waste on the final product's mechanical properties was studied, but also their synergies between each other, when mixed together. Statistic mixture designs enabled to develop interesting products for modern building applications, such as porous tiles and lightweight panels destined to insulation, with a purpose of fulfilling multifunctional properties.

Sommario

Grazie alle regole e normative ambientali europee istituite, il riciclaggio dei rifiuti è diventato una problematica sempre più rilevante. Per gli impianti di produzione, in particolare quelli che producono rifiuti pericolosi, le spese connesse allo smaltimento sono drasticamente aumentate negli ultimi decenni. Nel lavoro proposto, vari rifiuti, pericolosi o no, vengono utilizzati per elaborare diverse composizioni di vetroceramiche. Si distinguono rottami di vetro della produzione di finestre, di contenitori farmaceutici e di tubi catodici. I rifiuti non vetrosi invece sono calce esausta da residui di sistemi di filtrazione di fumi, scorie metallurgiche da leghe ferrose e non e ceneri da inceneritori. E' presentata nel presente lavoro la ricerca di un metodo di trattamento ad alta temperatura (minima 800 ° C) efficace per stabilizzare chimicamente il prodotto finale, tramite i diversi processi di sinterizzazione diretta, sinter-cristallizzazione e vetrificazione. Sono stati studiati gli effetti di ogni rifiuto sulle proprietà meccaniche del prodotto finale, ma anche le nuove funzionalità ottenute attraverso le sinergie risultanti dalla loro miscela. Miscele calibrate hanno permesso di sviluppare prodotti interessanti per applicazioni edilizie moderne, come le piastrelle porose e pannelli leggeri destinati all'isolamento.

Acknowledgments

Contents

Chapter I

Overall introduction: the GlaCERCo project

I.1 Introduction

For a few decades, companies have been financially encouraged in reviewing the entire design of their products, with the use of renewable materials or aggregates from recycling materials left on building demolition yards. States of European Union produced annually in the mid-1990 over 250 million tons of municipal waste and more than 850 million tons of industrial waste.

In the European countries that were OECD members, about 10 000 border crossings were registered per year (for a total of 2 million tons of hazardous waste). More than 55 000 contaminated sites were then known in only six European countries and the total area contaminated in Europe would represent 47 000 to 95 000 km^2, of which 1 000 to 3 000 km^2 were (contaminated) with discharges.

A deep knowledge of wastes would enable industries to reuse them as secondary materials in their processes and then become financially independent from prices fluctuations. To optimize the recycling and minimize costly landfill treatments, industrial wastes have been studied by researchers for over 40 years. As an example, a wide-spread research on characterization, co-financed by world leaders groups of coal manufacture, was developed to enlighten the inherent properties of so called "fly ashes" coming from coal calcination: granularity, silica content, density, rheology, enabling to transform them in secondary raw materials. Nowadays, fly ashes have been successfully reintroduced in many ceramic compositions, mainly concrete and cement, in the field of building materials.

The ceramic industry consumes large amounts of energy, especially during the firing process (Agrafiotis and Toutsos, 2001). Firing temperatures greater than 1200° C are required to sinter typical ceramic raw materials into dense products. Modifications of the raw material formulations have led to reductions in firing temperatures, but the improvements are limited because of the types of raw materials used. Most traditional ceramic products, such as tile and brick, consist mainly of clay-based raw materials, which inherently require high firing temperatures. Other ceramic manufacturing steps, such as the drying processes, are also very energy intensive. It is why in building applications, other alternatives to ceramics are often searched, like plastic, wood, and so on. Energy costs are a major portion of the total manufacturing costs, and thus new methods to reduce the amount of energy required will be a great benefit to the ceramic industry. By reusing waste, many investigations are technically possible in the ceramic field. As any solution, glasses are tolerant to compositional deviations, and therefore not sensitive to waste compositional

variations. Glasses are solid materials, which with their topologically-disordered internal atomic structure are true solid solutions; that is, solutions which were frozen to a solid state without phase separation. The most universal materials which are durable enough and have a long track record proving that they can withstand corrosive environments for millennia are silicate glasses. The high chemical resistance of silicate glasses allows them to remain stable in corrosive environments for many decades. On the other hand, ceramics are thermodynamically stable materials often derived from glasses via controlled crystallization. Many crystalline materials are extremely durable. Glass and glass-ceramics based hosts are the most prominent materials to ensure protection of the environment now and in the future in any expected and unexpected circumstances.

The proposed work demonstrates the feasibility of manufacturing high quality glass and glass-ceramic using a well-established and low-cost glass-ceramic process (Colombo *et al.,* 2003 and Bernardo *et al.,* 2006). The effects of glass composition on the crystalline phases that form and the nature of the oxides formed after exposure to heat and a reducing atmosphere will be determined. The process will yield dispersed metallic particles supported by the oxide glass-ceramic that may have applications for building and architecture: tiles (Bernardo *et al.*, 2008, 2009, 2010), insulating panels (Bernardo and Albertini, 2006), bricks, concrete aggregates (Bernardo *et al.,* 2010), cement, plaster, pane of glass (Bernardo, 2008), and coatings (Binhussain *et al.,* 2014). This subject may probably help to increase energetic performance of building field (Blengini *et al.,* 2012, Cabeza *et al.,* 2014).

I.2 U.E. Roadmap on waste

In 2011, the European Commission has set a Roadmap to Resource Efficiency in Europe, in order to improve the management of raw materials as well as wastes in a common objective of international competitiveness and independence. One of the significant issues raised is turning waste into a resource. A number of decisions have been set, among them an impressive milestone:

"By 2020, waste is managed as a resource. [...] Recycling and re-use of waste are economically attractive options for public and private actors due to widespread separate collection and the development of functional markets for secondary raw materials. Waste legislation is fully implemented."

However the European Union is prepared to make the decisions the situation requires, such as: stimulate the secondary materials market and demand for recycled materials through economic incentives and developing end-of-waste criteria (in 2013/2014); review existing waste prevention, re-use, recycling, recovery and landfill diversion targets to move towards an economy based on re-use and recycling, with residual waste reasonably tending toward zero (in 2014); ensure that public funding from the EU budget gives priority to activities higher up the waste hierarchy as defined in the Waste Framework Directive (e.g. priority to recycling plants over waste disposal) (in 2012/2013).

As part of this commitment a supporting research and innovation is necessary and then, milestones have been defined also to trigger and give the necessary push for the transition to a green and low-carbon economy:

"By 2020, scientific breakthroughs and sustained innovation efforts have dramatically improved how we understand, manage, reduce the use, reuse, recycle, substitute and safeguard and value resources."

Examining the sustainment provided by European Union, we find a particular Focus Union research funding (EU Horizon 2020) on environmentally friendly applications, 'Innovation partnerships' and the 7th Framework Program which is the very context of this PhD Thesis. The total waste production in Europe is quite constant and around 250 000 Gton/Year. The most important waste production is made by construction and demolition, (for this reason Horizon 2020 Program has a dedicated call for the recycling of wastes from this sector, SPIRE and WASTE), but combined together, hazardous, manufacturing, mining and quarrying wastes are also an important target and most of them contain easier potentiality to be recycled in a ceramic product.

I.3 The European Project GlaCERCo

All the activities refer to the **European Project "GlaCERCo"** (Glass and Ceramic Composites for High Technology Applications – FP7-PEOPLE-2010-ITN); in particular they refer to the **Work Package 1** (Vitrification and reuse of waste), for which the University of Padua (Padova, Italy) is the leading research unit.

The aim of the "GlaCERCo project" is to offer a multidisciplinary training in the field of high-tech glasses and composites, in tight contact with companies and universities within this consortium. The scientific goals are to develop advanced knowledge on glass based materials and to develop innovative, cost-competitive, and environmentally acceptable materials and processing technologies.

More precisely in this context, the aim of the research at University of Padova is to develop **sintered or vitrified products** (glasses and glass-ceramics) from **wastes, hazardous or inert**, as "secondary" raw materials for building materials with improved properties (e.g. porous **lightweight panels** for building applications, of low density and low mater absorption). Indeed, the technology has the three advantages of being **valuable, environmentally friendly** and **low cost**.

The thermal process is thought to answer **industrial requests**: low temperature (<1100 °C) and direct heating (30 min) enables **fuel saving** for ceramic manufacturing. Replacing raw materials by wastes in glass-ceramic composition **diminishes final product cost**.

Moreover, instead of paying for **landfill storage**, concerned companies can decrease their cost of **waste treatment** by reintroducing them in another "product-life-cycle", and make easier any **environmental certification**.

Particularly **environmentally friendly**, the obtained glass-ceramic becomes **non-hazardous,** thanks to the vitrification and/or sintering process. Inside the product, **amorphous phase** surrounds the waste material and enables to decrease its polluting effect. In case of a glass-ceramic, grown **crystalline phase** depends on oxides composition of each waste and their interactions with other raw materials, bringing to the material either excellent mechanical properties or thermally insulating properties.

At the end, wastes are enhanced by their inherent properties to develop valuable products: wastes containing foaming agents for porous glasses, wastes containing fluxing agents for low-temperature vitrified glass, or waste containing high strength particles as composite additives.

References

Agrafiotis C. Tsoutsos T. (2001) Energy saving technologies in the European ceramic sector: a systematic review, Appl. Therm. Eng., 21, 1231-1249.

Bernardo E. Varasso M. (2006) Vitrification of wastes and preparation of chemically stable sintered glass-ceramic products, J. Non-Cryst. Sol., 352, 4017-4023.

Bernardo E. De Lazzari M. (2010) Lightweight Porcelain Stoneware by Engineered CeO_2 Addition, Adv. Eng. Mat., 12, 65-70.

Bernardo E. Esposito L. (2009) 'Glass based stoneware' as a promising route for the recycling of waste glasses, Adv. Appl. Ceram. , 108, 2-8.

Bernardo E. Esposito L. (2008) Recycle of waste glass into glass ceramic Stoneware, J. Am. Ceram. Soc., 91, 2156-2162.

Bernardo E. Albertini F. (2006) Glass foams from dismantled cathode ray tubes, Ceram. Int., 32, 603-608.

Bernardo E. Scarinci G. (2010) Recycling of waste glasses into partially crystallized glass foams, J. Porous Mater., 17, 359-365.

Bernardo E. (2008) Fast Sinter-crystallization of a glass from waste materials, J. Non-Cryst. Sol., 354, 3486-3490.

Binhussain M.A. Marangoni M. (2014) Sintered and glazed glass-ceramics from natural and waste raw materials, Ceram. Int., 40, 3543-3551.

Blengini G.A. Busto M. (2012) Eco-efficient waste glass recycling: Integrated waste management and green product development through LCA, Waste Manag., 32, 1000-1008.

Cabeza L.F. Rincón L. (2014) Life cycle assessment (LCA) and life cycle energy analysis (LCEA) of buildings and the building sector: A review, Renewable and Sustainable Energy Reviews, 29, 394-416.

Colombo P. Brusatin G. (2003) Inertization and reuse of waste by vitrification and fabrication of glass-based products, Curr. Op. Sol. St. Mat. Sci., 7, 225-239.

Chapter II

Inorganic waste in Europe

II.1 What is an inorganic waste?

Wastes are unwanted or unusable substances or materials, which derive from natural or human (civil and industrial) processes. Waste can be, in a first approximation, divided in two main categories: organic and inorganic, and each category includes both hazardous and non-hazardous waste (Bernardo *et al.*, 2012). We also distinguish them depending on their origin, as presented in figure II.1.
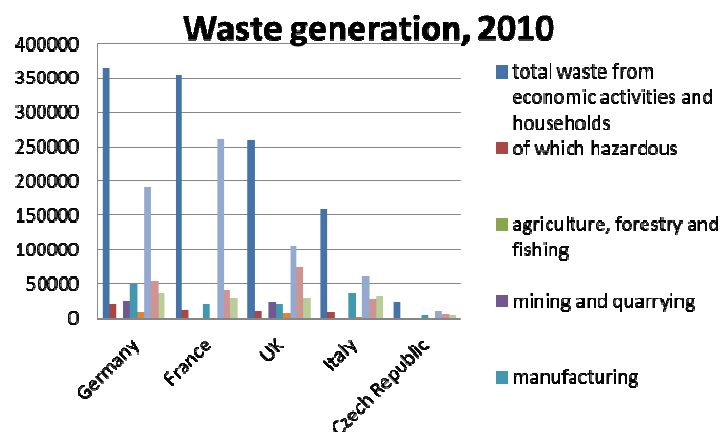
Figure II.1: Example of wastes distribution in some european countries (Eurostat, 2010)

Waste can be characterized by their composition, by proximate and elemental analysis, their calorific value, and by their biogenic and biodegradable function. Their composition type is separated in 8 major fractions: cellulosic materials (paper, cardboard); textile and wood; plastic (rigid: PET, HDPE, PVC or film: LDPE, PP) and rubber (and thermosetting plastic); metals (ferrous: steel, cast iron, iron scraps, and non-ferrous: aluminum, copper, stainless steel, others); glass and inert (ceramics, stones, rubble); organic materials (kitchen waste, garden waste); hazardous municipal waste (batteries, drugs); fines (everything smaller than 20 mm). Figure II.2 schematizes that a focus is done on the composition of unsorted residual waste (URW), by direct analysis at the gate of the recovery/ disposal plants (incinerators, landfills, …) and on the composition of gross waste (GW), to be calculated or estimated according to the existing type and level of source separation. In the "Polluter Pays" principle, the polluting party pays for the impact caused to the environment. This principle generally refers to the requirement for a waste producer

to pay for the appropriate disposal of the unrecoverable material. More specifically, for a company, there will be a range of solutions available to address the will or need to get rid of waste. As "inorganic" correspond every material that are solids, not-short term biodegradable and do contain as major components the 4 main atoms of so-called organic materials: C, N, O and H. It includes metals, glasses, rocks, and the derivatives of those materials and excludes polymers, compost, oils. These products are distributed as following: urban waste, industrial waste, construction/demolition waste and agriculture waste.

ISO14001 is an international standard that provides a framework for organizations to develop a systematic approach, implements strategies to reduce air pollution and that also fosters the development of an environmental management system. Along with the determination of Europe to improve the environmental economy through waste management, ISO 14001 has been upgraded in 2012, and the approach includes, from now, **water** and **CO_2** footprints, which may push manufacturers to take into account the water and gas consumption in their production process. Recycling waste in the heart of a production life cycle is already an environmental advantage for a company. The introduction of wastes in the process could present a benefit if it has a positive impact on these two components and then a key component in a business ability to obtain ISO14001 certification. It is indeed in accordance with the sustainability purpose of this norm. Sustainability is the ability to meet human needs at least environmental impact. In the industry, attention may be focused on materials selections, in this view. Environmental analysts and universities can be very strong external supports when they benefit of a growing knowledge on waste management and recovery market. The University of Padova is a good example of this, since the Department of Industrial Engineering combines both competencies into two services, chemistry materials and environment. It is relevant to remind that by definition the inorganic waste does not contain organic toxic substances, which are quite numerous. Indeed, in the list of toxic limits to apply in European countries laws, given by the European Commission (Regulation CE 1013/2006; Directive 1999-31/CE; Decision 2000/33/CE; Decision 2008/98/CE) to classify wastes by type (hazardous, non-hazardous, inert) for their admissibility in landfill storage, another part of elements to be analyzed are chloride, fluoride, FS, BTEX, PCB, sulfate, organic carbon, C10 and C40, HAP. These substances do not enter in the manufacture process of the inorganic wastes studied here. If some building materials such as concrete, bricks, ceramics and glasses, are directly admitted (except those coming from contaminated sites (Arrêté du 31/12/04)), however, a lot of powders are not admitted because of their volatility. For this reason, a low temperature ceramization of powder waste would give at first, the possibility to the producer to send it in landfill as inert materials.

II.2 Management technologies

One of the strategies of the management of waste production is called 4 R: **R**eduction, Energy **R**ecovery, **R**ecycling and **R**euse. Inorganic waste is frequently obtained after reduction: dusts and ashes are among the residues from a combustion process. Inorganic wastes are not so much concerned about energy recovery: in some cases, they dissipate heat that could be redistributed through pipes but usually it is accompanied by toxic fumes which make difficult the direct energy recovery from them. However, they are widely used for elements recovery, often, metals such as

rare earths from extraction plants residues, Pb from battery, etc. Iron was recovered from metallurgy process and eventually, H_2 release from metallurgical slags sludge or by products, has already been under investigation (Malfliet *et al.*, 2013). In general, there is already an existing recycling path for many considered wastes, as they may offer a technological advantage for the manufacturer, without mentioning the other practical advantages. Stoneware "chamotte" illustrates a typical example of closed recycling loop in the ceramic industry. If the waste is recycled inside the process of elaboration, it is called a closed recycling loop. The reuse of waste is not so developed, and is assimilated to an open recycling loop, when the waste is used in another process to elaborate another product. Glass cullet, when added among the ingredients of glass production, is in a closed loop, whereas, if used for the elaboration of insulating glass fiber, is in an open loop.
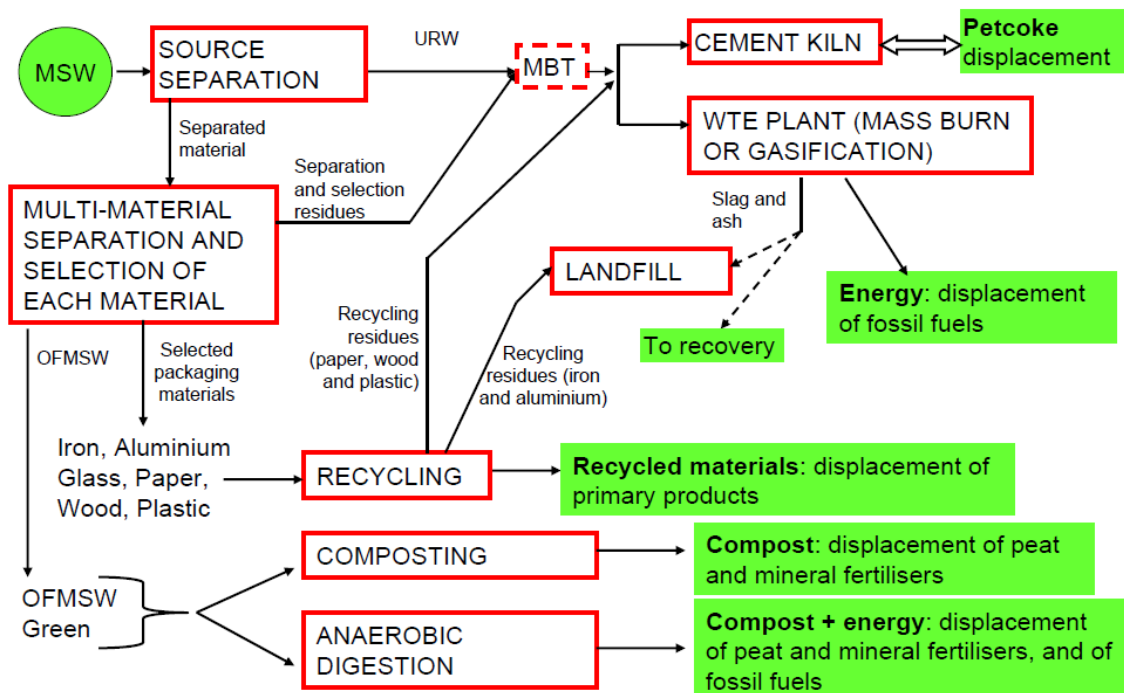
Figure II.2: Conceptual approach of a conceptual waste management scenario (Consonni, 2012)

Figure II.2 illustrates the complexity of municipal solid waste (MSW) selection. The separation between materials type enables to collect each of them for specific destinations. Iron, aluminum, glass, paper, wood, and plastic are recycled. Organics (Green) is composted. Among URW (urban residues waste), some part is sent to cement kiln or waste to energy (WTE) plants, and finally landfill. The recovery of URW (dash arrow) is always under investigation.

II.2.1 Thermal treatment by incineration

Nowadays, incinerators are most diffuse means of gross wastes thermal treatment. The incineration plants or municipal solid waste incinerators (MSWI) allow to decrease the volume occupied by waste in landfills and to recover energy by thermal utilization. In incineration is done the thermo-destruction of the waste but also the thermo-use: the difference is the energy recovery and then, the reduction of the life cycle impact factor.
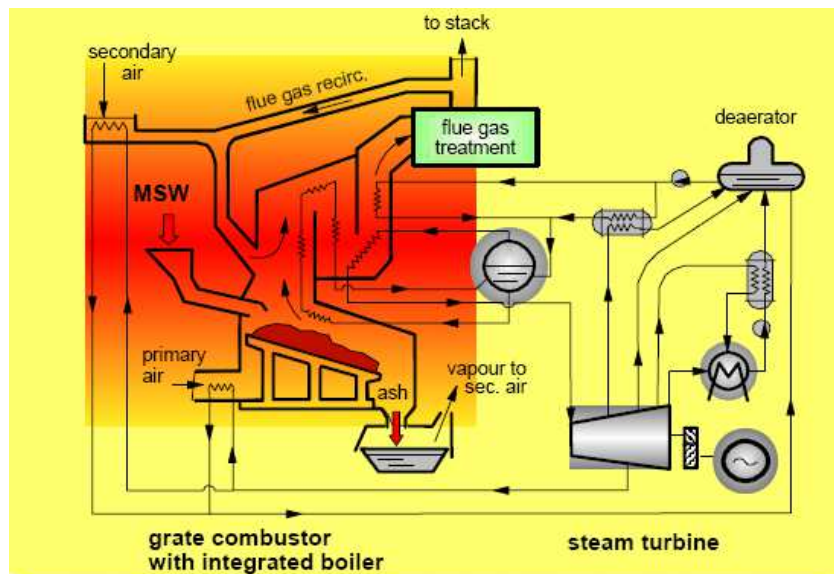
Figure II.3: Thermal cycle of the combustion in a modern thermouser
(grate combustor) (Consonni, 2012)

As shown in figure II.3, the MSW is converted into ash and the volatile compounds are collected by an important flue gas treatment system. The incinerator has the objective to sterilize, reduce the volume to 10-30 times and inert debris landfills. Those thermoelectric centrals are also modern thermo-users. But not all types of waste can be treated in an incinerator. It depends mainly on the heat capacity. We can differentiate on the basis of physical macroscopic characteristics (or on the basis of the chemical composition). The heat capacity (kJ) is the amount of heat obtained after oxidation of 1 kg of completely dry product at standard T and P. For example, the plastic has a heat capacity of 7500 kcal/kg against 3700 kcal/kg for the paper. Today the heat capacity of some waste can get to 2200 to 2800 kcal/kg against 700 kcal/kg to 900 kcal/kg at the beginning of the century. To summarize, the purpose of a thermo-user is a conversion of waste and air to combustions products: heat and slags. The entire combustion is done on a grate. There are combustors grate pan / tilt, fixed or mobile, air cooled or water cooled, belt or rollers (integrated with vertical boiler), grill fire bars (horizontal boiler). The distribution of combustion air is calculated for maximum energy savings, depending on the progress of combustion. It stands at least the primary air (undergrill) and the air above the second grate. All combustion is controlled with sensors. When the combustion is well controlled, i.e. complete, the emission of ultrafine particles waste is still important but not more important than those of the urban environment. A treatment is done (wet or dry with bag filter), with a steam cycle. The fumes are mainly dioxins, NO_x, SO_x, Cd, Hg, and MSWI powders.

II.2.2 Landfill storage

Landfill storage is the last destination of wastes, when they cannot be valorized anymore (Arrêté du 31/12/04). Previously, they usually are considered for a possible prevention, then minimization, then reuse, recycling and energy recovery, as presented in figure II.4. Landfills are separated depending on toxicity level of the waste stored: hazardous, non-hazardous and inert. Hazardous waste are waste that pose substantial or potential threats to public health or the

environment, and they can be flammable, radioactive, corrosive, toxic or have a genetic, carcinogenic, mutagenic and teratogenic potential.
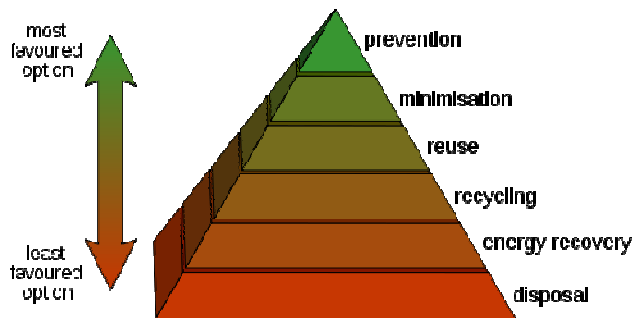
Figure II.4 : Schematic diagram of waste hierarchy (UNEP, 2013)

At these stages, they may undergo various chemical or thermal treatments: volume reduction, recovery, stabilization. Depending on available time, the emergency varies: immediately, it goes to landfill or it is exported, in medium times (years), recycling or energy recovery and, in long periods (< 10 years), sustainability can be studied through reduction of the production and re-use.

II.2.3 Waste vitrification

Vitrification is the transformation of a substance into a glass, typically accomplished via a process involving the formation a liquid phase at high temperature, in the presence of an adequate content of vitrifying oxides (i.e. the so-called "network forming oxides", normally SiO_2, B_2O_3, P_2O_5). This subsequently cools to a solid without the formation of any crystalline phases. In this context, the substance of interest is hazardous waste, with the addition or not of additional glass forming raw materials (Bernardo *et al.*, 2012) Table II.1 summarizes the main vitrification technologies. Among them, plasma torch is used by Europlasma, a European company that enables the inertization of asbestos, a hazardous waste from construction (figure II.5).
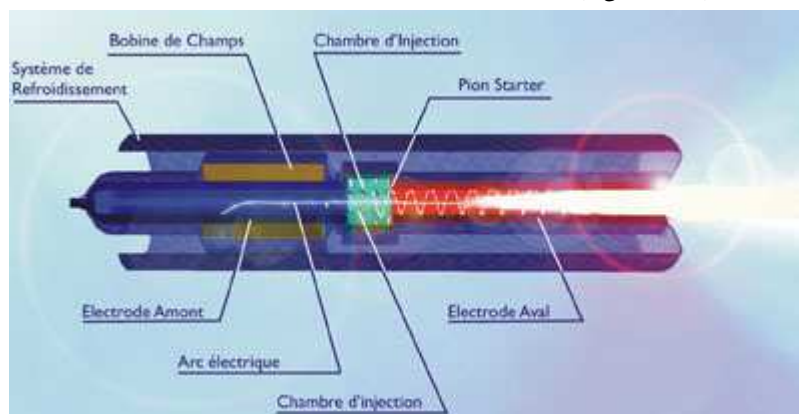
Figure II.5: Plasma torch technology (inertam.com, 2014)

The process is to burn by plasma-torch the fibers up to a complete melting, at 1350 °C to 1400 °C, making of it a one-piece amorphous material. The ability of glass to incorporate nearly all the elements of the periodic table into its structure is of fundamental importance: if formulated with an adequate composition, the resulting glass features a high chemical inertness, so that it can be landfilled without any particular concerns but it can also be recycled as secondary raw material for

the manufacturing of new products (Bernardo *et al.*, 2012). This process enables to transform a dangerous waste into a non-dangerous waste glass that will be safely stored in landfill. This thermal treatment is unavoidable to stabilize hazardous waste. From energetic views, it is relevant to imply this process in the elaboration of a new commercialized product.

Vitrification technology	Heat source	Advantages (A), Disadvantages (D) and Limitations (L)
Combustion based melters (tank melters, cyclone melters, surface melting furnaces and small-scale blast furnaces)	Combustion (natural gas, fuel oil, or coke)	(A) High reliability, long life, ability to vitrify waste of very different composition (tank melters). High processing rate (cyclone melters). (D) High capital cost. Inhomogeneous melt, volatilization of heavy metals, particulate in the off-gas, large volume of the off-gas (to be treated in large and expensive depuration plants). Pure oxygen as combustion agent decreases the off-gas volume by over 70% (but extra-cost has to be considered).
Fluidized bed gasifying melting systems	Combustion (natural gas, fuel oil, or coke)	(A) Optimum thermal efficiency. Complete destruction of toxic contaminants as dioxins. Melting of ashes into a vitreous slag.
Joule heated melters (JHMs): cold top JHMs, hot top JHMs, intensively stirred small volume-high throughput JHMs	Electrical power (Joule heating, due to ionic conduction inside the melt)	(A) Drastic reduction of the off-gas volume and thus of the purification plant size. By employing cold top JHMs it is possible to hinder volatilization of heavy metals and to obtain salts condensation. With hot top JHMs complete destruction of hazardous organics is obtained. (D) Free metals attack graphite or Mo electrodes and decrease the process efficiency. (L) System particularly suitable to vitrifying properly divided homogeneous inorganic materials (mud, soils and finely ground concrete). Careful formulation of the charge is required: water and organics must not exceed 5 wt%.
Terra-Vit melter (JHM)	Electrical power	(A) Reduced capital and operating costs. Increased melter life.
Electric arc furnaces	Electrical power (electric arc generated by three electrodes on the furnace top).	(A) Systems characterized by simplicity of construction, low thermal losses, high output. High process temperature (>1400°C). Fast ferrous materials melting. Risks of explosion minimized. (L) Technology most applicable to essentially inorganic, dry waste.
Plasma torch melters	Electrical power (ionization of a process gas by the electric arc generated, and formation of a very high temperature plasma)	(A) Compact plant (mobile units can be used). Very high temperatures attainable. High efficiency of toxic organic compounds destruction. Very wide flexibility, i.e. possibility of direct treatment of highly different types of waste, even containing large quantities of metals. Absence of waste products. (D) Limited yield of the plant. Plasma torch melters consume more energy, need frequent maintenance and are less durable than combustion-based or electric furnaces. (L) Technology most suited to waste requiring high destruction temperature or operating conditions that minimize risks to human health and the environment.
Cold-crucible induction melters	Electrical power (induction heating of a water-cooled crucible)	(A) Crucible protected against corrosion. Effective stirring of the melt. High purity melts attainable. Very high processing temperatures achievable, if required.
In situ vitrification	Electrical power (Joule heating of contaminated soils)	(A) Mobile equipment. High melting temperatures attainable. Highly effective process for remediating soils contaminated by heavy metals, chlorinated organic compounds and radioactive materials. (L) High cost of the process makes it sustainable only for hard to treat hazardous waste.
Self-sustaining vitrification	Exothermic chemical reactions between powder metal fuel and the waste	(A) No need of external power supply. Large and expensive equipment not required. (L) Technology most suited for small volume hazardous waste.

Table II.1: Main technologies used to vitrify waste (Bernardo et al., 2012)

The plasmalit product sheet® produced by Europlasma is a glass aggregate for pavements (in regard to EN 12620 Norm), from the melting of residues obtained by incineration of municipal solid wastes. A scientific program (Vivaldi Program, www.torchprocess.com) has been set to evaluate if the Plasmalit® can be considered safe for usage, and to show that it is not a hazardous waste. The chemical stability, the oxide content, and the content in crystalline phases are compared to specifications from the U.E. (EN 12457-2 Norm) and from the Vivaldi Program (XP X30-440 Norm). "The vitrified product deteriorates with a speed inferior of the initial speed Vo. Considering this speed, the lifetime of the vitrified product stored in the blocks is 12 million years. Its performances in terms of life time are similar to those of natural basalt. That's why the impact on the environment of storage of this vitrified glass should be as low as the one caused by basaltic rock. The concentration of toxic elements measured in the percolation water coming from the experimental blocks – assigned to reproduce the class III storage conditions – are widely inferior to the threshold values recommended in: The French Decree of 09 September 2007 on minimal criteria applicable on rejected liquid effluents in the natural environment , the Ministerial Proposal of January 1998 criteria and methods to evaluate the eco-toxicity of wastes and the Project related to class III storage installations (H or G category) of June 1998."

These promising conclusions enable to consider the alternative of a thermal treatment at lower temperatures, in which the melting is replaced by sinter-crystallization or sintering, leading to inert materials as well. Indeed, "ceramization" thermal process enables to decrease considerably the hazard risk of an inorganic substance, and then to develop an inert material presenting a new added value (environmental, technical and economic advantage). On another hand, the vitrification process is capital and energy intensive. The process is consequently hardly sustainable, if the economic advantage is related only to the avoided disposal costs. These costs are particularly significant for highly hazardous waste, such as asbestos-containing materials, which are vitrified even by employing the most expensive technologies, such as plasma heating. The obtained ceramic material, not only represent a security of safe landfill storage, in case of non-use, but also it can find a second application (Bernardo and Scarinci, 2009 and 2011b).

II.3 Inorganic waste that can be valorized in a ceramic composition

Many inorganic wastes contain a **relevant percentage of silica and other oxides**; their compositions could be comparable to those of raw materials traditionally used in ceramic and glass ceramic manufactures. Publications from Colombo *et al.*, 2003, Bernardo *et al.*, 2007a and 2007b; Rawlings *et al.*, (2006), give a huge overview of the feasibility of reusing such wastes in glass-ceramics. Most recent reviews (Rozenstrauha *et al.*, 2013; Chinnam *et al.*, 2013; M.A. Binhussain *et al.*, 2014) give an idea of the progresses during the last decades on this field.

II.3.1 Municipal Solid Waste Incinerator fly ashes

Municipal solid waste incinerated (MSWI) bottom and fly ashes have been deeply investigated for the elaboration of glass ceramics (Appendino *et al.*, 2004; Aloisi *et al.*, 2004 and 2006; Karamanov *et al.*, 2003 and 2008; Karamanova *et al.*, 2010) and ceramics (Karamanov et al., 2005; Lin, 2006; Schabbach *et al.*, 2011; Kasuriya *et al.*, 2008). In general, the sintering process allows an introduction of the waste at around 5 to 10 wt% in the composition, depending on

previous treatments, such as deironization. (Rambaldi *et al.*, 2010 and Vu, *et al.*, 2012) This kind of recycling path is the only one that ensures a positive leaching test, i.e. showing no heavy elements release, and has been widely experimented for the elaboration of novel eco-glass ceramics. Other possibilities of recycling such as mortars, cements, cement concretes, Portland cement, require the necessity to previously extract by leaching the heavy metals from them in order to get a safe product (Pera *et al.*, 1997; Rémond *et al.,* 2002; Lin *et al.*, 2003; Bertolini, *et al.*, 2004; Aubert *et al.*, 2004; Shi *et al*., 2009). An alternative process recently developed at Brescia University, allows these ashes to be incorporated in a mixture safely, thanks to a pre-stabilization of the particles by an organic silica layer (Guarienti *et al*., 2014).

II.3.2 Residues from fume abatement system

In the traditional ceramic manufacturing, i.e. in the production of pottery, earthenware, stoneware, chinaware, porcelain, and some technical ceramics, acid fumes escaping from kilns are ventilated and abated by chemical reaction with exhausted lime. Gaseous pollutant emissions come from firing and forming parts of the process, and consist in SO_2, NO_x, CO, CO_2, HF and Fluorides. Emissions of HF from kilns can be reduced through process modifications such as increasing the raw material lime content, but if not possible, dry sorption scrubbing also has been used to control HF emissions in the brick and ceramic industries. These devices use limestone as adsorption medium to produce CaF_2, which is removed by mean of a rotating screen, drum, or fabric filter. Control efficiencies of 95% to 99% have been reported for this type of scrubber (E.P.A., Mineral Products).

II.3.3 Metallurgical sludge from blast furnace

Historically, most iron ore is converted to iron using a blast furnace, although a number of newer technologies are replacing this process. The production of iron requires three important raw materials: iron ore, coal converted to "coke", and limestone.
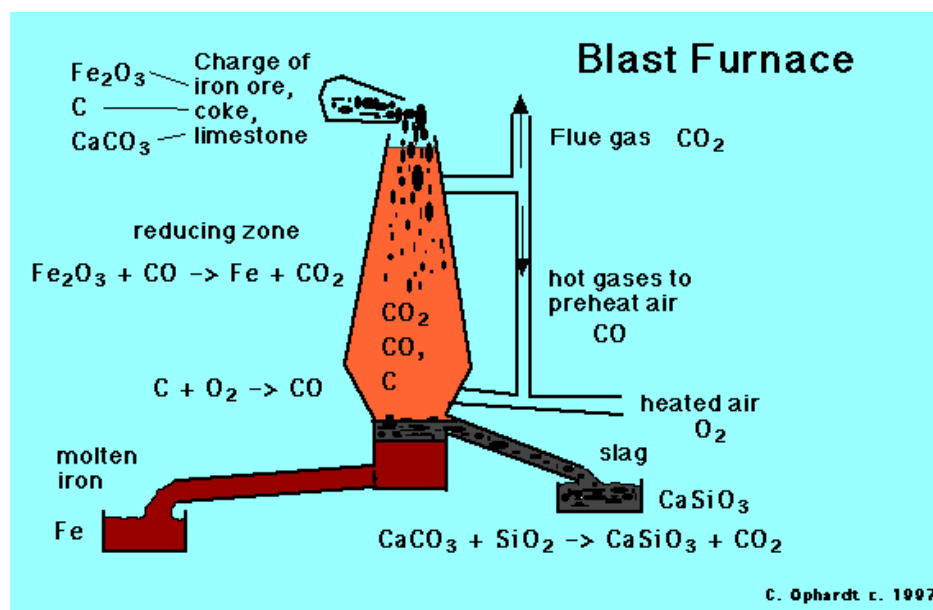
Figure II.6: Iron blast furnace (Ophardt, 2003)

The coal is converted to coke in coking ovens (figure II.6). The three raw materials are added to the top of the blast furnace. A blast of air containing oxygen is forced in from the bottom of the furnace. This causes the coke to burn with an intense heat of almost 2000 °C. The reaction is carbon plus oxygen to produce carbon monoxide (incomplete combustion due to lack of air).

The main reaction is then between the iron oxide, Fe_2O_3, with the carbon monoxide to produce molten iron metal and carbon dioxide. An alternate reaction is with the coke, C, to produce iron and more carbon monoxide. The molten iron collects on the bottom of the furnace and when cooled is called pig iron with many impurities. Much of the carbon dioxide is reduced with more carbon from the coke to make more carbon monoxide.

Impurities in the iron ore such as silicon dioxide react with the limestone to produce slag, $CaSiO_3$, and carbon dioxide. The slag floats on top of the molten iron and can be drawn off separately. The pig iron is treated in a second step called the basic oxygen furnace. Pure oxygen is blown into the molten pig iron to oxidize the impurities of sulfur, phosphorus, and carbon to their respective oxides: SO_2, P_2O_5, and CO_2. The result of this is the production of carbon steel. Other transition elements may be added to impart a variety of other properties. For example stainless steel contains 14-18% chromium and 7-9% nickel.

Blast furnace sludge or flue dust is a solid waste material from the integrated steel plant. It is a mixture of oxides expelled from the top of the blast furnace, whose major components are iron oxides and coke fines. It also contains silicon, calcium, magnesium and other minor elemental oxides in lesser amounts. The direct recycling is not usually possible since it contains some undesirable elements (like zinc, lead and alkali metals) that can cause operational difficulties in the blast furnace. In some cases the particles contain large amount of Zn and Pb as the volatile impurities. It is mainly due to the Pb–Zn containing scrap that is added into the blast furnace. Furthermore, in some cases the dust contains toxic elements (Cd, Cr and As), which make it hazardous and unacceptable for landfill. Usually the utilization of BF sludge is done by removal of alkalis, recovery of Zn and Pb, of C and magnetite, or Fe by complete reduction, or recycling as an absorbent to purify Cu^{2+} containing solutions (Das *et al.*, 2007).

II.3.4 Metallurgical slags from the copper smelting process

Historically, the most abundant copper bearing ore was called chalcopyrite, $CuFeS_2$. This ore is first enriched by flotation or beneficiation process (sulphite ores), in which powdered ore is mixed water as a slurry and then further mixed with oil and a chemical called amyl xanthate. The slurry, when agitated causes the copper sulphide minerals to float at which point they are skimmed off the surface and eventually dried. The dried material called concentrate is then sent to the smelter. As shown on figure II.7, oxide ores (and certain sulphide ores) are placed onto a leach pad and saturated with weak acid solutions that dissolve the copper mineral content. The resulting copper-bearing solution is collected and pumped to a solvent extraction plant. Compressed air is then blown through the mixture. The flotation process is dependent on pine oil droplets, but it's really xanthate-coated chalcopyrite grains sticking to air bubbles on their way up and over the tank. Pine oil simply makes the bubbles. Almost any frother would do, but pine oil is cheap and readily degrades in the environment. The less dense oil covered copper sulphide particles are carried to the top in the foam and are then skimmed off.

The next step carried out in an oxygen flash furnace is heated using natural gas to a high temperature. Next is added limestone, sand, and fresh copper ore concentrate (chalcopyrite) is blown into the furnace with oxygen. It is heated to 1100 °C. The combustion with oxygen is endothermic, and chalcopyrite is actually the fuel that keeps the furnace hot at that point. The oxygen in the air selectively reacts with the iron to form the iron oxide, FeO, and leaves copper in the form of the sulphide, CuS. Sulphur dioxide is a by-product and pollutant unless captured and converted to sulphuric acid.

The silicon dioxide in the sand reacts with the limestone and the iron oxide to form slag, $FeSiO_3$ and $CaSiO_3$. At the same time the excess sulphur in the ore reduces Cu^{2+} sulphide, CuS, to Cu^+ sulphide, Cu_2S, which melts and flows out of the bottom of the furnace. The slag is less dense and floats on the top. The molten Cu^+ sulphide, called copper matte, is run into a converter furnace, where air containing oxygen is blown through the copper matte to oxidize the sulphide ions to sulphur dioxide. At the same time some of the sulphide ions reduce the Cu^+ ions to impure blister copper metal. A final heating in an anode furnace is used to burn off the remaining oxygen. An interesting aside is that for every ton of copper produced, 1.5 tons of slag and 2 tons of sulphur dioxides are also produced as waste products.
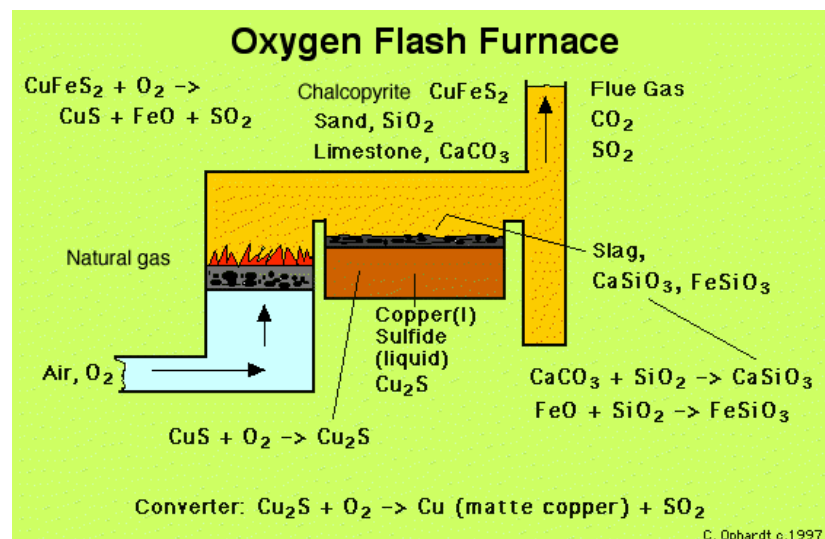
Figure II.7: Copper Smelting Process (Ophardt, 2003)

The final step is the conversion of the impure copper to pure copper. This is done by electrolysis where the impure copper is made into the anode electrode and the pure copper is formed at the cathode electrode. The copper electrodes are immersed in a solution of sulfuric acid and Cu^{2+} sulfate. Oxidation occurs at the anode; therefore copper metal is converted to Cu^{2+} ions with the release of two electrons. At the cathode the opposite reaction occurs: Cu^{2+} ions are joined with two electrons to form copper metal. During the transformation of copper metal into copper ions and back to copper metal, the impurities drop to the bottom of the electrolysis cell. Some of the impurities are gold, silver, nickel, platinum which are themselves recovered to be used.

The main constituents of a copper slag are FeO and SiO_2, each present at about 20 to 55 wt%. The copper content of a smelter slag is normally around 1 wt% while converter slag contains in general much more Cu (2 wt% to 25 wt%), which is much higher than that of copper ore (0,5 to 1

wt%), due to over oxidation and entrapment of metal droplets. Some Cu slags also contain Co and/or Ni at levels of interest for recovery. Toxic elements (e.g. As) and heavy metals (e.g. Pb) exist in some copper slags as well. The mineralogical compositions of slags generated from different origin are quite diverse due to many factors such as ore types, processing techniques and cooling rates. Normally, fayalite and magnetite are the two dominant phases. Ni and Co are present in the form of oxides while Cu in the form of oxides, metallic copper and various copper sulphides has been identified.

Fayalite based slag has already been present for a long time in copper metallurgy. The production of copper from both ores and secondary resources results in major amounts of fayalite slag at a rate of 2.2 ton slag per ton of produced copper. Fayalite slag still contains valuable metals in concentrations sometimes exceeding the content of current natural ores. Rather than being a waste, the slag residue itself can be used in different applications. In order to utilize fayalite based slag and improve the sustainability of the copper metallurgical process, new extraction techniques and slag applications need to be implemented or developed. Although fayalite is the main phase, the resulting microstructure and metals content of the slags lightly differs depending on the metallurgical process and the cooling practice (figure II.8). Applicable techniques for metal recovery and slag utilization depend on the final microstructure of the slag, according to a review on existing and novel routes for metal recovery and fayalite slag utilization (Hunt, 2013). Metallurgical slag without fayalite also was the object recent studies (Zaitsev *et al.*, 2009; Skuza *et al.*, 2009).
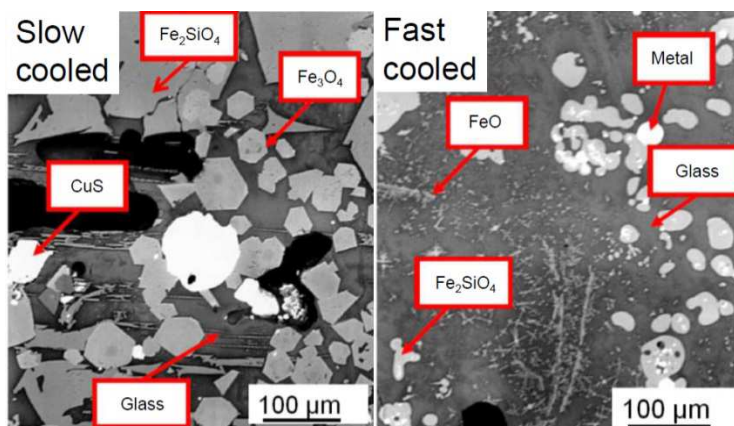
Figure II.8: High Magnification SEM view of two types of slags
from the non-ferrous metallurgy (Wang et al., 2013)

II.3.5 Glass Wastes

'Downcycling' and landfill of glass can be avoided - making container glass a valuable eco-friendly packaging material. In addition, for a glass manufacturer, the use of cullet (recycled glass) is extremely beneficial. Cullet is the technical term the industry uses for crushed glass and is a very important secondary raw material. Aside savings in virgin raw material consumption, around 2.5 - 3% in energy savings can be achieved for every 10% of cullet that replaces primary, 'virgin', raw materials, as no 'reaction energy' is needed to melt cullet. The increased use of cullet, replacing carbonates as well as other raw materials, also results in reduced CO_2 emissions. The use

of cullet leads to savings on both fuel and raw material costs - something the glass industry has known for some time. However, using cullet also brings down CO_2 emissions, as proved by a study carried out in the UK by Glass Technology Services Ltd (GTS) in collaboration with a group of leading manufacturers and The Carbon Trust.

Recycled glass can come from several sources, such as flat glass, glass bottles, light-bulbs, television screens, etc. Before it can be used in ceramic tile manufacturing, it has to provide certain characteristics: supply needs to be plentiful and its composition must be both homogenous and constant. The amorphous nature of glass and also its composition (rich in alkalis) give it a fluxing character. Because of these properties, recycled glass can be used both in ceramic body compositions (where it acts as a flux in a similar way as feldspars do), in ceramic pastes and glaze compositions as a substitute for frits (Karamberi *et al.*, 2006; Karamanov *et al.*, 2008).

II.4 Waste based glass ceramics

Thermal treatments of problematic wastes by glass-ceramic technology have been well-documented regarding its effectiveness in immobilising the toxic contents in their glass matrices. These kinds of heat treatment technologies have been widely used for treatment of several wastes usually processed to form glass-ceramic products. These wastes, coming from numerous sources, can be also considered raw materials and comprise (Rawlings *et al.*, 2006, Chinnam *et al.*, 2013, Cicek, 2013):

- Slag from metallurgical processes (iron and steel production)
- Coal Ash from Power Stations
- Residues from Urban Incinerators
- Slag from Gasification Processes
- Electric Arc Furnace Dust (Steel Fly Ash)
- Cement Dust
- Ore-Refining Quartz-Feldspar Waste
- Fluorescent Glass Waste
- Sewage Sludge
- Anodising Plant Industrial Waste
- Zinc-Hydrometallurgy Wastes
- Clay-Refining Waste (Kira)

Nowadays, recycling the products we consume has become an inevitable requirement in order to optimize natural resources usage while simultaneously preventing pollution from the disposal of such waste. The tile manufacturing industry in the US and in Europe scores highly in terms of effort made to reduce its carbon footprint. More companies are increasing the amount of recycled material used in their products, such as, in UK: Johnson Tiles, British Ceramic Tile, Natural Tile Company and Bottle Alley Glass, in US: Fireclay and Fired Earth, in Italy: Refin Ceramics, and in Spain: Roca, Onix Mosaico and Porcelanosa (Hari, 2013).

In recent years, the Spanish ceramic industry has undergone a period of crisis and uncertainty, with production levels dropping to 50% in less than three years. But this crisis may also herald new opportunities for the sector of ceramics by encouraging the development and manufacture of

more environmentally friendly, ecological tiles. Spain is one of the European countries where scientific research on waste-based products has been really increasing, particularly regarding the elaboration of ecological construction materials, defined as such due to their content of recycled glasses, manufacturing wastes and demolition wastes (Romero *et al.*, 1999 and 2001; Lazaron *et al.*, 2012; Rodriguez-Robles *et al.*, 2014).

In Italy, Lancellotti *et al.* (2013; 2014) have been focusing on chemical and thermal processes to transform waste by referring to End-of-Waste criteria (Directive 2008/98/CE), in order for it to be reused as "secondary raw material" in a traditional manufacture. In parallel, Bernardo, Colombo, Scarinci, Brusatin, *et al.*, have further oriented their interest toward chemical and thermal processes of products generated from wastes mixtures, such as innovative glasses, glass-ceramics, ceramics, and glass ceramic composites. The deepen characterization after sinter-crystallization, sintering, or vitrification allover involves to seek for the chemical stability of final products, but also for the enhancement of functional properties and the development of innovative ceramics (Colombo *et al.*, 2003; Bernardo *et al.*, 2006; Bernardo, 2007a, 2007b; Bernardo *et al.*, 2010a, 2010b, 2011a, 2012).

In Europe, more and more papers are published about waste based products and in 2013/2014 the Impact factors (IF) of the corresponding journals have reached interesting levels, showing the growing interest of waste valorization (as examples: Waste Manag. (3.157) vs. J. Eur. Ceram. Soc. (2.307) (according to citefactor.org, accessed online on 18/01/2015)). Referenced scientists are upraising as specialists of the new field of waste recycling, recovery and re-use (Portillo *et al.*, 2011; Hojamberdiev *et al.*, 2011; Nandi *et al.*, 2014). In international organizations on ceramics, it often exists a session on environmental issues that includes this problematic, such as the technical committees "Waste vitrification" (TC05) and "Environment" (TC13) at the International Commission on Glass.*

References

Aloisi M. Karamanov A. Pelino M. (2004) Sintered glass-ceramic from municipal solid waste incinerator ashes, J. Non-Cryst. Sol., 345-346, 192-195.

Aloisi M. Karamanov A. Taglieri G. Ferrante F. Pelino M. (2006) Sintered glass ceramic composites from vitrified municipal solid waste bottom ashes, J. Haz. Mat., 137 (1), 138-143.

Appendino P. Ferraris M. Matekovits I. Salvo M. (2004) Production of glass–ceramic bodies from the bottom ashes of municipal solid waste incinerators, J. Eur. Ceram. Soc., 24 (5), 803-810.

Arrêté du 31/12/04 (2005) relatif aux installations de stockage de déchets industriels inertes provenant d'installations classées, Journal Officiel, 50, www.ineris.fr.

Aubert J.E. Husson B. Vaquier A. (2004) Use of municipal solid waste incineration fly ash in concrete, Cement and Concrete Research, 34 (6), 957-963.

Bernardo E. (2007a) Fast sinter-crystallization of a glass from waste materials, J. Non-Cryst. Sol., 354, 3486-3490.

Bernardo E. (2007b) Micro- and macro- cellular sintered glass-ceramics from wastes, J. Eur. Ceram. Soc., 27 (6), 2415-2422.

Bernardo E. Scarinci G. (2009) Fast-Sintered Gehlenite Glass–Ceramics from Plasma-Vitrified Municipal Solid Waste Incinerator Fly Ashes, J. Am. Ceram. Soc., 92 (2), 528-530.

Bernardo E. Bonomo E. Dattoli A. (2010a) Optimization of sintered glass–ceramics from an industrial waste glass, Ceram. Int., 36, 1675-1680.

Bernardo E. Scarinci G. Bertuzzi P. Ercole P. Ramon L.(2010b) Recycling of waste glasses into partially crystallized glass foams, J. Por. Mater., 17 (3), 359-365.

Bernardo E. Dattoli A. Bonomo E. Esposito L. Rambaldi E. Tucci A. (2011a) application of industrial waste in 'glass-ceramic stoneware', Int. J. Appl. Ceram. Technol., 8 (5), 1153-1162.

Bernardo E. Esposito L. Rambaldi E. Tucci A. (2011b) sintered glass ceramic articles from plasma vitrified asbestos containing waste, Appl. Adv. Ceram., 110 (6), 346-352.

Bernardo E. Scarinci G. Colombo P. (2012) Vitrification of Waste and Reuse of Waste-Derived Glass, Encyclopedia of Sustainability Science and Technology, Editors Robert A. Meyers 1. RAMTECH LIMITED Pub. Springer New York, 11581-11613.

Bertolini L. Carsana M. Cassago D. Curzio A.Q. Collepardi M. (2004) MSWI ashes as mineral additions in concrete, Cement and Concrete Research, 34 (10), 1899-1906.

Binhussain M.A. Marangoni M. Bernardo E. Colombo P. (2014) Sintered and glazed glass-ceramics from natural and waste raw materials, Ceram. Int., 40 (2), 3543-3551.

Chinnam R.K. Francis A.A. Will J. Bernardo E. Boccaccini A.R. (2013) Review. Functional glasses and glass-ceramics derived from iron rich waste and combination of industrial residues, J. Non-Cryst. Sol., 365, 63-74.

Colombo P. Brusatin G. Bernardo E. Scarinci G. (2003) Inertization and reuse of waste materials by vitrification and fabrication of glass-based products, Current Opinion in Solid State and Materials Science, 7, 225-239.

Consonni S. (2012) I: Generalità sul recupero da rifiuti, II: Thermo-utilizzazione dei rifiuti, Gestione di rifiuti e termo-utilizzazione, Università di Padova, corso di dottorato di ingegneria industriale.

Das B. Prakash S. Reddy P.S.R. Misra V.N. (2007) An overview of utilization of slag and sludges from steel industries, Res. Cons. Recycl., 50, 40-57.

Decision 2003/33/CE (2003) Decision of the commission on criteria and procedures of admissibility of waste into landfill (EN), décision du conseil établissant des critères et des procédures d'admission des déchets dans les décharges (FR).

Directive 1999/31/CE (1999) Directive of the commission on waste disposal (EN), directive du conseil concernant la mise en décharge des déchets (FR).

Directive 2008/98/CE (2008) Directive of European Parliament and Commission on waste (EN), Directive du parlement européen et du conseil relative aux déchets et abrogeant certaines directives (FR).

E.P.A. (available online) ceramic products manufacturing, Mineral Products, 11, 7-13.

Eurostat (2010) epp.eurostat.ec.europa.eu, online data code env_wasgen, available online the 10-09-2014.

Guarienti M. Gianoncelli A. Bontempi E. Moscoso Cardoso S. Borgese L. Zizioli D. Mitola S. Depero L.E. Presta M.(2014) Biosafe inertization of municipal solid waste incinerator residues by COSMOS technology, J. Haz. Mat., 279, 311-321.

Hari A. (2013) Eco-friendlier ceramic, porcelain and glass tiles, DecoMagazine, decomag.co.uk/content/eco-friendlier-ceramic-porcelain-and-glass-tiles.

Hojamberdiev M. Eminov A. Xu Y. (2011) Utilization of muscovite granite waste in the manufacture of ceramic tiles, Ceram. Int., 37, 871-876.

Hunt A. (ed.) Wang, Gerven and Blanpain (2013) Chapter 2: metal recovery from metallurgical waste. A case study, Element recovery and sustainability, royal society of chemistry, RSC Green chemistry series, 39-54.

Karamanov A. Pelino M. Hreglich A. (2003) Sintered glass-ceramics from Municipal Solid Waste-incinerator fly ashes—part I: the influence of the heating rate on the sinter-crystallization, J. Eur. Ceram. Soc., 26 (6), 827-832.

Karamanov A. Aloisi A. Pelino M. (2005) Sintering behavior of a glass obtained from MSWI ash, J. Eur. Ceram. Soc., 25 (9), 1531-1540.

Karamanov A. Pelino M. (2008) Induced crystallization porosity and properties of sintered diopside and wollastonite glass-ceramics, J. Eur. Ceram. Soc., 28, 555-562.

Karamanova E. Schabbach L.M. Ranguelov B. Avdeev G. Lancellotti I. Karamanov A.(2010) Optimization of the heat-treatment regime of a sintered glass-ceramic from MSWI bottom ash, 10th International Multidisciplinary Scientific Geoconference and EXPO - Modern Management of Mine Producing, Geology and Environmental Protection, SGEM 2010, 2, 893-900.

Karamberi A. Moutsatsou A. (2006) Vitrification of lignite fly ash and metal slags for the production of glass and glass ceramics , China Particulology, 4 (5), 205-253.

Kasuriya S. Jiemsirilers S. Thavorniti P. (2008) Effect of MSW incineration bottom ash in clay based ceramics, Mat. Sci. Forum, 569, 205-208.

Lancellotti I. Ponzoni C. Barbieri L. Leonelli C. (2013) Alkali activation processes for incinerator residues management, Waste Manag., 33 (8), 1740-1749.

Lancellotti I. Cannio M. Bollino F. Catauro M. Barbieri L. Leonelli C. (2014) Geopolymers: an option for the valorization of incinerator bottom ash derived "end of waste", Ceram. Int., in press, available online.

Lazaron C. Trillesn V.R. Gomez F. Allepuz S. Fraga D. Carda J.B. (2012) Incorporation ceramic manufacturing waste and recycled glass into the integral ceramic process, Qualicer' 12, Castellon, Spain.

Lin K.L. Wang K.S. Tzeng B.Y. Lin C.Y. (2003) The reuse of municipal solid waste incinerator fly ash slag as a cement substitute, Res. Cons. Recycl., 39 (4), 315-324.

Lin K.L. (2006) Feasibility study of using brick made from municipal solid waste incinerator fly ash slag, J. Haz. Mat., 137 (3), 1810-1816.

Malfliet A. Jones P.T. Binnemans K. Cizer Ö. Fransaer J. Pengcheng Y. Pontikes Y. Guo M. Blanpain B. (2013) Proceedings of the 3rd Int. Slag Valor. Symp., The transition to sustainable Materials Management, KU Leuven, Belgium.

Nandi V.S. Raupp-Pereira F. Montedo O.R.K. Oliveira A.P.N. (2014) the use of ceramic sludge and recycled glass to obtain engobes for manufacturing ceramic tiles, J. Cleaner Prod., in press, 1-10.

Ophardt C.E. (2003) Iron Blast furnace, Virtual Chembook, elmhurst.edu/~chm/vchembook/326steel.html.

Pera J. Coutaz L. Ambroise J. Chababbet M. (1997) Use of incinerator bottom ash in concrete, Cement and Concrete Research, 27 (1), 1-5.

Portillo M.C. Gazulla M.F. Sanchez E. Gonzalez J.M. (2011) A procedure to evaluate resistance to biological colonization as a characterization for product quality of ceramic roofing tiles, J. Eur. Ceram. Soc., 31, 351-359.

Rambaldi E. Esposito L. Andreola F. Barbieri L. Lancellotti I. Vassura I.(2010) The recycling of MSWI bottom ash in silicate based ceramic, Ceram. Int., 36 (8), 2469-2476.

Rawlings R.D. Wu J.P. Boccaccini A.R. (2006) Glass-ceramics: Their production from wastes-A Review, J. Mat. Sci., 41 (3), 733-761.

Règlement 1013/2006 (CE) (2006) Regulation of the European Parliament and Commission concerning waste transfer, 14 June 2006.

Rémond S. Pimienta P. Bentz D.P. (2002) Effects of the incorporation of Municipal Solid Waste Incineration fly ash in cement pastes and mortars: I. Experimental study, Cement and Concrete Research, 32 (2), 303-311.

Rodriguez-Robles D. Cargia-Gonzales J. Juan Valdes A. Moran del Pozo J.M. Guerra I. Romero M. (2014) Quality assessment of mixed and ceramic recycled aggregates from contruction and demolition wastes in the concrete manufacture according to the Spanish standard, Materials, , 5843-5857.

Romero M. Rawlings R.D. Rincón J.M. (1999) Development of a new glass–ceramic by means of controlled vitrification and crystallization of inorganic wastes from urban incineration, J. Eur. Ceram. Soc., 19 (12), 2049-2058.

Romero M. Rincón J.M. Boccaccini A.R. (2001) Use of vitrified urban incinerator waste as raw material for production of sintered glass-ceramics, Mater. Res. Bull., 36 (1-2), 383-395.

Rozenstrauha I. Lodins E. Krage L. Drille M. Balode M. Putna I. Filipenkov V. Chinnam R.K. Boccaccini A.R.(2013) Functional properties of glass–ceramic composites containing industrial inorganic waste and evaluation of their biological compatibility, Ceram. Int., 39 (7), 8007-8014.

Schabbach L.M. Andreola F. Karamanova E. Lancellotti I. Karamanov A. Barbieri L.(2011) Integrated approach to establish the sinter-crystallization ability of glasses from secondary raw material, J. Non-Cryst. Sol., 357 (1), 10-17.

Shi H.S. Kan L.L. (2009) Leaching behavior of heavy metals from municipal solid wastes incineration (MSWI) fly ash used in concrete, J. Haz. Mat., 164 (2-3), 750-754.

Skuza Z. Kolmasiak C. Prusak R. (2009) Possibilities for the utilization of metallurgical slag in the conditions of the polish economy, Metallurgua, 48 (2), 125-128.

U.N.E.P. United Nations Environmental Program (2013) Guidelines for National Waste Management Strategies , Moving from Challenges to Opportunities.

Vu D.H. Wang K.S. Chen J.H. Nam B.X. Bac B.H.(2012) Glass–ceramic from mixtures of bottom ash and fly ash, Waste Manag., 32 (12), 2306-2314.

Wang X. Geysen D. Padilla S.V. D'Hoker N. Huang S. Jones P.T. Van Gerven T. Blanpain B. (2013) Fayalite based slags: metal recovery and utilization, Poster, Department of Metallurgy and Materials Engineering, K.U. Leuven, Belgium, available online on 15/11/2014.

Zaitsev A.I. Shakhpazov E.K. (2009) Development of a modern theory for metallurgical slag, Metallurgist, 53 (5-6), 255-260

* www.icglass.org/technical_committees.

Chapter III

Glass and glass-based products

III.1 Definition of glass

Solids that do not have a three-dimensional, periodic structure are said to be amorphous or glassy. Such materials do not exhibit significant level of crystallinity. Many classes of materials are capable of forming amorphous or glassy structures under certain conditions, including metal alloys, organic polymers and oxide or non-oxide compounds. In this discussion we will focus primarily on oxide-based glasses. The main types of glass include borosilicate glass, soda-lime Commercial glass, glass fiber (and Lead glass). Types of special glass include Alkali-barium Silicate glass, Aluminosilicate glass, Optical glass, Sealing glass, Technical glass, Vitreous Silica. Glass Ceramics can enter also in special glasses definition but here they will be considered apart. Most types of glass are made up of network-forming oxides and network-modifying oxides, the bases of which are principally either silicon oxide, calcium oxide or sodium oxide.

Main glass formers	Conditional glass formers	Intermediate oxides	Network modifiers
SiO_2	Al_2O_3	TiO_2	MgO
B_2O_3	Bi_2O_3	ZnO	Li_2O
GeO_2	WO_3	PbO	BaO
P_2O_5	MoO_3	Al_2O_3	CaO
	TeO_2	Zr_2O_3	Y_2O_3
			K_2O

Table III.1: Abbreviation list of oxides commonly used in glass

The structural relationship between the oxygen and the cation of the oxide compound strongly influences the glass-forming ability of the oxide. Table III.1 details the classification of oxides depending on their role in the glassy structure. The main glass former oxides have suitable structure and crystallization rates slow enough to form glasses when cooled from a liquid state with relatively slow cooling rates. Conditional glass-forming oxides will form glasses under certain circumstances. Intermediate oxides cannot form glasses, on their own or when mixed with glass formers. However, they can modify the properties of the glass because they can weaken the glass network by affecting Si-O bonds. These oxides are used to control properties such as the softening point or hardness. Oxides with crystal structures such as A_2O, AO, AO_4, A_2O_7, where A represents a cation, are so symmetric that they generally crystallize from a melt rather than form glasses. In its glassy state, the structure is seen to be disordered, where the positions of the atoms

are not correlated and with a chaotic behavior similar to a liquid, so that it displays an amorphous structure.

One of the characteristic properties of glass is its **viscosity**, which is a measure of its resistance to flow. Viscosity depends on any factor that can influence the ease with which molecules slip past each other. Liquids tend to become more viscous as the molecules become larger, or as the intermolecular forces become stronger. They also become more viscous when cooled. In glass production, certain steps are defined by the glass viscosity and lead to the definition of various points (figure III.1). Among them, T_g, glass transition temperature is defined as the point at which the elongation becomes discontinuous and characterizes non-crystalline solids; strain point at $10^{13.5}$ Pa·s; annealing point, at 10^{12} Pa·s; penetration point at 10^{11} Pa·s; dilatometric softening point at $10^{10.3}$ Pa·s and "true" softening point at $10^{6.6}$ Pa·s; finally flow point at 10^4 Pa·s; and working point at 10^3 Pa·s. At the melting point, vibrating lattice elements of a crystalline solid will no longer return to sites bonded to their neighbors. Glasses have three characteristics that make them more closely resemble "frozen liquids" than crystalline solids. First, and foremost, there is no long-range order. Second, there are numerous empty sites or vacancies. Finally, glasses do not contain planes of atoms.
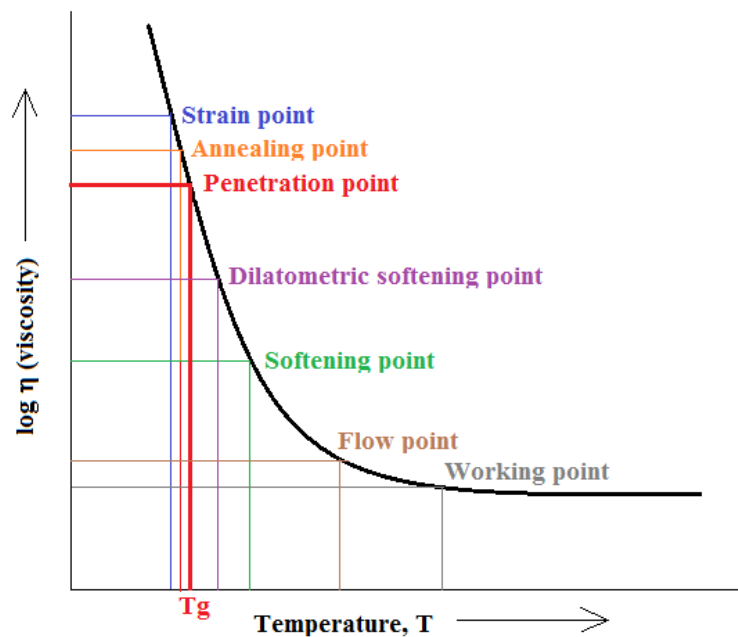
Figure III.1: Typical viscosity versus temperature curve for glass

In general, the glassy state is metastable. Because the amorphous state is "quenched in" by cooling a liquid fast enough to prevent crystallization, the glass state has a thermodynamic driving force to transform to a crystalline state. However, in many glasses the kinetic for the reaction can be so slow that for all practical purposes, the glassy state is stable. Some compositions of glass may be marginally stable over time or with elevated temperature aging, and the glass may transforms from an amorphous state to a crystalline state. This phenomenon is known as *devitrification*. Certain classes of ceramics, glass-ceramics, are based on this devitrification mechanism. With glass-ceramics, an article may be formed in the glassy state by processes such as casting or compression molding and then transformed to a predominately crystalline ceramic via

devitrification. Glass-ceramic can have improved mechanical properties over completely amorphous glasses.

Another characteristic is the volume expansion. When liquid or molten glass cools slowly, the volume (measured as specific volume- inverse of density) contracts based on the coefficient of thermal expansion of the material as shown in the figure III.2.
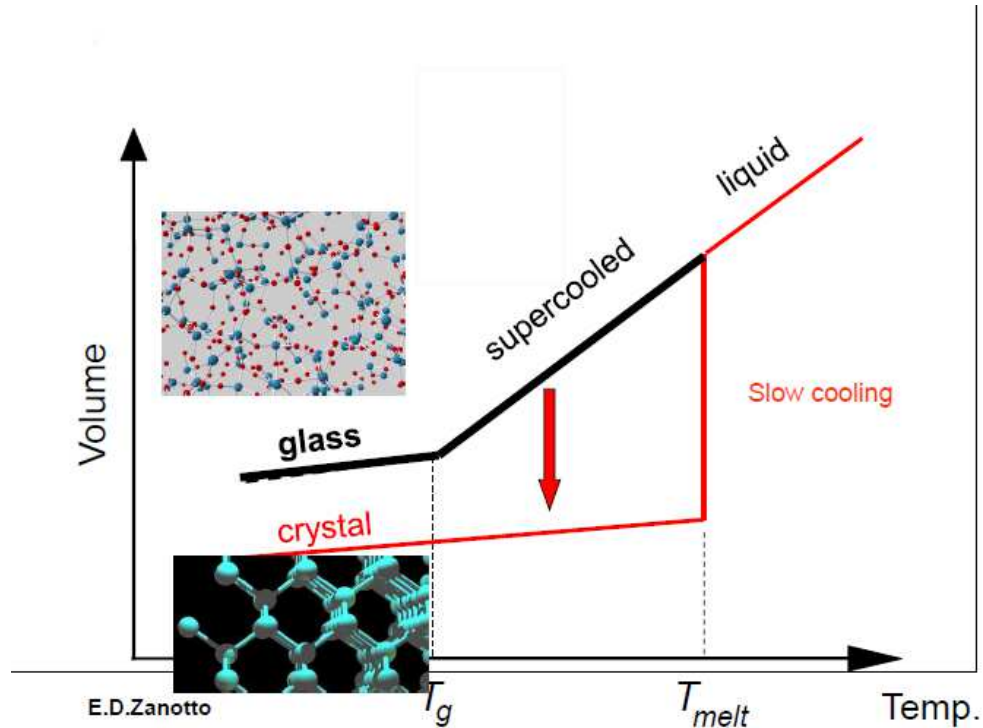
Figure III.2: Glass transition (volume expansion in function of the temperature)

Correspondingly, the viscosity of the glass increases, as show in the figure III.1. If the viscosity is still relatively low, structural changes (reorientation) can occur at the same rate as the cooling rate and the glass structure rearranges into a more dense arrangement as the viscosity of the glass increases. At some point the viscosity of the glass increases at a higher rate than the rate of structural rearrangement. At this transition temperature, the slope of the specific volume versus temperature curve changes. This change in slope occurs at the glass transition temperature, Tg. (Budinski and Budinski, 2004)

III.1.1 Common glass (soda-lime)

Most of the glass we see around us in our everyday lives in the form of bottles and jars, flat glass for windows or for drinking glasses is known as commercial glass or soda-lime glass, as soda ash is used in its manufacture. The main constituent of practically all commercial glass is sand. Sand by itself can be fused to produce glass but the temperature at which this can be achieved is about 170 0 °C. Adding other minerals and chemicals to sand can considerably reduce the melting temperature. The addition of sodium carbonate (Na_2CO_3), known as soda ash, to produce a mixture of 75% silica (SiO_2) and 25% of sodium oxide (Na_2O), will reduce the temperature of fusion to about 80 0 °C. However, a glass of this composition is water-soluble and is known as water glass. In order to give the glass stability, other chemicals like calcium oxide (CaO) and magnesium oxide (MgO) are needed. These are obtained by adding limestone which results in a pure inert glass.

Commercial glass is normally colorless, allowing it to freely transmit light, which is what makes glass ideal for windows and many other uses. Additional chemicals have to be added to produce different colors of glass such as green, blue or brown glass. Most commercial glasses have roughly similar chemical compositions of: 70% - 74% SiO_2 (silica) 12% - 16% Na2O (sodium oxide) 5% - 11% CaO (calcium oxide) 1% - 3% MgO (magnesium oxide) 1% - 3% Al_2O_3 (aluminum oxide).

Chemical composition [wt%]	
SiO_2	71.6
Al_2O_3	1.0
Na_2O	13.5
K_2O	0.4
CaO	9.0
MgO	3.9
Fe_2O_3	0.1
SO_3	0.2
BaO	<0.1
Physical properties	
fusion point Log=2	1145 °C
Flow point Log=3	1188 °C
working point, Logη=4	1024 °C
Softening point of Littleton, Logη=7.6	725 °C
annealing point, Logη=13	590 °C
strain point, Logη=14.5	550 °C
Coefficient of thermal expansion α	$8.67 \ 10^{-6}$ °C^{-1}
Density ρ	2.497 g/cm^3

Table III.2: Chemical and physical characteristics of soda-lime silicate glass (Bernardo, 2004)
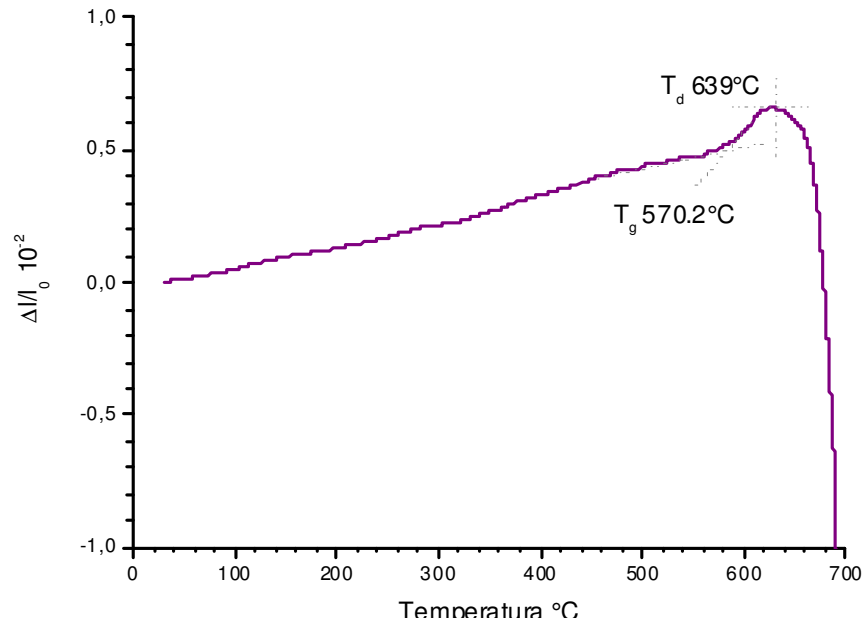
Figure III.3: Dilatometric analysis of a piece of soda-lime silicate glass

Flat glass is similar in composition to container glass except that it contains a higher proportion of magnesium oxide. Within these limits the composition is varied to suit a particular product and production method. The raw materials are carefully weighed and thoroughly mixed, as consistency

of composition is of utmost importance in making glass. Nowadays recycled glass from bottle banks or kerbside collections, known as cullet, is used to make new glass. Using cullet has many environmental benefits, it preserves the countryside by reducing quarrying, and because cullet melts more easily, it saves energy and reduces emissions. Almost any proportion of cullet can be added to the mix (known as batch), provided it is in the right condition, and green glass made from batch containing 85% to 90% of cullet is now common. Although the recycled glass may come from manufacturers around the world, it can be used by any glassmaker, as container glass compositions are very similar. It is, however, important that glass colors are not mixed and that the cullet is free from impurities, especially metals and ceramics.

The chemical and characteristic properties of a typical commercial transparent soda-lime glass are presented in the table III.2 and figure III.3. The DTA enabled to confirm the thermal expansion coefficient and to determine the glass transition point and the dilatometric softening, respectively of 570 °C and 640 °C. The DTA softening point is essential for the sintering and the sinter-crystallization of glass mixtures.

III.1.4 CRT glasses

CRT glasses are recognized as diffused non-recyclable glasses. In the cathode ray tube glasses are implied glasses containing heavy metals, based on Pb and Ba (Hreglich et al, 2001). The use of heavy metals in the composition of glasses for television monitor and computers, comes from the necessity of absorbing the electromagnetic radiations, particularly at high frequency, emitted from the electronic gun (see figure III.4). Without this type of glass, watching TV is very dangerous, as televisions produced X-rays that must be absorbed, otherwise they could in the long run cause health problems. The X-rays are absorbed by glass with minimum amounts of heavy oxides (lead, barium or strontium). The concentrations in heavy metals vary with the function of the glass in the TV (see tables III.4 and III.5). Lead glass is commonly used for the funnel and neck of the TV tube, while glass containing barium is used for the screen. A cathode ray tube (Bernardo, 2008 and dalle Vedove, 2013) is an electrical device composed mainly of an evacuated glass tube, inside of which is an electron gun that emits by thermionic effect rays of electrons that enable to see pictures on a screen.
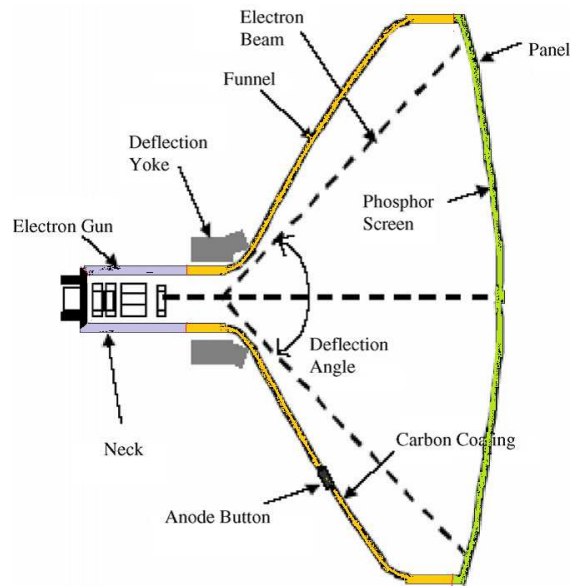
Figure III.4: Structure of monochrome kinescope

Figure III.4 represents a CRT glass tube. We can note that is it is composed of 4 parts, panel, funnel, neck and frit. According to Andreola *et al.* (2007), it is estimated that approximately 65% of the weight of a television set or a computer monitor is constituted of cathode ray tube (CRT) or kinescope, and it is composed for 85% of glass (65% panel and 30% funnel and 5% neck glass) as a screen, a neck glass, in which an electron gun is inserted and a back funnel glass that connects the panel and the neck (Figure III.4). The panel and funnel glass are formed by pressing individually and later they are sealed together without a junction. The color CRT structure is essentially similar to the monochrome one with some technical differences. The base is the monitor's "screen" that is coated on the inside with a matrix of thousands of tiny phosphor dots. Phosphors are chemicals which emit light when excited by a stream of electrons: different phosphors emit different colored light. Each dot consists of three blobs of colored phosphor: one red, one green, one blue. These groups of three phosphors make up what is known as a single pixel. In the neck there are three electron guns for the red, blue and green. Three electron beams from each electron gun pass through a hole in the shadow mask and excite phosphor uses vertical wires under tension, an aperture grill instead of a shadow mask. The main properties required for CRT glasses are X-ray absorption, electric resistivity and a thermal expansion suitable to the other glass parts and sealing metal. High light transmittance is also important for the panel glass to display clear pictures. In addition, it is essential that light transmittance is not deteriorated by electron beam or X-ray irradiation. Different kinds of glasses for each part of black and white (B&W) and color CRTs are used according to their technical specifications:

1. Panel (screen, the front part): a very homogeneous barium–strontium glass, of a greenish-blue color, whose weight is about two-third of the whole CRT;

2. Cone (the hidden part inside the TV set): a lead glass, whose weight is about one-third of the whole CRT;

3. Neck: a glass with a very high lead content enveloping the electron gun;

4. Frit (the junction between the panel and the cone cone): a low melting lead glass, included only in color CRTs.

Type	PbO (wt%)	ρ (g/cm^3)
Panel TV	2.25	2.695
Cone TV	22.5	3.02
Tube TV	28.4	3.18

Table III.4: Typical data of glass used in color CRT (Bernardo, 2004)

Type of glass	Transition glass temperature, T_g (°C)	Softening temperature, T_s (°C)	Dilatom. coefficient, α ($\times 10^{-6}$ °C^{-1})
Colour panel	535	855	9.99
Colour funnel	505	750	9.79
B&W mixed	490	720	9.15

Table III.5: Thermal properties for color (TV+PC) and B&W CRT glasses (Andreola et al., 2007)

The CRT glass coming from color equipment, presents important differences in composition between panel (screen) and funnel (cone). The screen is characterized by high levels of BaO (9 to 11 wt%) and SrO (8 to 10 wt.%), the cone instead contains a significant quantity of PbO (18 to 20 wt%) that is moreover completely absent in the panel.
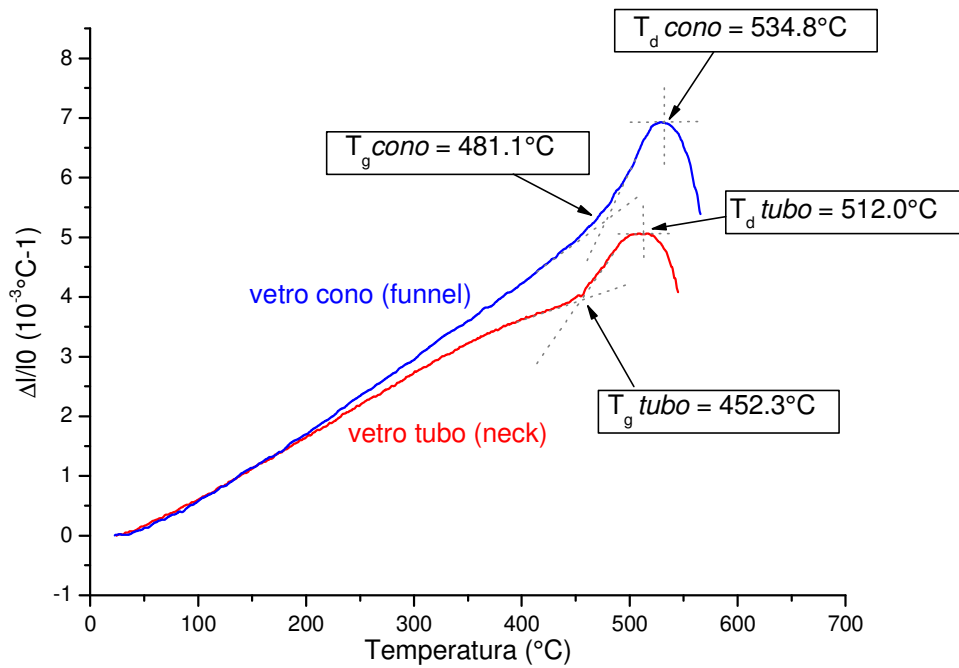
Figure III.5: Dilatometric analysis of lead glasses from tube and cone (funnel) (Bernardo, 2004)

27
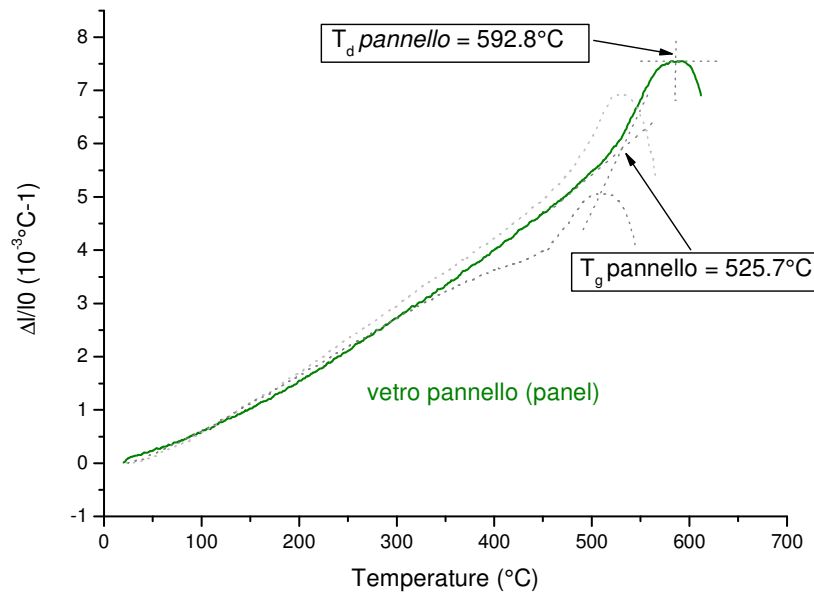
Figure III.6: Dilatometric analysis of panel glass, richer in BaO (Bernardo, 2004)

According to figures III.5 and III.6, the higher content of lead in tube glass determines the displacement of the glass transition temperature and the softening point of around 25-3 0 °C, with respect to cone glass. And the characteristic temperatures of panel glass are around 100 °C lower than those of a common soda-lime glass which makes this glass easy to process from 600 °C. By extension, not only for reasons of electric resistivity (absorption of electromagnetic radiations), the presence of Lead in the glass is due to the necessity to increase the coefficient of thermal expansion ($\alpha \sim 10 \ 10^{-6} \ °C^{-1}$), in order to make it compatible with platinum, used for the electric contact of lamps and lightening systems. The composition of the glasses for incandescent light contained Pb until the 1920', and then with the automatization of production, it became possible to limit the percentage of Pb.

III.1.5 Status of the recycling (closed- and open-loop cycle)

Normally for the manufacture of new CRTs, the two glass fractions (the leaded and the unleaded glass) are accurately separated and cleaned. The event of the new LCD and PDP technologies allows the shift of production sites to emerging countries as India, China and Southeast Asia. From these considerations it is possible to hypothesize a drastic reduction of the close-loop recycling. On the other hand, open-loop recycling is not easy, because it is forbidden to introduce dangerous elements (such as lead, arsenic, cadmium) into products like glass containers, tableware or glass fibers. In this context, the glass industry is an excellent potential consumer only for glasses without the abovementioned elements, such as carefully selected glass from the screens. In the ceramic industry the restriction is not so restrictive and both glass from screens and cones are potentially acceptable as secondary raw material even if they must be supplied with particular characteristics of homogeneity, cleanness, etc. Some EU experiences of open-loop recycling are below listed: Potential use in brick manufacturing; Potential use in foam glass; Use of CRT glass in tableware glass production; Use of CRT glass in insulating glass fiber production; Use of CRT glass on ceramic bodies.

As regards glazing manufacturing, CRT glass could be considered as a substitute for non-plastic materials, in particular ceramic frits. Moreover, it contains barium, strontium, zirconium and lead oxides, which represent components that are often added to glazes in order to obtain specific properties (brightness, chemical resistance, matt effect, etc.). Thus, CRT cleaned glass could represent an important raw material able to help to reduce the energy consumption and to shorten production times. This idea derives from the generally accepted concept for which the use of recycled materials is environmentally preferable to that of virgin raw materials.

III.1.2 Borosilicate glass

Most of us are more familiar with this type of glass in the form of ovenware and other heat-resisting ware, better known under the trade name Pyrex. Borosilicate glass (or sodium-borosilicate glass) is made mainly of silica (70 °C to 80%) and boric oxide (7-13%) with smaller amounts of the alkalis (sodium and potassium oxides) and aluminum oxide. This type of glass has a relatively low alkali content and consequently has both excellent chemical durability and thermal shock resistance - meaning it do not break under a rapid temperature change. As a result of these properties, sodium borosilicate glass is widely used across the household and chemical industry, the pharmaceutical sector but also various high intensity lighting applications and as glass fibers for textile- and plastic reinforcement. The typical characteristics of a borosilicate glass are presented in table III.4.

Chemical composition [wt%]	
SiO_2	72
B_2O_3	12
Al_2O_3	7
CaO	1
Na_2O	6
K_2O	2
BaO	<0.1
Physical properties	
working point, $Log\eta=4$	1140 °C
Softening point of Littleton, $Log\eta=7.8$	785 °C
annealing point, $Log\eta=13$	570 °C
strain point, $Log\eta=14.5$	530 °C
Coefficient of thermal expansion α	$5.5 \ 10^{-6} \ °C^{-1}$
Density ρ	$2.33 \ g/cm^3$

Table III. 4: Chemical and physical characteristics of a borosilicate glass for pharmaceutical applications (Bernardo, 2004)

The borosilicate glass is not generally made of a single phase, but of a mixture of two immiscible phases SiO_2-B_2O_3. The first is rich in Silica and the second is rich in boric-anhydrates and other components (network modifiers). From the thermodynamic, the system is more stable if the two phases are separated, because the necessary energy to bind the distinct components is not sufficient with regard to the binding energy of same components.
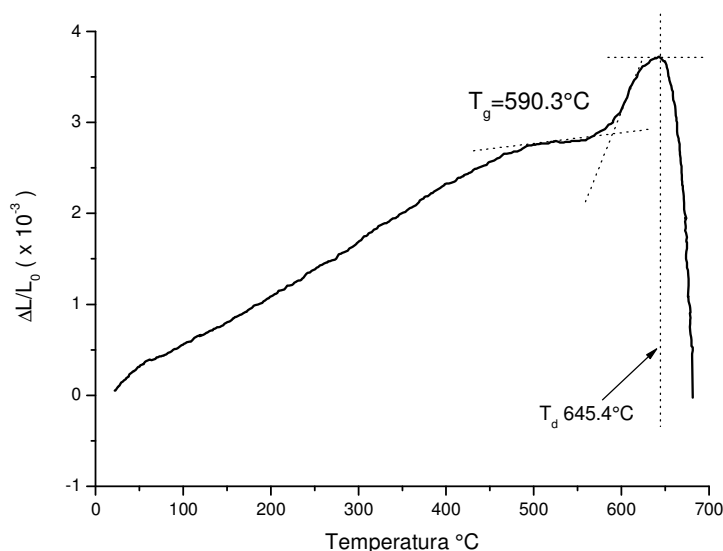
Figure III. 7: Dilatometric analysis of a glass powder piece for the pharmaceutical industry
(Bernardo, 2004)

However, there exist two mechanisms of separation, by nucleation and growth or by spinodal decomposition. In first case, a principal phase englobes isolated spherical particles of the second phase; in the second case, two continuous interconnected phases develop, both accessible at the surface. The borosilicate glasses of high chemical stability represent typical application of glass separated in phase of nucleation and growth; indeed, the SiO_2 rich phase is actually the most chemically stable, stops the diffusion of acid attack and the leaching of cations (present in the second phase) happens only on a few micrometers at the surface. The Vycor glass, at 96% SiO_2, is an application of spinodal decomposition. By a chemical attack, the interconnected soluble phase of borate is completely removed, leaving place to a micro porosity. (Bernardo, 2004)

The temperatures of softening point by DTA and glass transition are typically respectively at 645 °C and 590 °C (figure III.7).

III.1.1 Glass production

Note: acknowledgments to Prof Nicoletti (Honor President of the International Commission on Glass and part-time consultant at Stevanato, Nuova Ompi, Italy) Silvia Molinaro (Environment Engineer at Stevanato) for their explanations.

Raw materials for the glass are mixed in the most homogeneous possible way, in liquid phase. Indeed, temperatures in the fusion glass bath should overpass the melting point of every involved material. Then furnace temperature can reach 155 0 °C. The raw materials are principally composed of sand or quartz-containing products, natural or synthetized, then of soda Na_2O, of carbonates "A"-CO_3 and an input of Alumina Al_2O_3. The glass of bottles and windows (90% world glass production), contains Ca and Mg ions brought by dolomite or marble. Global glass production is around 150 Mton/year.

These materials all have very diverse aspects: their densities and granularities differ strongly, which makes their homogeneous mix almost impossible. Over the thermal process in the fusion furnace, cords lie ahead, richer in one or another raw material. These unavoidable defects are visible under SEM microscope. Knowing that fusion temperature can go quite high, depending on

composition, (for the record, pure quartz at 170 0 °C), the objective is to produce in the least energy consuming way. A compromise is to realize between a good chemical resistance, brought by alumina and silica, both of high fusion temperature, and a low glass fusion temperature, achieved by the addition of Na^+ ions, which act as fluxing and modifying agents in the glass network, but consequently diminish the chemical resistance properties.

Soda-lime glass is composed of ~72% silica SiO_2, ~10% soda Na_2O, then comes Na, Ca and Mg, and then ~ 6% alumina Al_2O_3, that can be brought by feldspars and nephelines (syenite, etc.), which further contain, Na, K and Mg, and which decrease fusion temperature. For example, the basic composition of float glass, one type of soda-lime glass, is of 72.6% sand, 13% soda, 8.4% lime and 4% dolomite. (ref: Pilkington glass website).

Should a high chemical resistance really be required, it may necessary to decrease soda and increase silica and alumina amounts, still without the possibility to increase the furnace temperature (refractories would not stand). A borosilicate glass is then elaborated. Indeed, bore is an atom that does not modify the structure of the glassy network, but acts as fluxing agent. The composition can then be this one: Si_{O2} 75%, Al_2O_3 6.5%, Na_2O 7.5%, B_2O_3 10.5%, CaO-BaO 0.5-1%. Sand, borax (containing soda), or a pure boric acid, then feldspars or alumina, and eventually soda, still form part of the glass compounds, and then soda in quantities deduced from the initially present percentages of the other materials.

The chemical reactions stages in the fusion furnace are various: first is evacuated humidification water, which hydrates in the same time anhydrous compounds (NaOH, CaOH, etc.), then evaporates the borax hydration water with a dissolution of sand. Then, at 45 0 °C takes place the borax decomposition. At 80 0 °C carbonates decompose with the gaseous release of CO_2. The fusion is recognized as such when there are no more solid particles in the mix, (by thermodynamic definition).Viscosity at the melting of the mixture is then a 100 times those of water, and is actually comparable to glycerin. Because of this, glass is full of tiny bubbles that cannot come up to the surface. Minor elements, in quantities 0.1% to 0.3% are incorporated to facilitate bubbles evacuation by agglomeration. It is called fused glass refinement (or refining process), that provides "bubbles cleaning" without increasing the temperature (115 0 °C). The refining agents derivate from CaF_2, AsO_3, and NaCl ions. They don't enter in the glass composition as they evaporate fast in doing "big bubbles", taking the smaller ones along to the surface. For those reasons, cords, unfused and bubbles are typically defects of a glass after manufacture. At the end of the fusion process, "ready-made" glass is evacuated by canals: conditioning zones. Then, forming process is variable: bottles are blown, glass tubes are made by Danner machines, and flat glass is produced according to float glass process established by Pilkington (glass floating on a fusion stain bath, allowing for a perfectly plane surface). To make amber colored glass (whose objective is to stop light emissions at high frequency (UV)) are added in the composition 1% to 2% Fe_2O_3 and 2% to 3% TiO_2.

During the shaping process of glass containers, the chemical transformation still takes place: the high temperature treatments (boring, cutting, and forming with pulleys and points) provoke the migration of Na^+ ions. Some components are sublimated. To certify the chemical resistance of the employed container, an autoclave test is made by laboratory. Indeed, the attack of vapor water (12 0 °C) on Na^+ ions creates a basic medium that dissolves glass. It is the European pharmacopeia, Japanese or American that will decide the necessary chemical resistance. Is designed valuable

either the borosilicate glass or reinforced soda-lime glasses: an ammonium treatment enables to reduce the sodium quantity in surface indeed, the NH_2SO_4 dissociates and liberates SO^{3-} which reacts with Na^+ ions to give Na_2SO_4, an opaque white precipitate, very soluble and eliminated with distilled water. Then the glass, that contains 7% Na, does not contain at all of it on a few microns thickness in surface.

Because of the differences in the various methods of manufacture, the industry is divided into 5 main sections under the general headings: Container glass; flat glass; scientific/technical glass; domestic glass; and fiber glass. Glasses may be devised to meet almost any imaginable requirement. There are many different types of glass with different chemical and physical properties and each can be made by a suitable adjustment to chemical compositions. For many specialized applications in chemistry, pharmacy, the electrical and electronics industries, optics, the construction and lighting industries, glass, or the comparatively new family of materials known as glass ceramics, may be the only practical material for the engineer to use.

III.2 Viscous flow sintering of glass

The sintering of glasses follows an absolutely characteristic mechanism. In general, the sintering may be regarded as the densification of powders, generally pressed, through the progressive removal of the porosity located at interstices between the granules, by application of a temperature significantly lower than the melting temperature of the material. Densification is thermodynamically favored abasement of the free energy of the system related to the reduction of the specific surface area ratio (area/volume ratio). The sintering mechanisms feature the absence or the formation of a liquid phase, upon heating of pressed powders. The following mechanisms of sintering are generally recognized (Various authors, 1996):

1. *Solid state sintering by diffusion mechanism;* this is the mechanism recognizable in advanced ceramic materials. It is characterized by the absence of a secondary amorphous phase to tie the crystalline grains. It involves the formation of a grain boundary by displacement of matter (and opposed displacement of crystal vacancies) from the internal part of the grains to the outside, with a progressive decrease of the distance between the centers of adjacent granules. The absence of a secondary intergranular phase allows for the manufacturing of materials with excellent high temperatures mechanical properties; in contrast, the diffusive mechanism is rather slow and often involves the need to compensate the activation energy (corresponding to the transfer of matter) not only with the thermal energy but also with the mechanical energy corresponding to a mechanical stress, associated to hot pressing (uniaxial or isostatic).

2. *Solid state sintering by evaporation-condensation*; this is the prevailing mechanism for solids with high vapor pressure, such as alkali halides (poorly interesting for engineering purposes), in which the transfer material is carried out by transition to the external gas phase and subsequent condensation.

3. *Sintering with the formation of the liquid phase*; powders of the substance to be sintered contain additives forming a liquid phase, for a content not exceeding 5%; the liquid phase "lubricates" the grains in the sense that it allows for the mutual sliding to compress the porosity and at the same time partially dissolves the base material (the associated change of the geometry of the grains provides a more favorable stacking). This mechanism of sintering is found in important

"technical" ceramic materials, such as alumina Al_2O_3 (with addition of MgO and SiO_2), silicon nitride Si_3N_4 (with addition of MgO).

4. *Sintering by vitrification or viscous flow sintering*; most of the starting powders are transformed into a highly viscous liquid phase; the glassy phase infiltrates in the pores, removing them. This mechanism is found typically in silicate raw materials, used for example in the manufacturing of traditional dense ceramic products, such as porcelain stoneware and more refined porcelain; the sintering of the glass represents a particular case, since all of the mass is transformed into liquid.

Glass-based materials refer to viscous flow sintering, The equation that governing the densification, according to this mechanism, is that provided by Frekel (Bernardo, 2004):

$$\frac{\Delta V}{V_0} = \frac{9}{4} \cdot \frac{\gamma \cdot t}{r_0 \cdot \eta}$$

where V_0 is the volume of the powder compact before sintering, ΔV is the volumetric shrinkage from the compact to the sintered product, γ the surface energy, the radius of curvature r_0 of the particles, t the holding time and η the viscosity of the glassy phase at the adopted sintering temperature. This law applies to spherical particles, homogeneous in size, and in case of interconnected porosity. When the sintering proceeds and the open porosity turns to closed porosity, we should refer to the McKenzie-Shuttleworth equation (Bernardo, 2004):

$$\frac{d\rho}{dt} = \frac{3\gamma}{2a_0\eta}(1-\rho)$$

where ρ is the density of the material and a_0 is the initial radius of the pores.

The new functional dependence of sintering time is symptomatic of a certain slowing of the densification with the additional contribution of changes in the thermodynamic conditions (the specific surface area of a compact being densified is gradually lower than that of the original powders). For completeness, it is necessary to point out that the viscosity of the glassy phase (η) has a dependency only on the temperature ($Log\eta \propto 1 / T$) in the case of exclusive sintering of a glass; in the general case, if the glass phase dissolves part of the crystalline phase, the modification in the composition of the glass during the sintering sometimes involves a strong change in the viscosity.

An important research in the literature (Ray and Tiwari, 2001) has reported that the dilatometric softening point is a fundamental reference for the sintering of glass powders. At this temperature, the viscous flow (associated to the compression of rods in the dilatometer) exactly counterbalances the thermal expansion, and the viscosity η is in the order of approximately 10^{11} poise (with 1 poise=10 Pa·s); it may be a direct reference in case of hot pressing. Empirically, for sintering without pressure, a temperature increase of at least 50 °C is needed (viscosity in the order of $\eta= 10^8$ poise). It should be noted that for a variety of compositions is not acceptable, a strong increase of the sintering temperature than the softening temperature, when setting up the concurrent crystallization: the uncontrolled crystallization of the glass involves a drastic increase in viscosity and a strong delay in the densification.

III.3 Glass foams

Glass foams represent a particularly interesting type of components for thermal and acoustic applications (Bernardo *et al*., 2012). They are produced in limited quantities due to high processing costs, but their characteristic of un-flammability, thermal and chemical stability will lead to an increased use in substitution for organic foams. Moreover, the closed cell structure makes the material watertight and an efficient barrier against soil humidity. The production of glass foams may follow two distinct processes: the first, dating back to the 1930s, consists of the direct introduction of gases ("blowing") into molten glass; the second one, much less expensive, is based on the viscous flow sintering of fine glass powders, which creates a pyro plastic mass which is foamed by the action of specific powder additives (foaming agents), owing to decomposition or oxidation reactions. The decomposition reactions involve carbonates and sulfates, while oxidation reactions are due to the interaction of carbon-containing species (C, SiC) with oxygen, coming mainly from the atmosphere of the sintering furnace. The adoption of a sintering approach paved the way for the use of glass not specifically designed for foam production; significantly, the sintering approach led to the extensive use of cullet for this application. Soda-lime glass is the common raw material; however, a number of recent investigations showed that it is possible to fabricate foams using other glasses, such as CRT glass. The low characteristic temperature of these glasses enables foaming at particularly low temperature (even below 75 0 °C), through the decomposition of added calcium carbonate. Furthermore, this foaming procedure has the significant advantage of producing chemically stable foams, avoiding any risk of reduction of heavy metal oxides into metal colloids, which is often experienced when using reducing compounds (SiC or TiN).

Glass foams represent an interesting way to directly use industrial residues, without converting them into a glass, with the addition of recycled soda-lime glass. Brusatin *et al*. (2002) used fuel oil-derived fly ashes (with SiC as foaming agent), processing at temperatures between 800 and 90 0 °C, producing foams with a crushing strength of about 3.5 MPa and a density of ~0.35 g/cm^{3}. Bernardo *et al*. (2007) used a SiC-containing waste, deriving from the polishing operations of artistic glass articles, as the only foaming agent (although the oxidation of SiC was favored by the addition of MnO_2), obtaining very high porosities (up to 92%); the heavy metal oxides present in the waste (mainly lead and cadmium deriving from artistic glass) were found to immobilized in the glass matrix. Fernandes *et al*. (2009) also employed waste as raw materials containing a foaming agent, using ash produced after the burning out of SiC-based abrasive paper.

The foaming of waste-derived glasses is quite complicated, due the above discussed tendency of these glasses to crystallize upon heating. Significantly, a porous structure is associated to a high specific surface, which enhances surface nucleation. If extensive crystallization occurs during foaming, problems in the homogeneity and reproducibility of the overall foam morphology arise. This issue may be overcome by using a combined approach, i.e. by the foaming of mixtures of soda-lime glass and a glass undergoing crystallization (Tulyaganov *et al*., 2006), or again of soda-lime glass and selected waste (like in the case of "glass-ceramics" from direct sintering of silicate waste, Wu *et al*., 2009).In this case the crystallization may actually be useful, since it enhances the mechanical properties. A similar situation is found when using mixtures of soda-lime glasses with

cullet of other origin, more difficultly recycled but quite prone to crystallization (e.g. glass residue from the manufacturing of glass fibers, having a CaO-Al$_2$O$_3$-SiO$_2$ composition similar to that of many waste glasses used for the preparation of glass-ceramics).

The remarkable crystallization of waste glasses may be even advantageous when other types of cellular materials are desired. Common glass foams are mostly closed cell foams, thus maximizing the thermal insulation; on the other hand, this makes them unsuitable to filtering applications. Open-celled glass-ceramics may be obtained by the mixing of glass powders with polymeric micro-spheres or by the deposition of slurries onto polyurethane sponges, followed by the burn-out of the sacrificial polymers and sinter-crystallization. The crystallization, enhanced by the high amount of free glass surface, "freezes" the structure modeled by the polymeric templates, greatly limiting the viscous collapse. A similar concept was reported by Fidancevska *et al*. (2003) who used slurries composed of mixtures of coal fly ash and recycled glasses to coat polyurethane foam or to envelop sacrificial carbon fibers. (Bernardo *et al.*, 2012)

III.3.1 Historical background

The production of glass foam dates back to the 1930', when many patents were granted in the same period (Scarinci *et al*., 2005). The patented processes can be divided into two fundamental types: by the sintering of finely ground glass powders with a suitable foaming agent, and by the direct introduction of fluids into the molten glass. Originally, in the sintering process, foaming agents may come from a combustible material, such as coal, lignite, wood or CaCO$_3$ and its alternatives like anthracite and carbon black. The direct introduction of gases into molten glass is done by injection (forcing gas, such as CO$_2$ or vapor H$_2$O) or by the evaporation of dissolved gas from a low softening point glass (composed of silica, borax and zinc oxide. Improvements in the bubble expansion may be depressurization, local overheating, addition of solid foaming agents Na$_2$SO$_4$, NaNi$_3$ and later oxygen releasing agents SO$_3$, Fe$_2$O$_3$, Sb$_2$O$_3$.

III.3.2 Starting glasses

Glass foam production can be considered an effective way of recycling a great number of glass products (container and flat glass, borosilicate glass for the chemical industry and more recently, even fluorescent lamp glass. The glass is contaminated with metallic and non-metallic fragments (plastics, ceramics, aluminum, iron, paper, organic substances, and soon). The costs of color sorting and impurity removal are high, especially if a significant portion of the glass is finely divided. The use of recycled glass in the production of new glass articles is consequently barely profitable.

III.3.3 Foaming reaction

The main industrial process currently employed for glass foam manufacture is sintering of powdered glass mixed with suitable agents. On a thermodynamic point of view, the growth of foam bubbles is analogue, in the process, to the growth of crystals, in that homogeneous dispersion of gas may form a nucleus that is susceptible to grow, only from a limit radius and in defined environmental conditions.

III.3.3.a Chemical dissolved oxygen, carbon oxidation

A characteristic equilibrium always exists in an alkali silicate glass melt between trivalent and divalent iron with oxygen evolution. This phenomenon is of great importance in the foaming process, because the reduction of Fe^{3+} to Fe^{2+} is presumably the gas-forming reaction, since oxygen is used to oxidize carbon (the most foaming agent) in the pyroplastic glass.

The reduction of sodium sulfate, introduced during fabrication of most common glasses as fining agent, oxidizes carbon to CO:

$Na_2SO_4 + 4\,C \rightarrow Na_2S + 4\,CO$
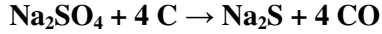
III.3.3.b Thermal decomposition

The most famous reaction is the decarbonatation of Ca- or Na- carbonates at 750 °C to 850 °C. During the gradual softening of the sintered glass under continuous heating, the calcium or sodium carbonate particles decompose to the oxide with simultaneous release of gaseous carbon dioxide. The oxide is incorporated into the molten glass mass and acts as a glass modifier, thus altering the viscosity of the molten glass. The released CO_2 is entrapped in the viscous glass mass and its pressure is gradually increased, forcing the molten glass to expand. On subsequent cooling the molten glass is solidified and a cellular structure is formed.

III.3.3.c Foaming by reaction

The production of CO and CO_2 by oxidation of carbon, in form of graphite or carbon black may lead to extensive foaming at 800 °C to 900 °C. Secondary reactions of carbon happen with some other compounds (from the atmosphere, present as further additives, from the glass) such as H_2O, alkali and sulfates, so that foaming can even be performed in non-oxidizing atmospheres, as follows:

$C + H_2O \rightarrow CO + H_2$
$C + 2\,H_2O \rightarrow CO_2 + 2\,H_2$
$Glass\text{-}SO_4^{2-} + 2\,C \rightarrow glass\text{-}S^{2-} + CO + CO_2$
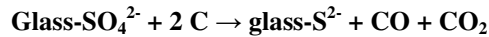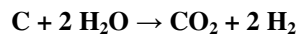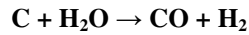
SiC is another important foaming agent, releasing CO or CO_2 by oxidation, typically 900 °C. The reaction leads to secondary compounds such as SiO or SiO_2, as follows in table III.6 (many reaction paths are possible):

Reaction	ΔH/kJ at 1000 K	ΔH/kJ at 1500 K
$SiC + [frac12]\,O_2 \rightarrow SiO + C$	−134.7	−179.08
$SiC + [frac12]\,O_2 \rightarrow CO + Si$	−157.3	−204.60
$SiC + O_2 \rightarrow SiO + CO$	−333.5	−412.3
$SiC + O_2 \rightarrow SiO_2 + C$	−656.1	−575.7
$SiC + O_2 \rightarrow CO_2 + Si$	−350.6	−357.3
$SiC + 2\,O_2 \rightarrow SiO_2 + CO_2$	−1048.1	−970.7
$SiC + 2\,CO \rightarrow SiO_2 + 3\,C$	−258.6	−91.2
$SiC + 3\,H_2O \rightarrow SiO_2 + CO + 3\,H_2$	−279.9	−327.2
$SiC + 4\,H_2O \rightarrow SiO_2 + CO_2 + 4\,H_2$	−281.6	−316.3

Table III.6: Possible reactions of SiC in various atmospheres (Scarinci et al., 2005)

Si$_3$N$_4$ and AlN can lead to extensive foaming, again by oxidation, but with the release of nitrogen; as an example we could have:

Si$_3$N$_4$ + 3 O$_2$ → 3 SiO$_2$ + 2 N$_2$
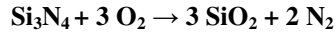
C, SiC and nitrides are particularly susceptible to the homogeneity of oxygen distribution. It may be that the external parts of glass/foaming agents compacts are subjected to extensive foaming, with the internal part, with limited access to atmospheric oxygen, practically unreacted. The homogeneity of foaming may be improved by addition of easily reducible compounds, such as oxides of metals with multiple valence states (MnO$_2$, Fe$_2$O$_3$, CeO$_2$ etc.). Sulfates (e.g. gypsum, Ca-sulfate) are useful as well, being reduced to sulfites or sulfides (as reported above). Oxides with multiple valence states can be provided also in form of an "oxidized" glass (Pittsburg Corning produces the well-known Foamglass ® by mixing recycled glass, carbon black and an oxidized glass, see figure III.8) (Scarinci *et al.*, 2005). Oxides with multiple valence states can be used as the only foaming agents, with the release of oxygen. As an example, MnO$_2$ is exploited following the equation:

2 MnO$_2$ → 2 MnO + 2 O$_2$
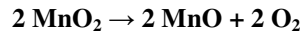
Mechanical properties of foams have been deeply studied by Ashby (2005) who established indexes to compare materials strength in function of their density. Foams and cellular materials are considered as structured material of which mechanical properties can be estimated by introducing the concept of lightweightness. The most diffused expressions applicable to the young modulus and to the bending strength are summarized in table III.7 (Bernardo, 2007).

	Stiffness problem	**Strength problem**
Simple tension	E/ρ	σ_f/ρ
Bending of bars (section free)	$E^{1/2}/\rho$	$\sigma_f^{2/3}/\rho$
Bending of panels (thickness free)	$E^{1/3}/\rho$	$\sigma_f^{1/2}/\rho$

Table III.7: Indices expressing the contribution of material to a given minimum mass or stiffness in mechanical strength. E is the young modulus in GPa and ρ is the material apparent density in g/cm^3

This comparison is useful is the materials selection, when a user seeks for a multifunctional application, such as lightweightness and mechanical strength (typical example of foams for building insulation or panel for ventilated façades). More particularly, foam glasses and glass-ceramics extend the field of applications of porous materials by linking porous ceramics and foams (see figure III.9).
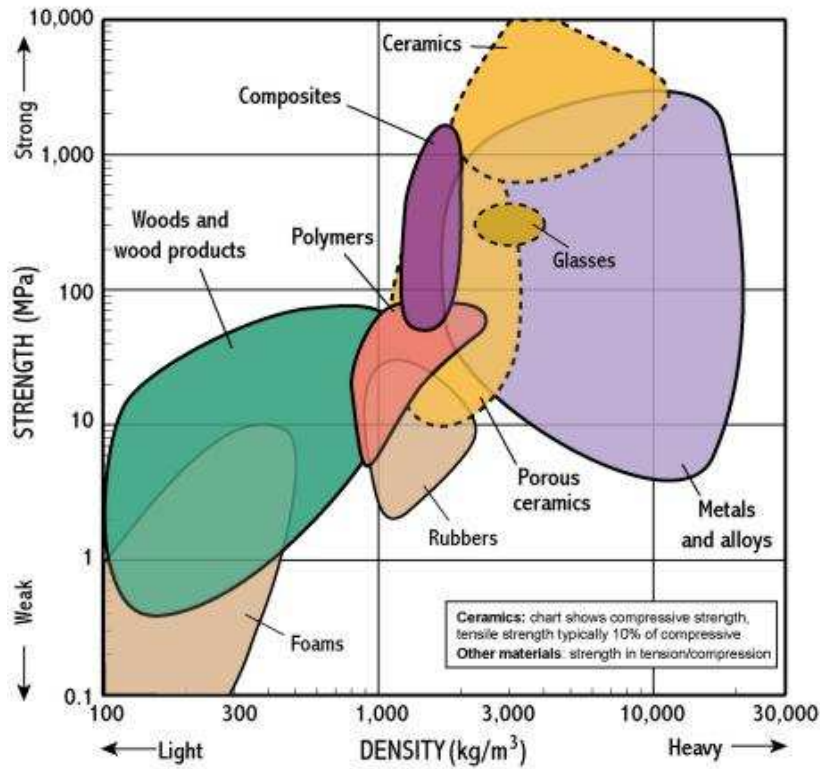
Figure III.9: Ashby graph - strength (MPa) in function of density (g/cm³) of current engineering materials

Figure III.8 details the steps of the production of the FOAMGLAS® product. In 1) we observe the addition and weighting of raw materials, recycled glass, feldspars, Na-carbonate, Fe_2O_3, MnO_2, Na_2SO_4, and NaNO3. Oxides, sulfates and nitrates are intended to lead to an "oxidized" glass. In the melting furnace (2), the temperature is around 125 0 °C. The melted glass (3) goes out of the furnace. In (5), pure glass is added in the mixer and carbon black is added in (6). Recycled glass (window glass) is ground and then introduced in the mixer (7). The whole mass is poured in specific containers for further expansion a secondary furnace at 850 °C where it will foam (8). A dispositive of energy recovery links the two furnaces ventilation pipes (9). The glass passes through a final furnace where a controlled cooling is applied (10) and finally the pieces are cut and shaped (11).

Il processo di produzione del FOAMGLAS®
(impianto di Tessenderlo, Belgio)
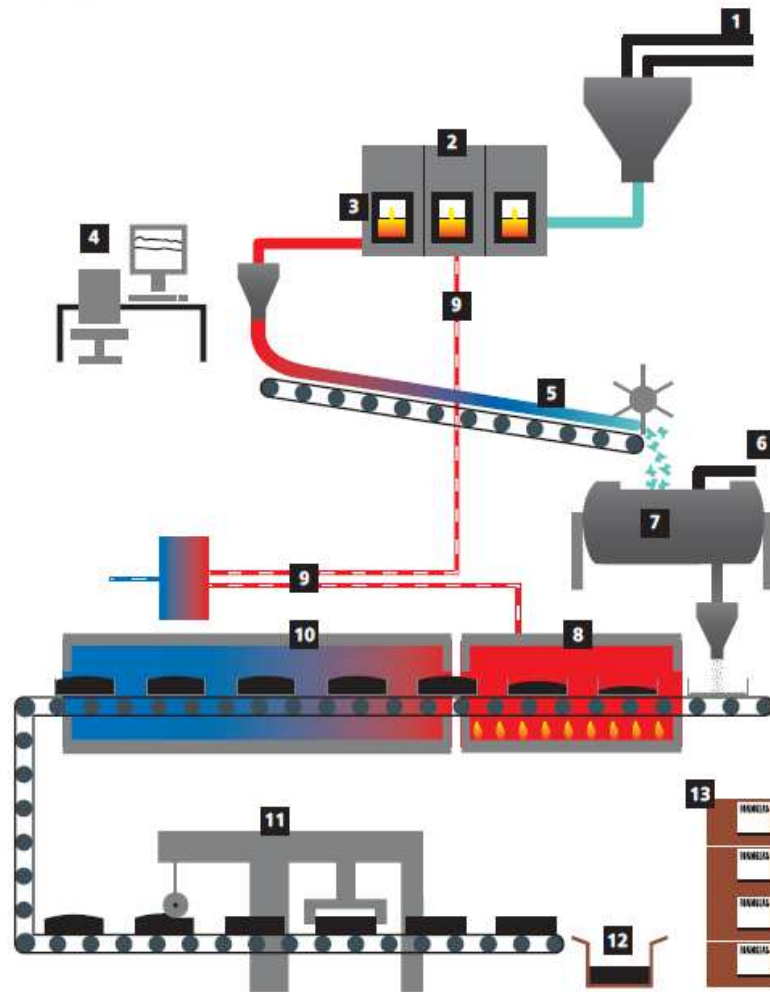
Figure III.8: The production process of FOAMGLASS®

III.3.4 Viscosity conditions

Glass can be transformed into a foam by addition of suitable substances with generate gaseous products by decomposition or reaction at temperatures above its softening (Littleton) temperature (corresponding to a viscosity of $10^{6.6}$ Pa·s). Then, the glass powder has not yet sintered to closed porosity, and the gaseous products cannot be retained by the ass, and if the gas generation takes place when the glass viscosity is too low, the gaseous products are released from the melt, as in the fining of glass melts.

Most convenient viscosity range for optimizing the foaming process for development of maximum porosity and minimum apparent density is at 10^5 Pa·s or 10^3 Pa·s, which corresponds for standard soda-lime glass, to temperature ranging between 800 °C and 1000 °C.

III.3.5 Properties of commercial glass foam products

Table III.8 shows various properties that can be asked for a commercial foam glass granulate for a use as filler in insulating applications of building and housing. The average size ("taille du grain") varies from 30 mm to 100 mm, the density ("densité en vrac") corresponding to the geometric density, is between 0.13 and 0.25 g/cm³. The water absorption ("absorption d'eau") is

lower than 7%. Lambda in W/mK corresponds to the thermal resistivity of the material and the thermal capacity ("capacité thermique") is expressed in J/m^3K. The compression strength is not directly expressed but is related to the compression coefficient and to the compression properties during the manipulation ("coefficient de compression", "capacité de compression au déversement", "module de déformation"). The porosity after compression ("pourcentage de volume vide après compression") corresponds to a test that will enable to determine the insulating property of such material even under standard compressions in buildings; here, it is lower than 35%. Temperature resistance is an important parameter and is presented resorting to the softening point ("point de ramollissement, grain") and the refractory behavior ("comportement au feu, grain"). Freeze resistivity ("resistance au gel"), chemical stability ("matériau de construction inerte", "aptitude au recyclage"), and thermal properties ("coefficient u sur dimension fixe") are finally expressed.

Propriétés	Unité	TECHNOpor granulat de mousse de verre			
		Standard	Commande spéciale		
		PERIMETER 50	FÜLL 100	DRUCK 50	Construction de route[1]
Taille du grain, non comprimé	mm	30/50	30/100	30/50	type 30/50
Densité en vrac	kg/m³	~ 170	~ 130	~ 220	~ 150 bis ~ 250
Absorption d'eau (grain)	vol. %	≤ 7	≤ 7	≤ 7	≤ 7
Niveau d'humidité de compensation	M %	≤ 0,01	≤ 0,01	≤ 0,01 [2]	-
Lambda, grain	W/mK	0,045 [2]	0,050 [2]	0,055 [2]	-
Lambda, déversement à sec ≤ 25 cm	W/mK	0,085	0,08	0,09 [2]	-
Lambda, déversement à sec > 25 cm	W/mK	0,075	0,07	0,08 [2]	-
Capacité thermique	J/m³K	~ 144500	~ 110500	~ 187000 [2]	-
Capacité thermique spécifique	J/kgK	~ 850	~ 850	~ 850 [2]	-
Hauteur minimum d'installation, non comprimé	cm	15	15	15	15
Coefficient de compression, type	coeff.	1,1 bis 1,3:1	1,0 bis 1,4:1	1,1 bis 1,3:1	1,2 bis 1,3:1
Pourcentage de volume vide après compression	%	≤ 35	≤ 35	≤ 35	≤ 35
Angle de déversement	°	~ 45	~ 45	~ 45	~ 45
Point de ramollissement (grain)	°C	env. 700	env. 700	env. 700	env. 700
Comportement au feu (grain)	Classe	A1	A1	A1	A1
Formation de fumée et de gouttes		non significatif	non significatif	non significatif	non significatif
Résistance au gel (déversement)		oui	oui	oui	oui
Module de déformation, sous-sol peu solide, $E_{V}2$	MN/m²	~ 45 [3]	-	~ 50 [3]	~ 50
Module de déformation, sous-sol solide, $E_{V}2$	MN/m²	~ 80 bis ~ 120[3]	-	~120 bis ~500[3]	~ 120 bis ~ 500
Résistance à la compression du grain	N/mm²	~ 6 [5]	~ 2 [5]	~ 10 [5]	~ 3 bis ~ 12 [5]
Capacité de compression au déversement	N/mm²	0,50 [4]	-	-	-
Matériau de construction inerte		oui	oui	oui	oui
Sans effet capillaire au déversement		oui	oui	oui	oui
Aptitude au recyclage/récupérabilité	%	100	100	100	100
Coefficient u 0,5 W/m²K sur dimension fixe	cm	16	15	17 [2]	-
Coefficient u 0,4 W/m²K sur dimension fixe	cm	20,5	19	22 [2]	-
Coefficient u 0,3 W/m²K sur dimension fixe	cm	24,5	23	26 [2]	-
Coefficient u 0,2 W/m²K sur dimension fixe	cm	36,5	34	39 [2]	-
Coefficient u 0,1 W/m²K sur dimension fixe	cm	74	69	79 [2]	-
Conditionnement/livraison:					
Big Bag 1,5 m³ / 3 m³	m³	oui	oui	oui	non/oui
en sac à déverser, env. 8 m³	m³	oui	oui	oui	oui
Vrac, par camion	m³	oui	oui	oui	oui

Table III.8: Technical data from a commercialized product Technopor Glass-schaum granulat

III.4 Glass-ceramics

An essential feature of glass is that it does not contain crystals. However, by deliberately stimulating crystal growth in glass it is possible to produce a type of glass with a controlled

amount of crystallization that can combine many of the best features of ceramics and glass. Actually, an accidental overheating of a glass furnace led to the discovery of materials known as glass-ceramics. When the glass was overheated, small crystals formed in the amorphous material that prevented cracks from propagating through the glass.

In most cases, for the production of glass-ceramics, a glass is first shaped (e.g. by rolling of the melt) and then subjected to a secondary ceramization treatment, aimed at nucleation and growth of crystalline phases (Höland and Beall, 2002). Further treatments on the glass-ceramic products, such as cutting and polishing, can be additionally requested, before commercialization and final use.

The first step toward glass-ceramics involves conventional techniques for preparing a glass. The product is then heated to 75 0 °C to 115 0 °C, until a portion of the structure is transformed into a fine-grained crystalline material. Glass-ceramics are at least 50% crystalline after they have been heated. In some cases, the final product is more than 95% crystalline.

III.4.1 Crystallization

Crystallization, as well as melting, is first order transition. It is identified by thermo analysis (DTA, DSC), by an exothermal peak that appear during the cooling, whereas melting is identified by an endothermic peak during heating. Changing the heating rate displaces the crystallization peak (a slower heating/cooling cycle translates the peak to higher temperatures). This is a key to justify that crystallization is the consequence of two processes that depend on temperature: nucleation and crystal growth. Figure III.10 represents "Tammann curves", showing that the maximum of nucleation and crystal growth rate is located at different states of super cooling. KG is the curve for growth rate and KV is the curve for nucleation rate (Deubener, 2012).
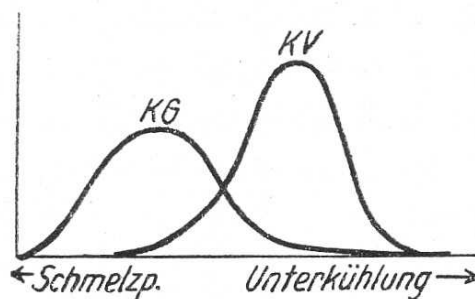

Figure III.10: Crystallization (KG) and nucleation (KV) rates in function of the super cooling

<center>**a**</center> <center>**b**</center>
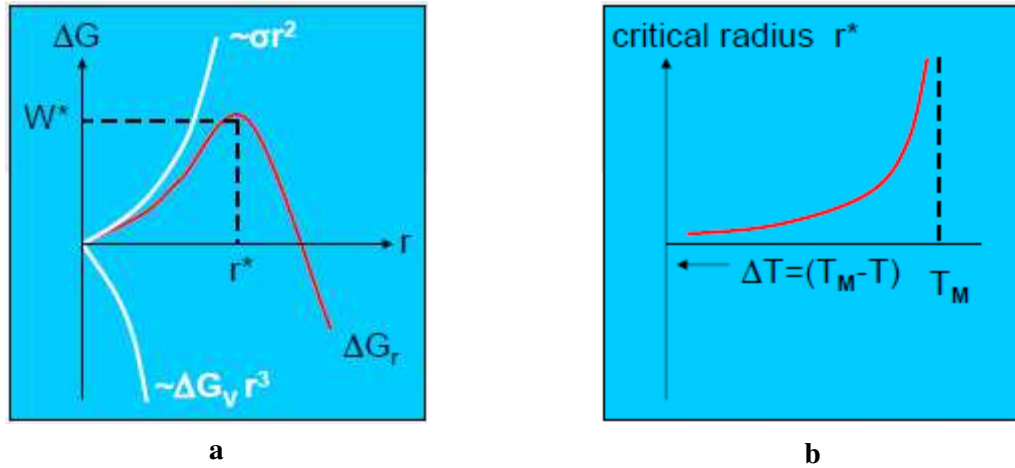
Figure III.11: General evolution of (a) the work formation in function of the nucleus radius; (b) the critical radius r* in function of the temperature

III.4.2 Nucleation processes

Thermodynamic fluctuations provoke agglomerations of molecules in the matrix. Such agglomerates may grow or collapse, depending only on the initial nucleus size. The nucleus has a defined level of free-energy for its growth within the surrounding network. The growth phenomenon as a function of time and temperature, and intrinsic properties of the system was deeply explained using thermodynamic and kinetics laws (Gutzow 1980 and Höland *et al.*, 2002, 2003, 2009).

The work of formation ΔG of a nucleus is a trinomial function of the radius of the growing sphere and has the evolution presented in figure III.11a. It also depends mainly on 2 terms of opposite sign: the negative term is linked to the free energy associated to the volume of the new formed phase, (related to saturation level) and the positive term includes the interfacial energy of the new surface. Schematically, the reaction happens as soon as ΔG is negative. At start, when r is near to zero, the free energy is unsufficient to maintain the cohesion so crystallization cannot occur. Then, the germs appear from a critical nucleus size, determined by the interfacial energy and the free energy (figure III.11b). For this reason, it is clear that a glass-ceramic can be full of crystals, as far as the interfacial energy is low enough (so the environment is not a barrier to their growth).

The kinetics of the nucleation rate were investigated by Gutzow et al. (1980), as an exponential function of time and temperature. It is then inversely related to the viscosity of the glass phase. Crystallization should be distinguished between volume or bulk (homogeneous) and surface (heterogeneous) nucleation. There are two types of nucleation: the first one is volume nucleation, which is commonly used technique for both homogenous and heterogeneous nucleation (figure III.12). Particular glasses, for example from the systems SiO_2-Al_2O_3-Alkali oxide, tend to phase separate into a SiO_2-rich glassy matrix and an alkaline or alkalike-earth oxide-rich glassy droplet phase or solid solution. Crystallization is achieved at earlier stage or delayed by changing the composition of the matrix phase (figure III.13). Surface crystallization or volume crystallization can thus be provoked or suppressed. Second, phase separation may lead to the formation of a low-viscosity phase demonstrating homogeneous crystallization, while the matrix crystallizes heterogeneously, either simultaneously or later. Third phase separation lead to the formation of interfaces that may be preferred sites for crystallization (figure III.14). At the end, in glass-

ceramics, the crystalline phases transformations are controlled after a good knowledge of temperature and viscosity of the system which can be determined by DTA analysis.
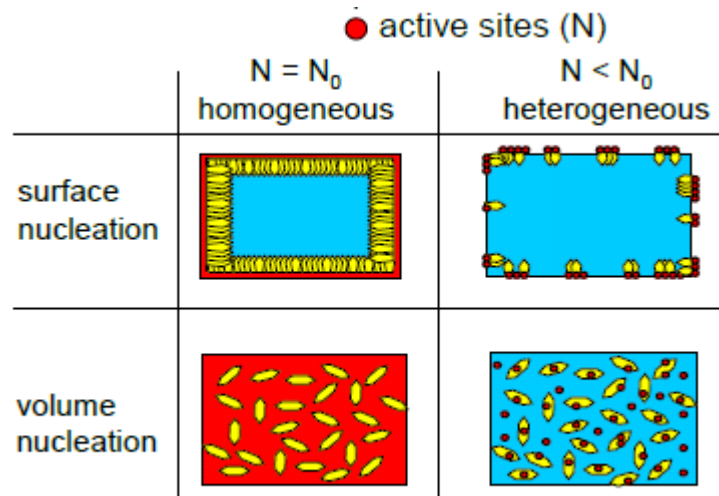
Figure III.12: Schematic summary of the nature of the crystallization process (Müller et al., 2000)
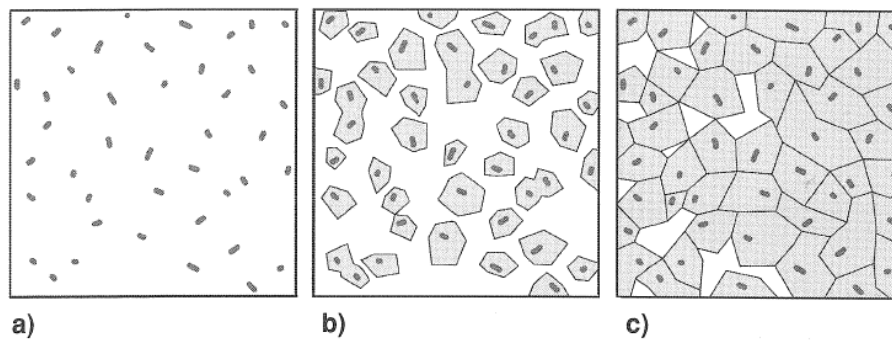
Figure III.13: From glass to glass-ceramic. (a) nuclei formation, (b) crystal growth, (c) glass-ceramic microstructure (Höland and Beall, 2002)
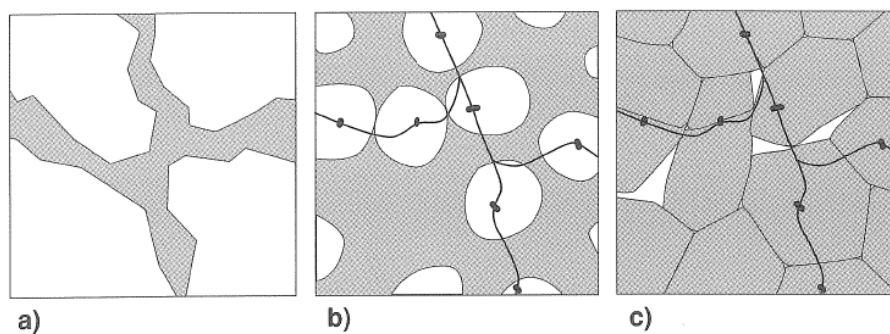
Figure III.14: Glass-ceramic from powdered glass. (a) powder glass compact (b) densification and insipient crystallization (c) frit derived glass-ceramic (Höland and Beall, 2002)

III.4.3 Properties of glass ceramics

Because glass-ceramics are more resistant to thermal shock, cookware made of this material can be transferred directly from a hot stove burner to the refrigerator without breaking. Because they are more crystalline glass-ceramics are also slightly better at conducting heat than conventional glasses. Glass-ceramics are also stronger at high temperatures than glasses. Thus, the glass-ceramic $MgO - Al_2O_3 - SiO_2$ is used to make electrical insulators that have to operate at high temperatures, such as spark plug insulators. For comparison, the properties and uses of some glasses and glass-ceramics are given in the table III.9.

For glass ceramics with important properties for technical, consumer, medical or biological applications, it is necessary to develop multi-component base glasses and still to apply the different nucleation mechanisms to convert the base glasses into glass ceramics. Glass ceramics of low thermal expansion involve two types of nucleation control: nucleation by phase separation and heterogeneous nucleation. First, nucleating agents TiO_2 or ZrO_2, incorporated in the system, form crystals at 78 0 °C by homogeneous nucleation. Then, SiO_2 β quartz small 100 nm crystals form at their contact, by heterogeneous nucleation, at 98 0 °C, and at the same time happens a phase separation of SiO_2 from the initial system (SiO_2-Al_2O_3, Li_2O for example). The low CTE (coefficient of thermal expansion) is achieved by forming those crystals of metastable solutions based on β quartz and β spodumene. For temperatures between 0 °C and 400 °C, any cracks that would be induced by a thermal shock are stopped by internal compression stress applied by quartz crystals on the glass, as quartz is highly mechanically resistant. Given the properties of low CTE and thermal conductivity, the glass ceramic has been successfully used as telescope mirror blanks in precision optics and for variety of household applications.

| Composition	Property	Use
Glasses		
Al_2O_3, MgO, CaO, SiO_2	Translucent, chemically resistant	Window glass, bottles
PbO, SiO_2	High refractive index	Lead crystal
B_2O_3, SiO_2, Na_2O	Acid resistant, low expansion on heating	Pyrex
Glass Ceramics		
MgO, Al_2O_3, SiO_2	Insulator with high mechanical strength at high temperatures	Spark plug insulators
$CaSiO_3$, $CaMgSi_2O_6$, $CaAl_2Si_2O_8$	Wear resistant	Building materials
$Li_2Si_2O_5$	Resistant to thermal shock	Nose cones on rockets, cookware

Table III.9: Properties and Uses of Some Glasses and Glass-Ceramics

Glass ceramics of high mechanical strength are produced by hot pressing at less than 1000 °C and involve both phase separation and volume nucleation. In base glasses of SiO_2-LiO_2-P_2O_5-ZrO_2 (20 wt% ZrO_2 –containing glass ceramics), nucleation is initiated by phase separation and primarily Li_3PO_4 crystals form during quenching of the glass melt. Then, ZrO_2 phases are formed as microcrystals growing up to 20 µm length; in the same way as quartz, they enhance the mechanical strength of the glass ceramic. SiO_2-LiO_2 (lithium disilicate glass ceramics system is a

heterogeneous nucleation by epitaxial growth of Li_3PO_4. This high strength materials (bending strength around 280 MPa) are also chemically durable. Other types of glass ceramics deriving from similar crystallization were developed, such as Al_2O_3 free, Al_2O_3 and La_2O_3 containing multicomponent lithium disilicate glass ceramic, with additional improved properties and bending strength reaching 400 MPa. For higher temperatures, quartz phase transformation is well known for its important volume expansion in a preferred direction, but we can consider that because of the random orientations of every β quartz crystals, the glass expansion is homogeneous in the 3 space directions.

III.4.4 Production modes

An increasing amount of investigation on glass-ceramic production has been made in recent years. These processing routes differ from each other in order to obtain unique properties such as expected microstructural or mechanical properties. The glass-ceramic production techniques can be listed as; Traditional methods, Sinter-crystallization method and Direct sintering.
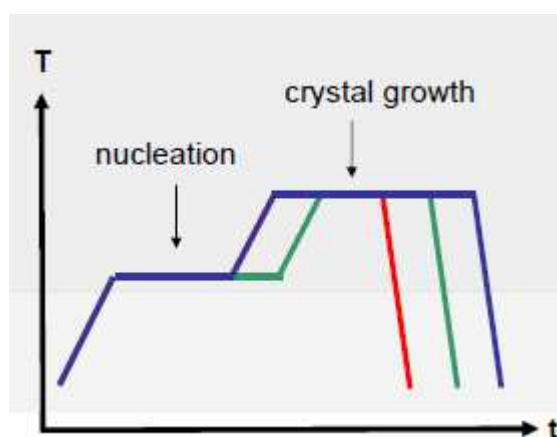
Figure III.15: Double stage heat-treatment to control microstructure

The crystal number density and time lag depend on condition of heat treatment of the second stage principally. First stage enables the nucleation whereas second stage enables the crystal growth. It is then possible to obtain desired number of crystals and size of crystals (figure III.15).

II.4.4.a Glass Ceramics by nucleation and growth

The following parts on glass-ceramics are available in the Encyclopedia of Sustainability Science and Technology (Bernardo *et al.*, 2012). Glass-ceramics represent a vast range of materials obtained by controlled crystallization of a glass of selected composition; the overall process leads to materials often possessing outstanding properties, such as high hardness and mechanical strength, a thermal expansion coefficient adjustable in a wide range of values (from negative to more than 12×10^{-6} °C^{-1}), high refractoriness, high chemical durability and excellent dielectric properties. The most valuable glass-ceramics, also known as "technical glass-ceramics", can be produced only from base glasses with a carefully controlled chemical composition, obtainable from particularly refined raw materials. However, the glass-ceramic technology has been applied to glasses obtained from waste since the early 1960', i.e. quite soon after the discovery of glass-ceramics occurred. The significant variability in composition of the inorganic

residues may be accommodated by using mixtures of different waste materials (changes in the waste ratio could compensate variations in the composition of a single waste) and by considering not particularly sophisticated applications, such as the manufacturing of tiles for the building industry.

Classical glass-ceramic technology relies on a double step treatment of a previously formed glass object (shaped into the desired form), corresponding to the nucleation of a crystal species within the base glass, favored by the separation of some glass components (such as Ag or Au colloids, or oxides like TiO_2 and ZrO_2), and to the crystal growth. These components are generally added to the formulation of the base glass, and are referred to as "nucleating agents". The base glass is heated first to the temperature of maximum nucleation and then to the temperature of maximum crystal growth (slightly higher than the previous one), with a holding time at each temperature, before cooling. These temperatures are different for each glass composition, and need to be determined precisely using, for instance, Differential Thermal Analysis (DTA).

Microcrystalline products obtained from extensive nucleation (i.e. containing a very large number of nuclei) possess of very remarkable mechanical properties, even when produced from waste. It must be observed that waste-derived glasses usually have an inherent strong tendency to devitrification, attributable to the presence of specific components in the formulation of waste, and therefore there is no need to add nucleating agents to the batch. The separation of magnetite (Fe_3O_4) crystals is particularly significant in iron-rich waste glasses. Karamanov and Pelino observed the dependence of crystallization on the ratio Fe^{3+}/Fe^{2+} (Karamanov *et al.*, 1999; Karamanov and Pelino, 2001). They showed that the crystallization of iron-rich glasses begins with the separation of small magnetite crystals, but the surface oxidation of Fe^{2+} to Fe^{3+} causes a change of the chemical composition, with the formation of hematite (Fe_2O_3), thus decreasing the total amount of crystal phase and changing the reaction order of the crystallization process. Bloomer *et al.* (1999) also showed that oxidized glass from dc arc melting of highly iron containing waste were highly durable, since oxidative conditions promote the dissolution of heavy metals, but poorly prone to devitrification. Iron-rich waste glasses are known also for the opportunity of obtaining glass-ceramics with interesting functional properties: Romero *et al.* (2001) showed that with Fe_2O_3 contents in the base glass superior to 26%, the precipitated magnetite particles were large enough to exhibit full magnetic order, so that glass-ceramics showed ferromagnetic behavior.

II.4.4.b Glass Ceramics by sinter-crystallization

The above described nucleation/crystal growth step may be difficult to control and economically expensive. A major drawback concerns the presence of defects in the glass articles, like pores, which remain in the glass-ceramic, causing a decrease in the mechanical properties. The evolution of gas bubbles from the glass melt requires high temperatures and long holding times, i.e. a carefully controlled refining step. This refining is particularly complicated with waste glasses, which are usually dark and feature a low thermal conductivity by radiation, due to the amount of heavy metals. A further detrimental issue for glass-ceramics obtained by the traditional route is their visual appearance, which is generally rather inferior to that of natural stones and traditional ceramics. With a sintering approach, the problems of defects and visual appearance are generally avoided. In fact, when applying the sintering route, there is no need to refine the melt

before casting into a frit, thus reducing cost and gaseous emissions. The ground glass powder is subsequently heated to a certain temperature, at which viscous flow sintering of glass powders occurs together with crystallization.

The simultaneous sintering and crystallization treatment is known as sinter-crystallization (Gutzow *et al.*, 1998), and it has been exploited commercially since the 1970', for the manufacturing of the well-known Japanese, wollastonite-based, "Neoparies" tiles for the building industry. As mentioned above, refining is not needed, so that the vitrification may be conducted in small plants and in particularly short times, favoring the immobilization of components which could vaporize with longer heat treatments. Furthermore, a relatively high degree of crystallization may be achieved in very short times; the surface of glass is in fact a preferred site for crystallization (Müller *et al.*, 2000; Prado and Zanotto, 2002; Francis *et al.*, 2004; Hernández-Crespo *et al.*, 2006), and thus ground glass is easier to devitrify than bulk glass with the same composition, and nucleating agents are not needed. In some cases, the holding time at the sintering temperature may not exceed 30 min, being also accompanied by very fast heating rates (even "direct heating" is possible, that is the direct insertion of glass powder compacts in the furnace directly at the sintering temperature), thus configuring a "fast sinter-crystallization" process (Bernardo, 2008). The base glasses for the manufacturing of sintered glass-ceramics have similar chemical compositions, except for lack of nucleating agents, to those of glass-ceramics from waste glasses obtained by conventional nucleation and growth. Pyroxenes, wollastonite and anorthite (with solid solutions) are very common crystal phases.

The sinter-crystallization process relies on a quite complicated balance between viscous flow sintering, surface crystallization and even bulk crystallization, i.e. crystallization operated by the separation of components acting as nucleating agents. This balance is sensible to many conditions, e.g. the oxidation state and the heating rate. Starting from an iron-rich waste glass, Karamanov *et al.* (2000) observed that the addition of C (1.5-2%) to the glass batch increased the magnetite phase and enhanced the crystallization rate. Bernardo et al., starting from a base waste glass with a low Fe^{2+}/Fe^{3+} ratio, observed that magnetite was promoted by oxidation, more sensible for fine glass powders (<40 μm) than for coarse ones (<80 μm). Karamanov *et al.* (2003 and 2005) reported that the balance between surface crystallization and bulk crystallization is strongly affected by the heating rate: low heating rates favor bulk crystallization, and sintering may be inhibited by the crystal phase, causing incomplete densification.

High heating rates favor sintering so that low porosity remains in the material; however the amount of crystal phase formation is lower, because crystallization occurs only at the surface. It has been shown in many papers that, in the presence of fine glass powders (<40 μm), the crystallization may be achieved right at the temperature of the crystallization exothermic peak in the DTA plot of the same powders (figure III.16). More recent investigations, however, highlighted that optimum crystallization is achievable only if the crystallization peak is located at a temperature suitably higher than that corresponding to the dilatometric softening point, i.e. the temperature at which viscous flow becomes appreciable (Ray and Tiwari, 2001). If the temperature difference is limited, the obtained glass-ceramics are remarkably porous and improvements in the densification are achievable only by increasing the sintering temperature and the heating rate (direct heating, as described above, enables sintering of the powders before the crystallization can

"freeze" the viscous flow, due to the very large increase in viscosity associated to crystal precipitation) (figure III.17).
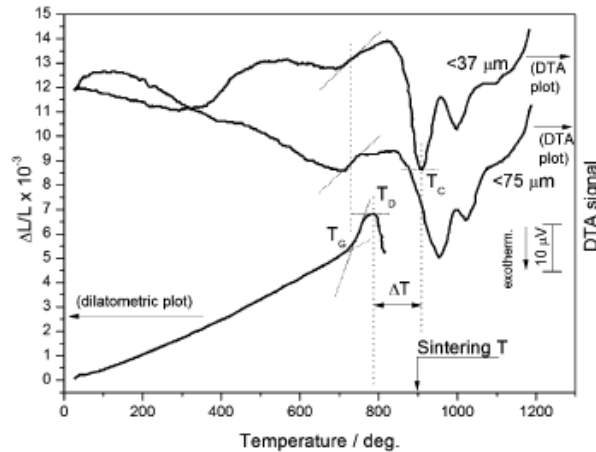
Figure III. 16: Thermal anaylsis showing the superposition of dilatometric and DTA plots for a glass (Bernardo et al., 2011)
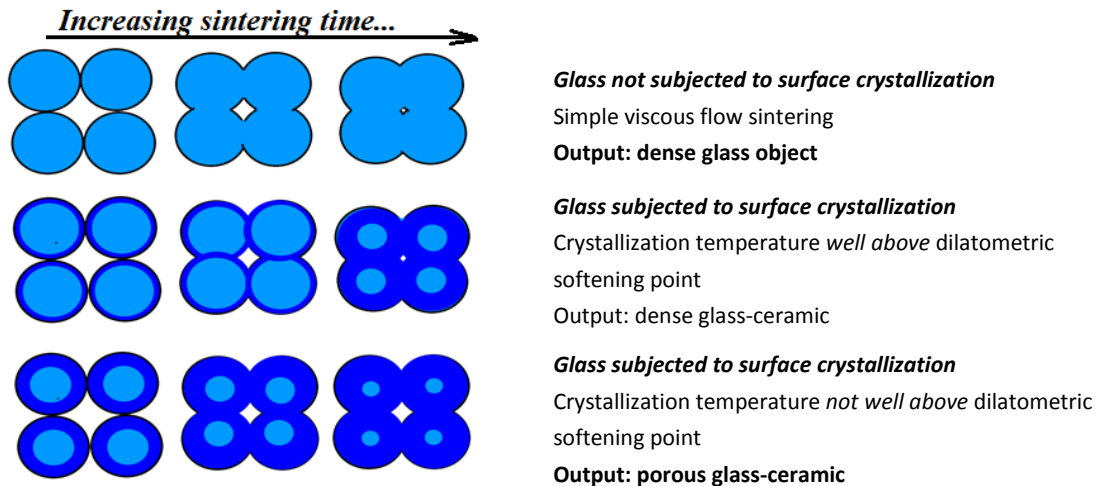
Figure III.17: Schematic representation of the different conditions starting from fine glass powders (Bernardo, 2013)

II.4.4.c Glass Ceramics by the petrurgic method

Glass-ceramics from waste may be produced by a third method, known as the "petrurgic method" (Romero and Rincón, 1999), named in this way because of the similarity with the process of crystallization of natural rocks. This method has actually been applied since the 1970s, with the development of "Silceram" ceramics from metallurgical slags. In this process, crystals nucleate and grow directly upon cooling of glass from the melting temperature, with an intermediate temperature holding stage, which can sometimes be avoided. A controlled cooling (from 1 to 10 °C/min) of glasses enables to obtained crystallization from mixtures of coal ash and soda lime glass melted at 1500 °C, without any intermediate step. The cooling rate is a dominant factor in controlling the formation and morphology of the crystal phase, particularly in relation to iron containing raw materials. Faster cooling rates allow for the formation of magnetite, with samples

exhibiting magnetic properties, while slow cooling rates cause the formation of plagioclase and augite.

II.4.4 *"Glass-ceramics" by direct sintering of silicate waste*

The above mentioned techniques for the manufacturing of glass-ceramic all involve the previous formation of a glass. However, some interesting sintered materials may be produced by mixing glass cullet, of various origins, with silicate waste, leading to components which cannot, strictly speaking, be termed glass-ceramics, since they are not produced by the (controlled) crystallization of any parent glass. Francis *et al.* (2002), as an example, produced glass-ceramics from high iron containing coal ash, adding Pyrex glass powder. The presence of iron led to soft magnetic materials, due to ferrite phases formation depending on the ash/glass ratio. A similar approach was followed by Fidancevska *et al.*, (2003). In these cases, the crystallization is associated to the interaction between recycled glass and the silicate waste.

References

Andreola F. Barbieri L. Corradi A. Lancellotti I. (2007) CRT glass state of the art case study- recycling in ceramic glazes, J. Eur. Ceram. Soc., 27, 1623-1629.

Ashby M.F. (2005) Materials selection in Mechanical Design, Third Edition, Butterworth Heinemann, Oxford, UK.

Bernardo E. (2004) PhD thesis, Materiali compositi innovativi a matrice vetrosa o vetroceramica, Università degli Studi di Padova, Italy.

Bernardo E. Cedro R. Florean M. Hreglich S. (2007) Reutilization and stabilization of wastes by the production of glass foams, Ceram. Int., 33, 963-968.

Bernardo E. (2007) Porous glasses and glass-ceramics as an environmentally sustainable application of Industrial Waste, 3rd level course, Advanced Glasses and Glass based compounds, Turin, 2013.

Bernardo E. (2008) Fast Sinter-crystallization of a glass from waste materials, J. Non-Cryst. Sol., 354, 3486-3490.

Bernardo E. Scarinci G. Colombo P. (2012) Vitrification of Waste and Reuse of Waste-Derived Glass, Encycl. Sustain. Sci. Technol., Editors Robert A. Meyers 1. RAMTECH LIMITED Pub. Springer New York, 11581-11613.

Bloomer P.E. Feng X. Chantaraprachoom N. Gong M. McCready M. (1999) Effect of crystallization, redox, and waste loading on the properties of several glassy waste forms, J. Am. Ceram. Soc., 11, 2999-3011.

Rawlings R.D. Wu J.P. Boccaccini A.R. (2006) Glass-ceramics: Their production from wastes—A Review, J. Mat. Sci., 41, 733-761.

Brusatin G. Scarinci G. Zampieri L. Colombo P. (2002) Foam glass from cullet, Glass Mach. Plants Acc., 1, 108-110.

Chinnam R.K. Francis A.A. Will J. Bernardo E. Boccaccini A.R. (2013) Review. Functional glasses and glass-ceramics derived from iron rich waste and combination of industrial residues, J. Non-Cryst. Sol., 365, 63-74.

Cicek B. (2013) Development of glass-ceramics from combination of industrial wastes with boron mining waste, PhD Thesis, University of Bologna, Italy.

dalle Vedove A. (2013) Materiali vetroceramici cellulari da miscele di rifiuti industriali, Master Thesis (Tesi magistrale), Università di Padova, Italy.

Deubener J. (2012) Transformation kinetics, 4th workshop for new researchers in Glass Science and Technology, Institute of Non-Metallic Materials, Montpellier.

Fernandes H.R. Tulyaganov D.U. Ferreira J.M.F. (2009) Production and characterization of glass ceramic foams from recycled raw materials., Adv. Appl. Ceram., 108, 9-13.

Fidancevska Mangutova B. Milosevski D. Milosevski M. Bosser J. (2003) Obtaining of dense and highly porous ceramic materials from metallurgical slag, Sci. Sintering, 35, 85-91.

Francis A.A. Rawlings R.D. Sweeney R. Boccaccini A.R. (2002) Processing of coal ash into glass ceramic products by powder technology and sintering, Glass Technol., 43, 58-62.

Francis A.A. Rawlings R.D. Sweeney R. Boccaccini A.R. (2004) Crystallization kinetic of glass particles prepared from a mixture of coal ash and soda-lime cullet glass, J. Non-Cryst. Sol., 333, 187-193.

Gutzow I. Pascova R. Karamanova A. Schmelzer J. (1998) The kinetics of surface induced sinter-crystallization and the formation of glass-ceramic materials, J. Mat. Sci., 33, 5265-5273.

Hernández-Crespo M.S. Romero M. Rincón J.M. (2006) Nucleation and crystal growth of glasses produced by a generic plasma arc-process, J. Eur. Ceram. Soc., 26, 1679-1685.

Höland W. Beall G. (2002) Glass-ceramic technology, Second ed., The American Ceramic Society, Westerville, OH..

Höland W. Rheinberger V. Scheiger M. (2003) Control of nucleation in glass ceramics, Phil. Trans. R. Soc. Lond. A., 361, 575-589.

Karamanov A. Cantalini C. Pelino M. Hreglich S. (1999) Kinetics of phase formation in jarosite glass-ceramic, J. Eur. Ceram. Soc., 19, 527-533.

Karamanov A. Pisciella P. Cantalini C. Pelino M. (2000) Influence of Fe3+/Fe2+ ratio on the crystallization of iron-rich glasses made with industrial waste, J. Am. Ceram. Soc., 83, 3153-3157.

Karamanov A. Pelino M. (2001) Crystallization phenomena in iron-rich glasses, J. Non-Cryst. Sol., 281, 139-151.

Karamanov A. Pelino M. Hreglich S. (2003) Sintered glass-ceramics from municipal solid waste-incinerator fly ashes-part I: the influence of the heating rate on the sinter-crystallization, J. Eur. Ceram. Soc., 23, 827-832.

Karamanov A. Aloisi M. Pelino M. (2005) Sintering behaviour of a glass obtained from MSWI ash, J. Eur. Ceram. Soc., 25, 1531-1540.

Morimoto N. et al. (1988) Nomenclature of Pyroxenes, Am. Mineral., 73, 1123-1133.

Müller R. Zanotto E.D. Fokin V.M. (2000) Surface crystallization of silicate glasses: nucleation sites and kinetics, J Non-Cryst Sol, 274, 208-231.

Peng F. Liang K. Hu A. (2005) Nano-crystal glass–ceramics obtained from high alumina coal fly ash, Fuel , 84, 341-346.

Prado M.O. Zanotto E.D. (2002) Glass sintering with concurrent crystallization, C. R. Chimie, 5, 773-786.

Rahaman M.N. (2003a) Chapter 8: Theory of solid state and viscous sintering, , Ceramic Processing and Sintering, , Second ed., Missouri, USA, Marcel Deker Ink 2003Ed, 470-537.

Rahaman M.N. (2003b) Chapter 10: Liquid phase sintering, Ceramic Processing and Sintering, , Second ed., Missouri, USA, Marcel Deker Ink 2003Ed, New York Basel, 620-685.

Ray A. Tiwari A.N. (2001) Compaction and sintering behaviour of glass-alumina composites, Mat. Chem. Phys., 67, 220-225.

Ray A. Tiwari A.N. (2001) Compaction and sintering behaviour of glass-alumina composites, Mat. Chem. Phys., 67, 220-225.

Romero M. Rincón J.Ma (1999) Surface and bulk crystallization of glass-ceramic in the Na2O-CaO-ZnO-PbO-Fe2O3-Al2O3-SiO2 system derived from a goethite waste, J. Am. Ceram. Soc., 82, 1313-1317.

Romero M. Rincón J.Ma Rawlings R.D. Boccaccini A.R. (2001) Use of vitrified urban incinerator waste as raw material for production of sintered glass-ceramics, Mat. Res. Bull., 36, 383-395.

Scarinci G. Brusatin G. Bernardo E. (2005) Chapter 2: glass foams, Glass technol., Colombo ,WILEY, UK, 158-175.

Tulyaganov D.U. Fernandes H.R. Agathopoulos S. Ferreira J.M.F (2006) Preparation and characterization of high compressive strength foams from sheet glass, J. Por. Mat., 13, 133-139.

Various authors (1996) Manuale dei materiali per l'ingegneria, (a cura di AIMAT), McGraw-Hill, Milano.

Wu J.P. Boccaccini A.R. Lee P.D. Kershaw M.J. Rawlings R.D. (2006) Glass ceramic foams from coal ash and waste glass: Production and characterization, Adv. Appl. Ceram., 105, 32-39.

Chapter IV

Samples preparation and characterization

IV.1 Preparation process

IV.1.1 Humid phase powder elaboration

After sieving under 90 µm, the components are mixed together and added with water (35%-40% of the total solid), obtaining aqueous slips, homogenized by mechanical stirring. If a grinding step is necessary, the aqueous mix is purred into a jar containing agate balls and ball milled for 30 min at 300 rpm. The slips are cast in wide glass containers (or aluminum, to avoid interaction of lime with glass containers) and dried at 110 °C overnight. The solid residues were manually ground and sieved to get fine granules of about 200 µm diameter and about 7% humidity.

IV.1.2 Uniaxial dry pressing

The powder mixture is weighted and slightly homogeneously humidified by droplets pulverization until 7 wt% water content, in a view to imitate the atomization process at laboratory scale. Obtained round granules are then pressed at 40 MPa, in different dies, to form discs (30 mm diameter, 2 mm height) and rectangular tiles (dimensions of $50 \times 35 \times 5$ mm).

Double-layer glass-ceramic samples are obtained by first lightly pressing (at 10 MPa) 15 g of the waste mixture in a square die (cross-section 50×50 mm) and then depositing 3 g of waste glass frit on this substrate at a surface density of 0.080 g/cm^2 by passing the powder through a 90 µm sieve. The layered samples are then uniaxially pressed at 40 MPa.

The samples are further dried at 110 °C for 30 min and then fired at the chosen process temperature for 30 min (heating rate of 40 °C/min, to mimic actual industrial processing, in case of rectangular tiles).

IV.1.3 Thermal treatment

For sinter-crystallization, the raw materials are first dried and homogenised by ball milling in an agate jar for 30 minutes at 300 rpm, then calcined at 900 °C(for 5 hours) and finally melted in a kyanite (Al_2SiO_5) refractory crucibles at 1400 °C for 90 minutes. The melt slightly reacted with the crucible thus inducing a limited increase of the alumina and silica in the final composition of the frit. Glass powders are produced pouring the melted glass into water; the drastic quenching provided a number of fragments that were successively dried and ball milled (30 minutes at 400 rpm). The milled powders were passed through a 240 mesh sieve to collect the particles < 63 µm.

Sintering experiments are performed after uniaxial pressing by direct introduction of samples, i.e. without heating stage. The molded specimens were dried at 110 °C for 1 hour and then directly put in an electric muffle furnace operating at the desired temperature (between 800 °C and 1150 °C). After 30 min holding time, discs samples were directly removed from the furnace, whereas small tiles were subjected to a cooling procedure, aimed at minimizing the thermal shock (furnace turned off, natural cooling at a rate of approximately 20 °C/min just at the end of the holding stage, until 600 °C and then natural cooling out of the furnace).

IV.2 Technical characterization

IV.2.1 Density

The apparent densities of the sintered materials are estimated by water displacement method, following Archimedes' principle, on electronic scale, of samples immersed in water (see figure IV. 1). Samples were hold by a leaky hamper which rested on the measurement plate. The measured weight m' comes from the forces balance m'g = mg - ρVg, where m is the effective mass of the sample, measured separately and ρVg is the hydrostatic push of the fluid, with V the sample volume. In water (distilled), ρ = 1 g/cm^3 and the volume in cm^3 is expressed from difference in g {m-m'}; and then sample density is: ρ_c = m/ (m-m').
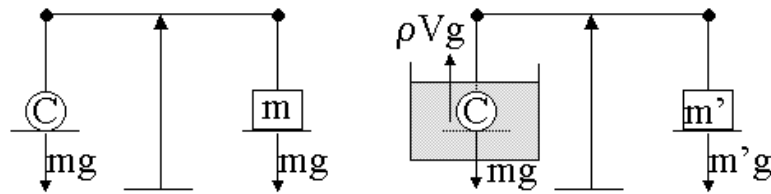
Figure IV.1: Schematic representation of the density measurement

The bulk density was assessed by He Pycnometer (Micromeritics®, model AccuPyc1330, Norcross, GA) after the grinding of the materials in fine powder shape, to avoid the influence of porosity in the calculated volume.

IV.2.2 Porosity

Porosiy was assessed by He Pycnometer (Micromeritics®, model AccuPyc1330, Norcross, GA). The characterization of the porosity of a cellular material is not so straightforward; in fact, with the same mass, several volumes can be detected, as illustrated by Fig.IV.2. The actual bulk density of a solid is its "intrinsic density", from pycnometry analysis on powders, i.e. ideally pore-free portions. If we consider a cellular material, we should consider other two density values: 1) geometric density (mass/volume ratio): the measurement does not consider pores, but only the external volume; 2) apparent density: the volume considered for the mass/volume ratio is the geometric volume deprived of open pores, i.e. those that can be reached by a fluid (in our case, **helium**) coming inwards (pycnometry analysis applied on whole samples). We may first define the outer volume (V_G), i.e. the "geometrical volume"; it comprises the volume of the solid phase (V_S) and the volumes of open and closed pores (V_{OP} and V_{CP}, respectively): $V_G = V_S+V_{OP}+V_{CP}$. The volume detected by pycnometry on whole samples, i.e. "apparent volume" (V_A) is the geometrical volume deprived of open pores: $V_A= V_S+V_{CP} = V_G-V_{OP}$. The volume detected by pycnometry on

powders is the volume of the solid phase (V_S): $V_S = V_G - V_{OP} - V_{CP}$. Finally, we can define geometric, apparent and bulk densities, for a generic mass m, as follows: $\rho_G = m / V_G$; $\rho_A = m / (V_G - V_{OP})$; $\rho_B = m / (V_G - V_{OP} - V_{CP})$. This means that: $\rho_G \cdot V_G = \rho_A \cdot (V_G - V_{OP})$ then $f_{OP} = 1 - \rho_G / \rho_A$, and $\rho_G \cdot V_G = \rho_B \cdot (V_G - V_{OP} - V_{CP})$ then $f_{CP} = 1 - f_{OP} - \rho_G / \rho_B$, with f_{OP} and f_{CP} the fractions of open and closed porosity, respectively. The fraction of open porosity is conditioned by the size of pores. A truly open-celled foam features apparent and bulk density values very close to each other. In many cases it may be that foams with the same external volume but different cell size (Fig.IV.2) have different open porosity, even if closed celled. This happens as an effect of the cutting of samples, opening some pores; bigger pores determine a higher "open volume" (white spaces in Fig.IV.3).
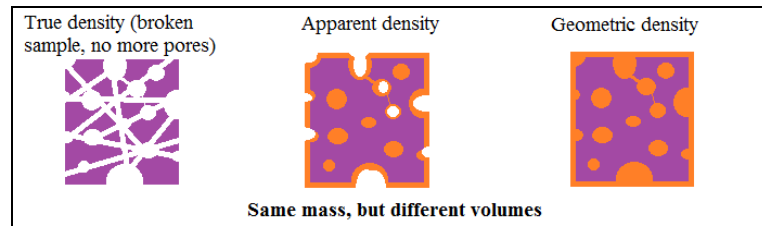
Fig. IV.2: Differences among bulk, apparent and geometric densities (purple: actual volume of the solid phase; orange: additional volume considered for apparent and geometric density determinations)
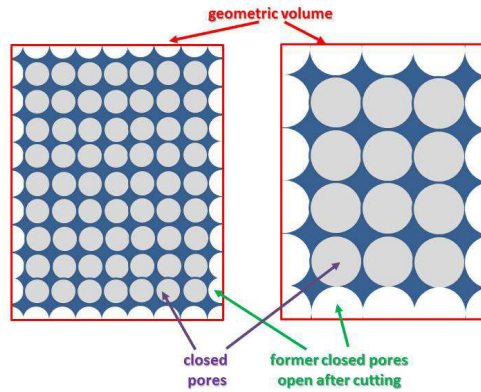
Fig. IV.3 – Example of the impact of cell size (left: small pores; right: big pores) on the open porosity detected starting from an ideally closed-cell foam [grey: closed porosity; white: open porosity]

IV.2.2 Water absorption

Immersion in boiling water is used for the evaluation of the water absorption, according to the current standard (ISO 10545-3, 1997).

IV.2.3 Differential Thermal Analysis

TG and DTA are applied on 100-150 mg powder samples with a temperature ramp of 10 °C/min until 1200 °C (DTA/TGA, STA 409; Netzsch Gerätebau GmbH, Selb, Germany).

IV.2.4 X-ray fluorescence analysis

In particular, the fluorescence analysis was conducted by R. Falcone (Stazione Sperimentale del Vetro, Venice, Italy) with a wavelength dispersive spectrometer (WDXRF, ADVANT'XP+, Thermo ARL, Ecublens, Switzerland) operating on pressed powder pellets (six measurements

performed on each sample; the net intensities of the F K_α line - λ=1.83 nm - were determined as the difference between the gross and the background counts).

IV.2.4 X-ray powder diffraction (XRD)

Mineralogical analysis is conducted by X-Ray Diffraction analysis (XRD) on powdered samples (Bruker D8 Advance, Karlsruhe, Germany - CuKα radiation, 0.15418 nm, 2θ=10-60°). Phase identification is achieved by means of the Match!® program package (Crystal Impact GbR, Bonn, Germany), supported by data from PDF-2 database (ICDD-International Centre for Diffraction Data, Newtown Square, PA).

As explained by Flewitt and Wild, (1998), X-ray diffraction has been extensively used for crystals analysis in many texts, from the years 1960s. X-rays are electromagnetic radiations, photons, with a wavelength of the order to a fraction of a nanometer compared with the hundreds of nanometers of light waves. Into crystalline materials, rows of atoms have spacing of ~0.3 nanometers. An X-Ray beam incident on a material penetrates many micrometers into the bulk and the direction of the diffracted beam intensity is determined by the periodicity of the atom planes in the crystalline solid. Consider the case where a beam of characteristic X-Rays of wavelength, lambda, is incident on a single crystal surface at angle theta, which produces a diffracted beam at an angle theta.
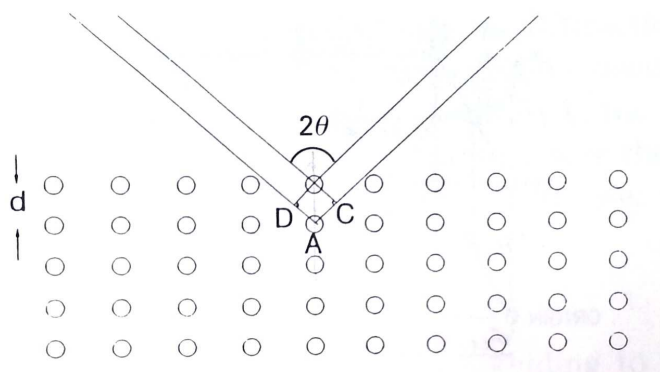
Figure IV4. X-ray diffraction from atoms in a crystalline material
(Flewitt and Wild, 1998)

The ray from the second row of atoms travels a distance greater than the ray from the top row. The two rows of atoms are separated by a distance d. For this to produce a diffraction maximum, the path difference must be an integral number of wave lengths. We obtain a condition for the diffraction maxima which is called Bragg equation:

$2d \sin \theta = n\lambda$, with d the distance between to plans of crystallization, theta the incident angle, and lambda the wavelength of the diffraction beam.

By this equation, d may be determined and the crystal spacing identified. Specific atom species will have an influence on the phase of the diffracted beam and dissimilar atoms in lattice positions can cause certain diffraction peaks to be absent. Thus by observing the diffraction pattern it is possible to identify the structure of the material. The reciprocal lattice is a construction to aid the interpretation of diffraction from crystal lattice. It would be to long developing this here but we cannot help reminding that this model enables to predict theoretically the diffraction of crystals according to lattice planes of spacing, and has enabled a lot to understand the theory of

crystallization. X-rays can most easily be produced by bombarding a material surface with relatively high energy electrons. When a high energy electron impinges on the material X-rays are produced. In practice it is normal to use metals to produce X-rays for use in X-ray diffraction instruments. This is because an intense beam of X-rays is desired and the good thermal conductivity of the meal allows the heat produced during bombardment with an intense high energy electron beam to be readily removed thus avoiding damage to the source. X-ray beam is detected using a counter tube, linked with associated electronic circuitry for data collection, treatment and recording. The powder method (employed here) corresponds to the one devised by Debye and Scherrer. An incident beam of monochromatic X-radiation interacts with a non-diffracting aluminum specimen filled with powder of very small grain size, the all forming a flat horizontal surface. This specimen must contain sufficient articles with the correct orientation to allow diffraction from all possible diffracting planes when the incident X-Ray angle varies. The angle between the incident and diffracted X-ray beam is 2θ and consequently each set of crystal planes products X-rays of semi-angle 2θ. The position of the intensity peaks in the diffracted beam is characteristic of the material being examined and unknown phases may be identified by comparison with standards JCPDS.
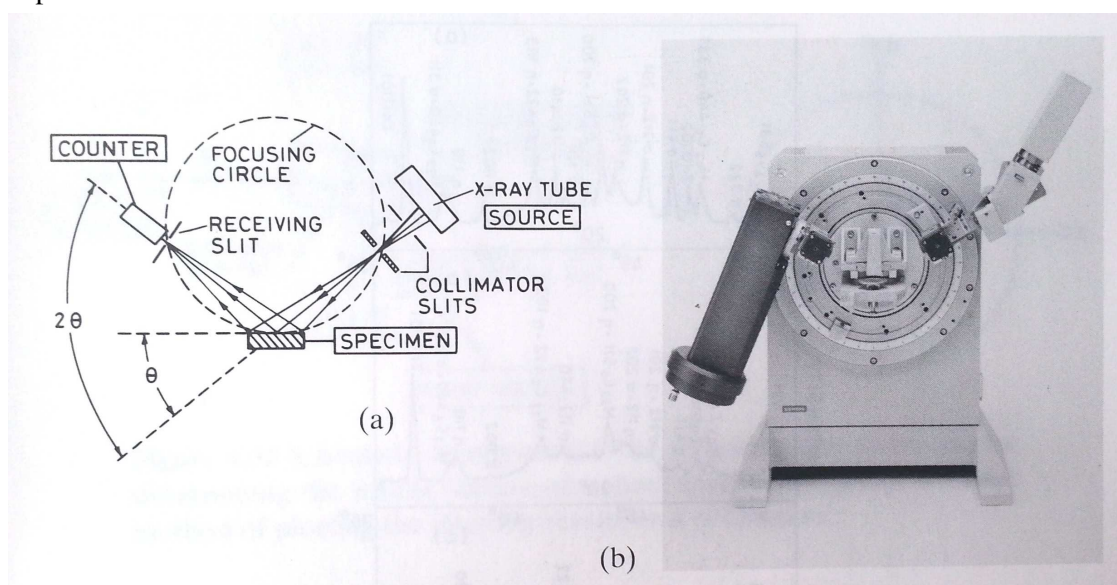
Figure IV.5. Powder diffraction (a) geometry of a conventional diffractometer
(b) diffractometer (Courtesy Siemens Ltd.)

Locked couple (LC) is activated, meaning that both source and detector move around the specimen symmetrically with a θ angle to the horizontal, at an angular speed which is determined by angular step and time between 2 steps (see figure IV.5). From Bragg law, the **peak positions** provide both the crystal structure and the lattice parameters for each phase contained in the powder specimen. The diffracted beam **intensity** provides a measure of the distribution and position of atoms within the crystal.

IV.2.5 Fourier Transform Infra-Red spectroscopy

Powdered samples were subjected also to FTI-R spectroscopy using KBr as supporting materials for the spectroscopy analysis. 1 wt% dry powder (after 1 hour at 200 °C) was introduced

in 1 g KBr pellet of diameter 10 mm. The mixture was carefully mixed and strongly grinded in an agate mortar and eventually pressed at 10 MPa just before the measure.

IV.2.5 Induction heating test

Discs of 5 mm mean thickness and 25 mm mean diameter were subjected to induction heating tests. The samples were placed at the center of the copper coils (9 turns and $\phi = 50$ mm) of a Nova Star 5 kW® power supply (Ameritherm Inc, Scottsville, NY, USA) operating at 21 kA/m with the frequency of 168 kHz. The temperature was measured with an IR THERMACAM® (FLIR Thermacam E65, FLIR System, Boston, MA, USA).

IV.2.6 Image analysis

IV.2.6.a Scanning electron microscopy (SEM)

Most interesting samples are studied to investigate the microstructural development with back scattered electron imaging (BEI) mode in a scanning electron microscope (ESEM Quanta 200, FEI Company, Eindhoven, The Netherlands). Before analysis, surfaces are polished with 1 µm and 0.5 µm diamond pastes except for powder samples. To reduce electrical charging of non-conducting specimen which can be induced by the incident electron beam, the surface can be sputter coated with a conducting metal such as gold.

SEM is a technique using, instead of X-rays, monochromatic beams of electrons with a wavelength that is function of the applied accelerating potential (Flewitt and Wild, 2003). The specimen is scanned by the incident electron beam and electrons emitted from the surface are collected and amplified to form a video signal. When the electron beam penetrates the sample, it diffuses more or less deep depending on the nature of the elements (atomic number). It is the combination of the high resolution with a large depth of focus that makes the SEM well suited to examine topography (secondary electrons), for example fracture surfaces or porosity. To achieve an SEM image, use is made of the different signals produced when the electron beams interacts with the bulk specimen. The contrast obtained from refracted electron signals depends upon the local orientation of the surface to the incident electron beam offering the ability to provide quantitative topographic images. Unfortunately for specimens with very pronounced surface roughness and re-entrant relief, contrast is modified by surface collection contributions but any improved contrast is usually accompanied by degradation of image detail. A part of the electrons from the electron beam are backscattered. The backscattered electron yield from a specimen in a SEM is dependent on the incident electron beam energy and intensity, the mean atomic number density and the surface orientation. And then, filtering the backscattered electrons signal gives indication on the atoms presents on samples surface.

IV.2.6.b Stereomicroscope

Macroporosity qualitative characterization was performed using a stereomicroscope.

IV.2.6.c Fluorescence microscope

Qualitative evaluation was performed using a Fluorescence microscope ZEISS Scope A1, with Digital camera AxioCam Icc 1 S/N 28591065, HXP120C Kübler fluorescence light source, / BF,

Light blue (Dapi fluorescence markers) and green (Calcein markers), and pictures were analyzed using Software ZEN® (blue edition) 2006-2011 CarlZeissmicroImaging GmbH.

IV.3 Mechanical characterization

For the evaluation of mechanical properties, small beams of $45 \times 3 \times 4$ mm are cut from bigger tiles and carefully polished up to a 5 μm finish and chamfered at the edges, by using diamond tools. This treatment is necessary due to the low fracture toughness of ceramic materials in general, but also because the preliminary cutting step lets the borders rough and irregulars, which may be responsible for the creation of new defects with a relevant concentration of stresses, which are not inherent to the material itself. The chamfering enables to decrease the inertia moment of the tested section. One set of beams can be left unpolished, in the case of studying the impact of surface on the bending strength.

IV.3.1 Four point bending tests

One of the most significant mechanical tests on ceramic materials is the bending test, and is fundamental in modelling. Compared to metallic materials, the traction strength of ceramics is very sensitive to dimension, geometry and superficial roughness of the samples, due to their lower fracture toughness: defects of various dimensions bring an important dispersion of rupture loads. The test itself then implies a difficult preparation of samples.
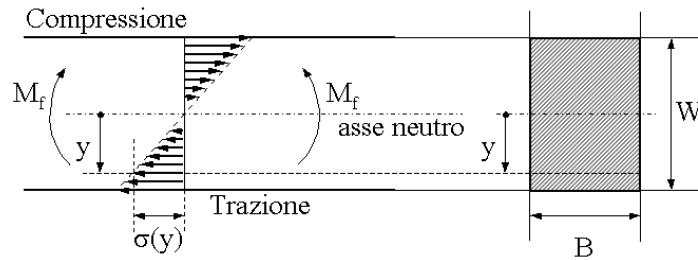
Figure IV.5.: Section of a " De Saint Venant" bar submitted to a flexural couple M_f with the distribution in traction and compression stresses indicated in function of the distance from the central axe (neutral).

For these reasons, the bending test present more advantages in the case of ceramic materials. Indeed, it is an indirect traction test, as traction and compression forces applies on a transversal section of a bar, in function of the central axe, according to the "De Saint Venant" relation: $\sigma = \dfrac{M_f \cdot y}{J}$, where M_f is the bending moment in the inflection plan, J is the inertia moment of the section, y is the distance from the central axe (see figure IV. 5).

For rectangular sections, of highness W and width B, we have:

$$J = \frac{B \cdot W^3}{12} \rightarrow \sigma(y) = \frac{M_f \cdot y}{B \cdot W^3} \cdot 12$$

Rupture happens when the strength σ, at the maximum distance y=W/2, over goes the traction strength of the material, (in the section where traction forces apply only); this strength is either called bending strength or modulus of rupture, M.O.R.

$$\sigma \max = \sigma(W/2) = \frac{M_f}{B \cdot W^2} \cdot 6 \geq MOR$$

In the 3 points test, the bar is charged in the middle. The section submitted to a bending couple $M_f=PL/4$ is a triangle, as figured below (figure IV.6, left). The maximal load is then:

$$\sigma\max = \sigma(W/2) = \frac{M_f}{B \cdot W^2} \cdot 6 = \frac{3}{2}\frac{P \cdot L}{B \cdot W^2} = \sigma\max(P)$$

The bending rupture load corresponds to the maximum transversal charge supported by the sample at the rupture time (P_{rott}):

$$M.O.R. = \sigma\max(P_{rott}) = \frac{3}{2}\frac{P_{rott} \cdot L}{B \cdot W^2}$$
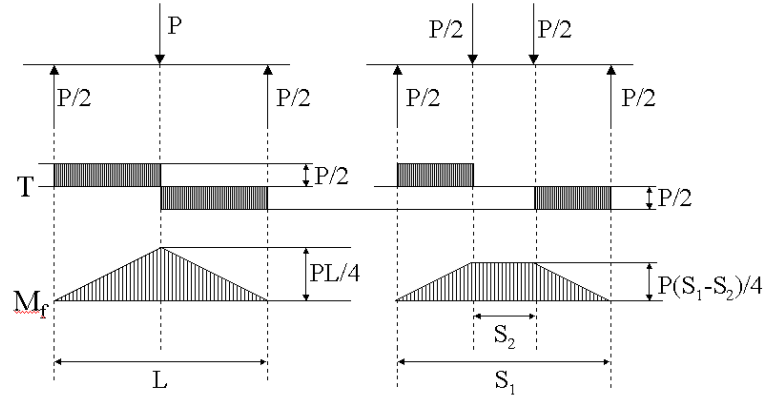
Figure IV.6: Representation of the cutting load T and bending moment M_f for configurations of 3-point and 4-points bending test.

A fundamental characteristic is that the central part is submitted to the maximum bending moment, and in the 3 points test, this part is limited (only a line), so the probability to meet critical defects is limited.

The 4 points bending test shows a symmetric transversal load P of a bar, two supporting points separated from a distance S1 and two contact points at S2 distance (figure IV.6, right). The load is reparsed on application points submitted to P/2. The bending moment worth $M_f=P(S_1-S_2)/4$.

$$M.O.R. = \sigma\max(P_{rott}) = \frac{3}{2}\frac{P_{rott} \cdot (S_1 - S_2)}{B \cdot W^2}$$

So the 3 points test can be considered a particular case of the 4 points test, where $S_2=0$.

The volume of the section submitted to a maximum load is higher and then increases the probability to find a critical defect in this section. Consequently, the rupture load by 4 points test is lower than by 3 points test (around 20%) but is more representative of the reality.

Four-point flexural tests (span of 28 mm) are carried out by using an Instron 1121 UTS (Instron, Danvers, MA); each data point represents the average of ten individual tests. The procedure for the bending test follows the conventional standards and the loading speed should remain in the interval 0.2-0.5 mm/min.

Various effects during the test can disturb the right bending strength evaluation: errors in the measurement of the distance between contact points or asymmetric positioning; shifting on the loading points; defects of articulation (one of the two contact points has a lower or null load); twisting effect due to non-parallel surfaces; highness of the section too low (limits of validity of the model reached); excessive chamfer implying an underestimation of the bending rupture load.

For these reasons, a good preparation is necessary and a maximum dispersion of samples is useful to get a proper estimation of the dispersion in the results (Bernardo, 2004).

IV.3.2 Compression tests (for porous samples)

Ceramic materials that do not present a sufficient bending strength can be evaluated by compression test. Indeed, the compression strength of a material is much higher than his traction strength, particularly the ceramics. In the case of porous samples, the compression is first supported by the tridimensional structure coming from the presence of pores, and then by the material itself, packed. For foam glasses, this test is more significant that the bending test.

Cubic samples are submitted to a load with a speed of 1 mm/min, which is applied on the entire surface of one of the cube side. Like in bending test, the parallelism of the surfaces is important to avoid parasite bending effects and a diminution of the contact area (Bernardo, 2004).

IV.3.3 Vickers Hardness tests

The hardness gives information of the evaluation of the abrasion strength, an important parameter in metals and ceramic-metal or ceramic-ceramic composites. The Vickers tests are very famous in dense materials based on glass, like glass-ceramics. A diamond pin in pyramid shape is loaded on the polished surface of the sample (see figure IV.7). The hardness measured is actually a "conventional pressure" value: the applied load P on the surface is normalized to the surface of the pyramidal stamp, established by the measurement of the diametric length d:

$$H_V = 1.8544 \frac{P}{d^2}$$, with H_V in MPa, P in N and d in μm.

An important possibility of application of the micro hardness is given when, at important loads, a system of cricks from the angles of the stamp, of which length can be correlated to the material fracture strength (see part IX.3).
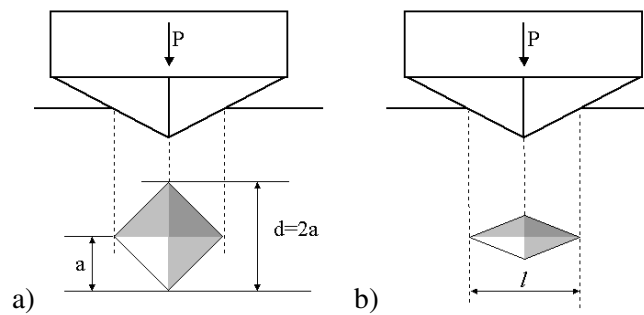
Figure IV.7: Schematic view of the two types of stamps Vickers (a) and Knoop (b)

IV.3.4 Elastic modulus

The elastic modulus was calculated on the base of non-destructive resonance frequency measurements. Young modulus was determined by the impulse excitation of vibration method (ASTM C 1259) using a flexure specimen configuration with nominal dimensions of 3 × 4 × 45 mm. Output information such as resonance frequency was manually recorded via data acquisition incorporated with the excitation system (GrindoSonic Mk5, Leuven, Belgium).

IV.4 Environmental characterization

Inorganic wastes often contain metallic trace-elements that could present a toxicity risk and confer a hazardous behavior to the environment. Some of these elements also interact in biological processes: for example, Iron is an essential component of hemoglobin; Zinc and Copper are important for cellular processes e.g. protein/DNA interactions. Their concentration in the elaborated material and their interaction with living organisms is a relevant factor to determine if these materials are chemically inert and can be used safely. To assess the compatibility of those materials with a natural marine environment, some studies refer to Daphne algae's eco-toxicity test (Rawlings and Boccaccini, 2006). The cytotoxicity test is a convenient alternative to evaluate materials compatibility with an environment centered on human activity such as public buildings and works. Here we present a cytotoxicity test, traditionally used for biomedical application, which could be a good indicator for sanitary accreditations in housing. Additionally presented, the leaching test is mandatory for the establishment of inert or the hazardous classification of waste, and extended to the final generated material from wastes.

IV.4.1 Notion of toxicity

Acute toxicity is the toxicity induced by the administration of a unique and massive dose of a product with a 50% risk to kill an organism, defined as the LD 50 (Lethal Dose). Another concept is that the effects are dose-dependent; indeed, this is very well used in medicine since the "venom does not make the poison, but the dose". Toxicity can be measured directly on a population range, or by comparison to similar exposures in similar conditions. When a single toxic product is involved, a "safety factor" can be added to account for uncertainties in data and evaluation processes. The safety factor from rat to humans is of 10 and from fish to mammals is of 100, meaning that rats are 10 times and fishes 100 times less resistant than humans. It is more difficult to determine the toxicity of chemical mixtures than a pure chemical, because of the effects of interactions. Common mixtures include gasoline, cigarette smoke and industrial waste, such as the discharge from a malfunctioning sewage treatment plant, with both chemical and biological agents.

IV.4.2 Toxicity of metallic trace-elements (MTE)

Naturally present as trace amount in the soil, a lot of MTE will be found among the presently studied components. Indeed, human activity may have reinforced this presence as they have an important role in every-day life. The list below gives an overview.

- Iron (Fe) and Fe allies, steel, stainless steel;
- Lead, (Pb) in accumulators' batteries (cars), pipes, binders, anti-corrosion paintings, bullets;
- Mercury (Hg) in teeth amalgams and electric batteries;
- Uranium (U) for boats quills, anti-protection munitions;
- Chromium (Cr) as red pigment, and for pieces chroming;
- Copper (Cu) in the domain of electronic and as fungicide. (Cu sulfate in grapes trees treatment);
- Cadmium (Cd) used in electric accumulators Ni-Cd is used in aeronautics for anti-corrosion;

- Silver (Ag) for jewelry, photography, mirrors, many electronic and electric industrial uses, money and medals;
  - Gold (Au) for jewelry, precious objects, electric contact, dentistry;
  - Zinc (Zn) for galvanization of steel, and molded pieces in automotive;
  - Titanium (Ti) for its chemical inertia in chemical reactors, and for bone (hump) replacement.
  - Nickel (Ni) for stainless steel;

The combustion of solid or liquid fossils is also susceptible to reject metals in ashes, vapors and fumes. Above all combustibles, the energy-wood is (in France) the main emitter of heavy metals into the atmosphere (except Hg and Ni). In the year 2000, a general definition was set by the UE for European Rights and Member States, in particular in the waste field: 1) heavy metal designs "and compound of antimony, arsenic, cadmium, chromium, copper, lead, mercury, nickel, selenium, tellurium, thallium and Stain, 2) those materials under metallic form, as far as they are classified as hazardous substances" and more generally, a hazardous substance is " a substance that has been or will be classified as dangerous (Directive 67/548/CEE and its updated modifications)". In fact, mainly nanoparticles and aerosols shaped MTE are an issue for sustainability and health. When present in the air (road, industry pollution, combustion, etc.), they are usually abated by humid deposit. Ashes and incineration residues as well as carbon-ashes from individual or industrial installations (incinerators and thermal centrals) often are suspected to contain those MTE among the toxic products such as carbonated residues, heavy metals, organic-chlorides and traces of radionuclides. These products are partly chemically reactive in powder shape.

IV.4.3 Cytotoxicity[*] test

Cytotoxicity tests are performed for many different applications, generally in the biological field. The classic *in vitro* cytotoxicity tests is "USP" and is a semi-quantitative evaluation of cell damage using a scale from 0 to 4. Three cytotoxicity tests exist: the Agar Diffusion Test, the Direct Contact Test, and the Elution Test. In comparison, ISO 10993-5 (2009) provides further guidance to quantitatively measure cellular activity. Thus, ISO group measurements of cytotoxicity determination can be designated into groups: 1) assessments of cell damage by morphological means [like USP], 2) measurements of cell damage, 3) measurements of cell growth and 4) measurements of specific aspects of cellular metabolism. The most sophisticated tests 2-4 help researchers to investigate potential anti-cancer and anti-viral drugs.

IV.4.3.a Cell biology introduction

The cells presently studied here are mouse embryonic fibroblasts (MEFs). MEFs are used as a feeder layer in the culturing of mouse Embryonic Stem (ES) cells. They provide both a substrate for the ES cells to grow on and secrete many factors necessary for ES cells to maintain their pluri-

---

[*] Note on cytotoxicity: The chemical stability of the produced glass-ceramics was assessed by combining together a method from waste toxicity control (TCLP testing) and an in vitro cytotoxicity test (ISO 1993, 2009), usually from biocompatibility control, but in this study, using traditional window glass, as biocompatibility reference. A very few research works used both TCLP and cytotoxicity together, and the objectives and methods were different (Huang *et al.*, 2008; Amaral *et al.*, 2009). In order to confirm, after TCLP, the non-toxic behavior of elaborated glass-ceramics, both direct and indirect method (elution) were used as complementary information regarding samples-cells interaction: indirect method referred to cells reaction to released ions and direct method linked to surface properties.

potency. Fibroblasts are derived from mesenchymal cells, which are very abundant in the embryo. Fibroblast cells are mostly present in the non-specialized connective tissues which are in particular resident of the derma layer and which ensure its coherence and suppleness. They create a gluing matrix which helps to attach and strengthen the organs (see figure IV.8b). In adults, various specialized tissues exist such as fat tissue, reticulated tissue, cartilage and bone. In the embryo, only non-specialized conjunctive tissues are found and fibroblasts are also important in quantities. Their function is to maintain the structural integrity of connective tissues by continuously secreting precursors of the extracellular matrix fulfilled with the creation of proteoglycans (binding molecules that entrap water molecules) responsible for the synthesis of collagen or elastin, and proteinases, enzymes able to degrade and remodel the extracellular matrix. Fibroblast shape is elongated with at least two branches (see figure IV.8a). Its length is around 5 µm wide and 30 µm long, depending on its development state. The cells contain nuclear chromatin which makes them visible using specific markers: Dapi is absorbed and intercalates into the DNA and so enables the identification of the nucleus; Calcein passes through the cellular membrane and then enables the identification of cytoplasm shape. The cytoplasm is rich in mitochondria, which reveals the cellular viability: the more they are active, positively correlated with cellular growth and proliferation. Water, mineral salts and proteins provide the nutritive supply (Nissan, 2010; Saker *et al.*, 2014).
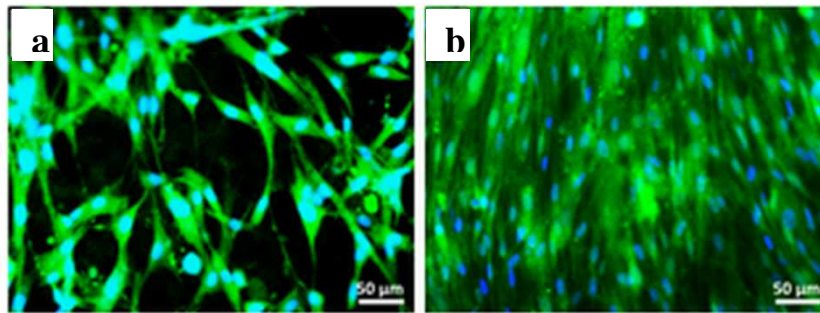
Figure IV.8: Fluorescence Magnification images of human fibroblasts adhered on hydrogel after 4 days (a) and 7 days (b) of incubation. The cells were stained for live cells (green) and nuclei (blue). Scale bar: 50 µm

Mitochondria are cellular organisms (see figure IV.9), functional units situated in the cytoplasm. They are involved in the "cellular respiration", where they burn nutrients by oxidation in order to produce the necessary energy (ATP synthesis) for the cell living. Their dysfunction may appear with the saturation of the system in free electrons (free radicals) coming form an incomplete reaction between complex components. Thus, measuring mitochondrial activity enables to evaluate cytotoxicity.
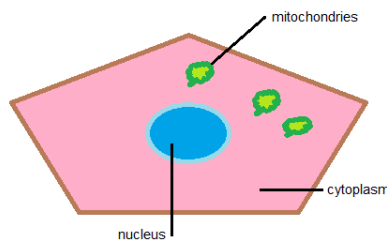
Figure IV.9: Schematic representation of a MEF cell

IV.4.3.b Procedure employed

For the evaluation of cytotoxicity, 6 samples are prepared (3 for direct method and 3 for indirect method). 0.5 g dry powder mixtures are pressed at 40 MPa using a 13 mm diameter mold, then direct heated (i.e. direct insertion the furnace at high temperature and cooling in air) during 30 min, at 1050 °C, to obtain small caps of 2 mm thickness. Samples are then gradually polished using 20 µm, 10 µm and 5 µm roughness diamond discs and finally at 1000 nm and 350 nm.

In order to assess the cell response to materials degradation, hereby different direct and indirect methods were applied (Hoppe *et al.*, 2011). Suspension of Mouse Embryonic Fibroblast (MEF) cells was cultured for 24 hours in a Dulbecco's Modified Eagle Medium (DMEM) containing 10% Fetal Bovine Serum (FBS) and 1% of penicillin-Streptomycin, at 37 °C, in a humidified atmosphere of 5% CO_2 in air. In the direct method, samples of test and control materials were applied directly to monolayers of cells covered with nutrient medium during a 24 hours incubation time. In indirect method (elution test), extracts were obtained by placing the test and control materials in separate cell culture media under standard conditions. Each fluid extract obtained after 1, 2 and 3 days was then applied to a cultured-cell monolayer, replacing the medium that had nourished the cells to that point. In this way, test cells were supplied with a fresh nutrient medium containing extracts derived from the test and control material. The culture were then returned to the 37 °C incubator and removed for examination after 24 hours. For cell viability quantification, Water Soluble Tetrasodium Test (WST) with Cell Counting Kit-8 (CCK-8) (Sigma Aldricht®, Germany) was used as recommended by the manufacturer. Cell viability after direct and indirect method was reported in a histogram. Cell viability of window glass is set at 100%, as a reference.

IV.4.4 Leaching test

The study of leachates from wastes and/or construction materials is relevant in the evaluation of the environmental impacts. In fact, many rules and regulation on leaching tests are available, which enables to model, evaluate and compare diverse scenarios, e.g. acidic/basic environment or short/long term leaching. The main purpose of a leaching test is to quantify hydro-extractable pollutants amounts from a material for a given scenario. Of course, the leaching depends on several chemical and physical conditions linked to the material and to the environment (table IV.1). To evaluate the impact of these factors on the leaching behavior, it exist either characterization trials or conformity trials.

Intern Factors		Extern Factors
Chemical process	Physical process	
Dissolution (solubility rate)	Percolation	Lixiviate quantity (L/S)
pH	Diffusion	Contact time
Chemical species	Superficial washing	Temperature
Total composition/ availability	Granulate/monolith	Medium Redox potential
Redox potential	particles size	Adsorption
Acid/base tampon capacity	Porosity	DOC
Dissolved organic carbon (DOC)	Permeability	
Leachate composition	roughness	
Temperature	Erosion	
Time		

Table IV.1: Intern and extern factors that can influence the leaching process (Coutand, 2007)

Characterization trials enable to evaluate the influence of external parameters on the leaching and the short term behavior, so specific landfill environmental conditions will be determined for a given type of waste. Conformity tests do not translate a real scenario, but enable to compare the leachate rates of evaluated material with referring regulation limits, for its storage or valorization. In table IV.2 is presented a non-exhaustive list of conformity leaching tests. It shows the wide variability of existing procedures. In general, for the assessment of waste based glass-ceramics conformity, TCLP is the most common procedure but the method requires the use of acidic solution, whereas the UE procedure requires water. By commodity the UE test was chosen, and samples were evaluated according to the European thresholds instead of USA thresholds.

Test -Origin-	Size (mm)	Solvent	pH	Leaching steps	L/S ratio by step	Time	mixing	Filtration (µm)
EN 12 457 (1-4) -U.E.-	<4 or <10	water	NC	1 or 2	2 or 10 or 2 and 10	24 hours or 6 and 18h	Yes	0.45
DIN 38 414 S4 -DE-	<10	water	NC	1	10	24h	Yes	
Waste research unit -GB-	<10	water or acetic acid	NC or 5	5	5 to 6	2 to 9 days	Yes	filtration under void
TCLP 1310 -U.S.A.-	<9.5	water + acids	3 initial or 5	1	20	24h	Yes	0.45

Table IV.2: Some regulated protocols of waste leaching – conformity tests

The leached elements, after quantification by ICP, will be evaluated in comparison to the limits corresponding to the selected procedure. As shown on following table, the limits defining inert or non-hazardous elements are different: European regulations separates landfill waste between inert, non-hazardous and hazardous definition.

Element	Limits (D.M.) / ppm L/S =10 l/kg		Limit (E.P.A.) / ppm
	inert material	non-hazardous material	
As	0.05	0.2	5.0
Ba	2	10	100
Cd	0.004	0.1	1.0
Cr	0.05	1	5.0
Cu	0.2	5	5.0
Hg	0.001	0.02	0.2
Mo	0.05	1	-
Ni	0.04	1	-
Pb	0.05	1	-
Sb	0.006	0.07	-
Se	0.01	0.05	1.0
Zn	0.4	5	-
Ag	-		5.0

Table IV.3: Criteria for waste acceptance in landfill according to
Italian (D.M.) and US (E.P.A.) regulations

The limit for the TCLP procedure, EPA, is far from the limits for the EN 12 457 procedure, DM. The release of heavy metals is evaluated by applying the conformity test EN 12457-2. Small fragments from bending strength determinations (dimensions of approximately 9 mm × 3 mm × 4 mm) are placed in an extraction solution, consisting of pure distilled water, with a pH value of about 7 for a liquid to solid ratio of 10, and gently stirred at 25 °C for 24h. The resulting solutions are filtered through a 0.8 μm filter and analyzed by inductively coupled plasma (ICP, SPECTRO analytical Instruments GmbH, Kleve, Germany). A blank sample, containing distilled water only, is used as a reference.

References

Amaral M. Gomes P.S. Lopes M.A. Santos J.D. Silva R.F. Fernandes M.H. (2009) Cytotoxicity evaluation of nanocrystalline diamond coatings by fibroblast cell culture, Acta Biomaterialia , 5, 755-763.

ASTM C 1259 (2005) Test Method for Dynamic Young's Modulus, Shear Modulus, and Poisson's Ratio for Advanced Ceramics by Impulse Excitation of Vibration, Annual Book of ASTM Standards, Vol. 15.01, American Society for Testing and Materials, West Conshohocken, PA.

Coutand M. (2007) Etude technologique et environmentale des résidus d'incineration de farines animales valorisés dans la matrice cimentaire. Evaluation écotoxique des matériaux et étude du piégeage des métaux. thèse INSA, laboratoire matériaux et durabilité des constructions INSA-UPS, Toulouse, France.

Directive 67/548/CEE (1967) Directive on the approximation of laws, regulations and administrative provisions relating to the classification, packaging and labelling of dangerous substances, Dangerous Substances Directive, to be replaced by the C.L.P. regulation (2008) from 2016.

EN 12457 - 2 (2002) Characterization of waste - Leaching. Compliance test for leaching of granular and sludges, Part 2., One stage batch test at a liquid to solid ratio of 10 l/kg for materials with particle size below 4 mm (without or with size reduction), index X30-402-2., UNI 10802 (2004) Manual sampling and preparation and analysis of eluates.

European Directive (1999) Council directive 1999/31/EC on the landfill of waste, Off. J. Eur. Commun. L 182, 1-19, eur-lex.europa.eu.

Flewitt P.E.J. Wild R.K. (2003) Physical methods for materials characterization, Sec. Ed., Institute of Physics Publishing Bristol and Philadelphia.

Gibraltar Laboratories (2014) Cytotoxicity and cell viability applications, , available online on 26-11-2014, gibraltarlabsinc.com/gibraltarblog.

Hoppe A. Güldal N.S. Boccaccini A.R. (2011) A review of the biological response to ionic dissolution products from bioactive glasses and glass-ceramics, Biomat., 32, 2757-2774.

Huang W.J. Tsai J.L. Liao M.H. (2008) Cytotoxicity of municipal solid waste incinerator ash wastes toward mammalian kidney cell lines, Chemosphere, 71, 1860-1865.

ISO 10545 - 3 (1997) Ceramic Tiles – Part 3: Determination of Water Absorption, Apparent Porosity, Apparent and Relative Density and Bulk Density, Stage 60.60, TC 189, ICS 91.100.23.

ISO 10545 - 4 (2004) Ceramic tiles - Part 4: Determination of modulus of rupture and breaking strength.

ISO 1993 - 5 (2009) Biological Evaluation of Medical Devices-Part 5: Tests for in vitro cytotoxicity

Nissan X. (2010) Etude des mécanismes moléculaires et cellulaires de l'engagement épidermique des cellules souches pluripotentes humaines, Thèse de doctorat, Université d'Evry Val d'Essone, France.

Sarker B. Singh R. Silva R. Roether J.A. J. Kaschta, et al. (2014) Evaluation of Fibroblasts Adhesion and Proliferation on Alginate-Gelatin Crosslinked Hydrogel, PLoS ONE, 9, doi:10.1371/journal.pone.0107952.

USP, Reference Documents for Biocompatibility and Class I-VI Testing, United States Pharmacopeia.

Chapter V

Direct sintering for waste stabilization and valorization

V.1 Concept: glass-ceramics from direct reactive sintering

The processing consists in the analogy with traditional ceramics (TC) (Colombo *et al.*, 2013).
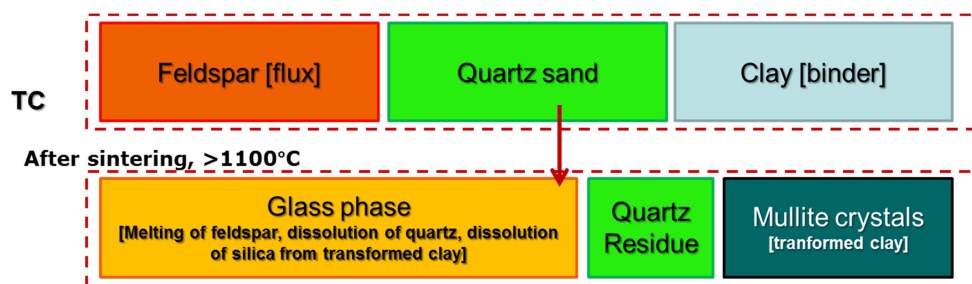
Figure V.1: Overall phases transformation in the traditional system

In the porcelain stoneware mixtures, we use a ternary system: feldspar, quartz sand and clay. Other added components vary slightly according to manufactures requirements and can be part of one the three acting elements for the preparation: fluxing agents (including feldspar), network formation (quartz sand), and binder (clay) (figure V.1).

After sintering, usually at temperature higher than 1100 °C, a glass phase comes from the melting of feldspar, dissolution of quartz and dissolution of silica from the transformed clay. As pure quartz fusion point is at 1700 °C, its partial decomposition is favored at lower temperatures such as 1100 °C by the action of feldspar. Some residues of quartz remain. Finally are found mullite crystals, coming from the transformation of clay.
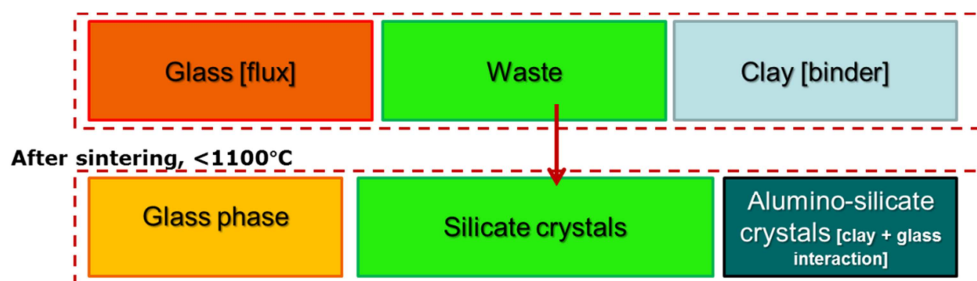
Figure V.2: Overall phases transformation in the waste-based system

Many types for waste (especially if combined) may lead to an abundant liquid phase upon direct sintering.

Reproducing the same ternary system logic, feldspar is replaced by glass and the network formation agents by inorganic waste. Clay may be kept as a binder. In this case, the absence of quartz enables a sintering under 1100 °C (figure V.2). The sintering process is a reaction sintering, as the crystalline phases do not come from the glass crystallization alone, but merely from chemical reactions between waste components and glass phases (for example, glass with $Ca(OH)_2$). The resulting phases are a glass phase, silicate crystals and alumino-silicate crystals (from the clay+ glass interaction). In some case, we may find mixtures according to a binary system (only glass/waste) (figure V.3).

Figure V.3 : Overall phases transformation in the waste-based system with two phases only

Waste-derived glasses may represent an opportunity for the development of a new type of porcelain stoneware, fired at much lower temperatures than the traditional ones and with a much reduced use of natural raw materials. For instance, feldspar sands were completely replaced by a $CaO-Al_2O_3-SiO_2$ waste-derived glass, obtaining a ceramic (fired at 1000 °C) with the same mechanical properties than that produced from traditional raw materials (fired above 1150 °C). The key advantages in the replacement of feldspars are the fact that the waste glass may provide a liquid phase by softening at much lower temperature than that required by the melting of feldspars, and the fact that some crystallization occurs, leading to an increase of viscosity that stabilizes the shrinkage. The complete replacement of feldspar with recycled soda-lime glass and CRT glasses has been recently proposed. The stabilization of shrinkage could be caused by a viscosity increase, operated by the addition of calcium hydroxide (for soda-lime glass) promoting the formation of wollastonite, or by the addition of alumina platelets (for CRT glasses). In both cases, the firing temperatures were particularly low (880 °C to 920 °C and 750 °C to 775 °C, respectively) (Bernardo *et al.*, 2012).

Glass compositions are suitable for the obtainment of (sintered) glass-ceramics from the mixing of different waste. The sinter-crystallization experiments enable to produce dense or porous glass-ceramics depending on the balance at the viscous flow sintering. By applying changes in the sintering/crystallization balance, waste derived glass powders can be mixed with recycled glass powders having a fluxing action (increased viscous flow, increased densification). The attention is to keep on many types of glass not usable in the manufacturing of original articles (e.g. CRT glasses, pharmaceutical glass, etc. presented in chapter II). The recycling step becomes then a "recovery" process. Finally, the several types of recycled glasses, depending to their characterization, can be used as raw materials for waste derived glasses, as additives for waste derived glass powders, or as fluxing agents in stoneware and other traditional ceramics.

V.2 Stabilization of fluorine-contaminated waste

SUMMARY - Calcium hydroxide is normally used to neutralize acid fumes escaping from furnaces for glass and ceramic manufacturing, leading to huge amounts of waste material known as "exhausted lime". The presence of calcium fluoride greatly complicates the use of this waste as Ca-rich secondary raw material. The present study is aimed at the development of a new type of glass-ceramics, allowing a significant fixation of fluorine (maintained as CaF_2 or in form of calcium silicon oxyfluorides), by direct sintering of exhausted lime mixed with clay and recycled glass from dismantled cathode ray tubes. The low softening temperature of recycled glass allowed a substantial viscous flow at relatively low temperature.

Sintered glass-ceramic samples of optimized composition (glass/clay/waste weight proportion equal to 50/30/20), featured water absorption below 2%, a good specific strength and, above all, a substantially unchanged F content, compared to the starting mixture. The obtained glass-ceramics could be used as low cost tiles, especially for insulation purposes, exploiting the residual porosity (30 - 40%).

V.2.1 Introduction

Elemental fluorine F is a member of the halogen family. In combination, it comprises 0.065% of the earth's crust, being the 13th element in abundance, and it is inevitably present in the raw materials for the ceramic industry (Monfort *et al*., 2008). A significant drawback of F-containing raw materials is the hazardousness of F-rich gaseous compounds that could evolve upon thermal processing; in fact, especially in recent years, environmental legislation in the European Union has set strict limits on the emission of fluorine-containing compounds into the atmosphere, the specific emission limit values for ceramic industries being about 5 – 10 mg HF/nm^3 at 18 %O_2 (IPTS, 2006; Ponikvar, 2008). Both glass and ceramic industries are known to abate F emissions by treating acid fumes with calcium hydroxide. This strategy provides some fluorine stabilization, by the formation of CaF_2 (Denissen and Vries, 1998), but also implies the accumulation of huge amounts of waste, known as ''exhausted lime'', with limited valorization possibilities. In fact, any thermal treatment applied to F-contaminated calcium hydroxide may cause fluorine to escape again, by the decomposition of calcium-based compounds. Previous studies exploited exhausted limes imply as Ca- and F-rich raw materials, for the development of waste glasses (i.e. glasses from combinations of waste materials),to be converted into frit-derived glass-ceramics(''sinter-crystallized'' glass-ceramics) (Bernardo *et al*., 2006; Bernardo, 2008; Lin, 2012), with no specific control of fluorine evolution. This part of Chapter V starts from a different approach, leading to glass-ceramics by direct sintering mixtures of exhausted lime, clay and recycled glass. The approach resembles that of traditional ceramics (e.g. Porcelain stoneware), in which wastes are no longer introduced in limited quantities (as shown by a vast literature (Rambaldi *et al*., 2007; Raimondo *et al*., 2007; Reinosa *et al*., 2010; Yürüyen and Toplan, 2009), but can represent the basic raw materials. Glass is a fundamental component, since it allows viscous flow sintering at much lower temperatures than those required for feldspar fluxes; in addition, it reacts with the other raw materials, giving origin to silicate and alumino-silicate crystals (Bernardo et al., 2008 and 2009).

In particular, we refer to glass-ceramic products based on a glass hardly recycled in the manufacturing of the original articles (i.e. panel glass from dismantled cathode ray tubes, CRTs), pure kaolin clay and exhausted lime. Lightweight materials, with limited water absorption, were obtained at low temperatures (900 °C to 1100 °C) (IPTS, 2006), with the key result of a substantial fixation of F, posing the conditions for a successful recycling of exhausted lime. Additional

experiments concerned the application of a glassy layer at the surface of sample to increase the mechanical properties and promote fluorine fixation.

V.2.2 Characterization of starting materials

The starting materials consisted of exhausted lime, glass from dismantled CRTs and pure kaolin clay. Exhausted lime comes from fume abatement systems of a plant for the production of blue-colored glass frits (Colorobbia SpA, Vinci, Italy), whereas CRT glass (provided by SASIL SpA, Biella, Italy) is actually a mixture of glasses from the recovery of panels of old TV and PC screens (Ba-Sr glasses, with a very limited content of PbO). The chemical composition of exhausted lime, according to XRF analysis (performed by the same Colorobbia SpA) and the composition ranges of CRT glass (provided by SASIL) are reported in Table V.1.

Compound	Exhausted lime (wt%)[a]	CRT glass (wt%)
SiO_2	6.40	59–61
CaF_2	14.50	–
CaO	52.40	0–2
B_2O_3	6.21	< 0.2
K_2O	2.60	6–7
Na_2O	1.11	7.5–8
MgO	0.69	0–1
Al_2O_3	0.37	1.5–3
CoO_2	0.16	–
Fe_2O_3	0.10	< 0.1
MnO_2	0.03	–
TiO_2	0.02	< 0.6
PbO	–	< 0.3
BaO	–	10–12
SrO	–	4.5–8.5
ZrO_2	–	1–5
LOI	Balance	–

LOI = lost on ignition.
[a]Tested after calcination at 500 °C.

Table V.1: Chemical composition of the employed exhausted lime and panel glass

Exhausted lime was mixed with the other components in three different weight proportions, labelled A (lime/glass/clay=20/70/10), B (20/60/20) and C (20/50/30). The amount of lime was kept constant in order to assess the impact on sinterability, phase evolution and stabilization of F of different glass/clay ratios.

As shown by figure V.4a exhausted lime, in the as-received condition, featured calcium hydroxide (PDF#01-1079) and $CaCO_3$ (calcite, PDF#86-2339) as the main crystal phases. Weaker diffraction peaks were attributed to CaF_2 (fluorite, PDF#87-0971) and quartz (PDF#85-1780). The thermal plots in figure V.4b are consistent with the characteristics of the phases detected by x-ray diffraction: the thermogravimetric (TG) plot exhibits two weight loss effects, at 450 °C to 500 °C and 750 °C to 800 °C, both with endothermic character, according to the DTA. These effects are consistent with decomposition reactions, occurring at 450 °C for $Ca(OH)_2$ (evolution of water vapor (García-Ten *et al.*, 2011)) and 750 °C for $CaCO_3$ (evolution of CO_2 (Halikia *et al.*, 2001). The weight change between the two reactions is also consistent with the preliminary information about chemical composition of exhausted lime, shown in table V.1.
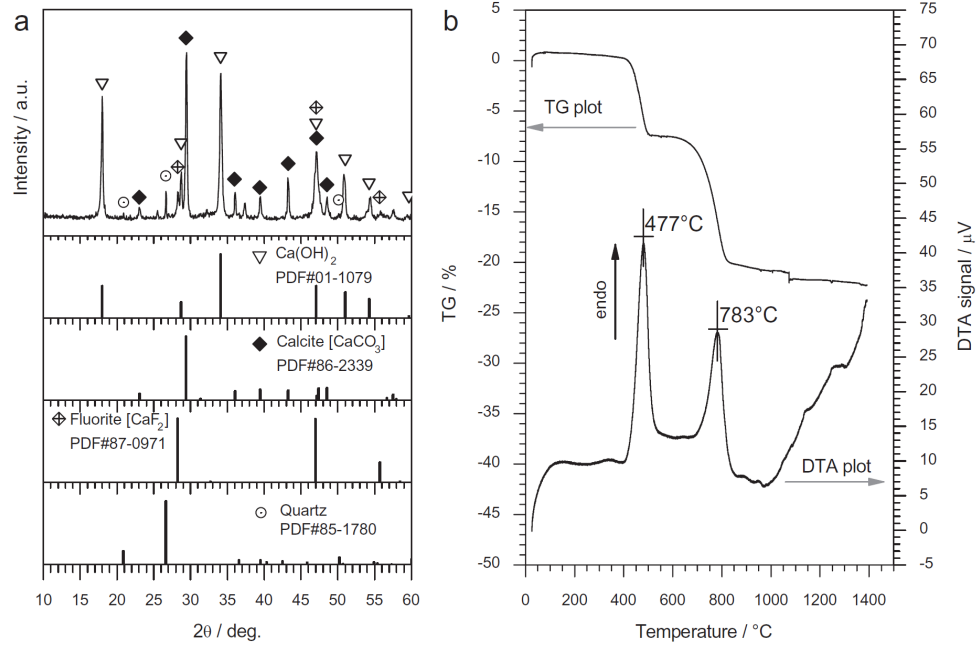
Figure V.4: Preliminary analysis on exhausted lime in the as-received condition: a) x-ray diffraction analysis; b) thermal analysis (DTA/TG plots)

Finally, the weak loss above 1000° C, accompanied by not well defined endothermic effects, may be attributed to the decomposition of calcium fluoride, as reported in the literature (Garcia-Ten *et al*., 2006). The presence of calcium carbonate and its decomposition explains the generally decreasing trend of density with increasing temperature, as illustrated by figure V.5.
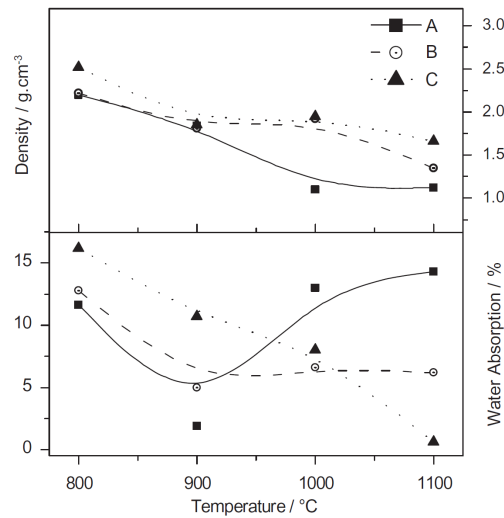
Figure V.5: Water absorption and apparent density trends with firing temperature (lines are simply guides for the eye – disc samples)

In fact, $CaCO_3$ is known to cause some foaming when mixed with glasses having a low softening point, such as CRT glasses (Bernardo *et al*., 2006). Due to the direct insertion of samples at the firing temperature also the water release, from decomposition of $Ca(OH)_2$ and clay dehydration (occurring at 550 °C Ring, 1996), probably contributed to the foaming.

The water absorption has more complex trends. All formulations generally led to a decrease of water absorption, up to 900 °C; above this temperature, the different balances among glass, clay and exhausted lime are associated to different behaviors. The formulation featuring the highest glass/clay ratio (formulation A), exhibited a dramatic increase of water absorption above 900 °C, whereas the one with the lowest glass/clay ratio (formulation C) exhibited a further decrease; the intermediate formulation had a stationary absorption above 900 °C.

V.2.2 Characterization of sintered materials

Densification and absorption trends could be caused by conflicting effects, involving the reduction of viscosity of the liquid phase, provided by the glass component, with increasing temperature. On the one hand, the viscous flow promotes the sealing of open porosity and the decrease of water absorption, on the other a low viscosity favors uncontrolled foaming by gas escape. In particular, the water absorption might be enhanced by the collapse of gas bubbles at the surface of samples (reasonably the hottest part of the samples, upon firing).
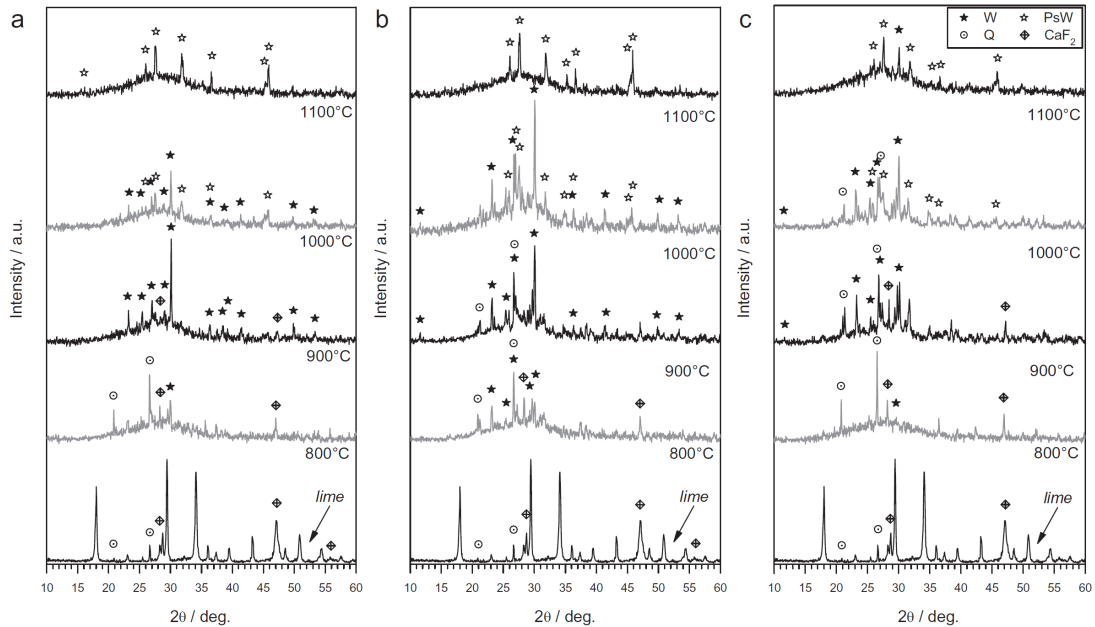
Figure V.6: Phase evolution with increasing firing temperature:
a) formulation A; b) formulation B; c) formulation C [pattern for exhausted lime represented out of scale
– W=wollastonite; PsW=pseudowollastonite; Q=quartz]

Operating with a high glass/clay ratio, the viscosity of the mixture was obviously lower than in the other cases, so that the "sealing effect" occurred at much lower temperature (900 °C) than extensive foaming (1000 °C to 1100 °C). On the contrary, for a low glass/clay ratio sealing and foaming likely occurred progressively and "simultaneously" (water absorption and density with similar decrease with increasing temperature). For all the formulations, the viscous flow was complicated by the crystallization, as illustrated by the diffraction patterns reported in figure V.6. The proposed approach does not properly lead to glass-ceramics, since there is no glass undergoing controlled crystallization by itself (Höland and Beall, 2012). However, we can observe that most of the crystal phases are "newly formed", i.e. they were formed by reaction among the components.

The signals for both Ca(OH)$_2$ and CaCO$_3$, well recognizable in exhausted lime (even if the pattern, already shown in figure V.4a, is represented out of scale, for comparison purposes), are practically absent in samples fired at only 800 °C. The calcium oxide available from the decompositions led to other Ca-rich crystal phases, by reaction with CRT glass, dominant above 900 °C. In fact, the main crystalline phase is wollastonite, in its low temperature form (β-CaSiO$_3$, PDF#84-0655), accompanied by pseudo-wollastonite (α-CaSiO$_3$, PDF#74-0874), i.e. its high temperature polymorph, appreciable especially above 1000 °C. The two phases are consistent with the formulation; more precisely the same phases were developed in frit-derived glass-ceramics, i.e. starting from a melting process (involving both CRT glass and exhausted lime as raw material) (Höland and Beall, 2012).
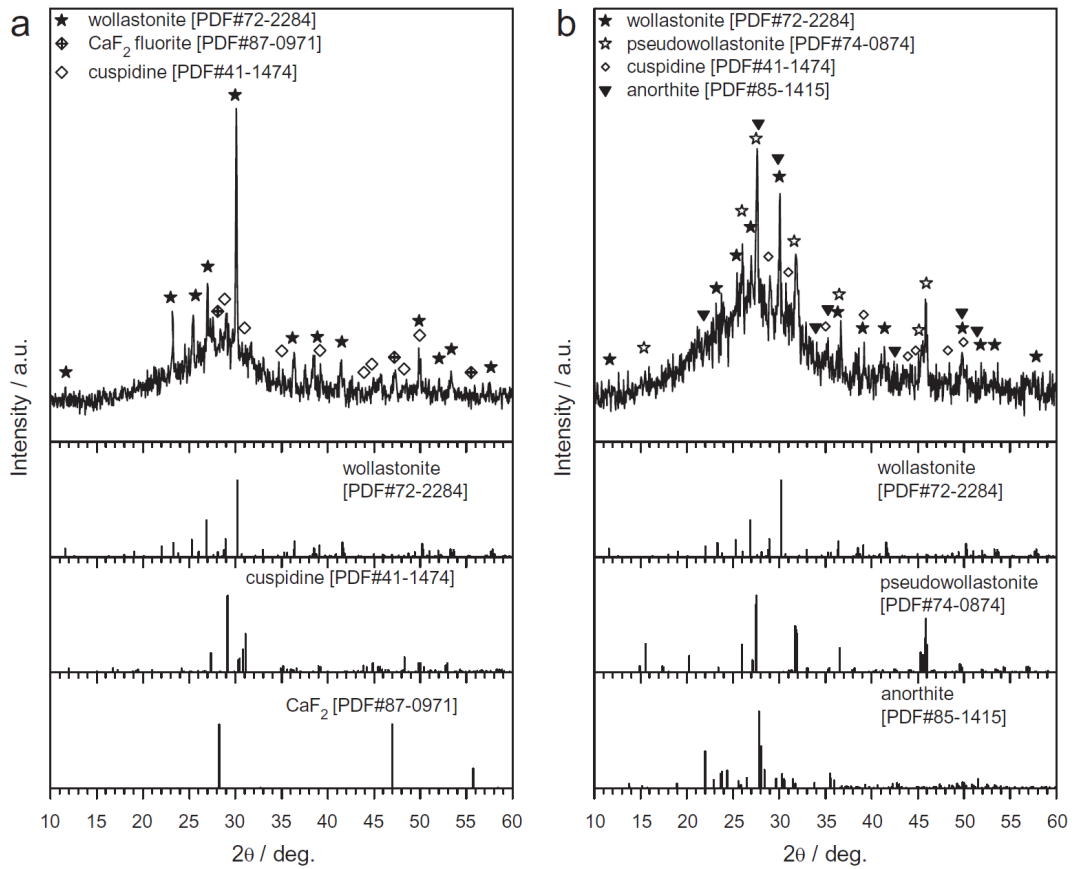
Figure V.7: Phase identification for reference sintered materials: a) formulation A sintered at 900 °C (A900); b) formulation C sintered at 1100 °C (C1100)

Quartz and CaF$_2$, the other two phases detected in the waste, were substantially maintained, but only in samples sintered at low temperatures. The quartz peaks are less intense for the mixture with the highest glass/clay ratio (formulation A): the lower viscosity of the system upon firing reasonably evidently promoted also intense quartz dissolution. According to figure V.5, some conditions could be taken as references. In fact, two formulations, for specific firing temperatures, i.e. composition A fired at 900 °C (A900) and C at 1100 °C (C1100), exhibited a water absorption below 2%, a sort of threshold limit for building materials to be applied on external walls (Bernardo *et al*., 2010). Coupled to the low density (close to 2 g/cm^3), the low water

absorption makes the products suitable for innovative applications, such as tiles for ventilated façades (lightweight tiles constituting a thermally insulating structure, Bernardo *et al.*, 2010).

Figure V.7, reporting the detailed phase identification of the two reference samples (we report the most probable phases according to Match!), allows some clarification about the minor phases. CaF_2 was actually replaced by another F-containing phase, that is cuspidine ($Ca_4Si_2O_7F_2$, PDF#41-1474), due to the interaction among the constituents of the studied mixtures; the transformation is partial, for A900, whereas it is reputed to be complete for formulation C1100. For formulation C, also anorthite ($CaAl_2Si_2O_8$, PDF#85-1415) is present, in agreement with the formulation (anorthite and related solid solutions have been already found to develop by reaction between Ca-rich compounds or glasses and kaolin clay (Bernardo *et al.*, 2008 and 2009)).
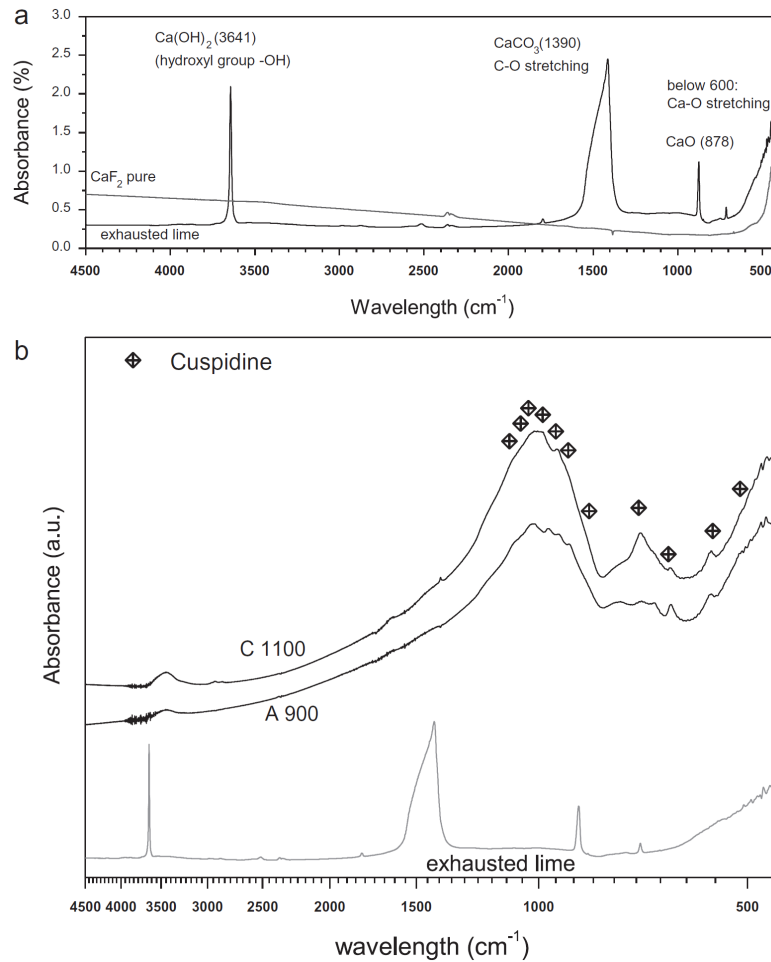
Figure V.8: FTIR characterization of the starting waste and of reference sintered glass-ceramics

FTIR analysis allowed a confirmation of the development of cuspidine. CaF_2 is infrared-transparent (it is known to be used for commercial IR windows), so that it is not surprising to find signals are attributable only to the other phases (Nasrazadani *et al.*, 2008) in the spectrum for as-received exhausted lime, as shown by figure V.8a. However, in sintered glass-ceramics, A900 and C1100, there are signals compatible with those for cuspidine, as illustrated by figure V.8b (Cruz-Ramírez *et al.*, 2011) (the symbols refer to the typical bands as described in the reference).

V.2.3 Mechanical characterization of optimized samples

Table V.2 summarizes the properties of test specimens cut from small tiles, sintered reproducing the reference conditions. The density and water absorption values practically confirm those determined for disc samples; the bending strength, considering the remarkable porosity, is quite substantial. Compared to a reference material, i.e. lightweight porcelain stoneware, specifically conceived for thermally insulating structures, samples from both formulations are denser, but possess almost the same specific strength (we considered, according to Ashby (1988), an index specifically concerning the structural efficiency of panels).

Sample	Apparent density, ρ (g/cm^3)	Water absorption[a] (%)	Total porosity (%)	Elastic modulus (GPa)	Bending strength, σ_f (MPa)	Specific strength, $\sigma_f^{0.5}/\rho$ (MPa$^{0.5}$ cm^3/g)
A900	1.84 ± 0.04	1.9 ± 0.1	31 ± 2	28 ± 2	20 ± 4	2.4
C1100	1.66 ± 0.04	0.6 ± 0.2	37 ± 3	21 ± 1	15 ± 3	2.3
C1100 glazed	1.62 ± 0.04	0.5 ± 0.1	39 ± 1	36 ± 3	20 ± 2	2.8
Lightweight porcelain stoneware, sintered at 1260 °C [18]	1.70 ± 0.05	1.5 ± 0.1	30	34 ± 2	22 ± 2	2.8

[a]Test performed on tiles.

Table V.2: Mechanical properties of selected sintered samples

V.2.4 Analysis of fluorine content

The obtainment of lightweight construction materials, at relatively low temperature and using waste materials instead of valuable raw materials (lightweight porcelain stoneware, presented in recent papers (Bernardo *et al.*, 2010), is sintered above 1200 °C and is due to the addition of expensive foaming agents, such as CeO_2 and SiC, to conventional raw materials), cannot be considered as separate from the stabilization of pollutants. In particular, fluorine evolution is a critical issue: any product should be accompanied by a significant fixation of the element, in order to reduce the need for new lime upon manufacturing (if all F is lost, the same amount of lime recycled is needed to neutralize the fumes from the new process, i.e. the overall amount of waste is constant).

An affordable estimation of fluorine content comes from WDXRF analysis, summarized in table V.3. The total counts for the distinctive line of fluorine (F Kα λ=1.83 nm, corresponding to an energy of 0.68 keV) for A900 sample, compared to those for exhausted lime in the as-received condition, are in proportion with the content of exhausted lime in the mixture (the normalized count is 0.23, while the content of lime in the formulation is 20%=0.2). For C1100 sample the signal for fluorine is much weaker, the total counts being one half of those for A900, despite the same content of exhausted lime adopted.

Counts for F line Kα (E:0.68 keV, λ:1.83 nm)	Reference: exhausted lime, as received	A900	C1100	C1100 glazed
Average value (10^3 counts/s)	5.04 ± 0.33	1.16 ± 0.02	0.54 ± 0.08	0.55 ± 0.03
Normalized counts (counts for sample/counts for reference)	1	0.23	0.11	0.11
% exhausted lime in formulation (%)	100	20	20	18

Table V.3: Estimation of F fixation by WDXRF analysis
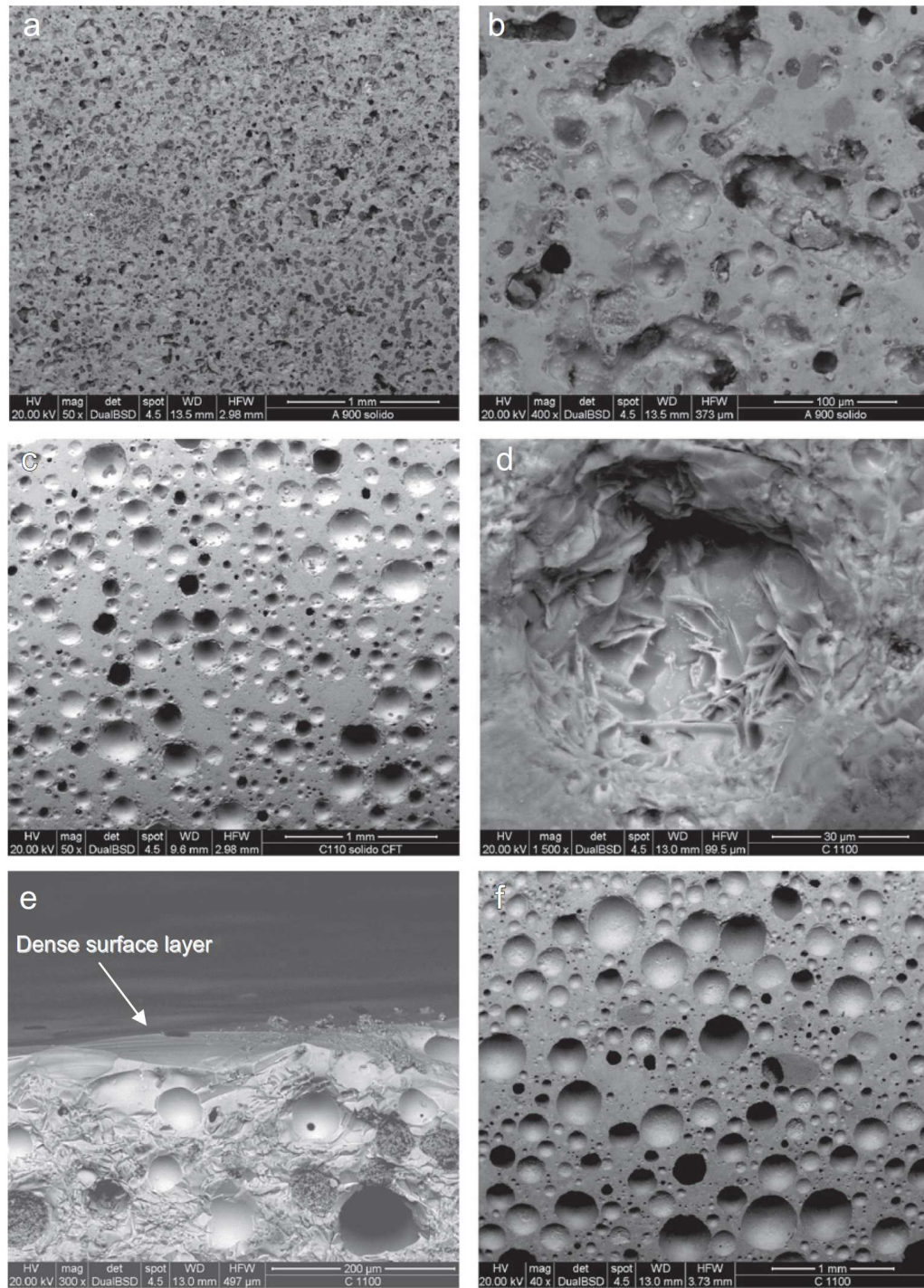
*Figure V.9: Microstructural details of selected glass-ceramic samples: a,b) A900; c,d) C1100;
e,f) C1100 with coating*

At 900 °C, the fixation of F is practically complete, while higher temperatures are associated to some F evolution, in form of gaseous compounds (e.g. hydrofluoric acid, silicon tetrafluoride (Garcia-Ten *et al*., 2006), in agreement with the thermal analysis (figure V.4); the slight formation of alumino-silicates, for sample C1100, is also thought to favor the evolution, due to their ability to dissociate fluorine-retaining crystalline phases (Garcia-Ten *et al*., 2006).

V.2.5 Application of a glaze

The fixation of F stimulates additional sintering experiments, based on double pressing. In fact, a second pressing operation is used to deposit a mixture of CRT glass and clay (in the proportion 63/37) on a base body of formulation C, thus forming a double layer green body with a weight proportion between top and substrate of 1:10. This procedure is mainly conceived to "seal" the F-containing body from the atmosphere, upon firing, with an F-free coating (glazes are effectively known to reduce gas emissions (Garcia-Ten *et al*., 2006)).

The results of WDXRF analysis, however, demonstrate that only limited F fixation is achieved: with a slightly lower overall content of F-containing waste, the counts for F are almost the same than those available from C1100 with no coating. The most significant effect concerns the density, well below 2 g/cm^3, much lower than in the glass-ceramic with no coating and not accompanied by any strength degradation; the coating, in other words, has a positive effect on specific strength. The coating probably helps the entrapment of gaseous compounds.

The porosity is substantial (more than 30%, from density determinations), but uniform, as testified by the low magnification images of the two reference samples (figure V.9a and figure V.9c). The crystallization is also evident from the images: in figure V.9b many micrometric grains are visible especially at the surface of pores, for formulation A; in Figure V.9d we can observe many interconnected acicular crystals, typical for wollastonite.

The good mechanical properties of the coated glass-ceramic sample, practically matching those of lightweight porcelain stoneware (both strength and elastic modulus are nearly the same, see table V.2) are a consequence of the quite homogeneous microstructures, as shown by figure V.9.

The presence of a dense surface layer (see upper part of figure V.9e), for glazed samples, is confirmed to positively influence the porosity (the sample shown in figure V.9f - C1100 with coating - is visibly more porous than that shown in figure V.9c - C1100).

In conclusion, further studies are probably needed to clarify the gaseous emission upon firing. In any case, the presented glass-ceramics achieve the starting objective of a substantial F fixation, and could be addressed to a specific application, in which they could be competitive with well-established ceramics, due to the intrinsic inexpensive character (in turn associated to the recovery of waste and the adoption of low firing temperatures). Future investigations will be probably dedicated to "engineered coatings", presented here only as an example, in order to improve both F-fixation and mechanical properties.

V.2.7 Additional tests

A second batch of around 200 g waste was supplied by Colorobbia after one year. In this, we could estimate the impact of the variability of waste composition from one batch to another. Same previous mixtures were prepared, the new batch composition replacing the exhausted lime in the proportions of exhausted lime (see table V.4), in order to compare the resulting changes due to the new batch composition. Compositions were realized by direct sintering in direct heating for 30 min holding time. 30 g of a glass formulation was provided by Smeacetto *et al*., (2012, Politecnico di Torino, Italy) to be used as a coating for the foamed glasses, named G10. The properties of the G10 glass are summarized in table V.5. All samples presented low densities (figure V.10). Only A1 700 presented an important water absorption (over 5%), and A1 800 water absorption reached ~2%. A2 900, prepared replacing CRT glass by G10 glass, and A1 900 showed a near-to-zero water absorption.

Reference	Components of Mixture A (20/70/10)			Sintering Temperature (°C)
A1 700	CaF waste batch 2	CRT glass	clay	700
A1 800	CaF waste batch 2	CRT glass	clay	800
A1 900	CaF waste batch 2	CRT glass	clay	900
A2 900	CaF waste batch 2	*G10 glass*	clay	900
A 900	*CaF waste batch 1*	CRT glass	clay	900

Table V.4: Mixtures compositions and thermal processing

Compositions (%wt)	SiO_2	Al_2O_3	CaO	Li_2O	Na_2O	K_2O	B_2O_3	BaO
G10	75	—	10	9	—	6	—	

	T_g (°C) (DTA)	T_x (°C) (DTA)	TEC (RT-400°C) °C^{-1}	T_{FS} (°C) (HSM)	T_{MS} (°C) (HSM)
G10	490	620	9.25×10^{-6}	515	630

Table V.5: Compositions and characteristic temperatures, First Shrinkage temperature T_{FS}, Maximum Shrinkage temperature T_{MS} and coefficient of thermal expansion (TEC) for G10 glass (Smeacetto et al., 2012)
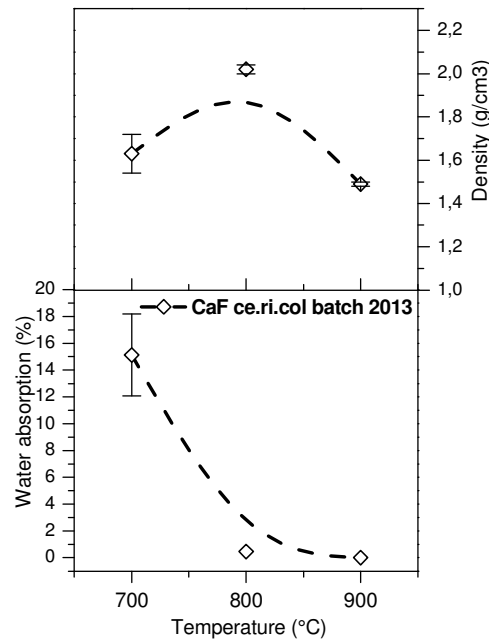
Figure V.10: Density and water absorption of mixture A from the second batch of exhausted lime, in function of the sintering temperature

The samples containing the waste from the second batch were probably richer in Cobalt oxide (more blue, see figure V.11) and presented an equivalent appearance to the samples containing the waste given to UNIPD, with a difference of processing temperature of 100 °C. For example as visible on figure V.12, sample A1 800 best fits with sample A 900.

A glaze composition {G10 (70 wt%); $ZrSiO_4$ (20 wt%); Al_2O_3 (10 wt%)} was applied on samples A900 and A1 900. G10 being fully transparent, a white appearance was brought by $ZrSiO_4$. Alumina, in addition not exceeding 10 wt%, was necessary to avoid foaming in the glaze,

to adjust the shrinkage of glaze to those of the substrate and to increase mechanical strength. The good adherence between the glaze and the substrate shows the good thermal compatibility of both compositions, and by extension, of CRT glass with G10 glass, at 900 °C.
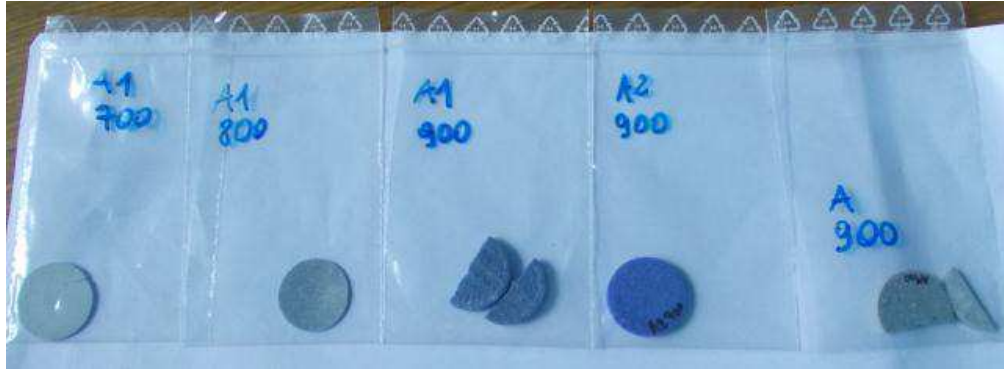
Figure V.11: Comparison of samples containing CaF waste from the second batch (A1 700; A1 800; A1 900; A2 900) and the first batch (A 900)
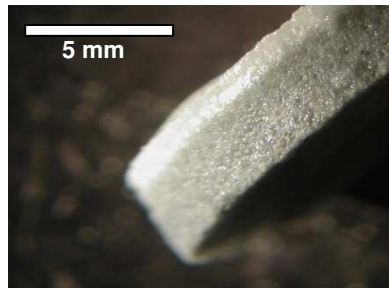
Figure V.12: Sample A900 covered of 0.5 g glaze composition

V.2.6 Cytotoxicity tests

Note: The conditions of preparation are described in the chapter IV.

Mouse Embryonic Fibroblasts directly seeded on samples surfaces and incubated for 24 hours (in a cell culture medium) were observed by fluorescent microscopy. Indeed, fluorescent microscope views give rapid information on cell dispersion on samples after 24 hours. They enable to measure qualitatively the short term cytotoxicity.

Cells growth depends on the concentration of ions released by the samples during leaching, which depends on ionic dissolution kinetic and oxide composition of samples. As visible on figure V.13 on glaze and on A 900, cells tend to spread on the surface and extend their contact area. Blue points represent the sites of cells core whereas green shapes present the sites of cells cytoplasm and are indicators of mitochondrial activity. Cells seemed attach to the surface particularly if it is rough, and inside porosity (see figure V.13). It was not possible to attribute the distribution of cells to the microstructure because the crystals were not visible. On another hand, cells repartitions seem to correspond more to topology. As this sample was porous (polished, then closed porosity was opened), the cells easily dispersed in the structure as particularly visible on figure V.13d. However, the studied glass ceramic are composed of many elements which are necessary to cells culture, (Si, Na, Ca, and several metallic ions) but also contain elements that may be toxic from a certain percentage (F). Referring to A. Hoppe, *et al.* (2011), CaF_2 are known for stimulating effects on osteoblasts cells when applied at moderate concentrations (25-500 ng/ml) whereas

higher concentrations (> 500 ng/ml) suppress osteoblast activity, impacting directly on cell viability.
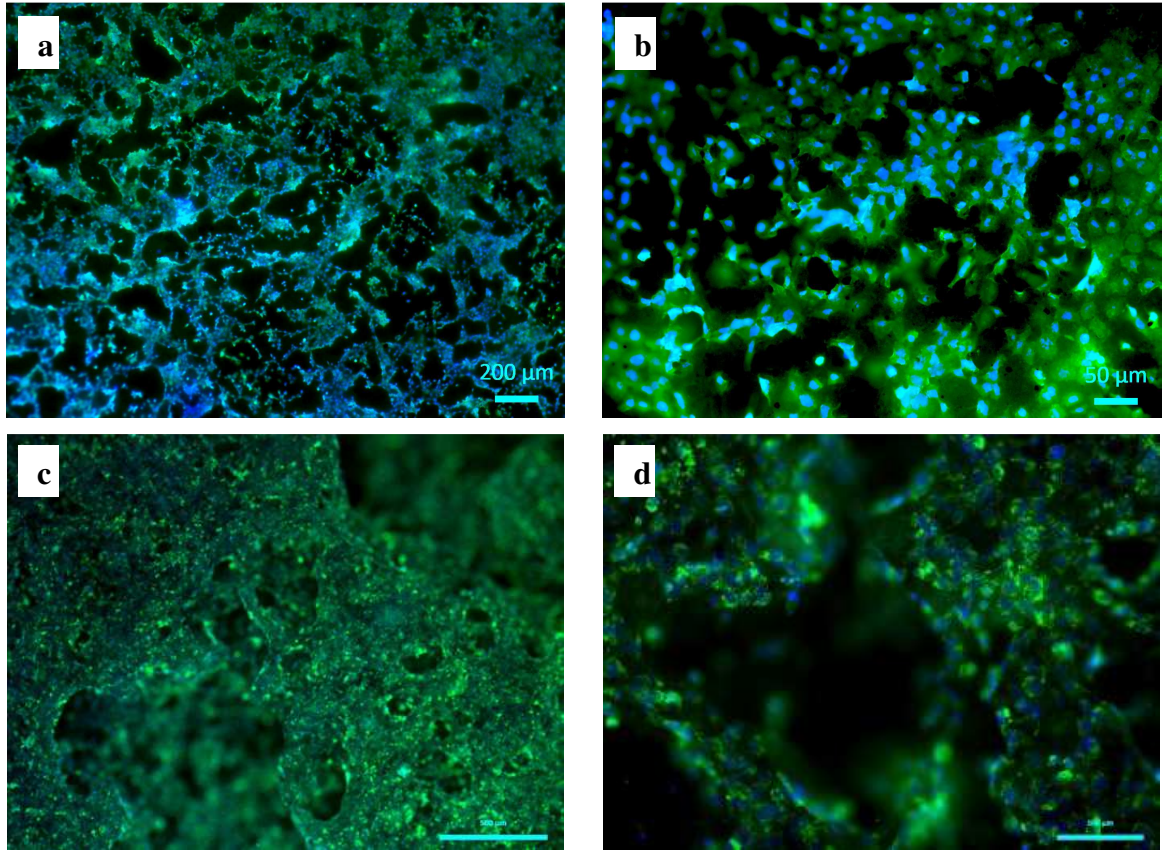
Figure V.13: Low (a, c) and High (b,d) Magnification views in fluorescence light (Dapi markers in blue, Calcein in green) of MEF seeded on the glaze (a,b) and on the sintered A 900 (c,d)

As visible on figure V.13, glaze as well as A900 sample presented a homogeneous dispersion of cells, and samples seem fully covered of cells. The absence of F in the glaze easily explains the compatibility of cells to the material. On another hand, the content of A 900 in F may be low enough to consider also its short term compatibility. If 24 hours is sufficient to evaluate short term toxicity, however on the long term, toxic behavior can also happen by accumulation. Up to date, it is almost not feasible to perform such a test on long periods as it requires an immobilization of the equipment for long times. Long term cytotoxicity (i.e. > 7 days) which may be relevant information for the presented samples is usually determined by calculation.

V.2.6 Conclusions

Exhausted lime, i.e. mainly F-contaminated calcium hydroxide, was successfully recycled in the formulation of lightweight glass-ceramics for building applications, based on low temperature sintering of glass-rich mixtures. The adopted strategy is particularly significant for its double impact; in fact:

- Rapid sintering treatments, for formulations comprising CRT glass (having a low softening point) promotes some foaming, thus obtaining micro-porous components; due to the uniformity of pore distribution, the specific strength is substantial; considering the low water absorption, the products may be attractive for the specific application as lightweight panels in ventilated façades (similar results have been presented for traditional ceramics, sintered at higher temperatures and prepared with valuable raw materials);

- Optimized formulations allow a remarkable fixation of fluorine; operating at low temperature (formulation A, sintered at 900 °C), fluorine is practically completely maintained, in form of CaF_2 or other F-containing compounds (cuspidine), while treatments above 1000 °C (formulation C, sintered at 1100 °C) determine only a partial stabilization; although preliminary, the present study evidenced possible improvements associated to a F-free coating.

V.3 Valorization of already-stabilized waste

A recent method of chemical inertization, based on the use of amorphous silica, offers the possibility to reduce the direct toxicity of MSWI fly ashes and use them as secondary raw material in low cost applications instead of landfill disposal. The present work was focused on the elaboration of an inert glass-ceramic comprising 20 wt% inertized fly ashes, coupled with recycled glass and clay. The chemical stability was confirmed by leaching tests and by cell culture studies to assess possible cytotoxicity using mouse embryonic fibroblasts. Optimized glass-ceramic tiles, processed at 1050 °C for 30 min, not only featured attractive aesthetic appearance and low water absorption (<2%), but also exhibited a remarkable specific strength (~3.6 $MPa^{0.5}·cm^3/g$) and no cytotoxicity.

V.3.1 Introduction

Vitrification has proved to be the safest technology for the treatment and remediation of non-combustible hazardous waste, among the various technologies for the disposal of inorganic waste (US E.P.A., 1992). The process implies the thermal destruction of waste and, when properly formulated, the resulting glass features a high chemical inertness, so that it can be landfilled without any particular concerns. Despite the soundness of vitrification technology, confirmed by numerous scientific studies and experimental tests (Colombo *et al.*, 2003; Schabbach *et al.*, 2011; Bernardo *et al.*, 2008), the method is associated with high energy consumption being also capital intensive. Vitrification of inorganic waste for which, differently from radioactive waste, environmental safety has not an absolute priority over cost, may be feasible only if the obtained glass could be reused in high value products, such as cellular and monolithic glass-ceramics for structural and functional applications (Binhussain *et al.*, 2014 ; Rawlings *et al.*, 2006; Chinnam *et al.*, 2013).

The entrapment of heavy metals present in waste, such as municipal solid waste incinerator fly ash, in a silica network, has been presented as a particularly effective inertization treatment (Bontempi *et al.*, 2013). This procedure is based on the mixing of colloidal silica with other fly ash residues, and the reaction occurs at room temperature (Bontempi *et al.*, 2010). The resulting material, named COSMOS® ("COlloidal Silica Medium to Obtain Safe Inert"), is washed and soluble salts can be recovered from solution simply by crystallization.

The obtained inert materials have been employed as filler for mortars, bitumen and resins. The chemical inertness of COSMOS has been recently exploited for its reuse as low cost filler for plastics. In particular, it was employed as a filler of polypropylene, showing promising properties as reinforcing filler (Besco *et al.*, 2013). However, to date no application has been reported regarding the reuse of COSMOS in ceramics. The present paper aims at presenting a first approach of using COSMOS to fabricate glass-ceramics, based on viscous flow sintering, considering suitable mixtures of recycled soda-lime glass, kaolin clay and COSMOS powder. Optimized formulations led to lightweight glass-ceramics possessing microstructural homogeneity and specific mechanical properties, to be used as low cost building material, with no negative impact on the chemical inertness of the products. The chemical stability of the produced glass-ceramics was assessed by combining a method to determine the leaching behavior of the sintered glass-ceramics (EN 12457-2) and an *in vitro* cytotoxicity test (ISO 10993-5:2009), usually considered for biocompatibility tests of materials (Amaral *et al.*, 2009). Indeed very few previous reports

dealing with waste-derived materials have considered such a combination of tests including cell culture studies to assess the material biocompatibility or safety (Huang *et al.*, 2008; Boccaccini *et al.*, 1997).

V.3.2 Materials characterization

COSMOS material was obtained by mixing three different types of fly ashes: ashes coming from MSWI (65 wt% in the composition), slag from desulfurization of FGD combustibles (20 wt%) and ashes from carbon combustion (15 wt%, Bernardo *et al.*, 2010).

Recycled soda-lime glass (SiO_2: 72 wt%, Na_2O: 13, CaO: 11, MgO: 2.5), pure kaolin clay and COSMOS powder were mixed together in four different weight proportions, labelled C1 (glass/clay/COSMOS=50/25/25), C2 (55/20/25), C3 (60/15/25) and C4 (65/10/25).

Element	Ashes MSWI (ppm)	Ashes FGD (ppm)	Ashes of carbon (ppm)	COSMOS (ppm)
P	n.d.	n.d.	0.3 ± 0.1	n.d.
S	n.d.	1.1 ± 0.9	67 ± 6	98 ± 9
Cl	2477 ± 234	980 ± 93	n.d.	3522 ± 288
K	433 ± 46	6.6 ± 0.8	6.6 ± 0.6	479 ± 41
Ca	1850 ± 171	794 ± 97	173 ± 14	2318 ± 177
V	n.d.	n.d.	0.29 ± 0.02	n.d.
Cr	n.d.	n.d.	0.031 ± 0.004	n.d.
Fe	0.18 ± 0.08	n.d.	0.29 ± 0.02	n.d.
Zn	3.7 ± 0.3	0.03 ± 0.01	0.013 ± 0.002	1.6 ± 0.1
As	n.d.	n.d.	0.048 ± 0.004	n.d.
Se	n.d.	n.d.	0.96 ± 0.07	n.d.
Br	33 ± 3	4.4 ± 1	0.012 ± 0.001	71 ± 6
Rb	n.d.	n.d.	0.012 ± 0.002	n.d.
Sr	n.d.	1.8 ± 0.1	2.4 ± 0.19	n.d.
Ba	n.d.	n.d.	0.19 ± 0.02	n.d.
W	n.d.	n.d.	0.053 ± 0.005	n.d.
Pb	13 ± 1	n.d.	n.d.	n.d.

Table V.6: Results of leaching test on several samples of fly ashes and COSMOS powder (Bontempi et al., 2013)

Component	Content (wt-%)
$CaCO_3$	24
$CaSO_4 \cdot \frac{1}{2}H_2O$	8
SiO_2	3
Si-rich Amorphous phase	65

Table V.7: Composition of COSMOS (Bontempi et al., 2013)

Table V.6 reports the results of leaching tests made on starting fly ashes and the obtained COSMOS powder. Fly ashes as well as COSMOS powder contained heavy metals such as Zn, Pb, Br, and Sr, but the released quantities were very different in each case. The leachate obtained from COSMOS powder showed very low concentrations of these elements, especially Pb, which confirmed the efficiency of COSMOS chemical inertization process (Bontempi *et al.*, 2013).

The presence of soluble salts and fine particles (<45 μm) could not be avoided, as testified by the relevant quantities of Br and Cl, in table V.6. This problem can be solved by means of a supplementary leaching purification step, which consisted in dissolution of exceeding salts in a liquid phase, in order to obtain totally inert COSMOS powder, according to Bontempi *et al.*, (2013).

Bernardo *et al*. (2009) have recently demonstrated that low cost ceramics may be obtained by extensive use of recycled glasses instead of conventional feldspar fluxes, with significant energy savings; in fact, glass/clay mixtures can be sintered at much lower temperature than traditional stoneware ceramics, with a stabilization of shrinkage (over a wide temperature range) offered by partial crystallization, owing to glass devitrification and/or reaction of glass with CaO-rich additives. The mixtures considered in the present paper were basically conceived to mimic the previously tested glass/clay mixtures (Bernardo *et al*., 2009) with a CaO-rich additive; "technical clay", i.e. a natural mixture of clay minerals and quartz, previously used, was replaced by pure kaolin clay mixed with COSMOS, providing also CaO. As shown by table V.7 COSMOS comprises silica-rich (mainly amorphous) and CaO-rich phases (carbonates).

The porosity that could be generated by the decomposition of Ca carbonate and sulfate, in COSMOS, was not considered as an issue, but as an opportunity. In fact, there is a growing interest in the ceramic industry towards lightweight tiles, to be used in highly thermally efficient façades (tiles mounted on metal frames, in turn attached to the main building walls; the air gap between tiles and wall providing excellent thermal and acoustic insulation) (Bernardo et al., 2010). Densities below 2 g/cm3 are typically appreciated, but with the constraint of water absorption below 2% (higher absorption values could compromise the freeze-resistance).
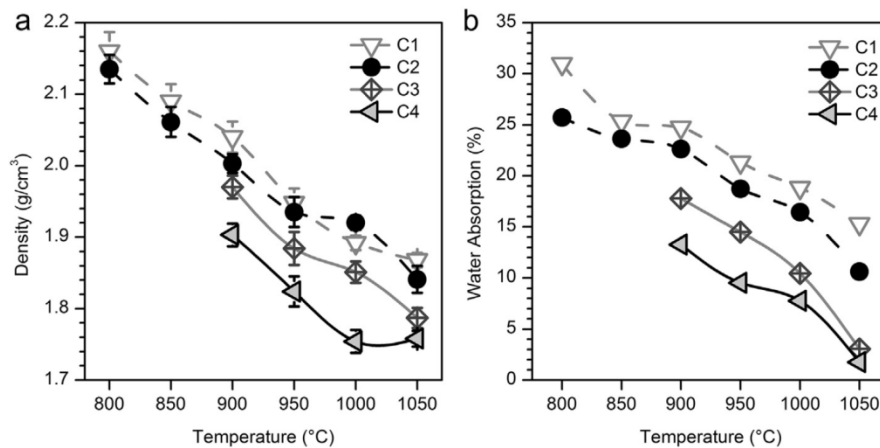
Figure V.14: a) density and b) water absorption trends with increasing temperature in different glass-ceramic mixtures

The newly developed ceramics, as presented in figure V.14, all showed decreasing density and water absorption with increasing temperature. The evolution of density is rather straightforward: the rapid heating (40 °C/min) reasonably forced $CaCO_3$ to decompose completely, being well above its characteristic temperature ($CaCO_3$ may decompose even below 800 °C (Ponsot *et al*., 2013), causing some foaming in the pyroplastic mass of softened glass. Higher glass contents and higher temperatures (1000 °C to 1050 °C) were obviously associated to a lower viscosity, and a consequent higher foaming ability, with some samples (C4 series) achieving a density below 1.8 g/cm³ (see figure V.14a).

The increasing viscous flow with increasing glass content and firing temperature, explains also the decreasing water absorption. The samples of C4 composition, sintered at 1050 °C, even fulfilled the above mentioned constraint for freeze-resistant tiles (water absorption below 2%). It should be noted that 1050 °C is well below the temperatures required for traditional stoneware

tiles to possess negligible water absorption (temperatures exceeding 1200 °C, Bernardo et al., 2010). The X-ray diffraction pattern of COSMOS powder, before any thermal treatment, as visible in figure V.15a, confirms the mineralogical composition provided by table V.7. The crystal phases correspond to calcite ($CaCO_3$, PDF#85-1106), hemi hydrated gypsum ($CaSO_4 \cdot _{0.5}H_2O$, PDF#84-0962) and quartz (PDF#84-0962). After firing treatment at 1050 °C, a sample of C4 composition contained practically only wollastonite (PDF#72-2284) and anorthite (PDF#84-0750), with traces of albite (PDF#09-0466), as a proof of the reaction between components. The same sample, as shown in figure V.15b, is interesting for the minimization of cristobalite ((PDF#39-1425); we refer to the intensity of the main diffraction peak, a well-recognized index of the quantity of a given phase; for C4 sample fired at 1050 °C, the intensity of the peak is about one fifth of the intensity for C1 sample fired at 900 °C, i.e. the quantity of cristobalite in the best sample is one fifth of the maximum obtainable for the full series of samples).
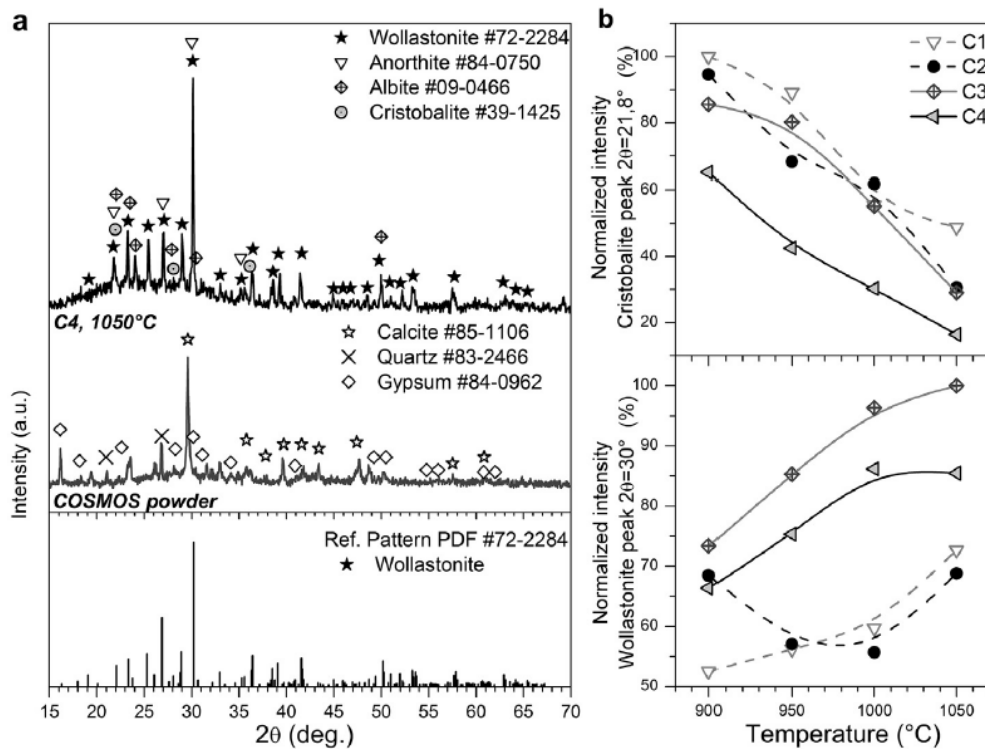
Figure V.15: a) XRD patterns confrontations of C4 composition sintered at 1050 °C and pure COSMOS powder; b) plots of normalized intensity of main XRD peaks of cristobalite and wollastonite

Cristobalite likely originated from the decomposition of clay and it could degrade the mechanical properties, owing to the well-known displacive transformation at around 200 °C, upon cooling, accompanied by a volume contraction of 3%. Extensive degree of viscous flow, associated to high glass contents and high temperatures, was evidently favorable to the dissolution of cristobalite. Finally, figure V.15b shows that, although not maximized, the content of wollastonite in the C4 sample sintered at 1050 °C was quite significant (80% of the maximum).

The obtained samples were not developed by a typical vitrification followed by controlled crystallization process. In practice, they cannot be considered, strictly speaking, as glass-ceramics (Höland and Beall, 2002). However, the developed phases are quite typical for glass-ceramics belonging to the $CaO-Al_2O_3-SiO_2$ system and formed, as mentioned above, by reactions between

constituents. The formation of wollastonite could be due to a reaction between glass and CaO (from $CaCO_3$, in turn provided by COSMOS). Anorthite and albite (calcium and sodium feldspars) could be formed from the chemical interaction of CaO and Na_2O, from both COSMOS and glass, with alumino-silicate residues from clay decomposition, as previously observed for glass/clay/CaO-rich additive mixtures.
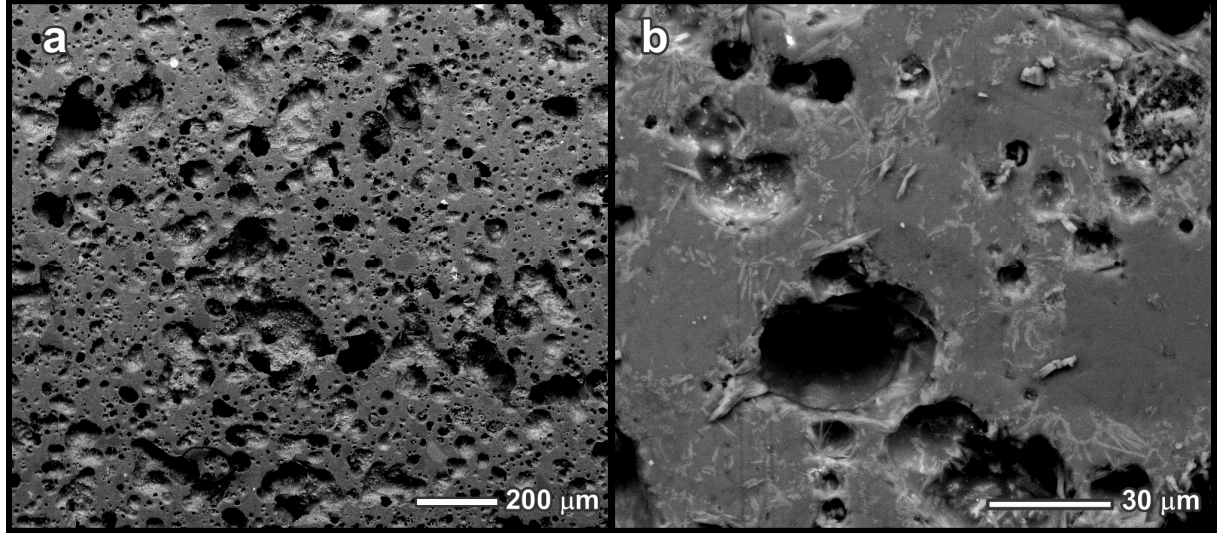
Figure V.16: SEM views of C4 sintered at 1050 °C: a) porosity, low magnification; b) phase distribution, high magnification

The microstructural details concerning the C4 sample sintered at 1050 °C, shown in figure V.16, confirm the foaming and the partial crystallization of this sample. The pore distribution is quite homogeneous (figure V.16a) and fibrous crystals (quite typical for wollastonite) are evident, especially around pores (figure V.16b). This fact may be seen as a proof of the double role of $CaCO_3$: pores were determined by decomposition of the carbonate, and crystallization was favored by local interactions between its residue (CaO) and glass.

	Values for C4 sintered at 1050 °C	Typical soda-lime-silica float glass[23]	Porcelain stoneware tiles[24]
Density, ρ (g/cm3)	1.8	2.5	2.3–2.5
Young's modulus, E (GPa)	44.0 ± 5.4	72	50–80
Bending strength, σ (MPa)	38.2 ± 5.4	41	35–85
Specific strength for lightweight panels $\sigma^{1/2}/\rho$ ($MPa^{0.5}$ cm^3/g)	3.6	2.5	2.6 − 3.7

Table V.8: Mechanical properties of ceramic C4, sintered at 1050 °C for 30 min compared to typical mean values of commercial equivalent products.

Due to the substantial porosity, both elastic modulus and bending strength were not particularly high, as reported in table V.8. However, the C4 sample sintered at 1050 °C compares favorably in terms of specific mechanical properties, of vital importance for lightweight design, (Ashby, 1988) with both dense soda-lime glass and even with porcelain stoneware. The excellent value of specific strength is in good agreement with the possible application in ventilated façades (Bernardo et al.,

2010). Such applications are supported also by the light coloration of the specimen (ivory-gray), as illustrated in figure V.17.

Figure V.17: Visual appearance of C4 sample sintered at 1050 °C for 30 min
(left: unpolished; right: polished surface)

V.3.3 Chemical characterization

Element*	Leachate from COSMOS (ppm)	Leachate from C4 − 1050 °C (ppm)	Limits for inert material (ppm)	Limits for non-hazardous material (ppm)
As	**0.0079**	0.0566	0.5	2
Cd	**<0.0002**	0.0006	0.04	1
Cr	**0.0849**	0.4496	0.5	10
Cu	**<0.0001**	0.0294	2	50
Mo	**0.0372**	0.0758	0.5	10
Ni	**<0.0014**	0.0163	0.4	10
Zn	**<0.0203**	0.0423	4	50

*Table V.9: Leachate of C4 ceramic (*elements below the detection limit not reported)*

The chemical stability of sample C4 sintered at 1050 °C for 30 min was verified by applying the TCLP test, as a preliminary approach. As reported in table V.9, the contents of toxic elements were all well below the limits for inert materials, except for chromium, only slightly below the threshold. Although successful, TCLP test was not considered as a definitive proof of inertness, since it is intended mainly for the certification of wastes, rather than for the characterization of products. The activity of MEF cells, generally applied in the characterization of biomaterials (Amaral *et al.*, 2009), was considered as a more conclusive test for characterizing the non-cytotoxicity of the material. Indeed the cell biology characterization of waste-derived materials, originally suggested almost 20 years ago (Boccaccini *et al*., 1997), should be increasingly considered as a convenient approach to test the safety of waste-derived products, contributing to tackle acceptability issues of such materials. In this context, our glass-ceramic was compared with a safe material of every-day use in building applications (window glass). Figure V.18 shows relative cell mitochondrial activity, in % (mean ± standard deviation, mitochondrial activity of window glass set at 100%), when measured after indirect and direct methods. Mitochondria are cellular sites whose activity is typically altered by toxic elements present in the surrounding medium, consequently, cytotoxicity is associated to mitochondrial dysfunction.
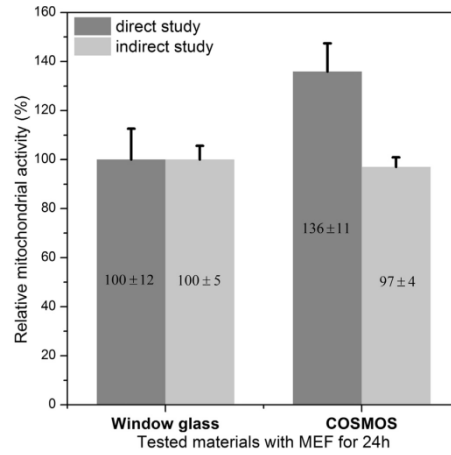
Figure V.18: Cell viability in contact with COSMOS ceramic [C4; 1050 °C], compared with window glass; direct study and indirect study

A higher mitochondrial activity was measured by the indirect method, namely 136% ± 11% in comparison to 97% ± 4% obtained by the direct method.
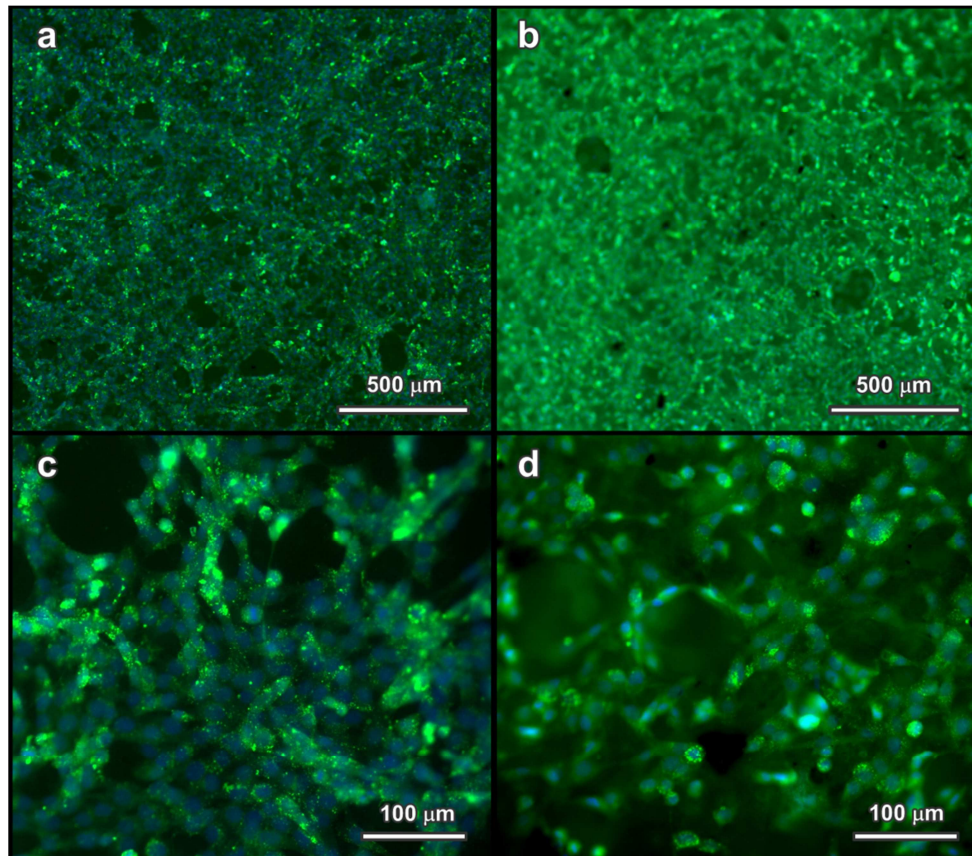
Figure V.19: Low magnification fluorescence microscope view with superposition Dapi (blue) and Calcein markers (green) of samples tested by the from direct method: a) window glass, b) C4 glass-ceramic

The mitochondrial activity of C4 was practically equivalent to that of the reference glass, according to both direct and indirect methods. Small variations in cell activity are usually complex to interpret, as they would depend on uncontrolled parameters, whereas a 50% (or higher) decrease

of activity can be reasonably attributed to cytotoxicity (Cicek *et al*., 2014). In this case, it can be assumed that the variation of activity is a direct and unique consequence of sample cytotoxicity. Then, the lower value of mitochondrial activity defining the samples as non-toxic was set at 50% relatively to the reference glass. This value refers to LD_{50} and LC_{50} indexes used in toxicology (Trevan, 1927). The results presented here are then positive, in that the sample did not present any toxicity effect after 24 hours neither by direct or by indirect cell biology studies.

As shown in tables V.6, V.7 and figure V.15, COSMOS ceramic contains many elements that usually promote cellular activity (Hoppe et al., 2012) particularly Si, O, Na, K and Ca (for example in bioactive glasses, Gerhart and Boccaccini, 2010). The other elements (Al, Cr) may be toxic but it seems that their concentration in the sample or their diffusion rate in the medium were not high enough to determine cytotoxicity. As illustrated by figure V.19, COSMOS C4 samples as well as window glass were fully covered by MEF cells, after 24 hours immersion. In addition, cells present an elongated morphology, which is typically for MEF cells. Furthermore, cells showed a fibroblast-like appearance with cytoplasmic expansions and cell–cell contact (Pollard, 2008; Amaral *et al.*, 2009).

The assessment of mitochondrial function (MTT assay) further suggested the low cytotoxicity of the glass-ceramic. Mitochondria are sensitive targets for toxic injury because of their crucial role in maintaining cellular structure and function via aerobic ATP production. The cells exhibit good cell attachment, spreading and mutual interconnections, well-recognized signs of successful biocompatibility.

V.3.4 Conclusions

Lightweight construction materials may be manufactured at relatively low temperature (1050 °C) using a mixture of waste materials instead of valuable raw materials. In particular, the developed glass-ceramic materials demonstrate the possibility to reuse significant amounts of COSMOS, i.e. fly ash from MSWI, subjected to a preliminary stabilization treatment with colloidal silica. The mineralogy of COSMOS was exploited here in combination with recycled glass and clay for the development of uniform cellular structures, as well as for partial crystallization, owing to glass/waste interactions.

According to leaching tests and cytotoxicity evaluation by cell culture, the glass-ceramic was safe and not toxic after 24 hours, exhibiting similar behavior to the reference soda-lime glass (considered as a safe product). Moreover, the material showed a spontaneous compatibility with MEF, which exhibited morphology and development similar to that observed on soda-lime glass. Indeed the cell biology study carried out represents a general convenient test for evaluating the biocompatibility of waste-derived materials, and it adds information about the safe behavior of this type of materials, thus we propose such cell biology tests for a comprehensive biocompatibility characterization of waste-derived products, which should help to tackle social acceptance issues for the broader exploitation of such materials.

V.4 Magnetic glass-ceramics

SUMMARY – Ceramics and glass ceramics based on industrial waste have been widely recognized as competitive products for building applications; however, there is a great potential for such materials with novel functionalities. In this paper, we discuss the development of magnetic sintered glass ceramics based on two iron-rich slags, coming from non-ferrous metallurgy and recycled borosilicate glass. The substantial viscous flow of the glass led to dense products for rapid treatments at relatively low temperatures (900–1000 °C), whereas glass/slag interactions resulted in the formation of magnetite crystals, providing ferrimagnetism. Such behavior could be exploited for applying the obtained glass ceramics as induction heating plates, according to preliminary tests (showing the rapid heating of selected samples, even above 200 °C). The chemical durability and safety of the obtained glass ceramics were assessed by both leaching tests and cytotoxicity tests.

V.4.1 Introduction

The recycling of inorganic waste into new usable ceramic products has been a key strategy for environmental protection for the last few decades (Lee, 2006), which has included also efforts to produce glass ceramics from waste (Rawlings *et al.*, 2006). Glass ceramics undoubtedly have constituted an important and established waste-derived product since the 1960s (Höland and Beall, 2002). Nevertheless, it must be acknowledged that the energy-intensive vitrification process at the basis of any glass ceramic manufacturing and the limited applications, mainly as building materials, remain as fundamental issues (Rawlings *et al.*, 2006; Colombo *et al.*, 2003).

The direct sintering of mixtures of inorganic waste, including recycled glasses, acting as fluxing agents, is an important alternative to conventional glass ceramics. The products cannot be nominally considered as glass ceramics, since there is no actual vitrification, *i.e.*, melting of an oxide mixture and cooling in an amorphous solid. However, a rich literature supports the classification of such products as "sintered glass ceramics", owing to the generally observed phase evolution (Rawlings *et al.*, 2006; Francis *et al.*, 2002; Dimech *et al.*, 2008; Bernardo and Dal Maschio, 2001). In fact, recycled glasses, besides promoting the densification by viscous flow sintering, react with the waste, leading to silicate and alumino-silicate crystals similar to those developed by devitrification of waste glasses. The process offers remarkable energy savings, due to the absence of a high temperature (>1350–1400 °C) melting stage and its simplicity.

As widely discussed by Chinnam *et al.* (2013), iron-rich waste materials, when incorporated in glass ceramics, demonstrate the potential of turning these waste-derived materials into functional glass-based products, appreciated for their magnetic, electrical and thermal properties. In particular, the magnetic functionality is interesting for the possibility of induction heating, exploited even in non-waste-derived iron-rich glasses and glass ceramics, such as those developed for cancer treatment by hyperthermia (Bretcanu *et al.*, 2005 and 2006); in fact, ferrimagnetic particles (such as magnetite crystals, embedded in a glass matrix) may provide intensive heating, owing to energy dissipation upon magnetization cycles (Deatsch and Evans, 2014).

In the present study, we have investigated mixtures of pharmaceutical borosilicate glass residues and two iron-rich slags, coming from non-ferrous metallurgy. One of the slags, in particular, contains fayalite, i.e. iron (II) silicate (Fe_2SiO_4), a typical crystal phase in many slags

from non-ferrous metallurgical processes (Gorai *et al.*, 2003; Mihailova and Mehandjiev, 2010). Whereas fayalite-rich slags have been already applied directly in working out foamed crafting concrete aggregates (Alp *et al.*, 2008), they have been used in glass-ceramic materials, to the authors' knowledge, only after a vitrification process aiming at the separation of iron from the glassy matrix (Francis, 2007; Çoruh *et al.*, 2006; Zhihong *et al.*, 2013).

In this investigation, the mixing of slags with borosilicate glass was successful in yielding dense products by fast sintering at relatively low temperature (900 °C to 1000 °C) with an excellent stabilization of pollutants (e.g. heavy metal ions) present in the slags, as assessed by direct leaching tests and by cytotoxicity tests. These tests using cell culture methods are being proposed to provide reliable data about the safety of waste derived products, e.g. when they become in direct contact with biological entities. The formation of magnetite, as main crystal phase in the resulting glass-ceramics, has been exploited considering the application of the new glass-ceramics to induction heating applications.

V.4.2 Raw materials characterization

The starting wastes consisted of metallurgical slags labelled S1 and S2. The drive for investigating these particular slags relates to the fact they are quite typical and can be seen as two end members for non-ferrous slags, i.e. Fe,Si-rich and Fe,Ca,Si-rich. The slags were mixed with recycled borosilicate glass, from the manufacturing of pharmaceutical containers (BS), in the following proportions (expressed in wt.%): 75 BS-25 S1, 50 BS-50 S2, 75 BS-25 S2 and 50 BS-50 S2. The chemical composition of the starting wastes, as well as of borosilicate glass is reported in Table V.10. The temperature necessary for an important densification was set at 900 °C, as a minimum firing temperature for glass/slag mixtures. In fact, because of the presence of secondary phases, some residual porosity could not be eliminated even operating at 850 °C, despite the possibility to achieve nearly full density at only 700 °C for the pure glass, in good agreement with previous experiences on the adopted borosilicate glass combined with alumina platelets, under 15 vol% (Bernardo and Scarinci, 2004).

Component	S1	S2	BS
Chemical composition (wt%)			
SiO_2	29	24	72
FeO	52	32	–
Al_2O_3	4	6	7
CaO	2	21	1
MgO	1	1	–
Na_2O	<1	<1	6
K_2O	<1	<1	2
ZnO	7	7	–

Table V.10: Chemical composition of the starting materials, S: slags, BS: borosilicate glass

V.4.3 Results and discussion

As shown in figure V.20, both density and water absorption exhibit quite particular evolutions, with increasing firing temperature depending on the composition. The most straightforward trends correspond to the samples containing a significant amount of slag (50wt% of S1 or 50wt% of S2),

which exhibited a slight increase of density (always below 2.5 g/cm^3), coupled with a sensible decrease of water absorption.
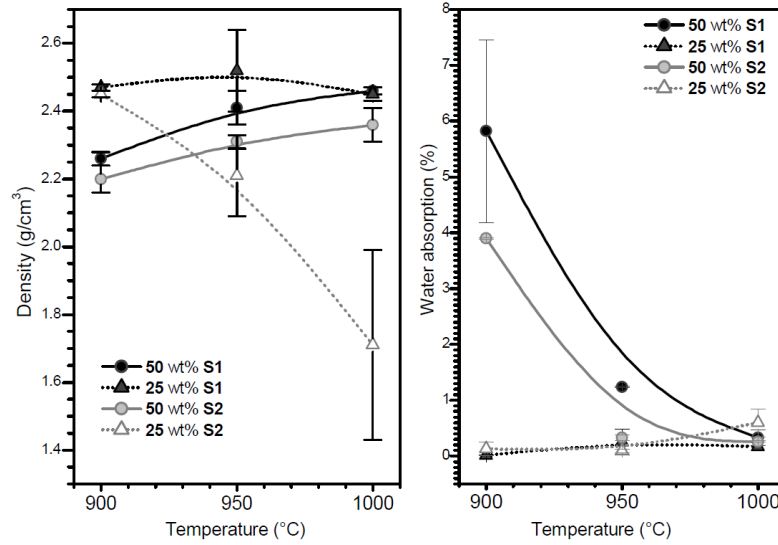
Figure V.20: Density and water absorption evolutions with composition and temperature (B-spline lines are provided simply as guides for the readers' eye)
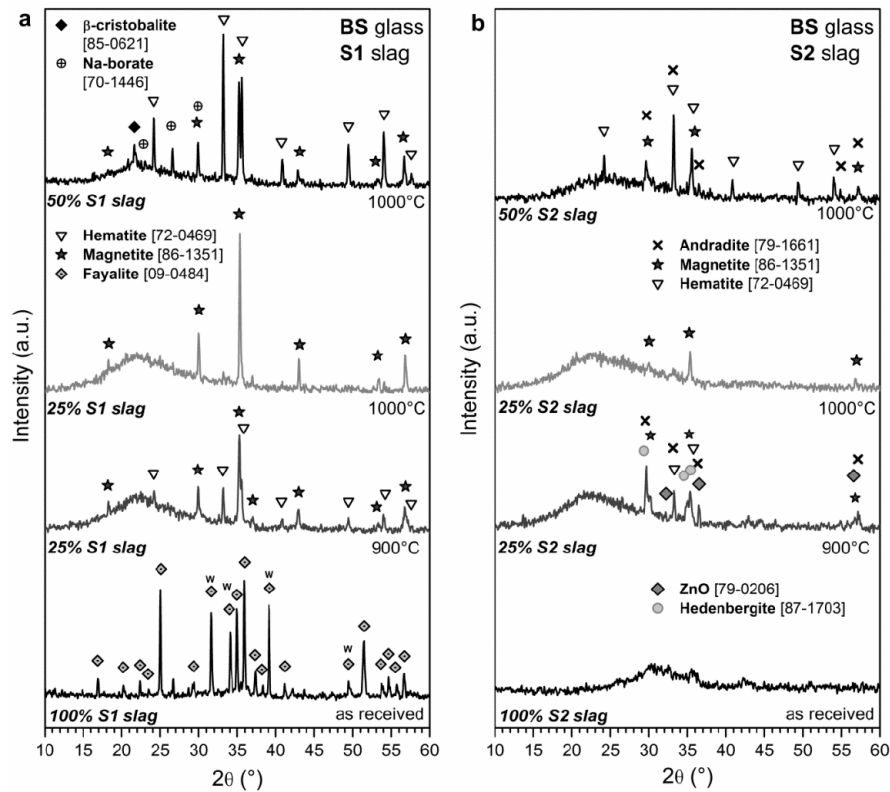
Figure V.21: Crystalline phase evolution of glass/slag mixtures based on (a) S1 slag, (b) S2 slag.

Softened borosilicate glass reasonably "glued" the slag particles, progressively removing the interstitial porosity. Such densification was more efficient with increasing temperature (causing a decrease of viscosity) and at the outer part of samples, obviously hotter (being closer to the heating

elements). In fact, the latter effect is clearly evident on some samples fired at 1000 °C, in which water absorption approached zero and only internal closed porosity remained (Bernardo, 2008; Bernardo *et al*., 2010).

The samples with low slag content (25 wt% of S1 or 25 wt% of S2) exhibited negligible water absorption even at 900 °C. The increased glass content evidently caused a more intensive viscous flow with the sealing of external porosity. The density, however, had quite surprising trends; whereas the density of samples featuring S1 slag remained almost stationary, the density of samples containing S2 slag exhibited a remarkable decrease with increasing firing temperature (from 2.45 g/cm^3, at 900 °C, to 1.7 g/cm^3, at 1000 °C).

The different behavior of samples with different slags and/or with different slag concentration is attributed to the specific glass/slag interactions. As demonstrated by the X-ray diffraction patterns in figure V.21, the borosilicate glass did not merely encapsulate the slags in a glass matrix, but promoted phase transformations.

The S1 slag, in the as-received conditions, as shown by figure V.21a, contained fayalite, i.e. Fe(II) silicate (Fe$_2$SiO$_4$ or 2FeO·SiO$_2$, PDF#09-0484). The intensity of some peaks (labelled with "w") is actually significantly higher than that of pure fayalite, which could be due to the incorporation of Zn^{2+} ions, with the formation of a solid solution; this is supported by the fact that willemite (Zn$_2$SiO$_4$ or 2ZnO·SiO$_2$, e.g. PDF#02-1413) effectively possesses strong peaks in the selected positions (label "w" in figure V.211a) and forms solid solutions with fayalite (Ettler et al., 2000; Raghavan, 2010).
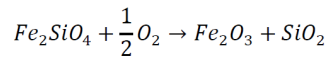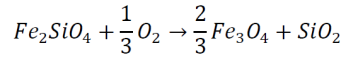
Air, i.e. an oxidative atmosphere, may cause the decomposition ("oxygenolysis") of fayalite, with the formation of iron oxides, according to the following reactions (O'Neill, 1987):

$$Fe_2SiO_4 + \frac{1}{3}O_2 \rightarrow \frac{2}{3}Fe_3O_4 + SiO_2$$

$$Fe_2SiO_4 + \frac{1}{2}O_2 \rightarrow Fe_2O_3 + SiO_2$$

(Note: all equations should be completed within a two column table with one line, centered, no boarders, as example see above).

At 900 °C, with S1 slag present in the amount of 25 wt%, both reactions likely occurred, with the formation of magnetite, i.e. iron oxide with both Fe^{2+} and Fe^{3+} (Fe$_3$O$_4$, or FeO·Fe$_2$O$_3$ – PDF#86-1351), and hematite, i.e. iron oxide with only Fe^{3+} ions (Fe$_2$O$_3$, PDF#72-0469), well visible in the pattern in figure V.21a. At 1000 °C, with the same concentration of S1 slag, magnetite was favored, consistently with the high temperature reduction of iron oxides in a viscous mass, associated to oxygen release, as discussed by Appendino et al. (2004). It can be noted that crystalline silica is not visible in the patterns for 25 wt% S1 slag: the secondary product of oxygenolysis reaction was probably dissolved by the borosilicate glass.

Operating with 50 wt% S1 slag, as illustrated by the upper pattern in figure V.21a, magnetite and hematite are confirmed as the main crystal phases. However, in this case, hematite is dominant. This behavior is likely due to more intensive oxygen diffusion, promoting the reaction induced by Eq.(2): the reduced viscous flow, associated to the lower glass content, probably did not allow an instantaneous sealing of the slag particles from atmospheric oxygen.

The minor phases detected in the X-ray diffraction pattern of sample with 50 wt% S1 slag are quite interesting. Whereas sodium borate [Na$_2$B$_6$O$_{10}$ or Na$_2$O·3B$_2$O$_3$, PDF#70-1446] could be attributed to the crystallization of the distinctive boron-rich phase of borosilicate glasses

(borosilicate glasses typically exhibit phase separation (Shelby, 2005)), the observed variety of crystalline silica, i.e. β-cristobalite, could be seen as a proof of glass-slag interaction. The detected phase could form by incomplete dissolution of silica from oxygenolysis, and it could be stabilized in the high temperature variant (β-phase) by incorporation of alumina, relatively high in the adopted borosilicate glass (Bernardo *et al.*, 2009) (SiO_4 tetrahedrons may be partially replaced by AlO_4 tetrahedrons, with extra cations, such as Na^+, Ca^{2+}, Cu^{2+} and Sr^{2+}, from both glass and slag, compensating the charge variation from Si^{4+} to Al^{3+}) (Thomas, *et al.*, 1994).

As shown by figure V.21b, S2 slag was practically amorphous in the as-received conditions; the mixing with borosilicate glass yielded again iron-rich phases, comprising both Fe^{2+} and Fe^{3+}, but mainly in association with calcium oxide. This is not surprising owing to the much more significant content of CaO in S2 slag compared with S1 slag. With limited slag content (25 wt%), the firing at 900 °C caused the separation of calcium-iron silicates, such andradite ($Ca_3Fe_2(SiO_4)_3$, PDF#79-1661), featuring Fe^{3+} ions, and hedenbergite ($CaFeSi_2O_6$), featuring Fe^{2+} ions. Magnetite and hematite, dominant with S1 slag, are reasonably still present, in form of traces, as well as zinc oxide (ZnO, PDF#79-0206). As observed for S1 slag, a temperature increase, starting from the same slag concentration, favored the formation of magnetite, with the rest of crystal phases dissolved by the borosilicate glass. The remarkable reduction of density could be due to the previously mentioned oxygen release, in turn provided by Fe^{3+}/Fe^{2+} reduction, causing some foaming. Indeed, due to the higher content of network modifiers provided by the S2 slag, it is expected that the glass phase would be less viscous and more prone to foaming, than in the case of S1 slag.

Operating with high content (50 wt.%) of S2 slag, in analogy with the samples made with S1 slag, the formation of more oxidized phases was favored. In fact, magnetite is present (see upper pattern of figure V.21b) coupled with andradite and hematite.

V.4.4 Mechanical characterization and functional properties

Sample	Sintering Temperature (°C)	Apparent density (g/cm³)	Porosity (%)	Elastic modulus (GPa)	Bending strength (MPa)	Vickers Hardness (GPa)
25% S1	900	2.34 ± 0.01	7.9 ± 0.5	69.0 ± 14.9	39.6 ± 11.1	5.3 ± 2.1
50% S1	1000	2.39 ± 0.01	16.4 ± 0.5	62.3 ± 13.4	33.0 ± 1.3	5.9 ± 1.1
25% S2	900	2.32 ± 0.01	9.6 ± 0.5	69.3 ± 4.8	37.6 ± 6.2	4.6 ± 0.7
50% S2	1000	2.39 ± 0.01	18.1 ± 0.5	56.8 ± 3.0	32.4 ± 7.6	5.4 ± 1.3

Table V.11: Physical and mechanical properties of selected glass-ceramics based on glass/slag mixtures.

Table V.11 summarizes the properties of samples based on S1 and S2 slag, sintered in the form of rectangular tiles. In this case, in order to mimic industrial firing, heating was performed at a steady rate (40 °C/min) and the samples were not removed from the furnace directly at high temperature, to avoid thermal shock. We focused on the conditions (concentration, temperature) that could maximize the density, on one hand, and minimize the water absorption, on the other.

The density values are in good agreement with those referred to small discs, subjected to direct heating. Despite the relatively high residual porosity (inferred from image analysis), varying from 8 to 18%, the obtained glass-ceramics compare favorably, in terms of elastic modulus, bending strength and Vickers hardness, with analogous waste-derived glass-ceramics (Cheng and Chen,

2004; Cheng et al., 2007). Like analogous waste-derived glass-ceramics, owing to the negligible water absorption, the developed materials could be used as low-cost building materials.
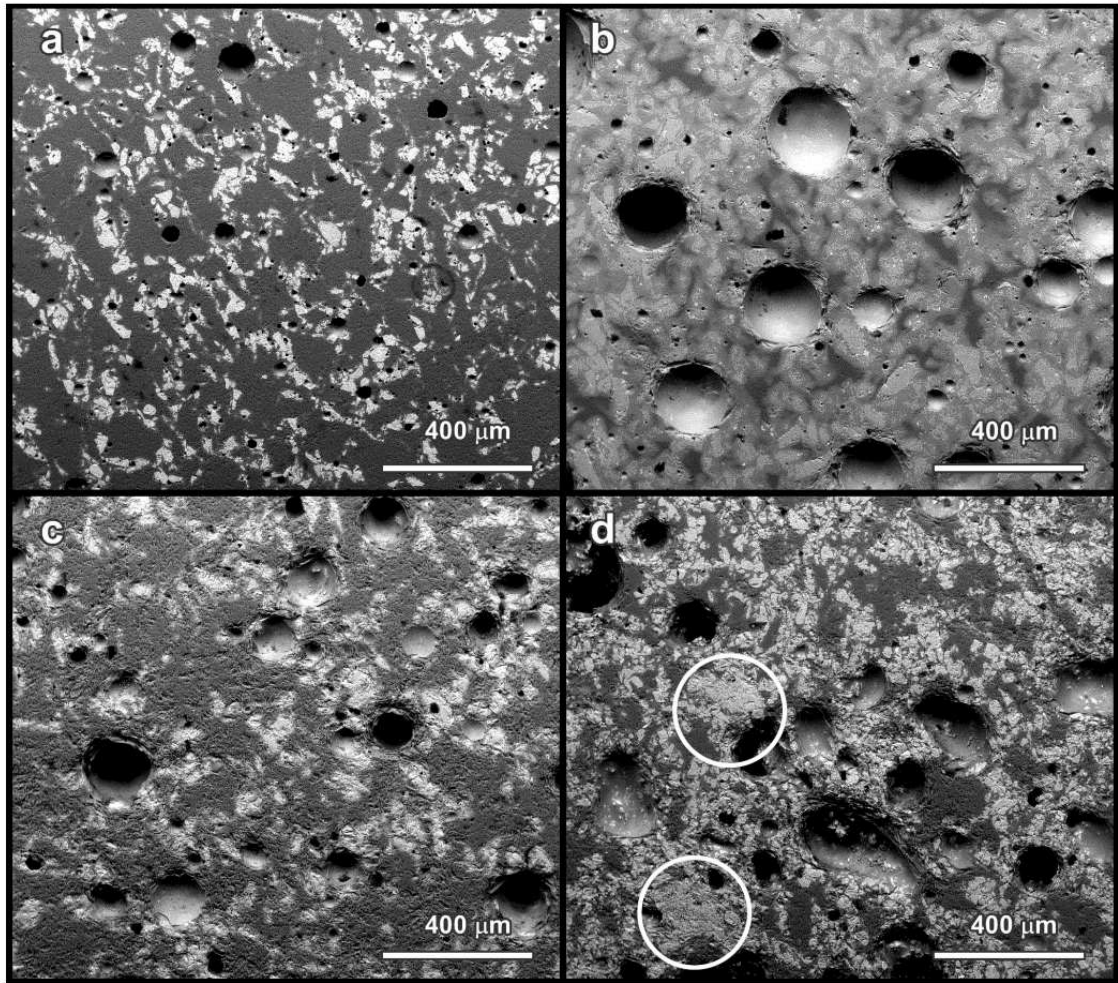
Figure V. 22: SEM micrographs of selected glass-ceramics (polished surfaces of bending bars, cut from rectangular tiles): (a) 25 wt% S1, 900 °C; (b) 50 wt% S1, 1000 °C; (c) 25 wt% S2, 900 °C: (d) 50 wt% S2, 1000 °C.

The SEM micrographs in figure V.22 confirm a quite homogeneous distribution of components in the glass-ceramic microstructure. In particular, iron-containing phases may be easily distinguished from the light color in the back-scattered electrons images. The homogeneity is particularly important for the stabilization of pollutants. In fact, the chemical homogeneity of a glass-ceramic from simple sintering of glass/slag mixture is obviously lower than that of a glass-ceramic obtained from melting, solidification of a glass and crystallization; pollutants may selectively accumulate in aggregates of slag particles not completely encapsulated in the liquid phase provided by the glass. Except for figure V.22d (see highlighted areas), showing a sample with 50 wt% S2 slag, sintered at 1000 °C, no large slag-derived aggregates are visible. On the contrary, the sample with 50wt% S1 slag sintered at 1000 °C, shown in figure V.22b, exhibits iron-rich phases (light spots) surrounded by a light halo. To our opinion, this could be due to iron diffusion in the borosilicate glass, a further evidence of glass/slag interactions.

The large pores, visible especially with 50 wt% S1, at 1000 °C (figure V.22b), are hardly explainable as derived from incomplete sintering. As reported above, the firing at 1000 °C could favor some oxygen release, from the reduction of iron oxides; magnetite could not be simply a product of the oxygenolysis of fayalite, but also a product of hematite reduction:

$$3 \, Fe_2O_3 \rightarrow 2 \, Fe_3O_4 + \frac{1}{2}O_2$$
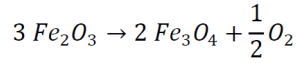
The phase development in the developed glass-ceramics suggests a possible application as tiles with a specific functionality. In fact, all the samples feature magnetite, i.e. a ferrimagnetic phase.

V.4.4 Induction tests

V.4.4.a Introduction to magnetism

Magnetic fields are produced by electric currents. At the atomic scale, the electronic orbitals or electron spins create magnetic fields, and then elementary magnetic moments. The result of the alignment more or less rigorous of the elementary magnets in a solid body is presented as an M magnetization which is the magnetic moment by volume unit. To realize this alignment, it will be in general necessary to apply a magnetic field H; the new can define the magnetic susceptibility of a material by: $\chi = M/H$, where χ is the susceptibility by cm^3.

More generally, solid compounds are shared, from a magnetic view, into two families, non-ordered magnets (non-cooperative magnetism) and ordered magnets (cooperative magnetism). In the first case, the interactions between atoms in the crystalline network are low (no long distance interactions) and then unable to develop a magnetic order. Those materials do not show spontaneous macroscopic magnetization. We distinguish: i) Diamagnetism an intrinsic property of the matter leading to a negative value of the magnetic susceptibility; ii) Paramagnetism, due to electrons not paired to ions or free electrons of metals.

However, some substances present a magnetic order spontaneous (cooperative magnetism) so that even in the absence of an external field, the electronic spins and the magnetic moments are arranged regularly due to the existence of the electrostatic exchange interaction. This order can be parallel (ferromagnetism), antiparallel with a compensation of the moments (antiferromagnetism) or antiparallel without compensation of the moments (ferrimagnetism) (see table V.12).

In the ferromagnetic bodies, the magnetic moments are already aligned: they form parallels under the effect of an internal field called "Weiss field". The magnetization is then present even without an excitation field. However, when the temperature rises, the thermal agitation tends to more and more compensate the effect of Weiss field, magnetic moments get disordered and over a critical temperature, Curie temperature, the body (e.g. metal) becomes paramagnetic with a magnetic susceptibility that decreases with the temperature. Ferrimagnets are materials in which the magnetic domains are subdivided into magnetic regions of varying intensities that cannot form opposite direction alignments, and which result in a non-zero magnetic moment.
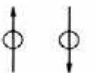
Table V.12: The types of magnetic behaviors

The ferrimagnetic bodies, represented by ferrites, a particular iron oxides family, have similar properties to ferromagnetic substances: they possess a resultant magnetization not zeroed in the absence of external magnetic field and then are considered as magnets. Contrarily to ferromagnetic materials, ferrimagnetic bodies are electric insulators, which make them interesting in the industry, notably in radio electricity. For example, magnetite counts among the ferrimagnetic substances and enables to product permanent magnets.
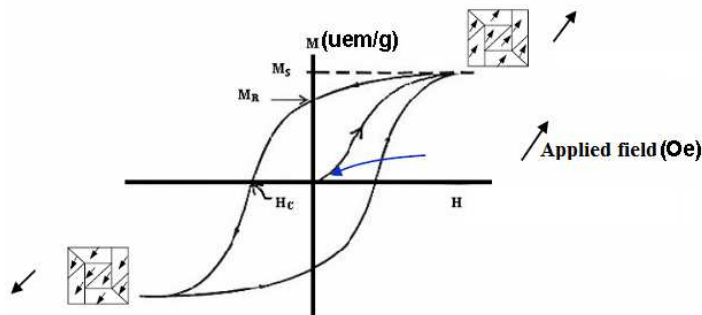
Figure V. 23: Hysteresis cycle of the magnetization in function of the magnetic field applied (H) where MS is the saturation magnetization, MR is the remanent magnetization and HC is the coercive field.

In the case of ferro- or ferrimagnetic materials, the magnetization is uniform inside each domain but vary from a domain to the other so that in the absence of external field, there is no global magnetization (figure V.23). The crystals of spinel structure AB_2O_4, in which A and B represent cations, have the possibility to show ferrimagnetism. Particularly in the present case, ferrites such as magnetite Fe_3O_4 show this property, indeed, the structure is built with FeO_6 octahedrons and FeO_4 octahedrons, corresponding to a separation between the oxidation states of iron as following : $FeO \cdot Fe_2O_3$, Fe^{3+} in FeO and Fe^{2+} in Fe_2O_3. Indeed, the spinel structure is composed of ions O^{2-}, ions Fe^{2+} situated in octahedral sites and half ions Fe^{3+} in ¼ of octahedral sites and the other half in 1/8 of tetrahedral sites (figure V.24, Daou, 2007).
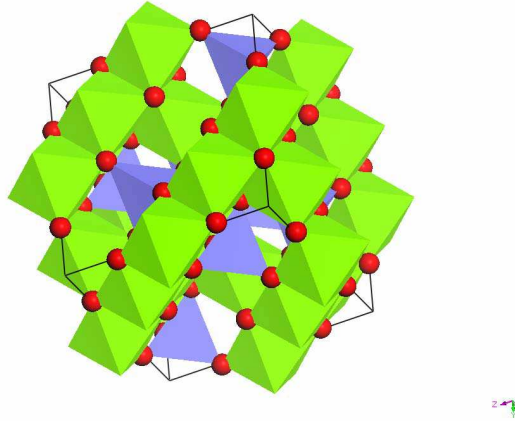
Figure V.24: Spinel structure, tetrahedral sites are represented in blue, octahedral sites in green and oxygen atoms in red. The elementary row is represented with a black line.

V.4.4.b Application to the elaborated materials

As presented in several reports concerning hyperthermia applications of ferrimagnetic materials (Andreu and Natividad, 2013; Jordan *et al*. 2009), when an alternating magnetic field (AMF) is applied to a ferrimagnetic material, the non-linearity and the delay of its magnetization with respect to the applied magnetic field originate a distinctive hysteresis loop; energy is dissipated, in the form of heat, for every cycle, i.e. for each alternation in the value of external field. Figure V.25a illustrates that the developed glass-ceramics effectively exhibited, for the samples with low slag content (25 wt% S1 and 25 wt% S2), an intensive heating when subjected to AMF. More precisely, the sample from S1 slag, sintered at 900 °C, reached 300 °C after only 60 s of application. Interestingly, the samples did not exhibit any cracking upon cooling, when AMF was switched off. The resistance to thermal shocks was probably favored by the relatively low thermal expansion of the adopted borosilicate glass (5.5 10^{-6} °C^{-1} , Bernardo *et al*., 2009) and by the porosity (reducing the elastic modulus). To our opinion, these findings could be the basis for the valorization of metallurgical slags, coupled with borosilicate glass, in the manufacturing of innovative heating elements, e.g. parts of cooking tops. Indeed fabrication of magnetic glass-ceramics from waste has been exploited in the past (Colombo *et al*., 2003; Francis *et al*., 2004; Francis, 2006; Rosenweig *et al*., 2002) but no detailed investigation on heat generation under AMF has been presented.

99
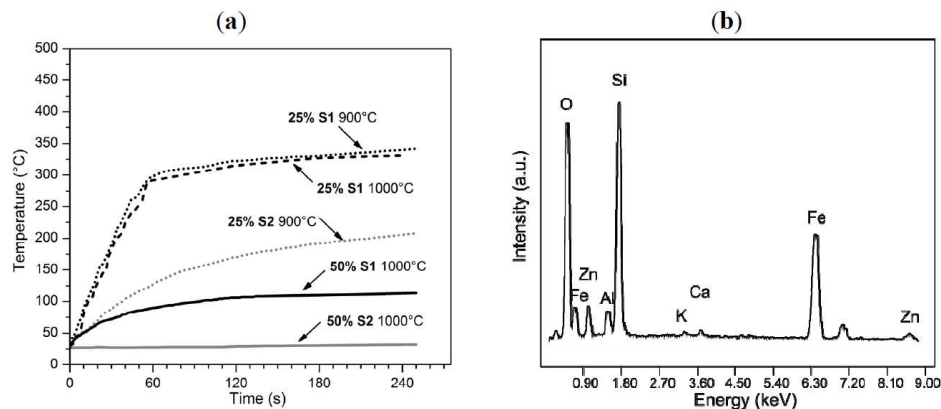
Figure V.25: (a) Heating of glass-ceramics from glass/slag mixtures under alternating magnetic field (AMF); (b) EDS spectrum of slag-derived aggregate in the sample with 50wt% S2, sintered at 1000 °C.

The samples with high slag content presented poor (50wt% S1) or even no (50wt% S2) temperature increase, despite the presence of magnetite. This phenomenological "anomaly" could be justified by the observed ionic inter-diffusion, as discussed earlier. Samples treated at 1000 °C did not feature pure magnetite, but a solid solution, comprising ions such as Zn^{2+}, as demonstrated by the EDS spectrum in figure V.25b. Ferrites, i.e. compounds with the general formula $M^{2+}O \cdot Fe_2O_3$ are known to exhibit lower heating rates compared to magnetite (Rosenweig, 2002). The formation of a Zn-containing solid solution, instead of pure magnetite, could be the reason also for the behavior of the sample containing 25% S1 slag, sintered at 1000 °C; despite the more intense peaks of ferrimagnetic phase (and no evidence of hematite) in figure V.20b, it was similar, in its electromagnetic heating behavior, to the sample from S1 slag, sintered at 900 °C.

The interdiffusion, at 1000 °C, between glass and slags, even in a low concentration (25 wt%), is testified by figure V.26. The SEM image in figure V.26a, referring to the sample with 25 wt% S1, clearly shows more "isolated" light spots (rich in iron), than in the case of the sample with the same composition sintered at 900 °C (figure V.25a), but also wide diffusion halos around the spots, like in the sample sintered at the same temperature, with higher slag content. The interdiffusion is so extensive for the sample with 25 wt% S2 that halos turn into "streaks", evident in figure V.26b, around big pores. The big pores, for this sample, as written above, actually correspond to a foaming effect, further evidenced by the optical stereomicroscope image in figure V.26c.
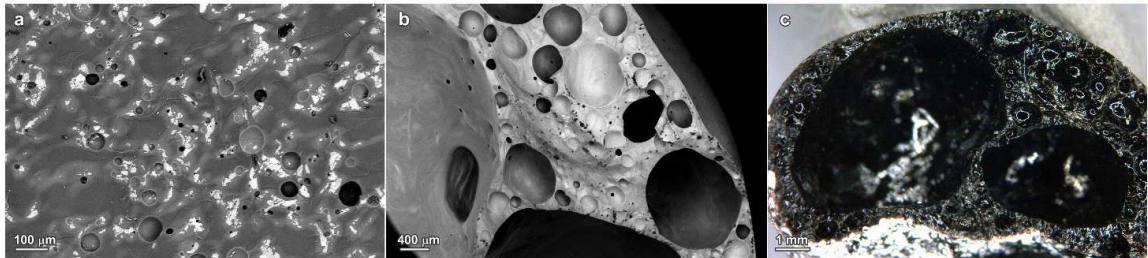
Figure V.26: Microstructural details of selected glass ceramics (a) 25 wt% S1, 1000 °C; (back) 25 wt% S2, 1000 °C (image (c) is from optical stereomicroscopy).

V.4.5 Chemical stability and cytotoxicity studies

Element	Leachate (ppm)		
Sample	25 wt% S1 900 °C	25 wt% S2 900 °C	EN Limits [#]
As	<0.0049	<0.0049	0.5
Ba	0.0029	0.0538	20
Cd	<0.0002	<0.0002	0.04
Cr	<0.0004	<0.0004	0.5
Cu	<0.0001	<0.0001	2
Hg	<0.0004	<0.0004	0.01
Mo	<0.0033	0.0048	0.5
Ni	0.0302	0.0166	0.4
Pb	<0.0047	0.0077	0.5
Sb *	n.d.	n.d.	0.06
Se	<0.0122	<0.0122	0.1
Zn	<0.0203	<0.0203	4

Table V.13: Chemical analysis of the leachate of samples subjected to TCLP testing (data not determined).*

The most interesting samples, i.e. those exhibiting intensive heating, were evaluated also in terms of chemical stability, a property essential for high value applications. TCLP test was applied as a preliminary approach. As reported in table V.13, the contents of toxic elements were all well below the limits for inert materials. Although successful, TCLP test was not considered as a definitive proof of inertness, since it is intended mainly for the certification of wastes, rather than for the characterization of products. In addition, antimony (Sb) was not determined, owing to problems of instrument calibration.
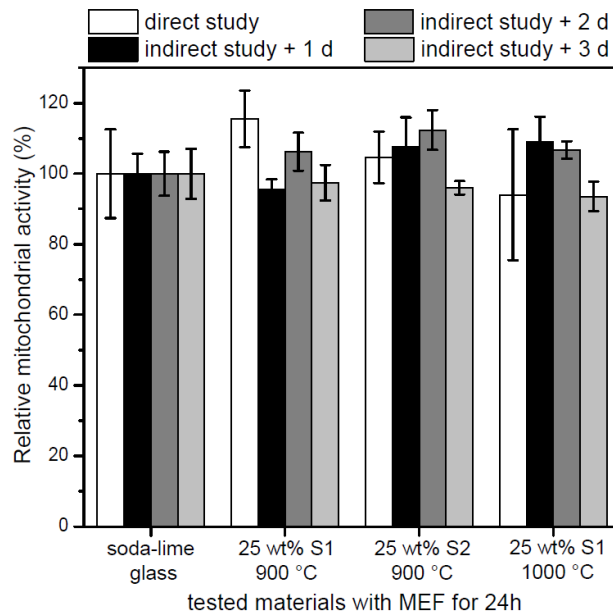
Figure V.27: Relative cell viability of slag/glass samples, compared with soda-lime.

The assessment of the biocompatibility of waste-derived products by cell biology investigations, although being of high relevance to certify the safety of these materials for general use, has been considered only to a limited extent in the past (Boccaccini *et al.*, 1997). As discussed recently (Ponsot *et al.*, 2014), there is therefore increasing interest to provide data about the safety of waste-derive products based on established cell-culture based cytotoxicity studies. In this

investigation, MEF cell cultures were considered to analyze possible cytotoxic effects of the glass-ceramics produced. Generally, MEF cells are applied in the characterization of biomaterials, e. g. materials for use in medical applications. In this study the iron containing glass-ceramics were subjected to cell culture tests and results were compared with those on materials considered to be safe for every-day use, i.e. soda-lime glass. In cell proliferation analysis, mitochondrial activity was considered as an index of the toxicity level of the examined materials. Soda-lime glass was taken as a reference as a well-known "safe" product. Its mean mitochondrial activity was set at 100% ± standard deviation. Figure V.27 illustrates the relative mitochondrial activity of MEF cells after 24 hours of seeding on waste-derived glass-ceramics and soda-lime glass, according to both direct and indirect studies. It can be noted that the mitochondrial activity of samples was practically equivalent to that of the reference glass. During the direct study, samples topology directly impacted on cells adherence. The higher values found for samples 25 wt% S1 900 (113% ± 9) and 25 wt% S2 900 (106% ± 8) could be attributed to porosity, which favors cells adherence. During the indirect study (black and grey bars), cells seeded on microplates were in contact with ions in the medium, released by samples after 1, 2 and 3 days dilution.
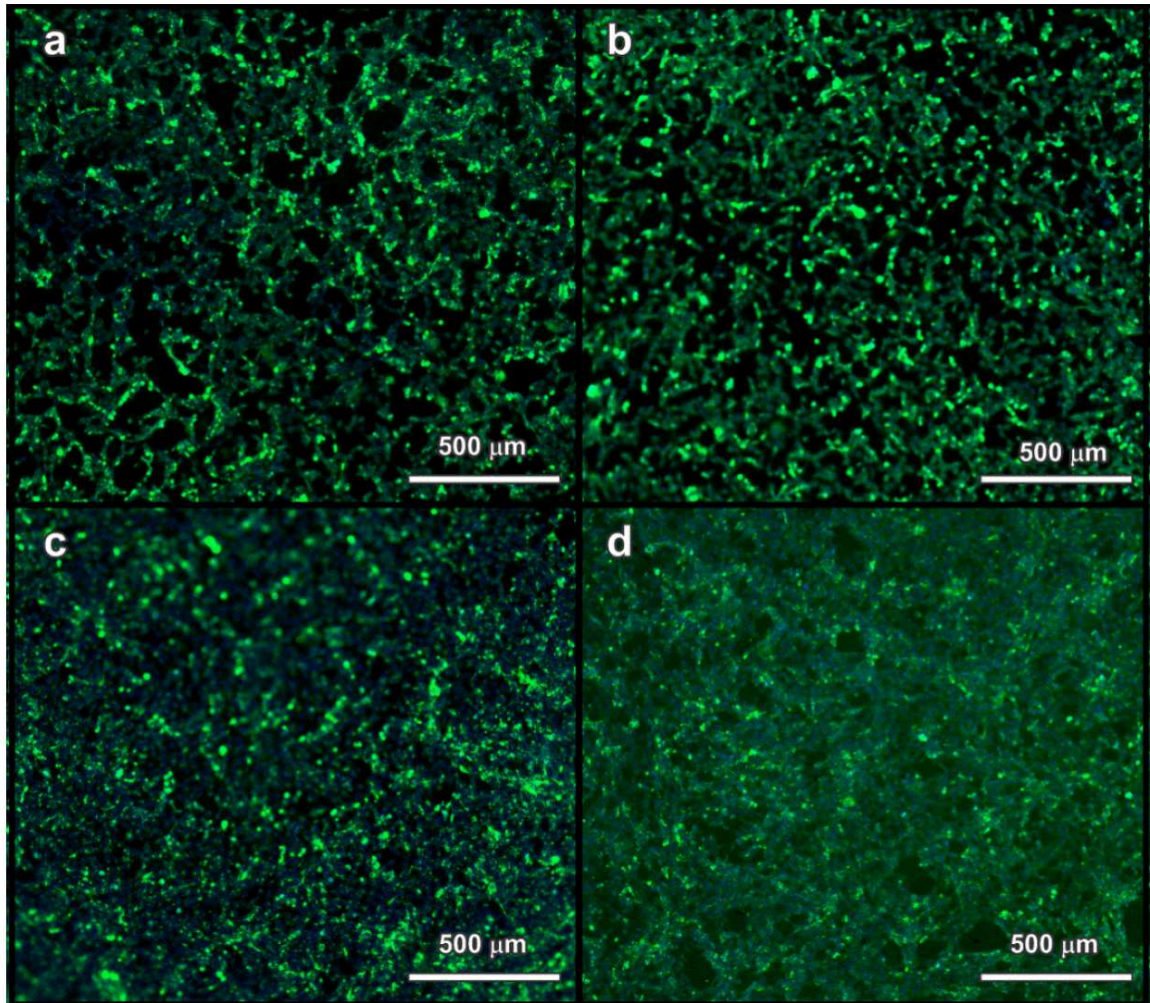
Figure V.28: Fluorescence microscope images of samples from direct test method (a) 25 wt% S1 900 °C; (b) 25 wt% S2 900 °C; (c) 25 wt% S1 1000 °C; (d) soda-lime glass (reference) [with superposition nucleus (blue) and cell body (green)].

The fluctuation of values was not interpreted further, but it might depend on parameters such as diffusion rate and concentrations of ions in the medium, synergies and interfacial cells/ions biological reactions. Only a significant drop of mitochondrial activity (not observed) could be reasonably attributed to environmental toxicity. In fact, the non-toxicity value limit value could be set at 50% mitochondrial activity, relatively to the reference glass, according to previous toxicology studies (Trevan, 1927). We can therefore state that, under the conditions of the applied test, none of the samples presented toxicity risk, even after 3 days (indirect study), which was accepted as a significant period to indicate cytotoxicity, considering the quasi instantaneous reactivity of MEF to their environment (Boccaccini *et al*., 1997; Ponsot *et al*., 2014).

As illustrated by figure V.28, glass-ceramic samples as well as soda-lime glass were fully covered by MEF cells. The cells exhibited spreading and mutual interconnections, with an elongated morphology, which are well-recognized features to indicate biocompatibility (Boccaccini *et al*., 1997; Ponsot *et al*., 2014). The glass-ceramics, as shown in table V.10, actually contained several elements promoting cellular activity, such as Si, O, Na, K and Ca. In addition, glasses doped with Zn, B, Mg or Fe have shown stimulating effects on cells growth; other minor elements (Al, Cr) are effectively toxic (Hoppe *et al*., 2011). The results of MEF activity indicate that the diffusion rate of toxic elements in the cell culture medium was reasonably limited. In other words, the chemical stability of the adopted borosilicate glass, employed in the pharmaceutical industry, was not degraded by the incorporation of slags in the present glass-ceramics.

V.4.6 Conclusions

The results obtained and discussed in this paper lead to the following conclusions:

- Metallurgical slags were successfully sintered, mixed with recycled borosilicate glass, at temperatures not exceeding 1000 °C. The developed glass-ceramics, owing to the negligible water absorption, could be used as low-cost lightweight tiles;
- Fe-rich phases developed according to slag/glass interactions;
- Owing to the presence of magnetite, the developed glass-ceramics (for a slag concentration of 25 wt%), exhibit intensive heating when subjected to an alternating magnetic field, so that they could be applied as novel heating elements;
- The chemical durability of the glass-ceramics was assessed by TCLP testing while the materials biocompatibility was confirmed by cytotoxicity tests.

V.5 Highly porous glass-ceramics from self-foaming mixtures

SUMMARY - Fe_2O_3 may transform to Fe_3O_4 or FeO by release of oxygen. This reaction provides an interesting alternative route for the manufacturing of glass foams. Additives, such as carbonates and C-containing compounds may be replaced by iron-rich wastes, mixed with different recycled glasses. Partial crystallization is also achieved, by glass/waste interactions. The obtainment of lightweight materials is coupled with the stabilization of pollutants (i.e. the iron-rich wastes are stabilized in the glass matrices), thus configuring a very promising synergy for industrial applications.

V.5.1 Soda-lime waste glass and iron-rich slag from refining of precious metals

Viscous flow sintering of finely powdered glass, at atmospheric pressure, gives the opportunity to prepare new valuable engineering materials, including innovative "glass-based stoneware", as presented in this paper. This new material derives from the substitution of expensive feldspar fluxes with glass, in turn allowing very low processing temperatures (even below 1000 °C) and promoting the incorporation of inorganic waste, such as iron-rich metallurgical slag. In the present case, glass-waste interactions were found to provide a homogeneous foaming, without other additives, and partial crystallization. The specific mechanical properties of the resulting cellular glass-ceramics, being comparable to those of conventional porcelain stoneware, sintered above 1100 °C, suggest an extensive use in the building industry as lightweight panels, considering also the negligible water absorption and the chemical stability.

V.5.1.a Introduction

Traditional ceramics have always been regarded as a reference for the disposal of inorganic waste (Lee, 2006). Since traditional ceramics have a mass market, even a small addition of a given waste to the usual formulations is associated with a remarkable recycling. This concept may be applied even to waste glasses, including glasses from the melting of hazardous waste as well as glasses hardly used in the manufacturing of original articles (Colombo et al., 2003; Kidalova et al., 2012).

Small glass amounts do not determine significant changes in the properties of traditional ceramics, as testified by the experiences with waste glasses introduced in formulations for porcelain stoneware (Brusatin et al., 2005; Karamanova and Karamanov), but this probably represents an underestimation of the potentialities of glass. If we consider glass additions, indeed, viscous flow sintering may occur at much lower temperatures than those required by conventional feldspar fluxes.

Extensive use of waste glass, either waste-derived or recycled, has been presented in recent papers (Bernardo et al., 2008 and 2009, Zhao et al., 2013). In particular, glass completely replaced the ordinary feldspar fluxes, allowing the obtainment of dense stoneware tiles ("glass-based stoneware") at temperatures not exceeding 1000 °C (instead of approximately 1200 °C for conventional formulations). The degradation of mechanical properties is prevented by crystallization, caused by interactions between glass and clay components. On the one hand the sintering temperature is not high enough for mullite formation, on the other residues of clay dehydration (i.e. metakaolinite) may react with calcium oxide, provided by the glass (Bernardo et al., 2008) and/or additives (such as Ca(OH)2) (Bernardo et al., 2009), yielding calcium alumino-silicates.

The present part of chapter V reports a further extension of the concept of revised formulations for stoneware, with most of the raw materials corresponding to waste; specifically, waste soda-lime glass (SL), i.e. a by-product of municipal glass recycling, was considered combined with a vitreous iron-rich metallurgical slag (MS). This slag, being highly concentrated in SiO_2 (see table V.14), cannot be considered for cementer use (Skuza et al., 2009).

The use of metallurgical slag is interesting for the possible interactions between glass and clay components, favoring the crystallization, and for the remarkable content of iron oxide, promoting the development of a highly porous structure by gas release ("bloating" effect, in turn associated to the reduction of Fe^{3+} into Fe^{2+}) (Appendino et al., 2004).

Porosity in materials for modern buildings is highly attractive, particularly for lightweight tiles to be placed vertically. Such tiles are interesting, above all, for ventilated façades, i.e. a new generation of coverings applied on the surface of large buildings, aimed at improved thermal insulation (Infield et al., 2004). As recently reported (Bernardo et al., 2010; Garcìa-Ten et al., 2012) a possible solution is represented by foamed porcelain stoneware, produced at high temperatures (those of conventional production), with the help of expensive additives (CeO2 or SiC). Cellular glass-ceramics, owing to their low water absorption, remarkable mechanical properties and good chemical stability, could be a valid alternative, especially when configuring savings in both raw materials and energy (due to the recycling of waste and low firing temperatures), as presented in this chapter.

V.5.1.b Characterization of the raw materials

The chemical composition of the employed starting materials is reported in table V.14. Pure kaolin clay (Carlo Erba Reagenti SpA, Milan, Italy) was mixed with soda-lime glass (SL), recovered from municipal recycling, and a metallurgical slag (MS), both kindly provided by SASIL SpA (Biella, Italy), in shape of fine powders (< 100 µm). SL does not refer to the fraction of recycled materials, after sorting, which consists of almost pure glass, ready for the industry, but to the fraction enriched in contaminants, which remains practically unemployed and mostly landfilled, in huge quantities (SASIL treats this waste in a quantity of about 180 000 tons/year). MS corresponds to slag from recovery and refining processes of precious metals.

Kaolin clay, SL and MS were considered in three proportions, according to table V.15, showing also the overall oxide contents. Mixture A (SL and MS in equal amounts) can be seen as the reference composition; it was conceived according to previous experiments with sintered glass-ceramics (Bernardo et al., 2012), in which pure kaolin clay, in an amount of 10 wt%, was successfully employed as binder for fine glass powders. Mixture B and C were conceived to evaluate the impact of an increased glass content, which was thought to enhance viscous flow (mixture B), and of an increased slag content, thought to favor crystallization and gas release, by reduction of Fe_2O_3.

Component	Soda-lime glass (SL)	Kaolin clay	Metallurgical slag (MS)
Oxides	Contents (wt %)		
SiO_2	72.3	43.5	55.3
Al_2O_3	2.2	39.0	12.0
Fe_2O_3	0.3	Traces	5.4
Na_2O	12.0		13.9
K_2O	0.9		1.0
CaO	10		12.4
MgO	2.0		Traces
TiO_2	0.1		

Table V.14: Chemical composition of the starting raw materials

Mix	A (reference)	B (glass rich)	C (slag rich)
Formulation	Contents (wt %)		
SL	45	54	36
MS	45	36	54
Kaolin clay	10	10	10
Oxides	Contents (wt %)		
SiO_2	61.8	63.3	60.2
Al_2O_3	10.3	9.4	11.2
Na_2O	13.0	12.8	13.1
CaO	11.2	11	11.4
Fe_2O_3	2.6	2.1	3.0

Table V.15: Formulation of the investigated mixtures

The amorphous character of MS is confirmed by the preliminary diffraction analysis shown in figure V.29. The same figure testifies the remarkable crystallization tendency of MS powders, fired at 1000 °C without additives. The developed crystal phases consist of calcium-sodium alumino-silicate ($2\ CaO \cdot Na_2O \cdot Al_2O_3 \cdot 4\ SiO_2$, PDF#76-0479), nepheline ($Na_2O \cdot Al_2O_3 \cdot 2\ SiO_2$, PDF#79-0993) and hematite (Fe_2O_3, PDF#87-1166). The separation of an iron oxide is interesting, since it reasonably acted as a nucleating agent, thus justifying the extensive crystallization (in figure V.29, the amorphous halo is practically absent for fired MS). This situation is rather similar to that of glass-ceramics from melted basalts, for which the separation of iron oxides is even promoted by adding oxidizing agents in the melt (Höland and Beall, 2002). In the present case, the oxidation (with the formation of ferric oxide, Fe_2O_3, i.e. the oxide associated to the higher valence state of iron ions) was favored by the high specific surface of glass powders (Chinnam et al., 2013).
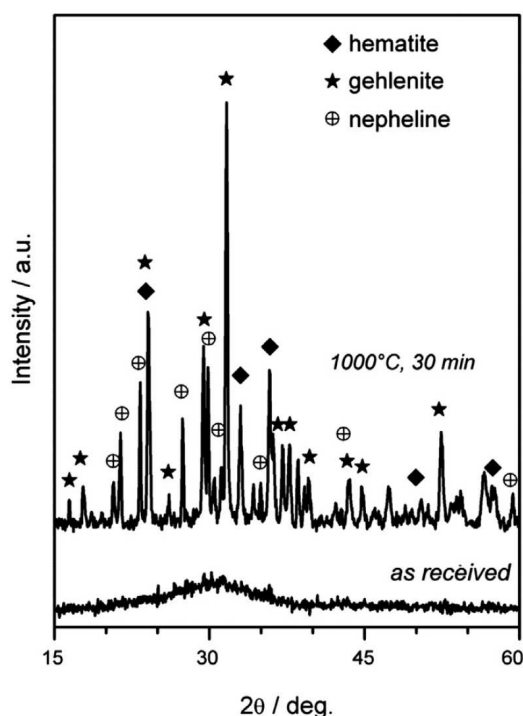
Figure V.29: Preliminary mineralogical analysis of MS slag, as received and after treatment at 1000 °C, with no additive, showing Nepheline $Na_2O.Al_2O_3.2SiO_2$

V.5.1.c Characterization of the sintered samples

As illustrated by figure V.30, both bulk density and water absorption of mixtures based on MS and SL decreased sensibly with increasing firing temperature. The general decrease of water absorption is not surprising, since the viscous flow of the liquid phase provided by glass softening is expected to seal the open porosity, at the surface. This sealing effect should be somewhat favored by the adopted firing strategy (direct introduction of samples in the furnace at selected temperatures), with the surfaces experiencing a much faster heating.

The remarkable decrease of bulk density could be attributed to the gas release from iron oxide reduction (release of oxygen according to $2 Fe_2O_3 \rightarrow 4 FeO + O_2$), causing a foaming effect (see Figure V.32). The foaming is not straight forward, since the partial crystallization (expected on the basis of the firing of MS alone) may complicate the viscous flow (rigid, crystalline inclusions are known to enhance the viscosity - Perrot, 1998). Above 1000 °C, the foaming was so intensive that bulk density was well below 2 g/cm^3 for all formulations; water absorption, however, was negligible only for formulation A. This formulation evidently featured an optimized balance between viscous flow, crystallization and gas release.

Figure V.31 confirms the crystallization of the samples, and evidences some changes according to the sintering temperatures and the formulations. Nepheline ($NaAlSiO_4$ or $Na_2O·Al_2O_3·2SiO_2$, PDF#79-0993), already found for pure MS, was visible especially at low temperatures. Wollastonite, i.e. calcium mono-silicate, was the other main phase, becoming dominant above 950 °C, as shown by figure V.31a. Interestingly, the best matching of diffraction data (see reference pattern) is provided by the iron-containing variant, that is $Ca_{2.87}Fe_{0.13}(SiO_3)_3$ (PDF#83-2198). The fact that this solid solution includes Fe^{2+} ions, coupled with the lacking of hematite, may be seen as a confirmation of the expected reduction of iron oxide.
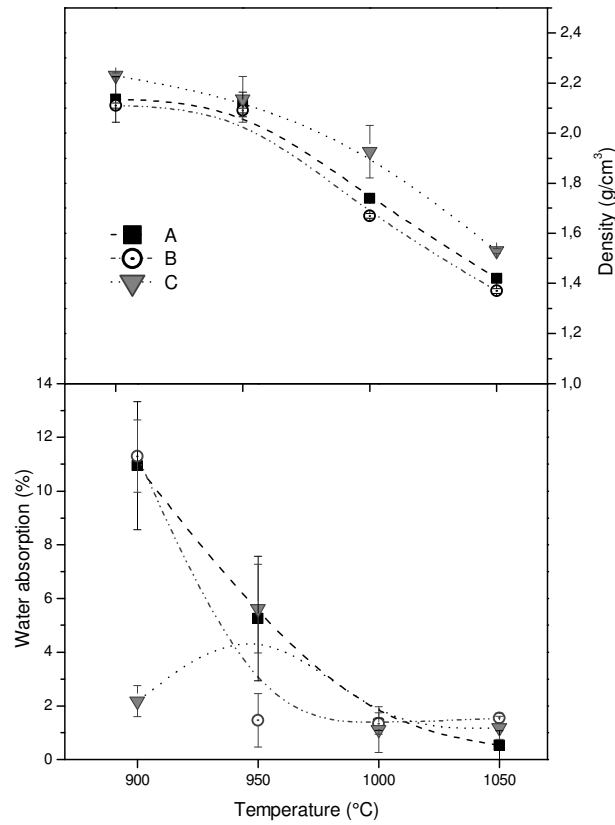
Figure V.30: Density and water absorption evolution with increasing firing temperature

Both wollastonite and nepheline exhibited a decreasing trend with increasing temperature, but with significant differences associated to the compositions, as shown by the "quantitative comparisons" illustrated in figure V.31b. It is well known that the intensity of diffraction peaks is proportional to the quantity of a crystal phase; for comparison purposes, we referred to the intensities of two characteristic main peaks ($2\theta = \sim 23°$ for nepheline, $2\theta = \sim 30°$ for wollastonite), for each sample and sintering temperature, and plotted them normalized by the maximum intensities in the whole set ("normalized intensities").

Nepheline was maximized at 900 °C, for formulation A, whereas wollastonite was maximized at 950 °C, for formulation B. It is evident that the "slag-rich" composition (C) promoted nepheline formation, in good agreement with a higher overall Al_2O_3 content (favorable to alumino-silicates); on the contrary, the "glass-rich" composition (B) favored wollastonite crystallization (at 1050 °C, the wollastonite normalized intensity is about 60%, while the nepheline normalized intensity is slightly above 20%).
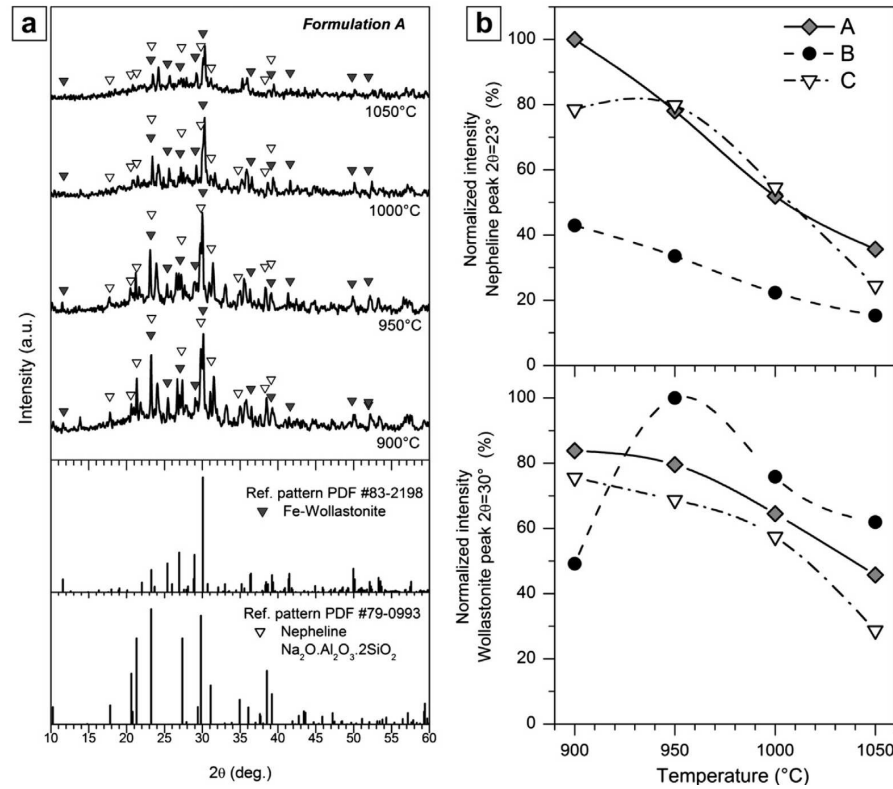
Figure V.31: Impact on crystallization of different processing conditions: a) phase evolution with increasing firing temperature (mixture A); b) intensity of distinctive peaks of major phases with increasing firing temperature, for different compositions

For the above cited application as lightweight tiles, to be placed vertically in the so-called ventilated façades, density and water absorption should be below 1.8 g/cm^3 and 2%, respectively, in order to minimize the weight of coverings and exhibit good frost resistance (Bernardo *et al.*, 2010). Such optimum conditions were reached in five cases (formulation A at 1000 °C and 1050 °C, formulation B at 1000 °C and 1050 °C, formulation C at 1050 °C), but the mechanical tests involved only the samples fired at 1050 °C, possessing values significantly below the limits. The mechanical properties, as reported in table V.16, are quite promising.

Sample	Sintering temperature (°C)	Density, ρ (g/cm^3)	Water absorption (%)[a]	Elastic modulus (GPa)	Bending strength, σ (MPa)[b]	Specific strength $\sigma^{1/2}/\rho$ (MPa$^{1/2}$ cm^3/g)
A	1050	1.52 ± 0.06	0.5 ± 0.5	16 ± 5	19.0 ± 2.0 [24.9 ± 7.1]	2.8 [3.3]
B	1050	1.30 ± 0.13	1.6 ± 0.2	24 ± 6	12.9 ± 3.1 [19.3 ± 12.6]	3.1 [3.4]
C	1050	1.72 ± 0.07	1.2 ± 0.4	27 ± 1	18.9 ± 4.1 [21.6 ± 14.1]	2.52 [2.70]

[a] Determined on as-fired samples.
[b] Data for unpolished specimens reported between square brackets.

Table V.16: Physical and mechanical properties of selected glass-ceramic foams

Compared to conventional dense porcelain stoneware, the developed materials are much weaker in terms of bending strength (according to Raimondo et al., 2011, the bending strength of dense stoneware is the range of 35 to 85 MPa), but quite similar considering the specific strength ($\sigma^{1/2}/\rho$, where σ is the bending strength and ρ is the density), i.e. an index of mechanical efficiency for materials to be applied in form of panels (according to Ashby's studies - Ashby, 1995).
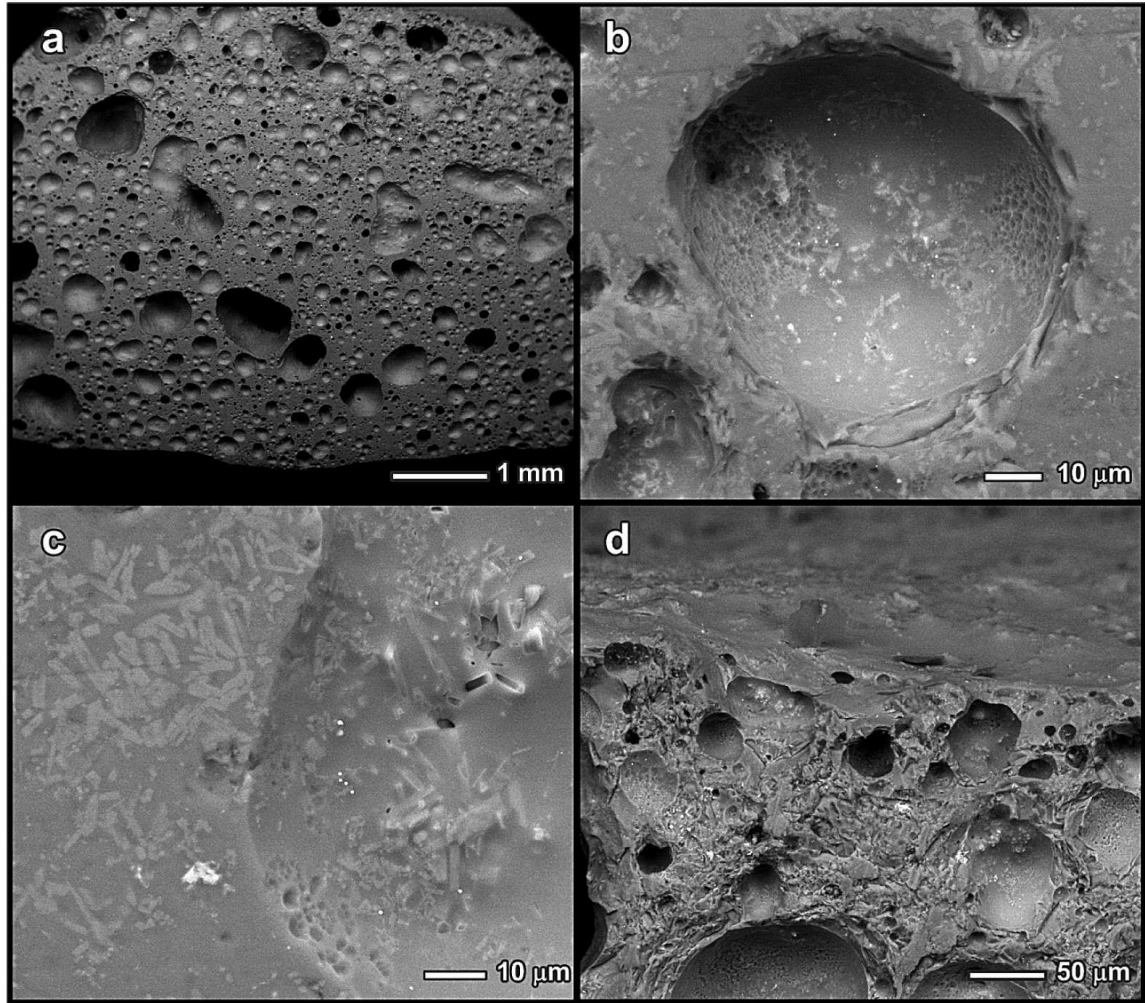
Figure V.32: Microstructure detail of a "self-glazed" glass-ceramic foam (formulation A): a) cross-section; b) crystallization at the surface of macro pores; c) degasification and sinter-crystallization micro pores; d) evidence of formation of a dense surface layer

The specific strength of the developed cellular glass-ceramics is close to the range of 3.4 to 3.8 $MPa^{1/2} \cdot cm^3/g$, reported for conventional stoneware (Bernardo et al., 2010). It should be noted that the bending strength was first determined on specimens cut from bigger samples and subjected to abrasion and polishing; since the preparation of specimens was associated to the removal of the dense layer at the surface, some stress concentration could be provided by the pores emerging at the surface. As reported in table V.16, unpolished specimens (bending bars from simple slicing of bigger tiles, upper and lower surfaces corresponding to the as-fired surface) exhibited a strong dispersion of strength data (reasonably due to cracks induced by cutting) but also a significantly higher average value (3.13 $MPa^{1/2} \cdot cm^3/g$) compared to the polished ones (2.80 $MPa^{1/2} \cdot cm^3/g$): the dense surface layer is evidently a reinforcing part.

The microstructure details reported in figure V.32 are in good agreement with the previous observations. The good mechanical properties (especially the specific strength) could be justified by the remarkable homogeneity of pore distribution, as clearly shown by figure V.32a. The partial crystallization is testified by figure V.32b, which depicts a multitude of crystals formed near the pore surface. As observed in other sintered glass-ceramics, this is consistent with the tendency

towards surface crystallization of calcium silicates (Gutzow and Shmelzer, 1995) (the surface of pores represents a "free surface", in which the volume variations associated to crystallization could be accommodated easier than in the bulk). Finally, figure V.32c evidences the presence of a dense layer (a sort of "self-glazing") on the outer part of unpolished specimens: the more intense heating at the surface promoted the viscous flow; any pore from oxygen release reasonably collapsed.

Element	Leachate (ppm)			EN limits L/S = 10 l/kg
	Sample A	Sample B	Sample C	
As	<0.0067	<0.0082	<0.009	0.5
Ba	<0.0071	<0.0162	<0.0201	20
Cd	<0.0002	<0.0002	<0.0002	0.04
Cr	<0.0028	<0.0105	<0.0117	0.5
Cu	<0.0213	<0.0279	<0.0108	2
Hg	<0.0004	<0.0004	<0.0004	0.01
Mo	<0.0033	<0.0033	<0.0033	0.5
Ni	<0.0085	<0.0044	<0.0061	0.4
Pb	<0.0047	<0.0047	<0.0047	0.5
Sb	<0.0099	<0.0099	<0.0099	0.06
Se	<0.0122	<0.0122	<0.0375	0.1
Zn	<0.0203	<0.0203	<0.0203	4

Table V. 17: Chemical analysis of the leachate of samples processed at 1050 °C and subjected to TCLP testing

The proposed approach is advantageous not only for producing low cost ceramics (sintered at low temperatures, from waste or cheap raw materials), but also for waste stabilization. Table V.17 reports the values obtained from the leaching of the samples A, B and C. The leaching for the various pollutants is negligible or below the limits reported in the European Directive (1999/31/EC).

The evaluation of more specific further tests (under more aggressive environment and longer period of time) should be preceded by the collection of standards about the reuse of secondary materials in the construction sector. Even though each country has different standards, in general, we should consider: i) TCLP has already been presented as a more unfavorable case than the suggested use of ceramics as tiles in the building industry (Fernández-Pereira *et al*., 2011); ii) The test was applied on polished specimens "recycled" from mechanical testing, featuring a higher specific surface (dense surface layer removed, many pores in contact with the leaching solution). In other words, the observed low release of pollutants may be considered as an effective proof of environmental safety of the newly produced ceramics.

V.5.1.d Conclusions

We may conclude that:

• The glass which is hardly recycled in conventional production can be used as very effective fluxing agent in the formulation of innovative stoneware ceramics, sintered at low temperature;

• The liquid phase provided by the softening of glass is able to dissolve some inorganic waste, such as metallurgical vitreous slag; the dissolution is followed by a secondary crystallization of calcium silicate and alumino-silicate phases;

- The high iron oxide content of MS waste can be exploited for the development of a foamed microstructure, owing to a "bloating" phenomenon;
- The residual porosity, in the "glass-based" stoneware here presented, is significant (above 30%), but it is not open; the lightness, combined with surface sealing and relatively good bending strength (in turn associated to crystallization) makes the investigated materials extremely interesting for the novel, high value application of ventilated façades; the strength is increased by the presence of a dense surface layer, which and makes the material "self-glazed".
- Ecological sustainability is enhanced by the possible superposition of low emissions in the processing (firing at low temperatures), saving of natural raw materials (recycled glasses replacing feldspar fluxes) and stabilization of waste (reduced leaching of heavy metals).

V.5.2 Borosilicate glass and iron-rich slag from refining of precious metals

*Note: Work in collaboration with R.K. Chinnam (University of Erlangen, Institute of Biomaterials, supervision by Prof. A.R. Boccaccini). The research in Padova mainly concerned the mechanical characterization of samples [manuscript "**Self-foaming glass-ceramics made of borosilicate glass and iron rich waste residue,** by R.K.Chinnam, I. Ponsot, E. Bernardo, A.R. Boccaccini in preparation].*

V.5.2.a Introduction

Two main choices to optimize the recycling products such as foam glass - ceramics are the additive type and the process parameters. In this study, an iron-rich scoria was used both as a foaming agent and as a filler mechanical reinforcement (in amounts ranging from 10 wt % to 50 wt %) in a glass-ceramic composition made from recycled pharmaceutical borosilicate glass. The compacts were pressed at 30 MPa and treated at 950° C using a direct sintering route (heating rate of ~ 150 ° C / min) at different annealing time (5, 30, 45 and 60 min) . DTA and XRD analyses, showing a significant loss of viscosity of the borosilicate glass during the oxidation of iron oxide Fe_3O_4 reaction justified the homogeneous distribution of the pores and the important blowing. The foam glass - ceramic with an average porosity of 72%, had a mean density of 0.6 g/cm^3. Strengthening the glass structure by scoria particles led to an impressive compressive strength, reaching 14 MPa. Considering the unusual strength-to-weight ratio (specific strength of ~ 4 $MPa^{1/2} \cdot cm^3/g$) and fast process possibilities, these glass - ceramic foams could find many interesting applications for the industry such as structural and functional lightweight materials.

V.5.2.b Description of the raw materials

Table V.18 shows the composition of BSG while the composition of MS waste in as-received state is taken from the paper published by Ponsot *et al*. (2013).

Components	Borosilicate glass (BSG)	Metallurgical slag (MS)
Oxides	**Contents (wt-%)**	
Al₂O₃	5	12
B₂O₃	10.5	-
CaO	1.5	12.5
Na₂O	7	14
SiO₂	75	55
Fe₂O₃	Traces	5.5
K₂O	Traces	1

Table V.18: Composition of borosilicate glass waste and MS

V.5.2.c Results and Discussion

The powders used in this study are BSG and MS wastes. BSG in powder form was completely amorphous and MS waste in as-received state was partially crystalline and under DH conditions at 950 ^{o}C MS fully crystallized (see figure V.33, peaks are hidden by an amorphous silica rich phase). Phases Hematite Fe_2O_3 #72-0469, Magnetite Fe_3O_4 #75-0449, Acmite $Na\ Fe\ (Si_2O_6)$ #71-1492 and Hedenbergite $CaFeSi_2O_6$ #71-1500 in MS wastes are rich in iron with a calculated Fe_3O_4 of 9.7%. Sintered MS at 950 ^{o}C for 30 min led to the growth of Nepheline, Ca-Na-Al silicate and Hematite phases. BSG powder when sintered under similar conditions resulted in crystallization of cristobalite phase (Chinnam *et al.*, 2013).

The influence of MS on the crystallization of BSG foams was analyzed using XRD (see figure V.34). With increase in MS, BSG+MS composition the inhibition to the growth of cristobalite was observed. In the case of 30, 40 and 50 wt% MS, the growth of cristobalite was almost completely inhibited leaving an amorphous material. A growth in the peak intensity of nepheline phase was observed with the increase in MS content in BSG.

It is known that at the sintering temperature of 950 ^{o}C the BSG can form a reasonably low viscosity fluid which improves the wetting behavior of glass towards the included refractory MS particles, thus leading to better encapsulation of un-reacted solids or crystallized particles with better glass to refractory interface. In the study related to the inhibition to the growth of cristobalite phase in BSG by Jean and Gupta (1993), the Al_2O_3 particles were added to BSG. The strong coupling between Al^{3+} ions from Al_2O_3 and Na^+ ions from BSG was found to change the glass network structure by substituting Si^{+4} by an Al^{+3} in the glass network. Due to the balance of charges a change in the composition could have occurred leading to the inhibition of cristobalite phase growth in BSG. Similarly in BSG+MS the inhibition to the crystallization could have occurred due to coupling between Al ions from MS and Na ions from BSG or any similar charge relaxation phenomenon which could have controlled the cristobalite growth (See figure V.34).
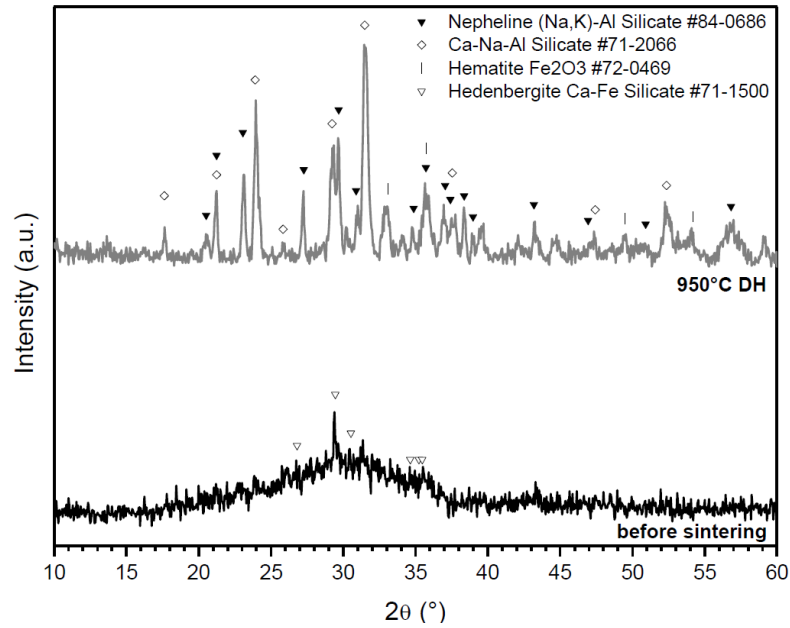
Figure V.33: XRD pattern of MS waste before and after direct heating at 950 °C
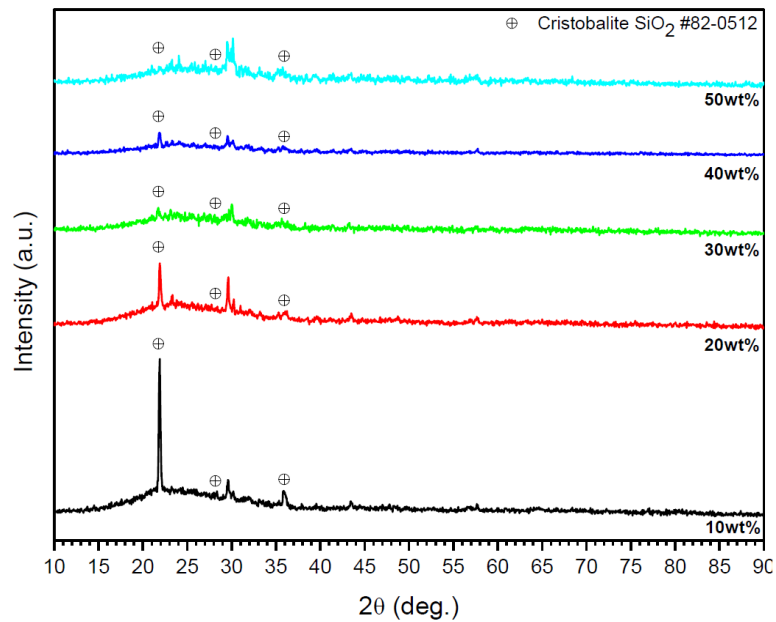
Figure V.34: XRD peaks of BSG + xMS foam GCs sintered at 950 °C for 30 min

To understand the softening behavior of BSG and MS the DTA measurements were performed (see figure V.35). At 825 °C, BSG exhibited small endothermic reaction representing the softening temperature. Though cristobalite formation is shown in XRD graphs (see figure V.34), there is no representative crystallization peak in DTA as the kinetic is probably too slow at the employed rate (10 °C/min). For MS, the endothermic peak at 820 °C is supposed to represent the initiation of softening (Lima and Monteiro, 2001) while complete softening was observed above 1000 °C.

Weight loss of BSG is negligible (0.4% is assumed as machine correction) while MS lost ~2%. The weight loss could correspond to iron oxidation and decomposition of carbonates present in the composition, as mentioned above in this paper.
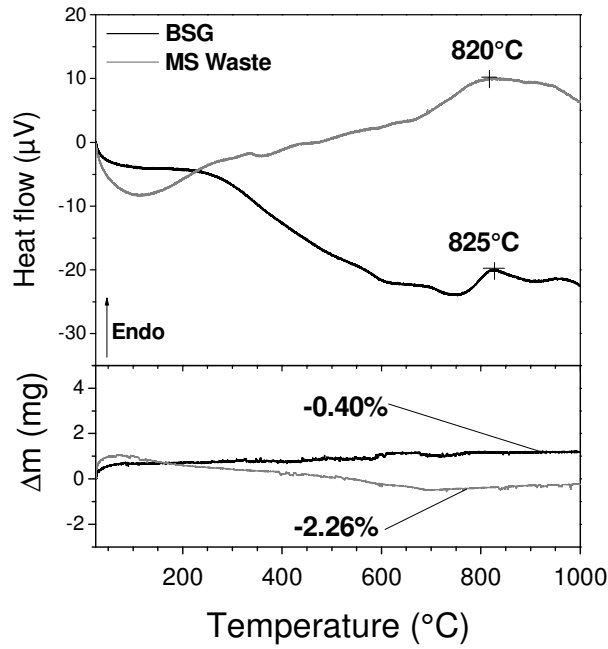
Figure V. 35: Thermal analysis of pure BSG and MS

The release of gas in the material due to phase change of certain elements in the composition provides basis for self-foaming effect. Such reactions in the matrix of the low viscosity glass can create foam like structure. The BSG when heated to 950 $^{\circ}$C attains low viscosity state and the release of oxygen from iron oxide decomposition in MS has self-foamed the material (see figure V.36).
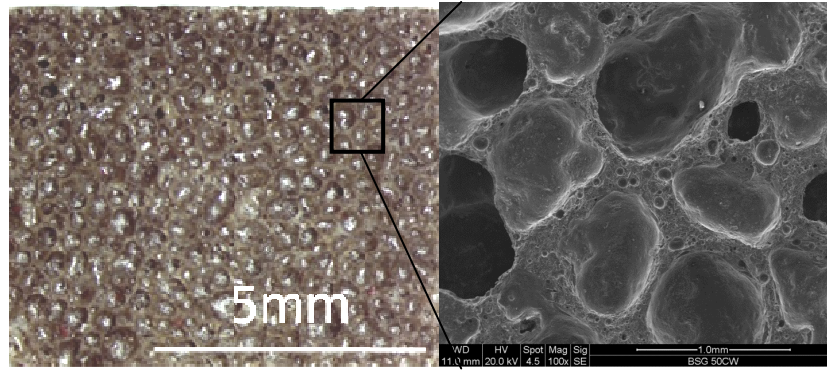
Figure V.36: Microscopic view of closed porosity in BSG-50 wt% sample.

It was observed that the sintered bodies with different concentrations of MS in BSG exhibited different physical properties. Using pycnometric measurements the volume porosity of 77% was recorded for 10 wt% MS while volume porosity of 67% was recorded for 50 wt% MS in BSG. The densities of 0.5 g/cm^3 and 1 g/cm^3 were measured for 10 wt% and 50 wt% MS in BSG. The changes in physical parameters of GCs could be attributed to the refractory elements present in MS. The presence of insoluble particles in viscous BSG could have affected growth of bubbles and thereby volume porosity and density of the foamed GCs. Therefore to further understand the influence of refractory elements on foaming of MS+BSG sintered bodies, annealing time was varied (15, 30, 45 and 60 min) on samples with different compositions (see figure V.37).

Samples with different compositions developed a similar pore size of ~0.5 mm when annealed for 15 min, while the pore size rose gradually with the increase in annealing time. The gas volume could rise in pores with temperature homogenization and further decomposition of gasifying elements in sinter body. Increase in the gas volume of pores creates addition pressure on walls which in turn pushes insoluble particles at walls to pack tightly causing a particle flow. If insoluble particles volume is considerably less, then an increase in annealing time can create thin wall, which will tend individual pores to coalesce and grow in size. If the insoluble particles volume is greater then it becomes difficult for particles to flow hence retains fine pores. Therefore, under the similar sintering condition less MS concentrations in BSG created larger pore size and higher MS concentration created fine pores even after 60 min of annealing. It can be observed that in GCs with 50 wt% MS, the standard deviation values are negligible. This indicates that structurally these GCs are reproducible by optimizing composition, heating rate and annealing time.
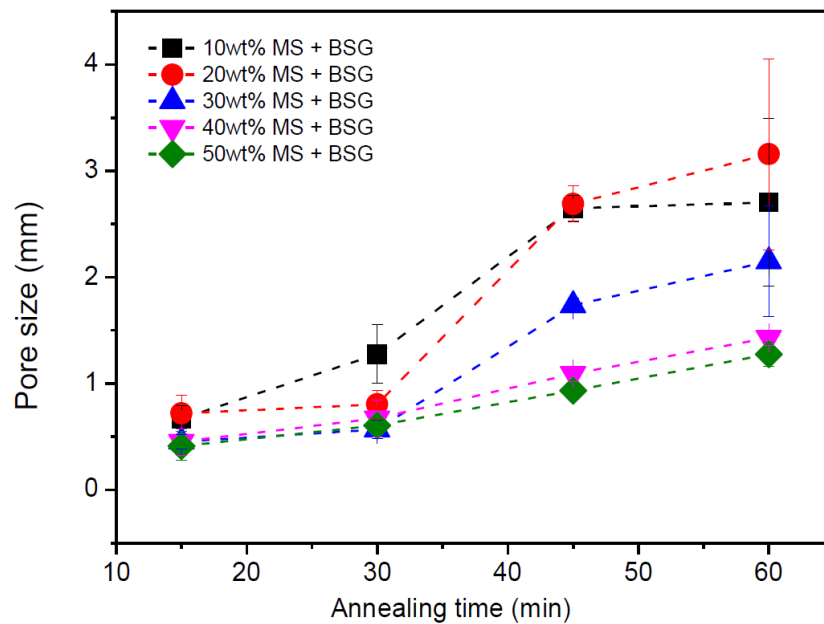
Figure V.37: Comparison between pore size distribution in Glass-ceramic composites made of 10, 20, 30, 40 and 50 wt% MS in BSG processed at 950 oC at different annealing times (15, 30, 45 and 60 min).

The change in thickness of pore wall leads to the change in mechanical properties. Foamed GC with thick and non-porous walls can exhibit greater strength compared to porous and thick walls (Bernardo *et al.*, 2010). The presence of cristobalite phase in the microstructure decreases the mechanical strength of GC because of its brittle nature. The addition of higher wt% of MS has inhibited the cristobalite growth as observed in figure V.34. Compressive strength measurements on low MS GCs showed less mechanical strength while with higher MS an increase in the compressive strength was recorded (see figure V.38). The direct effect of increased refractory elements, thick and non-porous wall structure (see figure V.36) led to the increase in compressive strength. A compressive strength of ~14 MPa with a total porosity of 67% and density of 1 g/cm^3 was obtained for samples of 50 wt% MS in BSG. Considering high standard deviation value for 50 wt% MS, it can be concluded that the faster cooling rate i.e., cooling samples in air directly from annealing temperature of 950 ^{o}C could have developed stresses in the material, such thermal shock

could have developed internal cracks deviating the absolute strength of the GC foam. Therefore, further studies on optimizing the cooling rates are necessary by keeping the processing conditions similar to the proposed once.
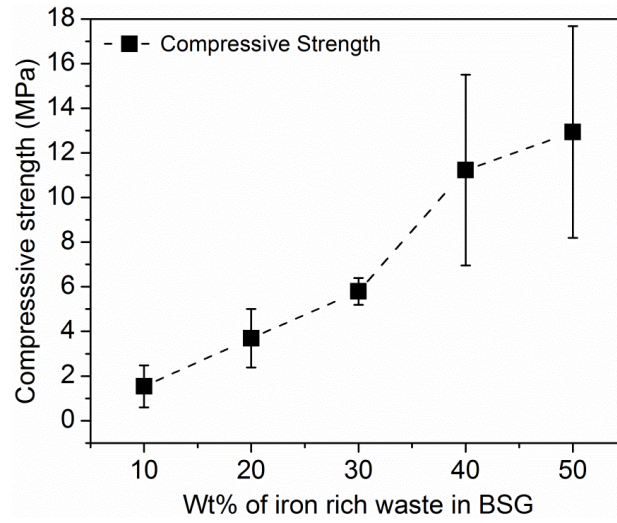
Figure V.38: Compressive strengths of BSG + xMS foams sintered under DH at 950 °C, annealed for 30 min and cooled in air to RT.
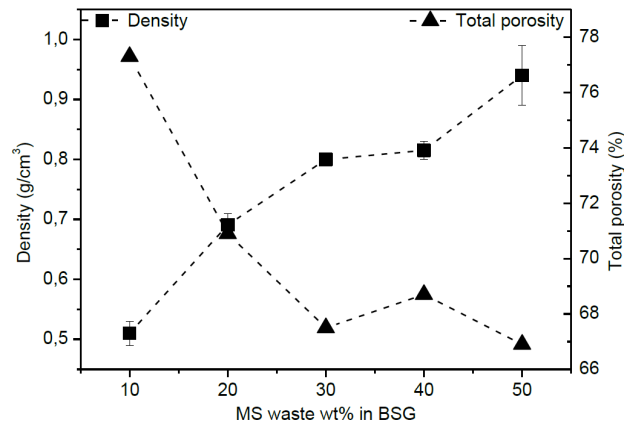
Figure V. 39: Geometric density and total porosity in function of MS waste wt%

As presented on figure V.39, the density of 0.5 g/cm^3 was recorded for 10 wt% MS waste while 50 wt% MS waste recorded ~1 g/cm^3. At a given temperature and annealing time, with the increase in MS content in BSG, a decrease in pore size and pore volume was recorded. MS is rich in refractory elements and the increase in particle volume in viscous BSG could affect the growth of pores, volume porosity and the density of the foam glass obtained.

The refractory or non-soluble particles presence in the viscous phase could restrict the flow or diffusion of gases within the compact (Jean and Gupta, 1993). The refractory particles could decrease the sinterability of the material (Chinnam *et al.*, 2013) which in turn helps the escape of gases while the material is being foamed thus decreasing the total volume porosity in the material. Hence, samples sintered at the same temperature with increasing wt% of MS waste resulted in the decrease in the volume porosity (see figure V.39).

MS content (wt-%)	Geometric density (g/cm^3)	Compression strength (MPa)	Specific compression strength (MPa$^{0.5}$·cm^3/g)
10	0.51 ± 0.02	1.7 ± 0.9	2.56
20	0.69 ±0.02	3.9 ± 1.2	2.86
30	0.8 ±0.01	5.8 ± 0.4	3.01
40	0.82 ±0.02	11.5 ± 3.9	4.16
50	0.94 ±0.05	13.2 ± 4.9	3.86

Table V.19: Specific strengths of glass-ceramic compositions DH at 950 °C for 30 min

Comparing to commercial glass foams mechanical strength (around 5 MPa), elaborated porous borosilicate glass-ceramics presented a relevant compressive strength, from 20 wt-% MS content. Growing bulk density by MS addition was compensated by a parallel growing porosity, which led to particularly relevant specific strength values (see table V.19), a prior index in construction field (Ashby, 2005).

V.5.2.d Conclusions

As a conclusion, we may say:

- Influence of foaming agents on the pore distribution in glass foam and their mechanical properties was successfully avoided by using self-foaming material. The influence of heating and cooling rates was successfully avoided by using direct heating conditions hence, lowering the reproducibility problems.

- Direct heating of foam glasses have given the opportunity to lower the total process time. Iron phase transformation has evolved gas which was helpful to self-foam the sintered body. The possible change in the network of BSG due to the charge relaxation phenomenon has inhibited the growth of cristobalite phase. Increase in refractory particles volume in the composition has helped to obtain ~14 MPa compressive strength for foam glass with a density of 1 g/cm^3.

- Waste derived materials and the processes involved in developing the form glass in this paper could attract industry to consider waste residues as the raw materials for processing functional materials.

V. 6 Glass foams from glass/sludge mixtures

A metallurgical by-product was tested, mixed with soda-lime glass, in order to produce cellular glasses. In particular we referred to Blast Furnace (BF) sludge. BF sludge is rich in C which is interesting in a perspective of exploiting foaming properties, as presented in chapter II, thanks to the oxidation of carbon and the possible concurrent reduction of iron oxides. The exploitation of high percentage of Carbon (~50 mol%) in the waste led to highly porous cellular glasses, proved to be chemically stable. The preparation of lightweight ceramics produced from such sludge was reported in the literature (Qi *et al.*, 2010).

V.6.1 First characterization

The chemical composition of the starting waste is available in table V.20. The metallurgical sludge used derived from the depuration system of the fumes from top furnace of steel plant ArcelorMittal. This sludge is good for the foaming because of its content in C and iron oxides. However, it cannot be reused in the top furnace because of its important content of Zn. Indeed, Zn would evaporate and condensate on the walls and damage strongly the refractory.

Element	*[wt%]*
Fe	19.80
C	44.70
S	3.00
CaO	2.84
Al_2O_3	2.83
SiO_2	5.75
PbO	1.30
ZnO	5.80

Table V.20: Chemical composition of the BF sludge
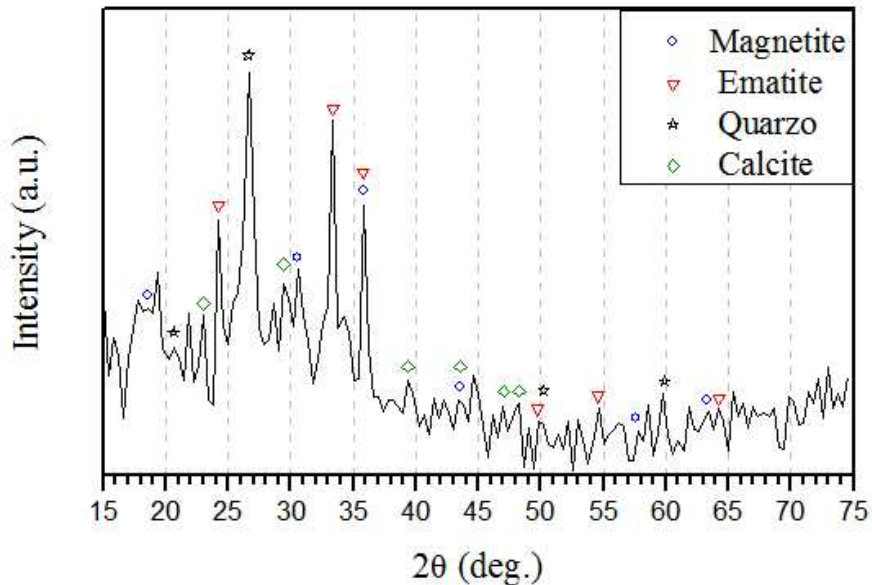
Figure V.40: X-Ray diffraction pattern of BF sludge before thermal treatment

The XRD analysis (figure V.40) indicates the presence of calcite ($CaCO_3$), hematite (Fe_2O_3), magnetite (Fe_3O_4) and quartz. Considering the presence of C, we could think at three reactions contributing to the foaming of glass/BF sludge, as follows:

$$CaCO_3 \rightarrow CO_2 \text{ [gas]} + CaO \qquad\qquad (1)$$
$$C + O_2 \rightarrow CO \text{ or } CO_2 \text{ [gas]} \qquad\qquad (2)$$
$$MO_x \rightarrow MO_y + O_2 \text{ [x>y]; mainly } 2\ Fe_2O_3 \rightarrow 4\ FeO + O_2 \qquad\qquad (3)$$
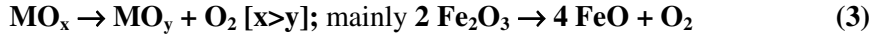
V.6.2 Additives

In order to find optimized formulations, the following additives were tested in the mixture, with the main aim of enhancing the oxidation of C:

- Gypsum ($CaSO_4 \cdot 2H_2O$)
- MnO_2
- Oxidized glasses (glasses from dismantled cathode ray tubes, glass from the vitrification of MSWI ash)

Panel glass from CRT and glass from MSWI, can be considered as oxidizing agents: in the first case, oxygen is known to be dissolved in the glass (CRT glasses are typically produced in oxidizing conditions, in order to prevent the reduction of heavy metal oxides), in the second case, oxygen may be provided by reduction of iron oxides, present in the formulation (this has been already exploited for the manufacturing of glass foams, according to Bernardo *et al*. (2013). The special Ba glass from cathode ray tubes, is not easily reused in the origin sector, since the original articles are no longer in the market. The glass from incinerator, rich in iron oxide derives from the vitrification of inorganic waste of the incinerator of Vercelli in Italy (VC).

Component	CRT panel glass (Andreola et al., 2007)	VC glass
CaO		13.9
Al$_2$O$_3$	4.36	14.0
MgO		4.60
SiO$_2$	66.1	41.1
Na$_2$O	7.63	10.3
K$_2$O	6.65	3.20
Fe$_2$O$_3$	0.25	4.10
MnO		0.20
TiO$_2$	0.13	
BaO	11.4	
SrO	0.99	
Sb$_2$O$_3$	0.44	

Table V.21: Chemical composition of secondary glasses

V.6.3 Optimization of the mixture

A simple mixture of 95 wt% SL glass and 5 wt% sludge led to inhomogeneous samples after direct sintering at 900 °C for 30 min. We can note a "black core"; this is likely due to inhomogeneous oxidation of C. At the surface, C reacted with atmospheric oxygen, leading to intensive foaming; the C in the internal part did not react with atmospheric oxygen, being "shielded" by the porous surface layers. This effect was quite expected; however, we expected also some oxidation of C, in the internal part, by reduction of iron oxide. The iron oxide from the

sludge evidently did not contribute. In order to improve the oxidation of "internal C" we added gypsum and MnO_2, still with poor improvements. On the contrary, an improvement was possible adding oxidized glasses.
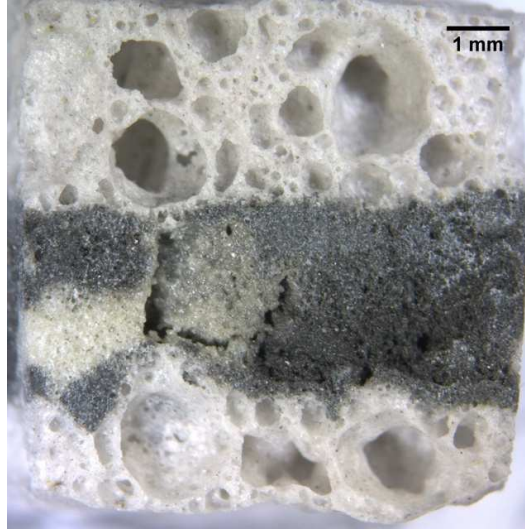
Figure V.41: Reduction of black core on sample cross section

SL glass, sludge, VC glass and panel glass were considered in the proportions indicated in the following table.

Compound Temperature	[wt%] 900 °C	[wt%] 800 °C
SL glass	90	85
BF sludge	5	5
VC glass	5	
Panel glass		10

Table V.22: Compositions of the optimized mixtures

We can note, with panel glass, the removal of black core with increasing firing time at 900 °C, from 15 to 30 min. However, the structure of foams from addition of panel glass was not satisfactory; due to its low softening temperature (lower than that of soda-lime glass, see Chapter III), there was a strong coalescence of pores (presence of big "bubbles" instead of a multitude of smaller pores, see figure V.41), generally associated with poor mechanical properties. The glass from MSWI, on the contrary, determined a homogeneous foaming, with no coalescence, due to the viscosity increase, associated to partial crystallization of wollastonite (see figure V.43). The partial crystallization is known to contribute positively to the mechanical strength. As shown by figure V.44, the optimized glass foam had a geometric density of 0.35 g/cm^3 with a corresponding porosity of 86% ± 2%. The compressive strength of 1.18 MPa is in the same order of magnitude of that of commercial foams with similar density (in particular, the relative compressive strength, i.e. the strength/density ratio $\sigma_{rel} = 3.37$ MPa·cm^3/g, shown as a black line in figure V.44, matches that of commercial glass foams).
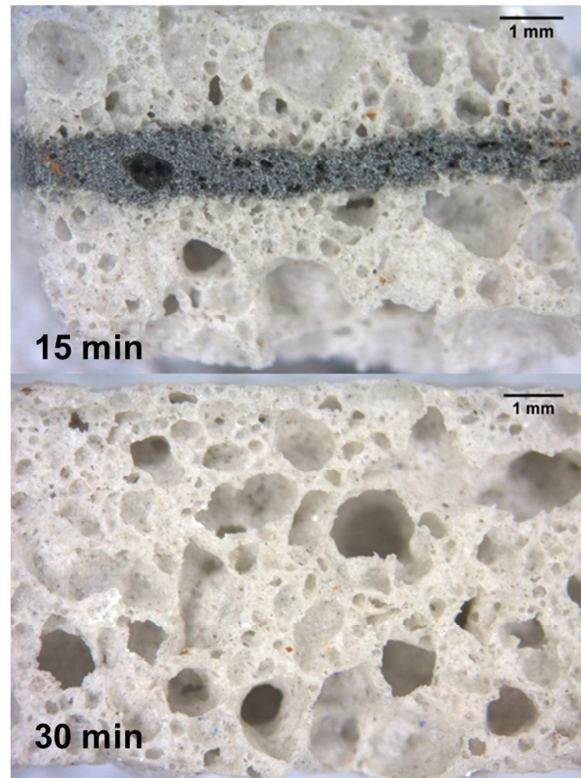
Figure V.42: Removal of black core in the mixture containing panel glass by increasing firing time from 15 to 30 min
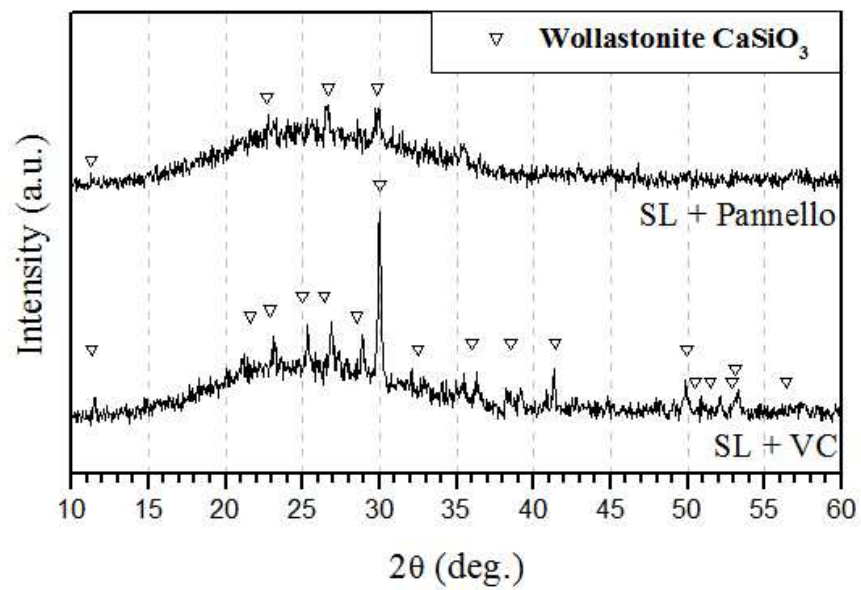
Figure V.43: X-Ray diffraction pattern of the mixture showing crystallization of wollastonite phase [PDF#76-0186]
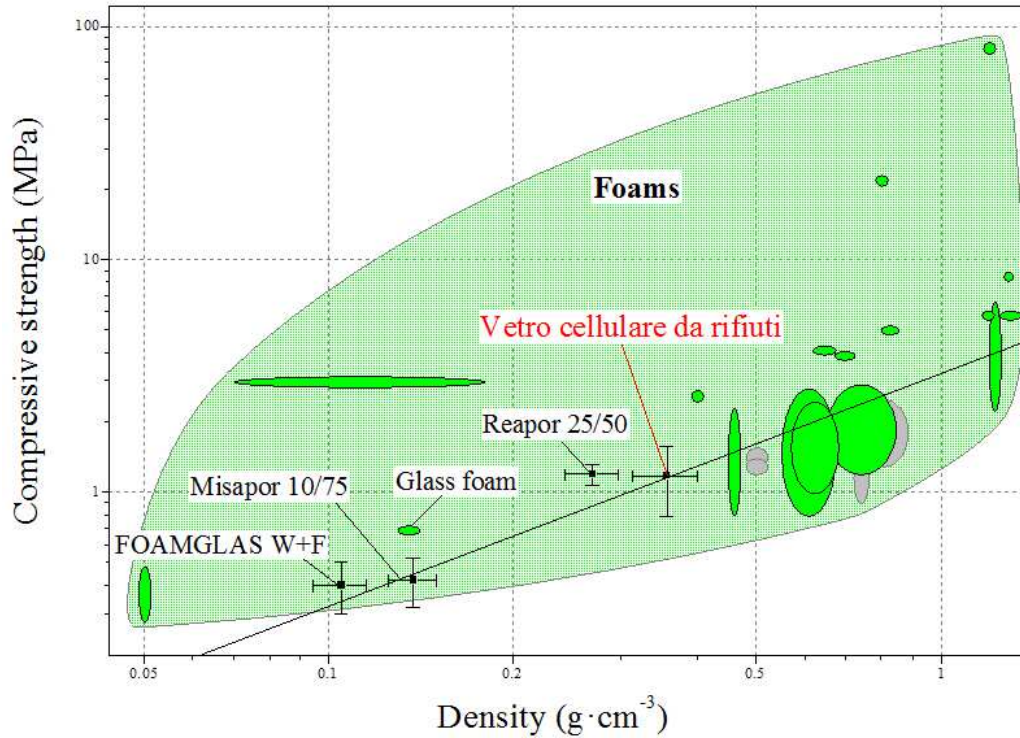
Figure V.44: Ashby graph including the foam sample from the optimized mixture ["vetro cellulare da rifiuti"=waste-derived glass foam]

V.6.3 Assessment of chemical stability

The optimized foams were subjected to TCLP test (EN 12457) for waste toxicity evaluation. The results in concentration of heavy metals and/or toxic elements are positive, i.e. all under limit value for toxicity.

Element	Leachate / ppm	Limit / ppm
As	<0.0049	0.5
Ba	<0.0000	20
Cd	<0.0002	0.02
Cr	<0.0004	0.2
Cu	<0.0001	0.1
Hg	<0.0004	2
Mo	<0.0033	0.5
Ni	<0.0014	2
Pb	<0.0047	0.2
Sb	<0.0099	0.06
Se	<0.0123	0.03
Zn	<0.0026	0.5
Ag	<0.0007	-

Table V.23: TCLP test on the sample from soda-lime glass, BF sludge
and oxidizing glass from waste incineration

It must be noted that TCLP was applied of fragment of foamed materials, so that the contact area (solution/foam) was particularly high. The test can be considered as highly severe. The only issue, still subjected to investigation (in collaboration with Stazione Sperimentale del Vetro, Venice, Italy), is the content of Zn. It is true that the release of Zn is negligible, but some Zn could be lost directly during firing, by volatilization of metallic Zn, possibly provided by

reduction of ZnO by C. The presence of oxygen from MSWI glass, however, could contribute to the stabilization of the same ZnO.

V.6.4 Examples of industrial applications

The cellular glass obtained can be used as a thermal insulating material. In panel form, it can be used in the internal or external insulation; in form of granules, it can be easily inserted in concrete. As previously discussed, cellular glass has several advantages compared to foamed polymers: it is incombustible, highly compression resistant, and it has a lower environmental impact in production and dismantlement. In the specific case, the partial crystallization could be useful to avoid alkali-silica reaction (ASR) in contact with concrete.

References

Alp I. Deveci H. Süngün H. (2008) Utilization of flotation wastes of copper slag as raw material in cement production, J. Hazard Mater., 159 (2-3), 390-395.

Amaral M. Gomes P.S. Lopes M.A. Santos J.D. R.F. Silva and M.H. Fernandes (2009) Cytotoxicity evaluation of nanocrystalline diamond coatings by fibroblast cell cultures, Acta Biomaterialia, 5 (2), 755-763.

Andreu I. Natividad E. (2013) Accuracy of available methods for quantifying the heat power generation of nanoparticles for magnetic hyperthermia, Int. J. Hyperthermia, 29 (8), 739-751.

Appendino P. Ferraris, M. Matekovits I. Salvo M. (2004) Production of glass–ceramic bodies from the bottom ashes of municipal solid waste incinerators, J. Eur. Ceram. Soc., 24, 803-810.

Ashby M.F. (2005) Materials selection in Mechanical Design, Third Edition, Butterworth Heinemann, Oxford, UK.

Bernardo E. Dal Maschio R. (2001) Glass-ceramics from vitrified sewage sludge pyrolysis residues and recycled glasses, Waste Management, 31, 2245-2252.

Bernardo E. Scarinci G. (2004) Sintering behaviour and mechanical properties of Al_2O_3 platelet-reinforced glass matrix composites obtained by powder technology, Ceram. Int., 30, 785-791.

Bernardo E. Albertini F. (2006) Glass foams from dismantled cathode ray tubes, Ceram. Int., 32, 603-608.

Bernardo E. Varasso M. Cadamuro F. Hreglich S. (2006) Vitrification of wastes and preparation of chemically stable sintered glass-ceramic products, J. Non-Cryst. Sol., 352, 4017-4023.

Bernardo E. (2008) Fast Sinter-crystallization of a glass from waste materials, J. Non-Cryst. Sol., 354, 3486-3490.

Bernardo E. Esposito L. Rambaldi E. Tucci A. Hreglich S. (2008) Recycle of waste glass into glass ceramic Stoneware, J. Am. Ceram. Soc., 91, 2156-2162.

Bernardo E. Esposito L. Rambaldi E. Tucci A. (2009a) 'Glass based stoneware' as a promising route for the recycling of waste glasses, Adv. Appl. Ceram., 108, 2-8.

Bernardo E. Esposito L. Rambaldi E. Tucci A. Pontikes Y. and Angelopoulos G. N. (2009b) , J. Eur. Ceram. Soc., 29, 2921-2927.

Bernardo E. De Lazzari M. Colombo P. Saburit Llaudis A. Garcìa-Ten F.J. (2010a) Lightweight Porcelain Stoneware by Engineered CeO_2 Addition, Ad. Eng. Mat., 12, 65-70.

Bernardo E. Bonomo E. Dattoli A. (2010b) Optimisation of sintered glass–ceramics from an industrial waste glass, Ceram. Int., 36, 1675-1680.

Bernardo E. Scarinci G. Bertuzzi P. Ercole P. Ramon L. (2010c) Recycling of waste glasses into partially crystallized glass foams, J. Porous Mat., 17 (3), 359-365.

Bernardo E. Ercole P. Bertuzzi P. (2012a) Porous stoneware based on recycled glass, Glass Worldwide, 42, 90-95.

Bernardo E. Scarinci G. Colombo P. (2012b) Vitrification of Waste and Reuse of Waste-Derived Glass, in: Encyclopedia of Sustainability Science and Technology, Robert A. Meyers (Ed.), 1. RAMTECH LIMITED, Springer New York, 11581-11613.

Bernardo E. Caldirola M. Ferraris M. (2013) Materiale termoisolante vetroceramico poroso in lastre e procedimento di ottenimento di tale materiale, Brevetto italiano, TO2013A000620.

Besco S. Brisotto M. Gianoncelli A. Depero L.E. Bontempi E. Lorenzetti and A. Modesti M. (2013) Processing and properties of polypropylene-based composites containing inertized fly ash from municipal solid waste incineration, J. Appl. Polym. Sci., 130, 4157–64.

Binhussain M.A. Marangoni M. Binmajed M.M. Bernardo E. Colombo P. (2014) Sintered and Glazed Glass-ceramics from Natural and Waste Raw Materials, Ceram. Int., 40, 3543-3551.

Boccaccini A.R. Petitmermet M. Wintermantel E. (1997) Glass-ceramics from Municipal Incinerator Fly Ash, Ceram Bull, 76 (11), 75-78.

Bontempi E. Zacco A. Borgese L. Gianoncelli A. Ardesi R. and Depero L.E. (2010) A new method for municipal solid waste incinerator (MSWI) fly ash inertization, based on colloidal silica, J. Environ. Monit., 12, 2093-2099.

Bontempi E. Struis R.PW.J. Pasquali M. Borgese L. Gianoncelli A. Gelfi M. Colombi P. Thiaudière D. Depero L.E. and Rizzo G. (2013) Inertization of heavy metals in municipal solid waste incineration fly ash by means of colloidal silica – a synchrotron X-ray diffraction and absorption study., RSC Adv., 3, 14339-51.

Bretcanu O. Spriano S. Verné E. Coïsson M. Tibero P. and Allia P. (2005) The influence of crystallized Fe_3O_4 on the magnetic properties of coprecipitation-derived ferrimagnetic glass-ceramics, 1 (4), 421-429.

Bretcanu O. Verné E. Coïsson M. Tiberto P. Allia P. (2006) Magnetic properties of the ferrimagnetic glass-ceramics for hyperthermia, J. Magnetism and Magnetic Materials, 305 (2), 529-533.

Brusatin G. Bernardo E. Andreola F. Barbieri L. Lancellotti I. and Hreglich S. (2005) Reutilization of waste inert glass from the disposal of polluted dredging spoils by the obtainment of ceramic products for tiles applications, J. Mater. Sci., 40, 5259-5264.

Cannillo V. Pierli F. Sampath S. Siligardi C. (2009) Thermal and physical characterisation of apatite/wollastonite bioactive glass–ceramics, J. Eur. Ceram. Soc. 29, 611.

Chen M. Zhang F.S. Zhu J. (2009) Lead recovery and the feasibility of foam glass production from funnel glass of dismantled cathode ray tube through pyrovacuum process, J. Haz. Mat., 161 (2-3), 1109-1113.

Chen B. Luo Z. Lu A. (2011) Preparation of sintered foam glass with high fly ash content, Mat. Lett., 65 (23-24), 3555–3558.

Chen X. Lu A. Qu G. (2013) Preparation and characterization of foam ceramics from red mud and fly ash using sodium silicate as foaming agent, Ceram. Int., 39 (2), 1923-1929.

Chen Q. Baino F. Spriano S. Pugno N.M. Chiara Vitale-Brovarone C. (2014) Modelling of the strength–porosity relationship in glass-ceramic foam scaffolds for bone repair, J. Eur. Ceram. Soc., 34 (11), 2663-2673.

Cheng T.W. Chen Y.S. (2004) Characterization of glass ceramics made from incinerator fly ash, Ceram. Int., 30 (3), 343-349.

Cheng T.W. Huang M.Z. Tzeng C.C. Cheng K.B. Ueng T.H. (2007) Production of colored glass–ceramics from incinerator ash using thermal plasma technology, Chemosphere, 68, 1937-1945.

Chinnam R.K. Boccaccini A.R. Bernardo E. Epstein H. (2013) Glass-Ceramic Composites From Borosilicate Glass and Alumina-Rich Residues, Int. J. Appl. Ceram. Technol., doi: 10.1111/ijac.12197.

Chinnam R.K. Francis A.A. Will J. Bernardo E. Boccaccini A.R. (2013) Review. Functional glasses and glass-ceramics derived from iron rich waste and combination of industrial residues, J. Non-Cryst. Sol., 365, 63-74.

Cicek B. Tucci A. Bernardo E. Will J. Boccaccini A.R. (2014) Development of glass-ceramics from boron containing waste and meat bone ash combinations with addition of waste glass, Ceram. Int., 40, 6045-6051.

Colombo P. Brusatin G. Bernardo E. Scarinci G. (2003) Inertization and reuse of waste materials by vitrification and fabrication of glass-based products, Curr. Op. Solid State Mater. Sci., 7 (3), 225-239.

Colombo P. Bernardo E. Marangoni M. Binhussain M.A. Binmajed M.A. H. Hamad H. Atalasi Alajmi A.M. and Al-Tamini A. (2013) Advanced lightweight glass-ceramics for interior and external building materials.

Çoruh S. Ergun O. Ergun N. Cheng T.W. (2006) Treatment of copper industry waste and production of sintered glass-ceramic, Waste. Manag. Res., 24, 234-241.

Cruz-Ramírez A. Romo-Castañeda J. de los Ángeles Hernández-Pérez M. Vargas-Ramírez M.A. Romero-Serrano A. and Hallen-López M. (2011) An application of infrared analysis to determine the mineralogical phases formation in fluxes for thin slag casting of steel, J. Fluor. Chem., 132, 323-326.

Daou T.J. (2007) Synthèse et fonctionnalisation de nanoparticules d'oxydes de fer magnétiques, Thèse de doctorat, Université Louis Pasteur, Strasbourg, 10-31.

Deatsch A.E. Evans B.A. (2014) Heating efficiency in magnetic nanoparticle hyperthermia, Journal of Magnetism and Magnetic Materials, 354, 163-172.

Denissen J.A.M. Vries A.H. (1998) Reduction of fluoride emission from clay materials, Z.I. Int., 51, 19-26.

Dimech C. Cheeseman C.R. Cook S. Simon J. Boccaccini A.R. (2001) Production of sintered materials from air pollution control residues from waste incineration, Waste Management, 31, 2245-2252.

Dufrane D. Delloye C. Mckay I.J. de Aza P.N. Scheider Y.J. Anseau M. (2003) Indirect cytotoxicity evaluation of pseudowollastonite, J. Mat. Sci. special issue: Materials in Medicine, 14, 33-38.

EN 12457-2 (2002) Characterization of waste - Leaching. Compliance test for leaching of granular and sludge Part 2., One stage batch test at a liquid to solid ratio of 10 l/kg for materials with particle size below 4 mm (without or with size reduction), index X30-402-2,.

Environmental Protection Agency U.S. (1992) Report EPA/625/R-92/002, Handbook of Vitrification Technologies for Treatment of Hazardous and Radioactive Waste, Office of Research and Development, Washington, DC.

Esposito L. Timellini G. Tucci A. (1995) Fracture Toughness of Traditional Ceramic Materials: a First Approach., Aetas 4a Conf. Soc. Ceram. Eur., Gruppo Editoriale Faenza Editrice S.p.A., Faenza, (Italia), 11.

Ettler V. Johan Z. Touray J.C. Jelínek E. (2000) Zinc partitioning between glass and silicate phases in historical and modern lead–zinc metallurgical slags from the Příbram district, Czech Republic , CR de l'Acad. Sci. - Series IIA. Earth Planet Sci., 331 (4), 245-250.

European Directive (1999) Council Directive 1999/31/EC on the landfill of waste, Official Journal of the European Community, L 182, 1-19 eur-lex.europa.eu.

Fernandes H.R. Tulyaganov D.U. Ferreira J.M.F. (2009) Preparation and characterization of foams from sheet glass and fly ash using carbonates as foaming agents, Ceram. Int., 35 (1), 229-235.

Fernández-Pereira C. de la Casa J.A. Gómez-Barea A. Arroyo F. Leiva C. and Luna Y. (2011) Application of biomass gasification fly ash for brick manufacturing, Fuel, 90, 220-232.

Francis A.A. Rawlings R.D. Sweeney R. Boccaccini A.R. (2002) Processing of coal ash into glass ceramic products by powder technology and sintering, Glass Technol., 43, 58-62.

Francis A.A. Rawlings R.D. Sweeney R. Boccaccini A.R. (2004) Crystallization kinetic of glass particles prepared from a mixture of coal ash and soda-lime cullet glass, J. Non-Cryst Sol, 333, 187-193.

Francis A.A. (2006) Crystallization kinetics of magnetic glass–ceramics prepared by the processing of waste materials, Mater Res Bull, 41, 1146-1154.

Francis A.A. (2007) Magnetic characteristics of iron-containing glass originated from the mixture of various wastes, Ceram. Int., 163–168.

Garcia-Ten J. Monfort E. Gomez P. Gomar S. (2006) Influence of calcite content on fluorine compounds emissions during ceramic tile firing, J. Ceram. Process. Res., 7, 65-82.

García-Ten J. Monfort E. Gómez-Tena M.P. Sanz V. (2011) Use of coating to minimize acid emissions during ceramic tile firing, J. Clean. Prod., 19, 1110-1116.

Garcìa-Ten J. Saburit A. Bernardo E. Colombo P. (2012) Development of lightweight porcelain stoneware tiles using foaming agents, J. Eur. Ceram. Soc., 32 (4), 745–752.

Gerhardt L.C. Boccaccini A.R. (2010) Review. Bioactive Glass and Glass-Ceramic Scaffolds for Bone Tissue Engineering, Materials, 3, 3867-3910.

Gibson L.J. Ashby M. (1997) Cellular Solids, Structure and Properties –second ed., Cambridge university press, Clarke D.R., Suresh S. Ward I.M. (eds.), FRS pub. Cambridge, UK, 510 pages.

Gorai B. Jana R.K. Premchand (2003) Characteristics and utilization of copper slag—a review, Res. Conserv. Recycl., 39 (4), 313.

Gutzow I. Shmelzer J. (1995) The Vitreous State-Structure, Thermodynamics, Rheology and Crystallization, Springer-Verlag, Berlin, Germany.

Halikia I. Zoumpoulakis L. Christodoulou E. Prattis D. (2001) Technical Note: Kinetic Study of the thermal decomposition of calcium carbonate by isothermal methods of analysis, Eur. J. Min. Proc. Env. Prot., 1, 89-102.

Hasheminia S. Nemati A. Eftekhari-Yekta B. Alizadeh P. (2012) Preparation and characterisation of diopside-based glass–ceramic foams, Ceram. Int., 38 (3), 2005-2010.

Hatch D.M. Ghose S (1991) The α–β phase transition in cristobalite, SiO_2: symmetry analysis, domain structure, and the dynamical nature of the β phase, Phys. Chem. Miner., 17, 554–62.

Höland W. Beall G.H. (2012) Glass-Ceramic technology, Sec. Ed., John Wiley & Sons, Westerville, Wiley-American Ceramic Society, New-Jersey.

Hoppe A. Güldal N.S. Boccaccini A. (2011) A review of the biological response to ionic dissolution products from bioactive glasses and glass-ceramics, Biomaterials, 32, 2757-2774.

Huang W.J. Tsai J.L. Liao M.H. (2008) Cytotoxicity of municipal solid waste incinerator ash wastes toward mammalian kidney cell lines, Chemosph., 71, 1860-1865.

Huang W.J. Tang H.C. Lin K.L. Liao M.H. (2010) An emerging pollutant contributing to the cytotoxicity of MSWI ash wastes: Strontium, J. Haz. Mat., 173 (1–3), 597-604.

Hummel R.E. (ed.) (1985) Electronic Properties of Materials, Second Ed., Springer-Verlag Berlin Heidelberg ISBN 0-387-54839-4,.

Infield D. Mei L. Eicker U. (2004) Thermal performance estimation for ventilated PV facades, Solar Ener., 76 (5), 93-98.

IPTS European Commission (2006) Reference Document on Best Available Technique in the Ceramic Manufacturing Industry, ITPS, Seville, Spain.

ISO 10993-5 (2009) Biological evaluation of medical devices, Part 5, Tests for in vitro cytotoxicity,.

ISO EN 10545-3 (1997) Ceramic Tiles –Part 3: Determination of Water Absorption, Apparent Porosity, Apparent and Relative Density and Bulk Density, stage 60.60, TC 189, ICS 91.100.23.

Jean J.H. Gupta T. K. (1993) Devitrification inhibitor in binary borosilicate glass composite, J. Mater. Res., 8, 356–363.

Jordan A. Wust P.S. Fahling H. John W. Hinz A. and Felix R. (2009) Inductive heating of ferrimagnetic particles and magnetic fluids: Physical evaluation of their potential for hyperthermia, Hyperthermia, 25 (7), 499-511.

Karamanova E. Karamanov A. (2009) Glass-ceramic frits from fly ash in terracotta production, Waste Manag. Res., 27 (1), 87-92.

Kidalova L. Stevulova N. Terpakova E. Sicakova A. (2012) Utilization of alternative materials in lightweight composites, J. Cleaner. Prod., 34, 116-119.

Lee W.E. (2006) Editorial: The contribution of ceramics to environmental clean-up, Adv. Appl. Ceram., 105, 1.

Lima M.M. Monteiro R. (2001) Characterisation and thermal behavior of a borosilicate glass, Thermochimica Acta, 373, 69-74.

Lin K.L. (2012) Recycling solar panel waste glass sintered as glass-ceramics, Environ. Prog. And Sustain. Energy, 31, 612-618.

Liu X. Morra M. Carpi A. Li B. (2008) Bioactive calcium silicate ceramics and coatings, Biomed. Pharmacother. 62, 526.

Méar F. Yot P. Ribes M. Ii U.M. (2006) Effects of temperature , reaction time and reducing agent content on the synthesis of macroporous foam glasses from waste funnel glasses, J. Rech. Carac., 60, 929-934.

Mihailova I. Mehandjiev D. (2010) Characterization of fayalite from copper slags, J. Univ. Chem. Tech. Metal, 45 (3), 317-326.

Monfort E. García-Ten J. Celades I. Gazulla Ma. F. Gomar S. (2008) Evolution of fluorine emissions during the fast firing of ceramic tile, Appl. Clay Sci., 38, 250-258.

Nasrazadani S. Eureste E. (2008) Application of FTIR for quantitative Analysis of Lime, technical report, N°FHWA/tX-0815-9028-01-1, University of North Texas.

O'Neill H St. C. (1987) Quartz-fayalite-iron and quartz-fayalite-magnetite equilibria and the free energy of formation of fayalite (Fe_2SiO_4) and magnetite (Fe_3O_4), Am. Mineralogist, 72, 67-75.

Perrot P. (1998) A to Z of Thermodynamics, Oxford University Press, ed., Great Britain, UK.

Pollard T.D. Earnshaw W.C. Lippincott-Schwartz J. (2008) Cell Biology, Easy reading, Second edition, Spektrum Akademischer Verlag, Saunders Elsevier, 1600 John F. Kennedy Blvd, Suite 1800, Philadelphia, PA9103-2899, Pub. Elsevier Inc. ISBN 1-4160-22554.

Ponikvar M. (2008) Exposure of human to fluorine and its assessment, in: Fluorine and Health, A. Tressaud, G. Haufe (Eds.), Elsevier B.V., pp. 487-549.

Ponsot I. Bernardo E. (2013) Self glazed glass ceramic foams from metallurgical slag and recycled glass, J. Clean. Prod., 59, 245-250.

Ponsot I. Falcone R. Bernardo E. (2013) Stabilization of fluorine-containing industrial waste by production of sintered glass-ceramics, Ceram. Int., 39, 6907-6915.

Ponsot I. Bernardo E. Bontempi E. Depero L. Chinnam R.K. Detsch and R. Boccaccini A.R. (2014) Recycle of pre-stabilized municipal waste incinerator fly ash and soda-lime glass into sintered glass ceramics, J. Clean Prod, in press,

Qi Y. Qinyan Y. Han S. Yue M. Gao B. Yu H. Shao T. (2010) Preparation and mechanism of ultra-lightweight ceramics produced from sewage sludge, J. Haz. Mat., 176, 76-84.

Raghavan V. (2010) Phase Diagram Evaluations - Fe-O-Si-Zn (Iron-Oxygen-Silicon-Zinc), J. Phase Equilibria and Diffusion, ASM International 201010.1007/s11669-010-9721-9.

Raimondo M. Zanelli C. Matteucci F. Guarini G. Dondi M. and Labrincha J.A. (2007) Effect of waste glass (TV/PC cathodic ray tube and screen) on technological properties and sintering behavior of porcelain stoneware tiles, Ceram. Int., 33, 615-623.

Raimondo M. Guarini G. Marani F. Fossa L. Dondi M. (2011) Producing large panels of porcelain stoneware, Tiles Today, 70, 48-55.

Rambaldi E. Carty W.M. Tucci A. Esposito L. (2007) Using waste as a partial flux substitution and pyroplastic deformation of a porcelain stoneware tile body, Ceram. Int., 33, 727-733.

Rawlings R.D. Wu J.P. Boccaccini A.R. (2006) Glass-ceramics: Their production from wastes—A Review, J. Mat. Sci., 41, 733-761.

Reinosa J.J. Silva A.C. Rubio-Marcos F. Mello-Castanho S.R.H. Moya J.S. and Fernandez J.F. (2010) High chemical stability of stoneware tiles containing waste metals, J. Eur. Ceram. Soc., 30, 2997-3004.

Ring T.A. (1996) Fundamentals of Ceramic Powder Processing and Synthesis, Acad. Press, ,.

Rosenweig R.E. (2002) Heating magnetic fluid with alternating magnetic field, J.Magnet Mat, 252, 370-374.

Sandu V. Nicolescu M.S. Kuncser V. Damian R. Sandu E. (2012) Magnetic glass-ceramics, J. Adv. Ceram., 1 (2), 138-143.

Scarinci G. Brusatin G. Bernardo E. (2005) Cellular Ceramics, Structure, Manufacturing, Properties and Applications, M. Scheffler, P. Colombo (eds.), Wiley-VCH, Weinheim, pp. 158-176.

Schabbach L.M. Andreola F. Karamanova E. Lancellotti I Karamanov A. and Barbieri L. (2011) Integrated approach to establish the sinter-crystallization of glasses from secondary raw material, J. Non-Cryst. Sol., 357, 10-17.

Shelby J.E. (2005) Chapter 4 Immiscibility/phase separation, Introduction to Glass Science and Technology second Ed., RSC, Alfred, NY, USA, 51-71.

Skuza Z. Kolmasiak C. Prusak R. (2009) Possibilities for the utilization of metallurgical slag in the conditions of the polish economy, Metalurgija, 48 (2), 125-128.

Smeacetto F. Salvo M. Ventrella A. Rizzo S. Ferraris M. (2012) Durable Glass-Ceramic coatings for Foam Glass, Int. J. Appl. Glass. Sci., 3 (1), 69-74.

Thomas E.S. Thompson J.G. Withers R.L. Sterns M. Xiao Y. and Kirkpatrick R.J. (1994) Further Investigation of the Stabilization of β-Cristobalite, J. Am. Ceram. Soc., 77, 49-56.

Trevan J.W. (1927) The Error of Determination of Toxicity, Proceedings of The Royal Society of London. Series B, Containing Papers of A Biological Character (1905-1934), 101 (712), 483-514.

www.sasil-life.com (2009) online access, official website, SasiL S.p.A., Italy.

Yürüyen S. Toplan H.Ö. (2009) The sintering kinetic of porcelain bodies made from waste glass and fly ash, Ceram. Int., 33, 2427-2433.

Zanelli C. Raimondo M. Guarini F. Marani F. Dondi M. (2013) Producing large panels of porcelain stoneware, Tiles Today, 70, 48-50.

Zhao H. Poon C.S. Ling T.C. (2013) Utilizing recycled cathode ray tube funnel glass sand as river sand replacement in the high-density concrete, J. Clean. Prod., 51, 184-190.

Zhihong Y. Qiao L. Jixiang X. Yong H. Guangdong L. and Yi K. (2003) Preparation and crystallization of glass–ceramics derived from iron-rich copper slag, J. Alloys Comp., 74, 354-360.

Chapter VI

Novel layered glass-ceramics

VI.1 Concept of sinter-crystallization and layered glass-ceramics

As previously mentioned, vitrification is the safest approach for the treatment of wastes but the process involves difficulties in establishing itself, being particularly cost-and capital-intensive. In the case of inorganic waste for which (in contrast to radioactive waste), environmental hazard does not impact on the environment by radiations, the feasibility of cost decreasing is justifiable, particularly if the glass obtained can be reused in high-value applications.

If glass-ceramics are the most significant application waste-derived glasses, due to their combination of good mechanical properties and chemical stability, the production of such high-value glass-ceramics from inorganic wastes incurs additional costs, however, particularly secondary ceramization treatments which double the energy consumptions. The production of the sinter-crystallized glass-ceramics has attracted much attention since the process is shorter compared to the traditional method. Quenching the glass frit obtained by a first rapid vitrification enables energy saving during both vitrification and ceramization steps. Finally, direct sintering of mixtures of inorganic wastes including recycled glasses acting as fluxes is an important alternative. The products cannot be strictly called glass-ceramics, since the vitrification of glass based components begins at the same time as the sintering and the phases transformations of other components. However, there is much evidence in the literature supporting the classification of such products as « sintered glass-ceramics », owing to their observed phase evolution (Francis *et al*, 2002).

The idea presented in Figure VI.1 is to cover the sintered body with a vitrified layer, made of the same raw materials as the body (Binhussain *et al.*, 2014). This would be a good solution not only to avoid problem of pollutants stabilization, but also to improve mechanical strength. Indeed, the glass ceramic layer offers mechanical reinforcement and enhances the stabilization of pollutants.

The production process described has the aim of combining direct sintering of waste mixtures and sintering of waste-derived glasses, with the creation of layered « hybrid glass-ceramics » (see figure VI.1, red square). The good mechanical properties and homogeneous microstructure of sinter-crystallized glass-ceramics were also exploited in a glaze, white or colored, designed on a porous base body obtained from direct sintering. Vitrification of waste is sustainable, since it is applied only to a limited amount of the starting material and, in addition, the single firing reduces the costs associated with glaze deposition. Owing to their negligible water absorption on the

glazed side, and their low density, layered glass-ceramics could be a viable alternative to the lightweight tiles currently used in building façades.
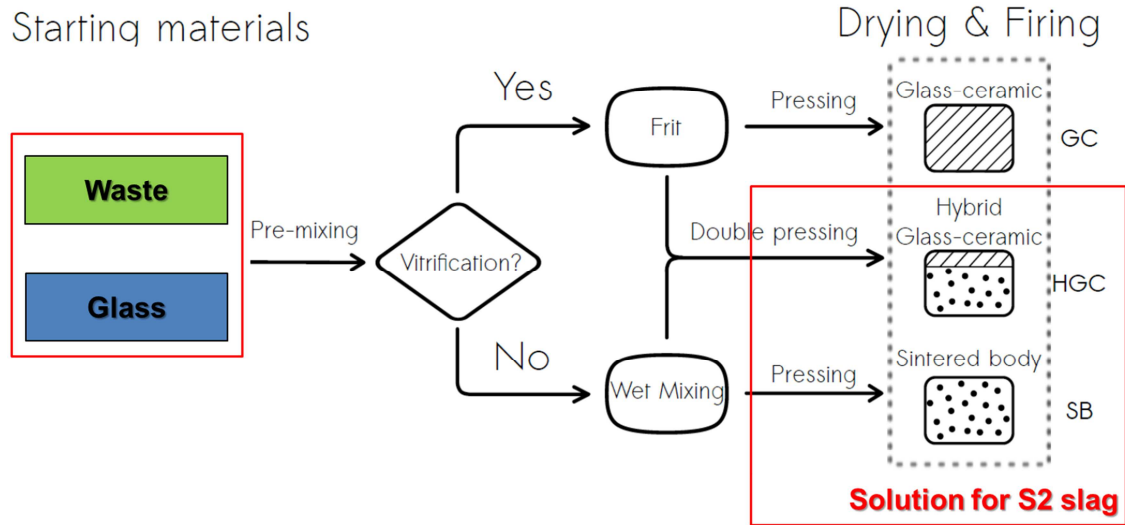
FigureVI.1: Schematic representation of the three routes for the process to obtain a layered glass-ceramic employing selected natural and waste materials

VI.2 Layered glass-ceramics from engineered mixtures of wastes

Monolithic glass-ceramics were produced by a novel sintering approach, involving both chemical composition and manufacturing operations. The surface porosity of a glass-ceramic body from direct sintering can be sealed by a dense sinter-crystallized glass-ceramic layer, produced from the same starting raw materials, consisting of a mixture of fly ash from thermal power plants, recycled soda-lime glass and boron waste (residues of the mining and purification of valuable boron containing minerals). The use of the latter waste, providing B_2O_3, allowed a substantial viscous flow, for the substrate, even at a relatively low sintering temperature (850 °C).

The dense sinter-crystallized layer, besides imparting improvements in the mechanical properties, was found to feature an enhanced chemical stability.

VI.2.1 Introduction

Vitrification is a well-recognized technology for the stabilization of many types of inorganic waste, including radioactive waste (U.S. Patent, 1992). However, being particularly energy and capital-intensive, there are some difficulties in establishing the approach on an industrial scale.

For non-radioactive waste the costs of vitrification can be compensated by the possible reuse of the waste-derived glass as a raw material for new products (Colombo et al., 2013). Glass-ceramics are undoubtedly the most established product from the reuse of inorganic waste, *after* vitrification (Rawlings et al., 2013). However, it should be noted that glass-ceramic manufacturing implies additional costs: the waste-derived glasses must be first shaped (e.g. by rolling of the melt) and then subjected to a secondary ceramization treatment, aimed at glass devitrification, i.e. nucleation and growth of crystalline phases. Further treatments on the glass-ceramic products, such as cutting

and polishing, can be additionally requested, before commercialization and final use (e.g. in buildings, replacing natural stones and traditional ceramics) (Höland and Beall, 2002).

Frit-derived or "sinter-crystallized" glass-ceramics have attracted much attention as an alternative to conventional glass-ceramic manufacturing, in order to reduce the costs (Schabbach et al., 2011). In fact, energy savings are associated with both vitrification and ceramization steps, since waste glasses may be poured just after homogenization, thus avoiding the expensive refining step, and crystallization may occur very rapidly (in one hour or less, at a sufficiently high sintering temperature) as a result of surface nucleation, even for glasses with a very low content of oxides that can act as nucleating agents (i.e., oxides with poor solubility in glass, such as TiO_2 and ZrO_2)(Gutzow et al., 1998). Grinding is generally an expensive step, but we should consider that the fragments produced by pouring a glass melt into water possess high internal stresses, favorable to milling, and fine glass powders can be easily converted into flat glass-ceramic tiles, by simple pressing and single-step firing, minimizing cutting and polishing operations (Bernardo et al., 2006).

Although shorter, the high-temperature (>1350–1400 °C) melting stage, with sinter-crystallization, remains. The melting stage can be even avoided when adopting a further sintering approach. Many investigations, from the literature, support a second type of "sintered glass-ceramics", derived from direct sintering of mixtures of inorganic waste including recycled glasses, which act as fluxes (Francis, 2002, Dimech et al., 2008). The products are not strictly glass-ceramics, since there is no formation, at any stage, of a homogenous glass to be crystallized later. However, the recycled glass component (present in significant amounts), besides promoting an increase in density as a result of viscous flow sintering, reacts with the waste, leading to the formation of silicate and alumino-silicate crystals (similar to those produced by devitrification of waste glasses) and of a new glass phase.

Like in conventional glass-ceramics, pollutants in products from direct sintering could be embedded in the crystalline and/or in the amorphous phase, but they could escape more easily, since the chemical homogeneity of a sintered solid is much lower than that of a glass obtained from melting (pollutants might remain concentrated in regions not completely dissolved by the liquid phase provided by the glass component).

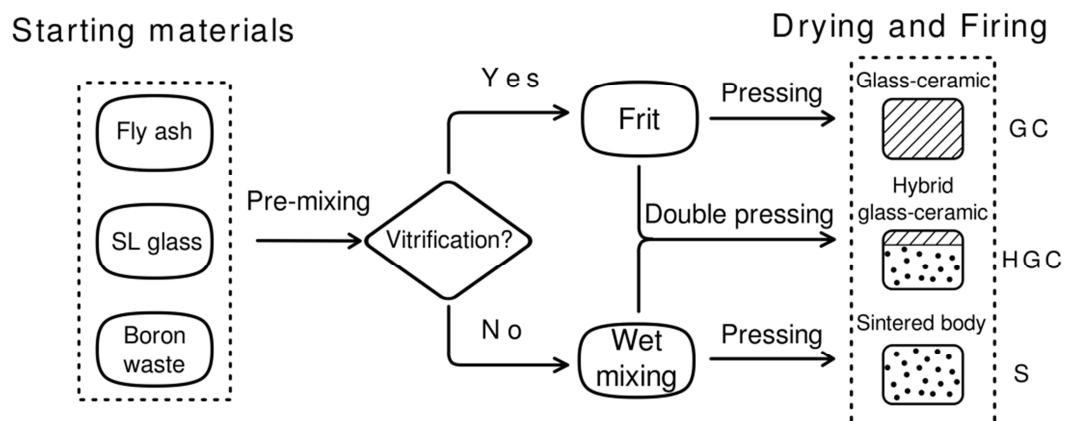*Figure VI.2: Schematic representation of the three routes for the production of glass-ceramic materials employed in the present chapter part*

The present section aims at providing an example of this new strategy, combining the advantages of direct sintering and sinter-crystallization, with the creation of "double layer glass-ceramics", recently presented (Binhussain et al., 2014) (see figure VI.2) with an engineered chemical formulation. A selected mixture of waste (fly ash from thermal power plants, recycled soda-lime glass and boron waste) is mostly used for direct sintering; the base body, however, is coated by a glaze, derived from sinter-crystallization of a glass from the melting of the same mixture. The glazed side is that to be directly exposed to the environment: the sinter-crystallization process provides a layer with negligible water absorption and enhanced chemical stability. The sinter/sinter-crystallization approach, in the present investigation, is favored by the specific choice of starting waste; in particular, the presence of B_2O_3, allows sintering treatments at only 850 °C, due to enhanced viscous flow.

2. Experimental procedure

The chemical composition of the starting waste raw materials in this study is reported in table VI.1. SL corresponds to the fraction of recycled soda-lime glass that is difficult to reuse in conventional glass production owing to its impurities; FA refers to fly ash from lignite combustion (Public Power Industry of Greece, Megalopolis plant); BW represents boron-rich residues from the extraction of commercially valuable borate minerals (from borate mine waste deposits in Bigadic, Turkey). BW residue was considered after ball milling, aimed at homogenization, and calcination at 500 °C, for 2 h, aimed at the removal of decompose hydrated boron salts (BW contains several types of calcium borate hydrates, e.g. colemanite - $CaO \cdot 3B_2O_3 \cdot 5H_2O$ -, mixed with calcite) (Cicek et al., 2013).

Oxides	SL glass	FA	BW	Waste glass	BS glass
SiO_2	71.6	49.4	16.1	50.2	72
Al_2O_3	1.0	22.7	0.9	7.6	7
Na_2O	13.5	0.9	0.2	5.8	6
K_2O	0.4	1.4	0.5		2
MgO	3.9	1.6	6.9	4.9	
CaO	9.0	8.9	26.4	17.3	1
B_2O_3		0	19.7	8.2	12
Fe_2O_3	0.1	7.4	0.1	2.3	
TiO_2		1.1			
SrO			1.2		
others	0.5	5.3		3.7	
L.O.I.		1.3	28.0		

Table VI.1: Chemical compositions (wt%) of the starting waste and of the resulting waste-derived glass

The waste materials were considered in the weight proportion SL/FA/BW=40/30/30.

3 Results and discussion

Figure VI.3 illustrates the evolution of both density and water absorption with increasing firing temperature, for the samples from direct sintering. We can note that the density increased almost linearly up to 1000 °C, reaching an almost stationary level of about 2.3 g/cm^3. The water absorption, well above 15%, from 800 to 1000 °C, went abruptly below 2% (1.3%) at 1050 °C. This behavior is reputed to be due to interactions between the components of the starting mixture;

the glass component caused some densification by viscous flow, with increasing firing temperature, but also some dissolution of the other components, in turn stimulating the crystallization. The formation of a rigid network, from the interlocking of crystal inclusions, limited the same viscous flow, up to 1050 °C; at this temperature the flow of the glass phase did not deter mine a complete removal of porosity, but sufficed for the sealing of the external surfaces of samples, obviously subjected to a more intense heating than the rest.
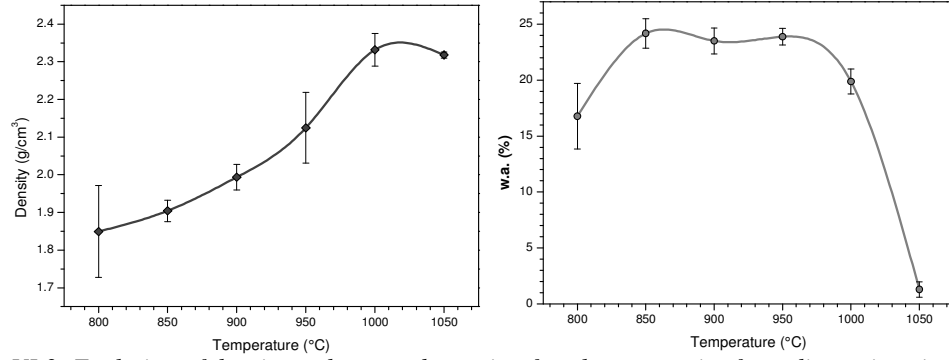

FigureVI.3: Evolution of density and water absorption for glass-ceramics from direct sintering (S)
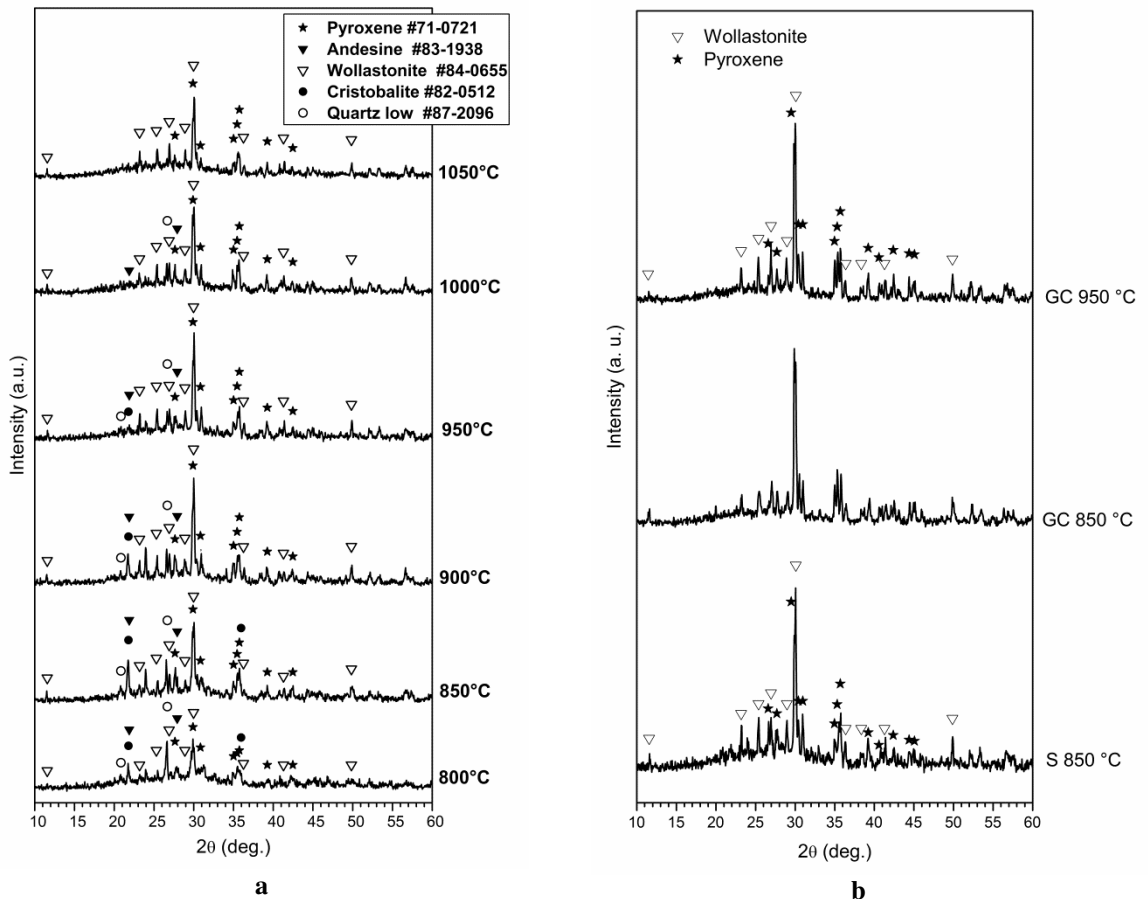

a

b

Figure VI.4: a) Phase evolution in glass-ceramics from direct sintering (S)
b) Comparison between glass-ceramics from direct sintering (S) and from sinter-crystallization of waste-derived glass (GC)

The starting composition was originally conceived with the aim of reproducing the molecular balance of main oxides, CaO, Al_2O_3 and SiO_2, present in most waste-derived glass-ceramics, e.g. the well-known "Slag-sitalls" (Rawlings et al., 2006; W. Höland, G. Beall, 2002), with the additional contribution of B_2O_3; calcium silicates and alumino-silicates were expected as typical phases of a glass belonging to the CAS (CaO-Al_2O_3-SiO_2) system, whereas boron oxide was expected to remain in the residual glass phase, lowering the viscosity.

The XRD patterns, reported in figure VI.4a, demonstrate the substantial crystallization of the expected phases, even at low temperature. More precisely, above 850 °C, wollastonite ($CaSiO_3$, PDF#84-0655) is clearly recognized as the most significant phase; the interlocking of crystals, previously hypothesized, is reasonable, considering the usual fibrous morphology of wollastonite crystals. Interestingly, at 1050 °C, only a secondary silicate, belonging to the pyroxene family (augite, $Ca_{0.818}Mg_{0.792}Fe_{0.269}Al_{0.42}Si_{1.751}O_6$, PDF#71-0721), is detected; variants of crystalline silica (α-quartz, PDF#87-2096, and α-cristobalite, PDF#82-0512) are detected in significant traces only below 950 °C; finally, another silicate phase (andesine, $Na_{0.622}Ca_{0.368}Al_{1.29}Si_{2.71}O_8$, PDF#83-1938) is visible up to 1000 °C.

No diffraction peak may be attributed to phases originally present in the BW waste (discussed by Cicek et al., 2013): B-rich compounds likely dissolved in the liquid phase provided by the softening SL glass, turning it into a boro-silicate phase. The developed Ca-rich silicate phases are practically identical to those developed from vitrification-crystallization process: this observation is supported by the comparison between S sample sintered at 950 °C (temperature at which wollastonite and augite peaks appear as well-defined) and samples from the sinter-crystallization of glass powders obtained from the same mixture, shown in figure VI.4b. Well-defined wollastonite and augite peaks are actually detected applying sinter-crystallization at only 850 °C; we may say that the selected mixture of raw materials yields, for both direct sintering and sinter-crystallization of glass powders, the same phases, in turn depending on the mixing of oxides; the higher homogeneity in the distribution of oxides, with vitrification, allows for lower precipitation temperatures. The substantial crystallization, already at 850 °C, for GC samples, is consistent with the DTA plot reported in figure VI.5: a strong exothermic effect, for fine powders of waste glass, is visible at about 870 °C.
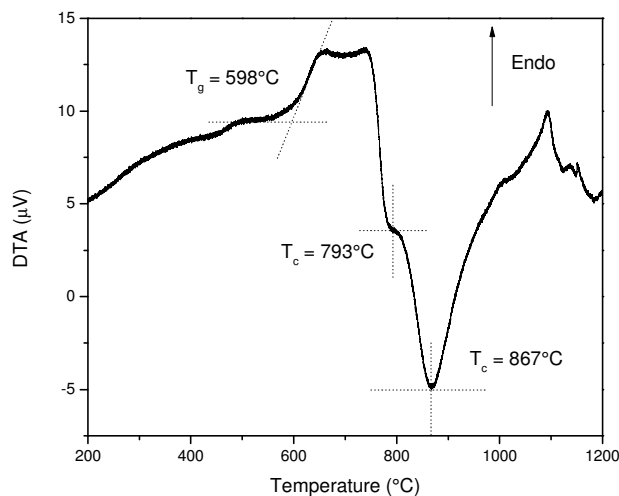

Figure VI.5: DTA plot for fine powders of waste glass

The sinter-crystallization process led also to improvements in the water absorption, which resulted negligible even starting from samples fired at 850 °C. This finding encouraged us to proceed with the development of "hybrid glass-ceramics" with a layered structure, i.e. materials with a main body from direct sintering of constituents and a glaze derived from a glass frit, in turn obtained by vitrifying the same constituents. In fact, materials developed according to this novel approach have the potential to fulfil the requirements of tiles for high values applications such as the so-called ventilated façades (Bernardo et al., 2010b), i.e. both low density (in the order of 2 g/cm^3 or below) and water absorption (below 2%).

From table VI.2 we can note that a firing temperature of 1050 °C was necessary for tile samples from direct sintering to possess an adequately low water absorption (<2%); although containing many isolated pores, as shown by figure VI.6a, it is much denser than that sintered at 950 °C. The sample fired at 1050 °C, illustrated by figure VI.6b (fracture surface), and the sinter-crystallized one, sintered at 950 °C, shown in figure VI.6c, both contain a multitude of randomly oriented fibrous crystals, confirming the analogy inferred from X-ray diffraction analysis.

Samples	Sintering Temp.	Water absorption	Density ρ	Elastic modulus, E	4-pt bending strength, σ
	°C	%	g/cm^3	GPa	MPa
S1	950	24	2.04 ± 0.09	22 ± 1	16 ± 1
S2	1050	1.3	2.32 ± 0.01	62 ± 2	44 ± 3
GC	950	<0.5	2.66 ± 0.05	56 ± 2	32 ± 4
HGC	950	<0.5*	2.16 ± 0.04	25 ± 3	14 ± 2
HGC-BS**	850	0.8 *	2.05 ± 0.06	19 ± 3	25 ± 4

Table VI.2: Physical and mechanical characterization data for tile samples data referred to the glaze; ** 5% Al$_2$O$_3$ – 95% glass (57% waste glass – 38% BS)*

A first "hybrid glass-ceramic" sample was fired at 950 °C, i.e. the minimum temperature at which, as discussed above, the phase composition of samples from direct sintering and that of samples from sinter-crystallization coincide. As illustrated by figure VI.6d, the coating was uniform, except for defects from manual handling, highlighted by arrows; the interface, shown in figure VI.6e, is visibly crack-free. As reported in table VI.2, while the density of the HGC sample was not particularly enhanced by the glaze, the water absorption of the glazed size is dramatically lower than that of the sintered body.

Despite the practical identity of phase composition, the sinter-crystallized glaze and the sintered body could differ in terms of chemical homogeneity, considering that, as reported in the introduction, pollutants might remain concentrated in regions not completely dissolved by the liquid phase developed upon firing. This observation is substantially confirmed by the leachates from TCLP testing, reported in table VI.3; the release of most metals, from the glass-ceramic from sinter-crystallization at 950 °C, is much lower than from the glass-ceramic from direct sintering at 1050 °C, with the exception of As and Pb (unchanged) and Ni (higher leaching after sinter-crystallization). In both cases, however, the release is much lower than the limits for an "inert" material. A further reduction of the ionic releases could be provided by the mixing of the waste glass with a glass with high chemical stability, such as recycled pharmaceutical borosilicate glass, already used to densify and stabilize waste-derived glass-ceramics (Cicek et al., 2012).
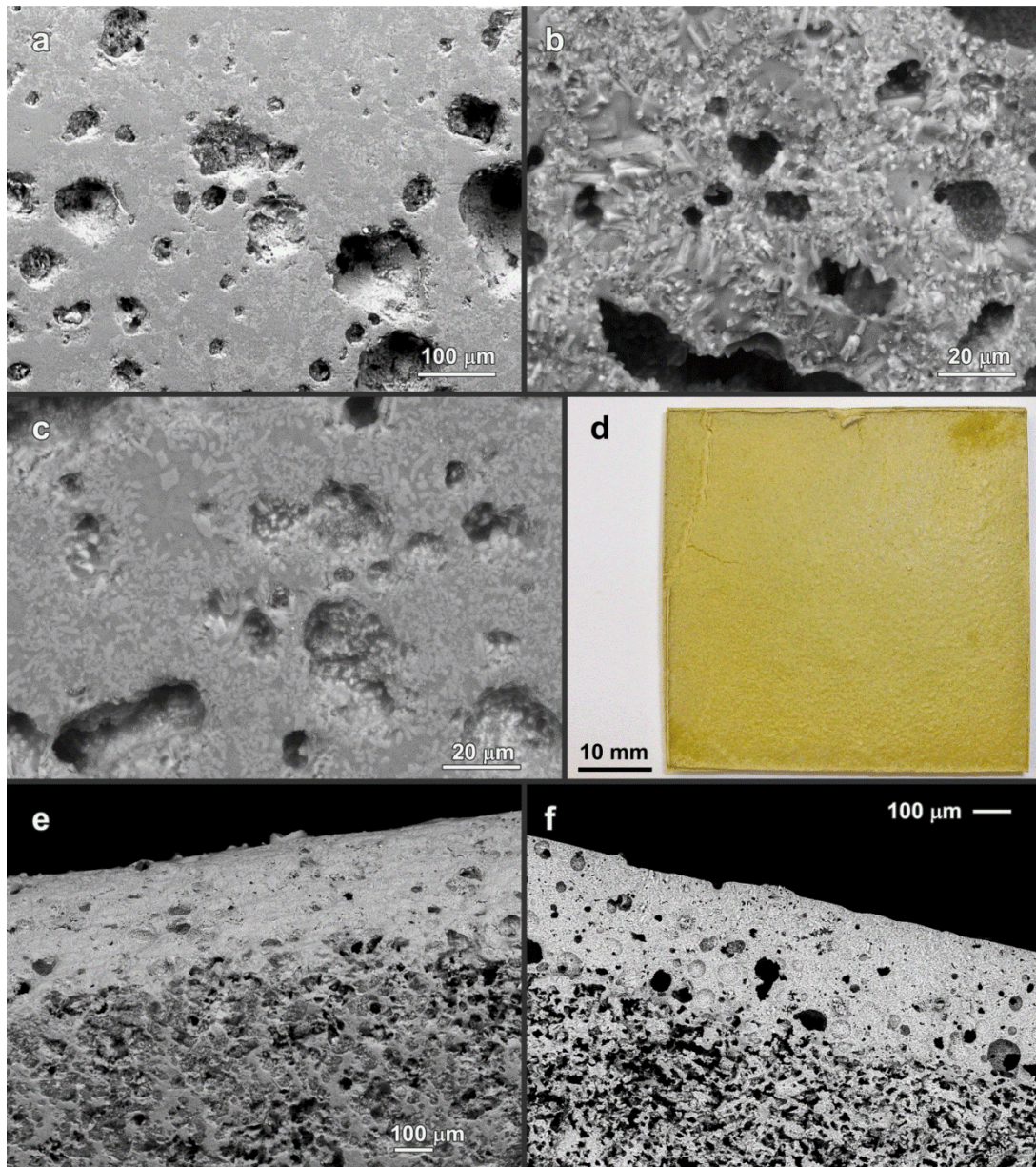
Figure VI.6: Microstructural details of sintered samples: a, b) S sample, fired at 1050 °C; c) GC, 950 °C; d) visual appearance of HGC sample, 950 °C; e) glaze-body interface, HGC sample, 950 °C; f) glaze-body interface, HGC-BS sample, 850 °C

The main purpose of the glass addition in the present case, however, was the control of shrinkage, when operating with a glaze even below 950 °C. In fact, the directly sintered body, fired at 850 °C, had a far lower shrinkage (~2%) than at 950 °C (~5%), causing the development of cracks in the glaze. The cracks were progressively removed by increasing the concentration of borosilicate glass; a slight amount of alu mina was introduced in order to lighten the yellow color of both glass-ceramic glazes. From figure VI.6f we can observe that operating with a mixture in the weight proportion alu mina/borosilicate glass/waste glass=5/38/57 (borosilicate glass and waste glass in the proportion 40/60), in a second hybrid glass-ceramic sample (HGC-Bs), the interface is again homogeneous and crack-free, after firing at 850 °C. As reported by table VI.3, the new formulation of the glaze had positive effects even on the leaching (TCLP was applied to

discs of glaze mixture fired in the same conditions than HGC-BS), with the exceptions of Ba, Ni and Pb.

Element	Leachates (ppm)			EN Limit for inert material (ppm)
	S 1050 °C	*GC (=Glaze HGC) 950 °C*	*Glaze HGC-BS 850 °C*	
As	0.0091	0.0108	0.0049	0.5
Ba	0.3783	0.0435	0.0711	20
Cr	0.1303	0.0071	0.0039	0.2
Cu	0.0293	0.0070	0.0014	0.1
Mo	0.1535	0.0191	0.0033	0.5
Ni	0.0014	0.0325	0.0513	2
Pb	0.0096	0.0107	0.0328	0.2
Se	0.0122	0.0122	0.0122	0.03
Zn	0.0380	0.0203	0.0203	0.5

Table VI.3: Chemical analysis of the leachate of selected samples subjected to TCLP testing
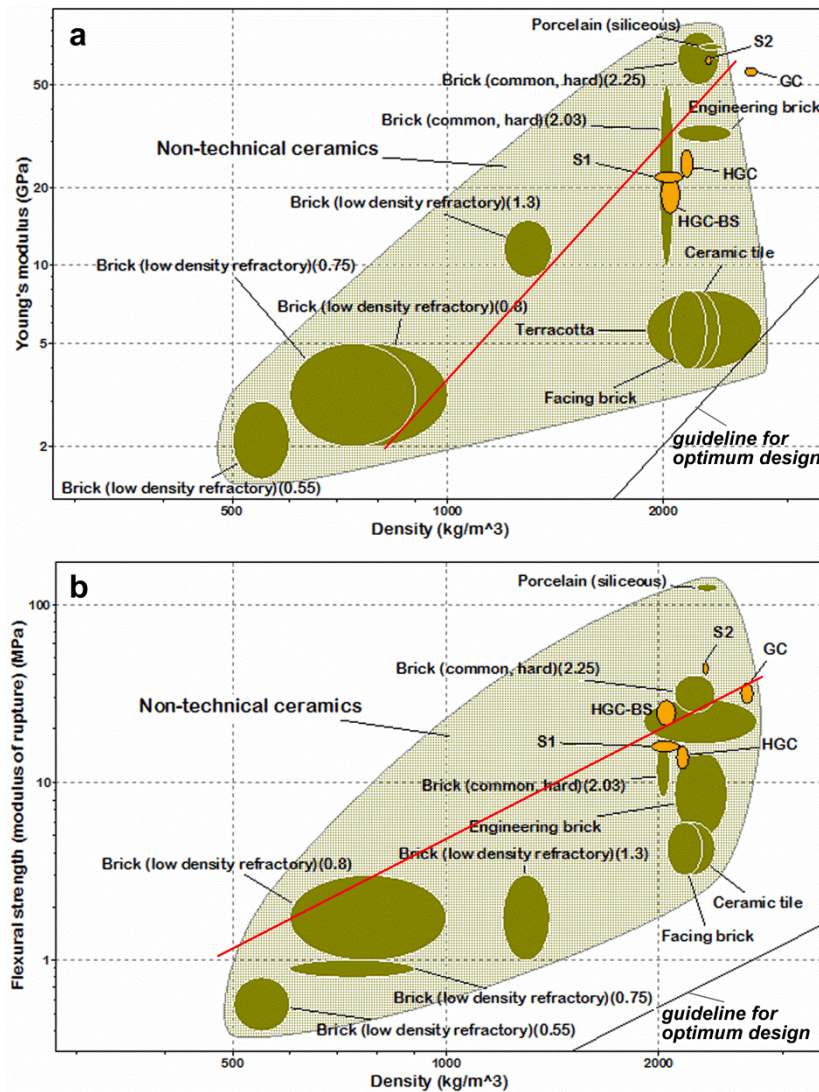
Figure VI.7: Ashby's plots of developed glass-ceramics compared with non-technical ceramics and glasses (a) Young's modulus; b) flexural strength

A final remark concerns the mechanical properties of the different types of glass-ceramics developed. Figure VI.7 illustrates the typical Ashby's plots (Ashby, 2005) considered for lightweight design (modulus/density, strength/density), representing data for traditional ceramics. The glass-ceramic materials here presented, highlighted in yellow, considering the guidelines for the manufacturing of lightweight panels (referring to the indices $I=E^{1/3}/\rho$ and $I'=\sigma_f^{1/2}/\rho$, where E is the elastic modulus, σ_f is the bending strength, or modulus of rupture, and ρ is the density; the performances of our samples are illustrated by the red lines), compare favorably with most construction materials available at the moment. More precisely, HGC-BS is the most efficient, considering the constraints of low density and low water absorption (penalizing GC and S2 samples, respectively) for the above mentioned application in ventilated façades.

4. Conclusions

We may conclude the following.

- The phase composition of glass-ceramics from direct sintering of a waste mixture and from vitrification and subsequent sinter-crystallization may coincide, operating above 950 °C; this was likely due to the extensive fluxing ability offered by both soda-lime glass and boron waste;

- Both types of glass-ceramics are chemically stable, according to the results of TCLP testing; the ionic releases, however, are lower for sinter-crystallized samples, than for directly sintered ones, owing to the higher chemical homogeneity;

- The surface porosity of a glass-ceramic body from direct sintering can be sealed by a sinter-crystallized glaze, produced from the same starting waste mixture, thus forming layered glass-ceramics, at the temperature at which the phase composition is nearly identical (950 °C);

- The characteristics of the waste-derived glass-ceramic glaze can be tailored by the addition of secondary components (pharmaceutical borosilicate glass and alu mina), allowing for the manufacturing of layered glass-ceramics at only 850 °C;

- Owing to their characteristic specific strength, layered glass-ceramics could find applications in the building industry as lightweight tiles, e.g. in ventilated façades.

VI.3 Optimization of glass-ceramics from mixtures of glass and metallurgical slags

Glass-ceramics based on iron rich wastes are produced following an innovative approach, combining direct sintering and sinter-crystallization processes. According to this method, a layered tile is manufactured by single firing at 900 °C, using a selected combination of wastes for both porous body and dense coating layer. The coating layer ("glaze") is due to sinter-crystallization of a waste-derived glass mixed with zircon and recycled borosilicate glass. The glaze sealed the porosity of body and enhanced both mechanical properties and chemical stability. Indeed, the results report a near-to-zero water absorption rate, despite a low geometric density (~2 g/cm3), accompanied by a Young's modulus of ~40 GPa and a bending strength of ~30 MPa. The results of leaching behavior are consistent with EN standard for chemical stability of wastes.

VI.3.1 Introduction

Vitrification technology has proved to be one of the most successful ways to stabilize inorganic wastes, and particularly radioactive waste (US E.P.A, 1992). As pointed out by Colombo *et al.*, (2003) the stabilization of non-radioactive wastes is subjected to sustainability constraints: vitrification may be feasible when waste-derived glasses can be used as secondary raw materials, i.e. the costs associated to high temperature treatments are compensated by the value of new glass-based products, among which glass-ceramics are undoubtedly the most established (Rawlings *et al.*, 2006).

In most cases, for the production of glass-ceramics, a glass is first shaped (e.g. by rolling of the melt) and then subjected to a secondary ceramization treatment, aimed at nucleation and growth of crystalline phases. Further treatments on the glass-ceramic products, such as cutting and polishing, can be additionally requested, before commercialization and final use (Höland and Beall, 2002).

Frit-derived or "sinter-crystallized" glass-ceramics have also raised much interest as a low cost alternative to conventional glass-ceramic manufacturing (Schabbach *et al.*, 2011). Indeed, if waste glasses are poured just after the homogenization, the (expensive) refining step is no longer required. Crystallization occurs more rapidly as a result of surface nucleation, in one hour or less, at a selected sintering temperature. Starting from pressed fine glass powders also cutting and polishing operations are minimized.

The viscous flow sintering approach can lead to glass-ceramics even avoiding the high temperature melting stage (1350 °C-1400 °C). In fact, wastes, combined with significant amounts of recycled glasses, can be subjected to "direct sintering". The dissolution of inorganic waste in the liquid phase provided by the recycled glass and the formation of new silicate and alumino-silicate crystals (similar to those produced by devitrification of waste glasses) support the identification of the products as glass-ceramics, although not derived only from a homogeneous parent glass (Rawlings *et al.*, 2006).

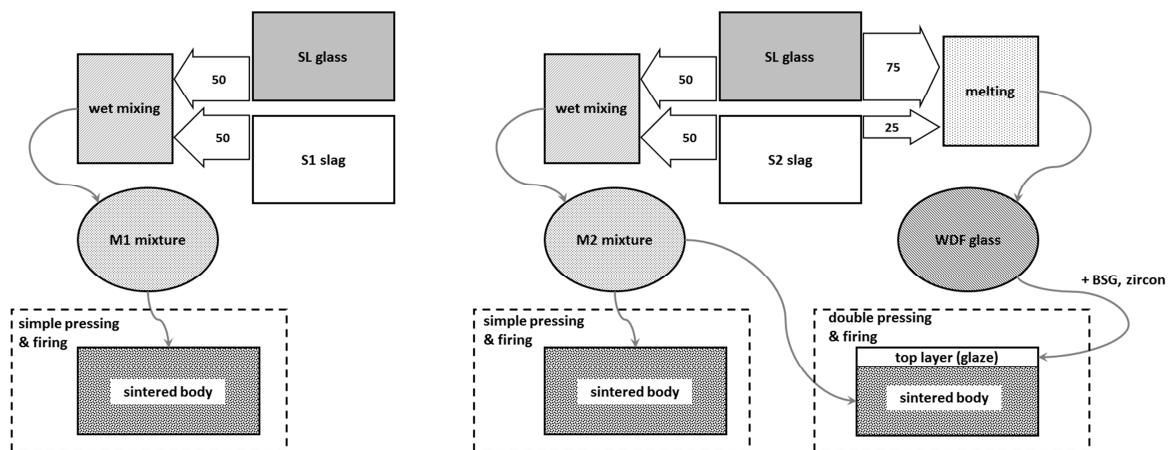*Figure VI.8: Schematic representation of the processes adopted for the development of glass-ceramics based mainly on metallurgical slags and soda-lime glass*

Glass-ceramics from direct sintering have one fundamental advantage and one fundamental disadvantage compared to "classical" glass-ceramics. Besides for the savings in energy required by the overall manufacturing process, the direct sintering is advantageous for reducing the

volatilization of some pollutants (e.g. fluorides, Ponsot *et al.*, 2013); on the other hand, some pollutants could remain concentrated in some areas of the samples.

This paper describes the obtainment of glass-ceramics from direct sintering of metallurgical slags, mixed with recycled soda-lime glass. A new strategy - recently proposed (Binhussain *et al.*, 2014) - combining the advantages of direct sintering and of sinter-crystallization, is also exploited. As illustrated by figure VI.8, "layered glass-ceramics" (LGC) could be considered as a third option, besides glass-ceramics from sinter-crystallization and direct sintering. A single-step treatment causes the direct sintering of a base body of glass/waste mixture, and the sinter-crystallization of a frit, from a glass in turn derived from the same starting materials. The chemical stability may be optimized, since the glazed side would be that to be exposed directly to the environment.

Vitrification of waste is reputed to be sustainable, since it is applied only to a limited amount of the starting materials; the single firing reduces the costs associated to the deposition of a glaze. In addition, there is a good matching of the concept of LGC with the requirements of modern building façades. In fact, there is growing demand for lightweight tiles, with low water absorption (below 2%, for optimized frost resistance), to be placed vertically, anchored to metal frames, in turn fixed on main building walls: the air gap between tiles and substrate walls contribute positively to the thermal insulation (mimimizing thermal losses, in winter, and minimizing overheating, in summer). A solution may come from traditional porcelain stoneware tiles with an engineered porosity, due to the use of foaming agents (Bernardo *et al.*, 2010); waste-derived LGC could be far more convenient, since we could exploit the porosity of the core, formed by direct sintering, coupled with the strength, low water absorption and possibly pleasant color of the glaze, avoiding the use of valuable natural materials.

VI.3.2 Experimental procedure

VI.3.2.a Sample preparation

Table VI.4 reports the chemical compositions of the starting raw materials and the formulations developed from them. "S1" and "S2" refer to two types of iron rich slags coming from non-ferrous metallurgy, provided by KU Leuven (Belgium). As previously reported (Ponsot *et al.*, 2014), "S1" is partially crystallized, with fayalite, i.e. Fe(II) silicate (Fe_2SiO_4 or $2FeO \cdot SiO_2$) as the main crystal phase, whereas "S2" is amorphous. Soda-lime glass (SLG), provided by Sasil SpA (Brusnengo, Italy), corresponds to the fraction of recycled soda-lime glass in which the amount of ceramic impurities impedes extensive reuse in the manufacturing of new glass containers (closed loop recycling). Borosilicate glass (BSG), provided by Nuova OMPI (Piombino Dese, Italy), derives from discarded pharmaceutical containers. Slags and glasses were first ground separately into fine powders by ball milling and then sieved up to 90 µm.

Mixtures of fine powders of SLG and slags, corresponding to the proportions 50%S1-50%SLG (M1) and 50%S2-50%SLG (M2), were sintered at 900 °C, 950 °C and 1000 °C.

The slag S2 was considered as raw material for a glass frit (WDF). This frit was obtained by melting a second SLG/S2 mixture (75%SLG-25%S2) at 1300 °C for 3 h, and later fired at 900 °C.

Layered glass-ceramics (LGC) were obtained by double pressing in a 50 mm × 34 mm rectangular die. A base layer of M2 mixture was first subjected to light pressing (10 MPa) and subsequently coated with WDF/glass/zircon powders (a weight proportion WDF-BSG-Zircon of 40-15-45 was the optimum one) in an amount corresponding to a surface density of 0.080 g/cm^2.

Component	S1	S2	Soda-lime glass (SLG)	Boro-silicate glass (BSG)	Mixture 1 (M1)	Mixture 2 (M2)	Waste-derived frit (WDF)
				Oxides (wt%)			
SiO$_2$	29	24	71.6	72	50.5	47.8	59.7
FeO	52	32			26	16	8
Al$_2$O$_3$	4	6	1.0	7	2.5	<1	2.2
Na$_2$O	<1	<1	13.5	6	7	7	3.7
K$_2$O	<1	<1	0.4	2	<1	<1	<1
MgO	1	1	3.9		2.5	2.5	3.1
CaO	2	21	9.0	1	5.5	15	12
ZnO	7	7			3.5	3.5	1.7
B$_2$O$_3$	<1	<1		12	<1	<1	
			Formulations (wt% balances)				
M1	50		50				
M2		50	50				
WDF		25	75				
Glaze for LGC*				15			40

* remaining 45% represented by zircon (ZrSiO$_4$) mineral

Table VI.4: Chemical compositions and formulations of starting wastes, recycled glasses and waste-derived glass-ceramics

The coating was performed by leaving the pressed powders inside the die, removing only the plunger; the WDF powders were manually passed through a sieve positioned over the open die. After repositioning the plunger, the interpenetration between the WDF/glass/zircon powders and the substrate was achieved by secondary pressing at 40 MPa. Layered glass-ceramics were subjected to the same thermal treatment applied to M1 and M2.

VI.3.2.b Results and discussion

The preliminary firing treatments, on small disc samples, were aimed at evidencing the impact of temperature on density and water absorption, critical to applications in the building industry (Bernardo *et al*., 2010). From figure VI.9 we can observe that the two slags, mixed with soda-lime glass, led to samples with quite particular density and water absorption trends. Increasing the temperature of sintering from 900 °C to 1000 °C, the density almost linearly decreased, in parallel with a visibly growing porosity. S1 actually leads to lighter bodies, with the density curve corresponding to M1 mixtures always lower than those of M2 mixtures; the water absorption, on the contrary, is minimized for M1 samples.
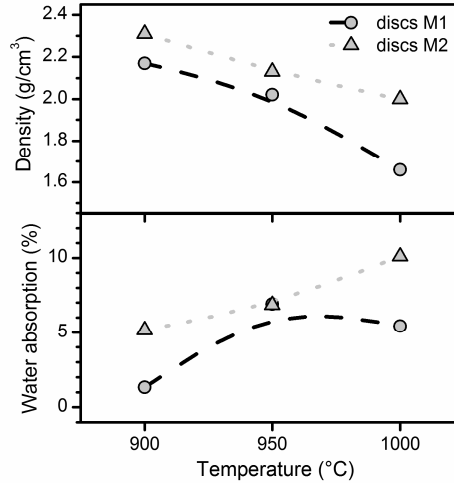
Figure VI.9: Density and water absorption of samples from direct sintering (preliminary firing tests)

The formation of pores is attributed to oxygen release (abundant in S1 and S2 slags). It may be observed that, from table VI.4, iron is in the Fe^{2+} (FeO) state, in the starting slags; for S1, in particular, this is consistent with the presence of fayalite (Fe_2SiO_4, PDF#09-0484), as actually shown in figure VI.10. However, a first oxidation by direct slag/air interaction (e.g. "oxygenolysis" of Fe_2SiO_4, yielding SiO_2 and Fe_2O_3 or Fe_3O_4) (see chapter V.4), could be followed by reduction, as a consequence of slag/glass interactions (the glass chemistry affects the stability of the iron oxides: this has been recently observed with soda-lime glass/basalt mixtures, leading to highly porous glass-ceramic) (Marangoni *et al*., 2014).
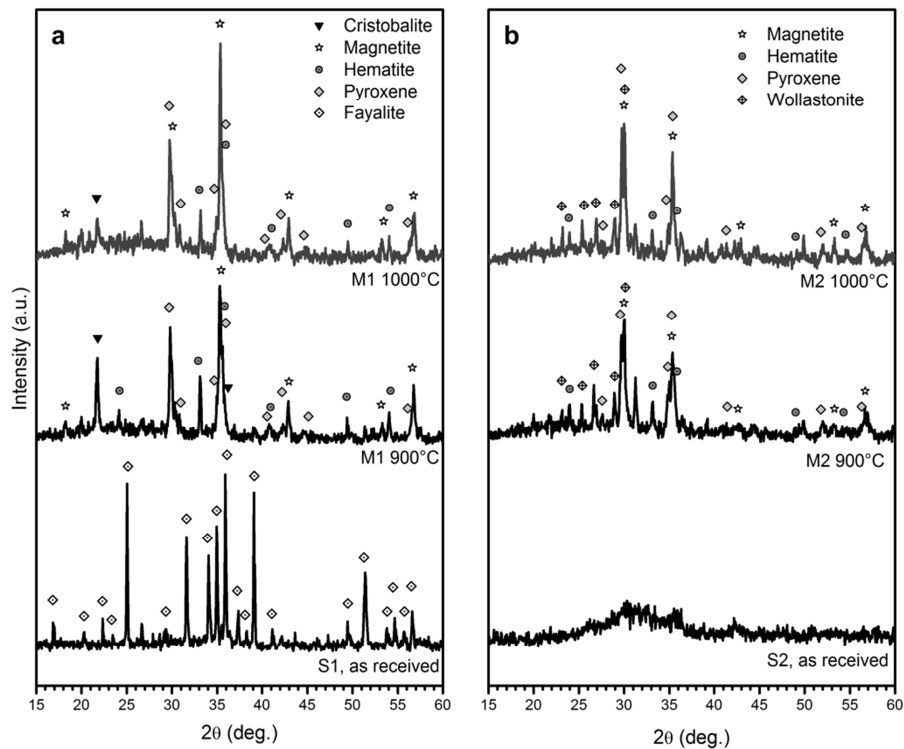

Figure VI.10: X-ray diffraction patterns of selected samples from direct sintering (preliminary firing tests)

The diffraction patterns of M1 and M2 fired sample, in figure VI.10, may be seen as a confirmation of the oxidation/reduction sequence. In fact, both magnetite (Fe_3O_4, PDF#86-1356)

and hematite (Fe_2O_3, PDF#72-0469) appear in samples fired at 900 °C, for both formulations. For M1, cristobalite (crystalline SiO_2, PDF#82-0512), is also evident, as a result of fayalite decomposition. The magnetite peaks (see, in particular, the strongest line at $2\theta \sim 35°$), for M1, become stronger with increasing firing temperature, whereas those of hematite (strongest line at $2\theta \sim 33°$) become weaker, consistently with a reduction reaction, providing oxygen release ($6\ Fe_2O_3 \rightarrow 4\ Fe_3O_4 + O_2$). The glass/slag interactions are further testified by newly formed silicates, relatively rich in silica (limited in both S1 and S2, abundant in SLG). Fort both formulations we can observe the presence of pyroxene, corresponding to the general formula $CaMg_xFe_{1-x}Si_2O_6$ (the position and the intensity of peaks are well-matched by $CaMg_{0.34}Fe_{0.66}Si_2O_6$, PDF#87-0701, and $CaMg_{0.52}Fe_{0.48}Si_2O_6$, PDF#87-0701). The chemistry of this phase is probably even more complicated, since it can incorporate additional ions, e.g. Zn^{2+} as well as Al^{3+} (from slags) (Rincón *et al.*, 1999). Finally, samples from S2 slag, richer in CaO, feature wollastonite ($CaSiO_3$, PDF#84-0655). The formation of wollastonite could be seen as a reasonable cause for the observed enhanced water absorption for M2 samples. The viscous flow sintering of the glass phase could fill the external porosity (the sample M1 fired at 900 °C, as an example, exhibited a water absorption of only ≈1%); however, the presence of rigid inclusions could delay the flow (Pascual *et al.*, 2005), especially in the case of inclusions represented by highly elongated crystals, like those usually associated to wollastonite (Bernardo, 2008).
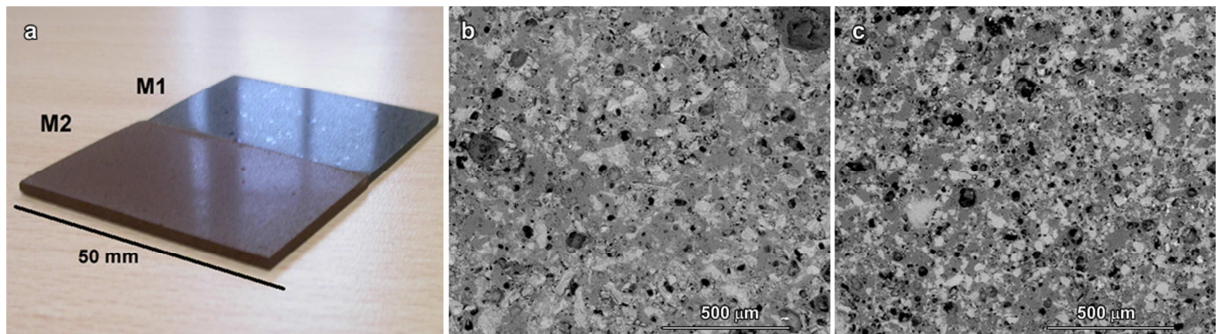
Figure VI.11: a) Aesthetic appearance of tiles samples from M1 and M2 mixtures; b) microstructural detail of sample M1; c) microstructural detail of sample M2

As shown by figure VI.11a, tiles samples from M1 and M2, fired at 900 °C, were quite different. M1, presenting a black color, became smooth and particularly brilliant, after polishing (up to 5 µm), in good analogy with porcelain stoneware and natural stones. On the contrary, M2, featuring a red color, remained quite opaque. The difference is evident also in the high magnification details, in figure VI.11b and VI.11c; the M1 sample exhibited isolated pores, whereas the M2 sample presented a widespread porosity, deter mining the observed opacity, by substantial scattering of reflected light and the smoothness of the glazed surface, after polishing.

Sample	Density (g/cm^3)	Water absorption (%)	Elastic modulus (GPa)	Bending strength (MPa)
M1	2.12 ± 0.03	0.6	44.3 ± 4.1	35.9 ± 9.0
M2	2.08 ± 0.04	5.8	37.9 ± 2.4	27.6 ± 2.7
LGC (M2 core)	2.16 ± 0.05	1.7	42.3 ± 6.5	31.4 ± 4.7

Table VI.5: Physical and mechanical properties of waste-derived glass-ceramics

The water absorption, for tile samples, as reported in table VI.5, is in good agreement with that of discs samples, despite the difference in heating and cooling (the conditions applied to tile samples were conceived to minimize thermal gradients, in bigger samples, upon heating, and thermal shock, upon cooling). We can say that M1 samples, from direct sintering, exhibit a good potential as lightweight tiles, even in the absence of a glaze; the complex of properties (density slightly higher than 2 g/cm^3, low water absorption, good bending strength) compares favorably with that of porous lightweight porcelain (Ponsot *et al.*, 2014). M2 samples, on the contrary, cannot be accepted, due to the excessive water absorption.

Following the scheme of figure VI.8, we considered the deposition of a glaze as a possible improvement of M2 samples. This glaze derived from the same starting raw materials (SLG and S2 slag) then M2 samples, but with a different balance. In fact, the mixing of 75 wt% SLG with 25% S2, instead of 50% SLG and 50% S2, could lead to a glass frit (waste-derived frit, WDF) with enhanced silica content, promoting the chemical stability.
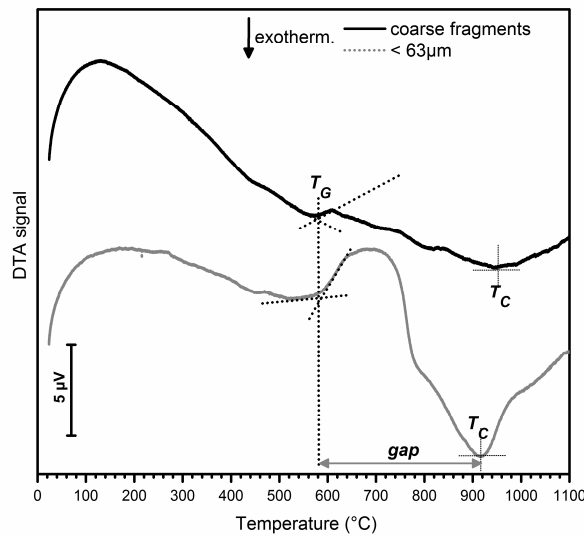
Figure VI.12: DTA analysis of fine and bulk powders of WDF

WDF was found to be sensitive to surface nucleation. As shown by figure VI.12, fine glass powders (with large specific surface) exhibited a significant crystallization exothermic peak at about 900 °C; on the contrary, coarse fragments (with limited specific surface) practically did not present any peak. Interestingly, WDF is also a good candidate for sinter-crystallization, i.e. crystallization with concurrent crystallization; in fact, dense glass-ceramics can be obtained by sintering at the crystallization temperature (temperature of the exothermic peak, T_C), if this temperature far exceeds the dilatometric softening temperature, recognized as the minimum temperature for extensive viscous flow (Ray and Tiwari, 2001). In the present case, the dilatometric softening temperature was not determined, but there is a particularly wide gap (nearly 300 °C) between the transition temperature (T_G) and T_C; considering that the dilatometric softening occurs only slightly above T_G, WDF had effectively the potential for developing a dense glass-ceramic layer, sintering at 900 °C (Bernardo, 2008).

The color and the shrinkage remained as open issues, concerning the application of WDF as a glaze for M2 bodies. In fact, pure WDF discs exhibited a quite unpleasant yellow-brown color and far higher shrinkage (~26%) than M2 samples (6.2 %), after firing at 900 °C; such mismatch could cause the development of cracks between the substrate and the glaze, in layered glass-ceramics.

This was corrected by considering WDF mixed with zircon and BSG powders. Zircon (well-known white pigment) improved the aesthetic appearance, leading to samples with a much lighter coloration, but also limited the densification. The shrinkage, operating with 45% zircon, fell dramatically, at about 1%, while the water absorption was above 7%. The addition of BSG enhanced the viscous flow sintering, being not subjected to crystallization: figure VI.13a shows that the progressive replacement of WDF with BSG, starting from a sample with WDF and zircon in the 55/45 weight proportion, effectively led to samples with moderate shrinkage and low water absorption. For the WDF/ BSG/zircon proportion of 40/15/45, the shrinkage matched that of M2 sample, whereas the water absorption reached 2%, the above mentioned threshold limit for optimum frost resistance.
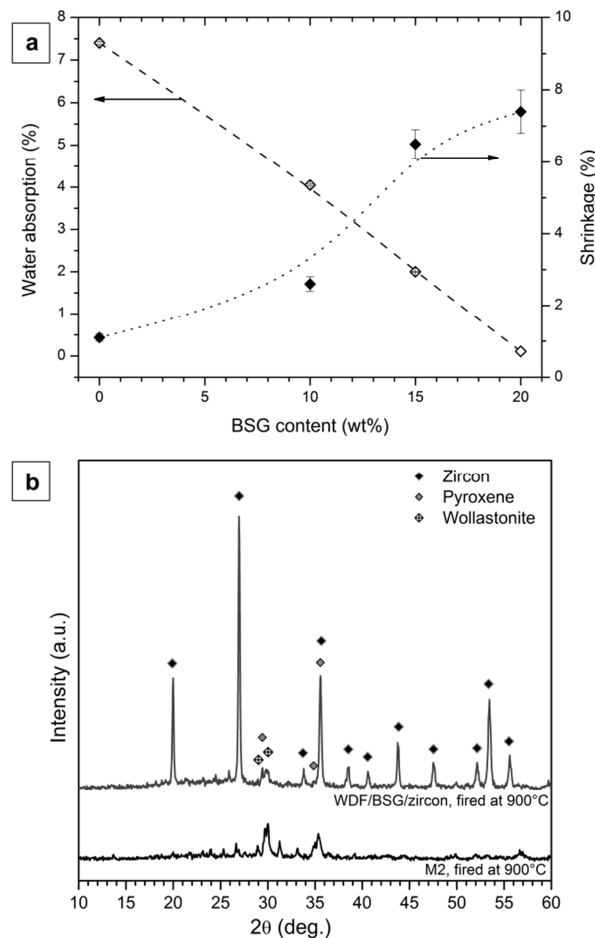
Figure VI.13: a) Water absorption/shrinkage evolution with increasing amount of BSG glass in frit-derived glass-ceramics fired at 900 °C, for 30 min; b) X-ray diffraction pattern of optimized glaze (WDF/ BSG/zircon=40/15/45)

The glaze can still be considered as the sinter-crystallization of WDF. In fact, from figure VI.13b, we can note that the strongest diffraction peaks correspond to zircon (ZrSiO4, PDF #71-0991); however, peaks attributable to both wollastonite and pyroxene (see the matching of positions with the pattern for M2) are still visible.

The layered glass-ceramic sample from direct sintering of M2 mixture accompanied by sinter-crystallization of WDF/BSG/zircon mixture is shown in figure VI.14a. The figure evidences the light color and the smoothness of the glazed surface, after polishing. The coating is uniform and

evidently crack-free; this is further confirmed by the SEM micrograph in figure VI.14b, clearly showing the good interpenetration of the glaze

(the high atomic weight of Zr makes the zircon-containing glaze lighter, in backscattered electrons images), still featuring some residual porosity, with the more porous body from M2 mixture. "Islands" corresponding to BSG and WDF are evidenced in figure VI.14c (in particular, due to the low atomic weight of B, BSG-rich zone appear darker). Finally, the previously discussed silicate crystals (wollastonite and pyroxene) are well visible in the WDF-rich areas, in the high magnification detail of figure VI.14d, while iron oxides are not visible as separate particles. Interestingly, fibrous silicate crystals appear concentrated at the interface with zircon particles, as a further proof of surface nucleation.

As reported in table VI.5, the introduction of a glaze, in LGC sample, did not particularly enhance the density, compared to M2; on the contrary, the water absorption (measured on a dense disc with the composition of the glaze) was much lower than that of M2. Elastic modulus and bending strength improved, and were quite close to those of M1 sample. LGC could be actually considered a good candidate for the manufacturing of ventilated façades, like M1, but with the additional advantage of a much lighter color.
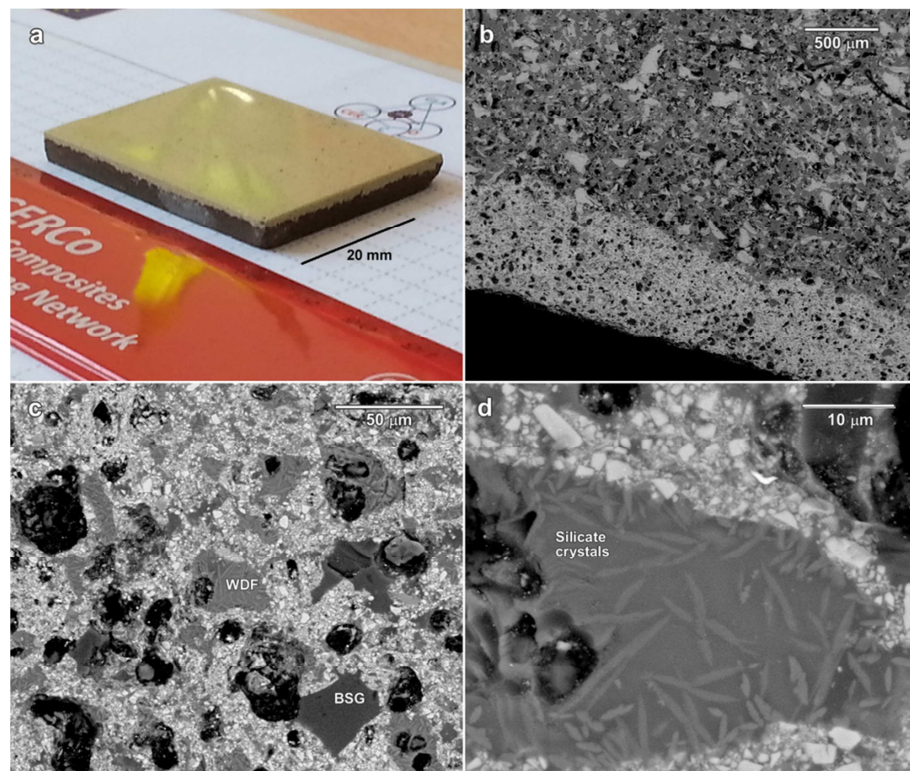
Figure VI.14: Aesthetic appearance and microstructural details of LGC sample, derived from S2 slag: a) photographic view; b) interface (SEM micrograph); c,d) high magnification details of the glaze (SEM micrographs)

The produced glass-ceramics were evaluated also in terms of stabilization of pollutants, by application of TCLP. The tile sample from M1 mixture, according to the leaching data reported in table VI.6, is chemically stable, with all metal ions well below the thresholds for inert materials, according to European Norm EN 12457. The tile from M2 had some ions above the thresholds (in particular Sb); the enhanced specific surface, due to open porosity (in turn associated to the observed high water absorption), reasonably maximized the interaction between material and

solution, favoring the leaching. In analogy with water absorption, also the leaching was improved by application of a glaze, with all metal ions well below the threshold for inert materials for a test applied on WDF/BSG/zircon glass-ceramic.

Element	Leachate / ppm			Limits [UE] / ppm	
	M1	M2	LGC (glaze)	inert material	non-hazardous material
As	0.0241	0.3284	0.0309	0.05	0.2
Ba	0.0514	>0.7382	0.0157	2	10
Cd	<0.0002	<0.0002	<0.0002	0.004	0.1
Cr	0.0046	0.0226	0.1152	0.05	1
Cu	0.0239	0.0602	0.0090	0.2	5
Mo	0.0148	0.1684	0.0760	0.05	1
Ni	0.0059	0.0045	0.0024	0.04	1
Pb	<0.0047	<0.0047	<0.0047	0.05	1
Sb	<0.0099	0.2498	<0.0099	0.006	0.07
Se	<0.0122	0.0697	<0.0122	0.01	0.05
Zn	0.0281	<0.0203	<0.0203	0.4	5

Table VI.6: Leaching results of samples heated at 900 °C for 30 min with 40 °C/ min rate

Figure VI.15 reports the cell viabilities (left), after a 24 hours exposition in a culture of mouse embryonic fibroblasts, and the spreading of cells on samples surfaces (right), with blue and green evidencing the nuclei (Dapi markers) and the cytoplasms (calcein markers), respectively.
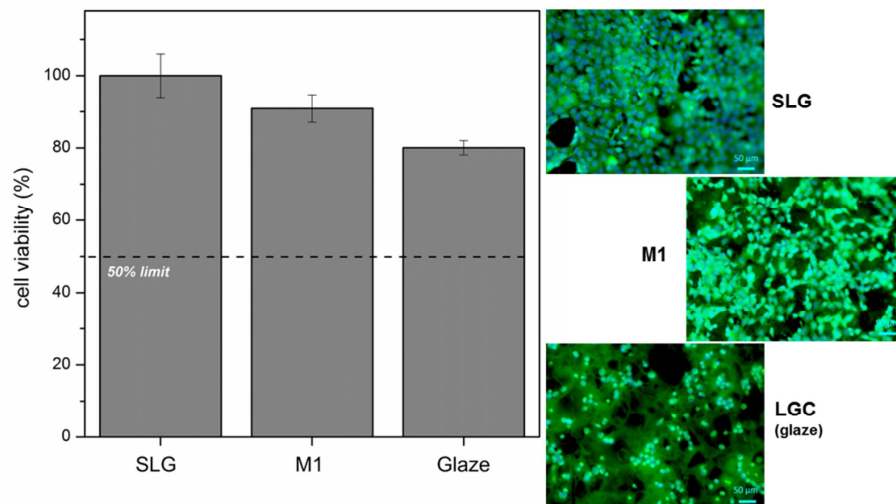
Figure VI.15: Cell viability (in %) referred to a commercial SLG (left); fluorescent microscope images of samples from direct cytotoxicity test (right)

Soda-lime glass is the most viable sample for cellular activity. Indeed, its composition is similar to simple biocompatible glasses, as Si, O, Na and Ca, present in high majority, are the elements that interact mostly in cellular growth (see chapter IV). The cell viability decreased, in M1 and in the glaze for LGC, in agreement with the lower percentages of the previously mentioned elements, but remained substantial (well above 50%, considered as a threshold for toxicity). As previously found with samples from S1 and S2 combined with BSG (Ponsot *et al.*, 2014), the cells exhibited spreading and mutual interconnections, with an elongated morphology, which are well-recognized features to indicate biocompatibility (Pollard *et al.*, 2008; Hoppe *et al.*, 2011). The results are undoubtedly preliminary (as an example, "indirect" tests, with samples were placed in a separate cell culture medium under standard conditions, are still in progress), but the

observed biocompatibility well matches with the chemical stability, assessed by TCLP leaching test.

VI.3.3 Conclusions

We may conclude the following:

- Direct sintering of metallurgical slag (S1) and soda-lime glass can lead to lightweight glass-ceramics, with limited water absorption, good mechanical properties and good chemical stability;
- The excessive water absorption and the poor chemical stability of glass-ceramics from the mixing of soda-lime glass with another metallurgical slag (S2) can be improved by application of a glaze;
- A single step thermal treatment can deter mine both direct sintering of a waste-derived base body and sinter-crystallization of the glaze;
- A waste-derived glaze can be adjusted, in term of color, shrinkage and viscous flow, by addition of zircon and recycled borosilicate glass;
- Layered glass-ceramics, comprising a waste-derived core and a waste-derived glaze could find applications in the building industry as lightweight tiles, e.g. in ventilated façades.

References

Ashby M.F. (2005) Materials Selection in Mechanical Design, third ed., Butterworth Heinemann-Elsevier, Oxford, UK.

Bernardo E. Castellan R. Hreglich S. Lancellotti I. (2006) Sintered sanidine glass-ceramics from industrial wastes, J. Eur. Ceram. Soc., 26 (15), 3335–3341.

Bernardo E. (2008) Fast sinter-crystallization of a glass from waste materials, J. Non-Cryst. Sol., 354, 3486–3490.

Bernardo E. Scarinci G. (2008) Fast sinter crystallization of waste glasses, Adv. Appl. Ceram., 107, 344–349.

Bernardo E. Scarinci G. Edme E. Michon U. Planty N. (2009) Fast-sintered gehlenite glass–ceramics from plasma-vitrified municipal solid waste incinerator fly ashes, J. Am. Ceram. Soc., 92, 528-530.

Bernardo E. De Lazzari M. Colombo P. Llaudis A.S. Garcìa-Ten F.J. (2010a) Lightweight porcelain stoneware by engineered CeO2 addition, Adv. Eng. Mater., 12, 65-70.

Bernardo E. Bonomo E. Dattoli A. (2010b) Optimization of sintered glass–ceramics from an industrial waste glass, Ceram. Int., 36, 1675-1680.

Binhussain M.A. Marangoni M. Bernardo E. Colombo P. (2014) Sintered and glazed glass-ceramics from natural and waste raw materials, Ceram. Int., 40, 3543-3551.

Cicek B. Esposito L. Tucci A. Boccaccini A.R. Bingham P.A. (2012) Microporous glass ceramics from combination of silicate, borate and phosphate wastes, Adv. Appl. Ceram., 111, 415-421.

Colombo P. Brusatin G. Bernardo E. Scarinci G. (2003) Inertization and reuse of waste by vitrification and fabrication of glass-based products, Curr Op Sol St Mat Sci. , 7, 225-239.

Dimech C. Cheeseman C.R. Cook S. Simon J. Boccaccini A.R. (2008) Production of sintered materials from air pollution control residues from waste incineration, J. Mater. Sci., 43, 4143-4151.

Environmental Protection Agency U.S. (1992) Report EPA/625/R-92/002, Handbook of Vitrification Technologies for Treatment of Hazardous and Radioactive Waste, Office of Research and Development, Washington, DC.

Francis A.A. Rawlings R.D. Sweeney R. Boccaccini A.R. (2002) Processing of coal ash into glass ceramic products by powder technology and sintering, Glass Technol, 43, 58-62.

Gutzow I. Pascova R. Karamanov A. Schmelzer J. (1998) The kinetics of surface induced sinter-crystallization and the formation of glass-ceramic materials, J. Mater. Sci., 33, 5265-5273.

Höland W. Beall G. (eds.) (2002) Glass-ceramic technology, The American Ceramic Society, 2002, Westerville OH.

Hoppe A. Güldal N.S. Boccaccini A.R. (2011) A review of the biological response to ionic dissolution products from bioactive glasses and glass-ceramics, Biomat, 32, 2757-2774.

Marangoni M. Secco M. Parisatto M. Artioli G. Bernardo E. Colombo P. Altlasi H. Binmajed M. Binhussain M. (2014) Cellular glass–ceramics from a self-foaming mixture of glass and basalt scoria, J. Non-Cryst. Sol., 403, 38-46.

Marchioni D. (2013) Vetroceramiche Sinterizzate da Rifiuti Industriali, Laurea Magistrale, Università di Padova, Italy.

Pascual M.J. Durán A. Prado M.O. Zanotto E.D. (2005) Model for sintering devitrifying glass particles with embedded rigid fibers, J. Am. Ceram. Soc., 88, 1427-1434.

Pollard T.D. Earnshaw W.C. Lippincott-Schwartz J. (2008) Cell Biology, Easy reading, Second edition, Spektrum Akademischer Verlag, Saunders Elsevier, 1600 John F. Kennedy Blvd, Suite 1800, Philadelphia, PA9103-2899, Published by Elsevier Inc. ISBN 1-4160-22554.

Ponsot I. Bernardo E. (2013) Self glazed glass ceramic foams from metallurgical slag and recycled glass, J. Cleaner Prod., 59, 245-250.

Ponsot I. Pontikes Y. Baldi G. Chinnam R.K. Detsch R. Boccaccini A.R. Bernardo E. (2014) Magnetic glass ceramics by sintering of borosilicate glass and inorganic waste, Mat., 7, 5565-5580.

Ponsot I. Falcone R. Bernardo E. (2013) Stabilization of fluorine-containing industrial waste by production of sintered glass-ceramics, Ceram Int, 39, 6907-6915.

Rawlings R.D. Wu J.P. Boccaccini A.R. (2006) Glass-ceramics: Their production from wastes-A Review, Journal of Materials Science, 41 (3), 733-761.

Ray A. Tiwari A.N. (2001) Compaction and sintering behavior of glass-alu mina composites, Mat CChem Phis, 67, 220-225.

Rincón J. Ma. Romero M. Boccaccini A.R. (1999) Microstructural characterization of a glass and a glass-ceramic obtained from municipal incinerator fly ash, J. Mat. Sci., 34, 4413-4423.

Schabbach L.M. Andreola F. Karamanova E. Lancellotti I. Karamanov A. Barbieri L. (2011) Integrated approach to establish the sinter-crystallization ability of glasses from secondary raw material, J. Non-Cryst. Sol., 357 (1), 10-17.

Chapter VII

Final remarks

VII.1 Novel application of waste-derived glass-ceramics: electromagnetic shielding tests

VII.1.1 Introduction

Ceramics and glass-ceramics based on industrial waste have been widely recognized as competitive products for building applications; however, there is a great potential for products with novel functionalities. As presented in chapter V.4, the substantial viscous flow of borosilicate glass led to dense products, for rapid treatments at relatively low temperature (900 °C to 1000 °C), whereas glass/slag interactions resulted in the formation of magnetite crystals, providing ferrimagnetism. In the case of soda-lime glass, the glass/slag interactions led to the evolution of oxygen (due to the reduction of Fe_2O_3 into FeO) upon sintering, with the development of highly porous foams, that could be used as thermally insulating materials, with no need for any foaming agent.

Moreover, the ferrimagnetic properties obtained may be benefic in electromagnetic shielding application for EMC chambers. According to Drivnosky and Kejik (2009), problems arise when it is necessary to measure the shielding effectiveness of the construction materials for those chambers or boxes. Especially in the development stage, before building the whole chambers or boxes, it is not possible to perform accurate measurements in the huge sizes: this approach would be expensive and time consuming. Constructional problems appears when it is necessary to know the shielding efficiency of the developed materials like bricks, plasterboard, concrete etc., and particularly composite materials which are necessary to the construction of chambers doors, the weakest part of these shielded chambers.

The generated material, if presenting suitable properties, could replace the current heavy construction materials that require both a complicated manutention and a supplementary additive coating to provide shielding efficiency in advanced microwave structures such as EMC or anechoic chambers.

VII.1.2 Sample preparation

The starting wastes consisted of the metallurgical slag labelled S2 presented in chapter V.4. The drive for investigating this slag relates to the fact it is Fe,Ca,Si-rich and then prone to sintering in the desired temperatures ranges. The slag was mixed with recycled soda-lime glass, in the following proportions: 75 wt% SL - 25 wt% S2. The chemical composition of the starting waste and of the recycled soda-lime glass is reported in Table VII.1.

| Oxide	S2	SL
Chemical compositions (wt.%)		
SiO$_2$	24	73
Fe$_2$O$_3$	32	-
Al$_2$O$_3$	6	-
CaO	21	11
MgO	1	3
Na$_2$O	<1	13
K$_2$O	<1	-
ZnO	7	-
B$_2$O$_3$	<1	-

Table VII.1: Oxide content of the starting wastes

Low densities (<1 g/cm^3) were generally obtained by an important foaming, upon viscous flow sintering, in turn associated to the oxygen release provided by the reduction of ferric oxide into ferrous oxide. In fact, the sample elaborated presented an important blowing already present after a thermal treatment by direct sintering at 900 °C for 30 min. The rapid expansion enabled to shorten the heating time from 30 min to 5 min.

Heating time	Geometric density (g/cm^3)	Bulk density (g/cm^3)	Total porosity (%)
30 min	0.36 ± 0.05	2.73 ± 0.00	87.2
20 min	0.38 ± 0.02	2.75 ± 0.00	87.4
10 min	0.45 ± 0.07	2.83 ± 0.00	82.6
5 min	0.32 ± 0.06	2.79 ± 0.00	88.4

Table VII.2: Total porosity of the selected sample {75 wt% SL ;25 wt% S1} sintered at 900 °C

Comparatively to the borosilicate glass (chapter V.4), soda-lime glass favored the mechanism of high temperature reduction of Fe$_2$O$_3$, leading to both oxygen release and magnetite Fe$_3$O$_4$ formation:

$$^{3}/_{2}\ Fe_2O_3 \rightarrow Fe_3O_4 + {}^{1}/_{4}\ O_2$$
$$Fe_2O_3 \rightarrow 2\ FeO + {}^{1}/_{2}\ O_2$$
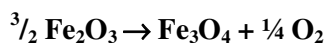
The obtained densities, summarized in table VII.2, were sufficiently low to enable an adjustment of the temperature at 880 °C. The obtained foam was lightweight and presented relatively good compression strength (see tableVII.3).

Heating time	Geometric density (g/cm^3)	Bulk density (g/cm^3)	compression strength (MPa)	Total porosity (%)
5 min	0.66 ± 0.03	2.67 ± 0.01	3.60 ± 0.57	75.2

Table VII.3: Total porosity of the selected sample {75 wt% SL ;25 wt% S1} sintered at 880 °C

To exploit the ferrimagnetic properties of the sample, a composite material was elaborated from the samples shaped in granules (see figure VII.1a) according to a typical laboratory granulation process (Citu *et al*., 2011 ; UniPD) and incorporated as fillers in a geopolymer preparation (Betonfix, UniPD) in volume proportions 60 % filler / 40 % geopolymer. The produced composite was shaped by wet casting (30 wt% water) into round plates of 15 mm thickness and 130 mm diameter, using a plastic mold (figure VII.1b). Because of the high density of the geopolymer, the

resulting plate presented an increased total geometric density, but still of reasonable value (2.0 ± 0.1 g/cm^3).
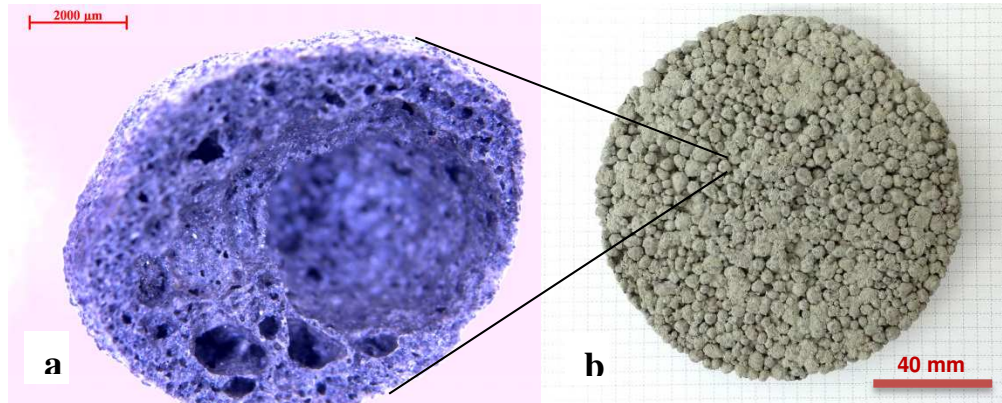
Figure VII.1: a) Diametric section of a foam granule; b) composite plate

The leachate of the obtained granules shown in table VII.4 indicates a good chemical stability lower than the limit for non-hazardous materials. Thus, by incorporating the granules among the (inert) geo polymer particles, the dilution of the heavy elements would be sufficient to reach the lowest limits of inert material.

Element	Leachate / ppm	Limits / ppm L/S =10 l/kg	
	Foam	inert material	non-hazardous material
	(*S2 25 wt%*)		
As	**0.1811**	0.05	0.2
Ba	0.0399	2	10
Cd	<0.0002	0.004	0.1
Cr	0.0111	0.05	1
Cu	0.0429	0.2	5
Hg	0.0007	0.001	0.02
Mo	0.0192	0.05	1
Ni	0.0078	0.04	1
Pb	0.0050	0.05	1
Sb	<0.0099	0.006	0.07
Se	**0.1018**	0.01	0.05
Zn	<0.0203	0.4	5
Ag	0.0143	-	

Table: Leachate from TCLP (EN version) on foam granules

The innovation here merely consists in combining electromagnetic properties to the lightweigthness, thanks to the already present ferrimagnetism. In the recent literature are reported similar studies, among them shielding effectiveness tests on low-cost civil engineering construction material based on cement containing waste (Migliaccio *et al.*, 2013).

The obtained plate in two replicates was then submitted to a first set of short electromagnetism tests showing a slight modification of the initial field of around 0.1 mT. It was noticed an inhomogeneity of the field along the disc superficial perimeter. The points of high concentration magnetic field corresponded to foam granules position and the zones showing an absence of magnetic field corresponded to geopolymer-rich zones, showing the inhomogeneous distribution of iron-containing particles in the disc. This was justified by the inhomogeneity resulting from the

particles/geopolymer mixture. Electromagnetic shielding effectiveness was tested according to the method established for thin films by Desideri *et al*., (2013) (figure VII.2).
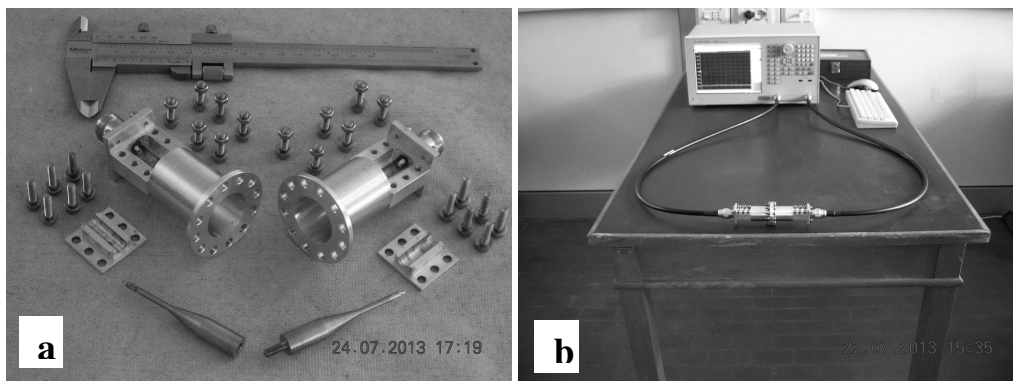
Figure VII.2: a) Sample holder ;b) Measurement experimental set-up

In the procedure, the frequency ranged between 100 kHz and 3 GHz. The electrical resistivity was measured and reported as an electromagnetic signal. Figure VII. 3 shows the results of the test performed on new discs of dimension suitable to the experimentation (disc of 35 mm diameter and 5 mm thickness, faces parallels and completely flat, with a 3 mm hole in the center).
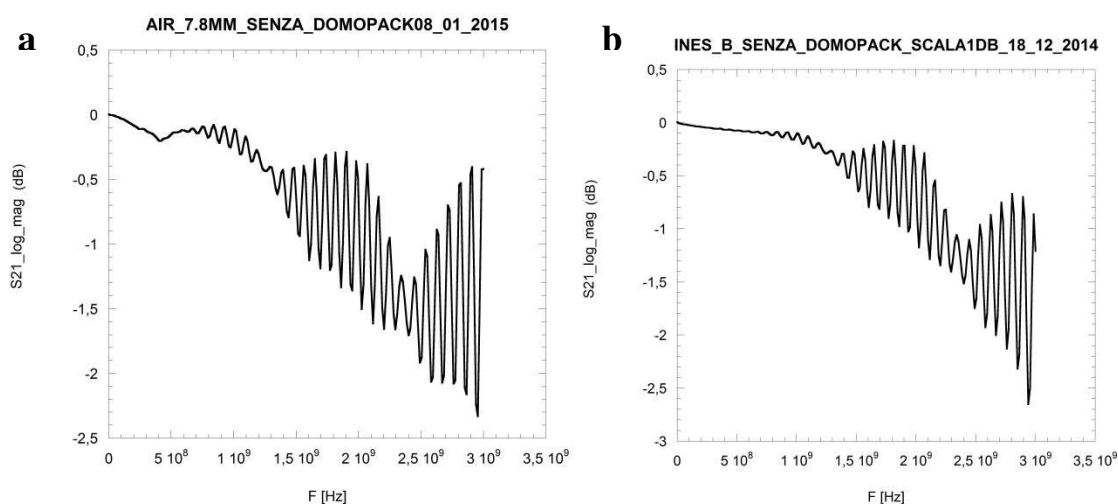
Figure VII.2: Electromagnetic response, in dB, in function of frequency (Hz); a) "zero – setting" curve, no sample; b) data with sample, no "zero – setting"

The zero-setting curve (figure VII.2a) corresponds to a blank measurement, "zero situation", i.e. the system in air, without the disc, done in the same geometric conditions as during the trial on the geopolymer-foam composite discs (figure VII.2b). Both measurements were done without domopack.

As a result, the obtained difference between the data with and without sample, reported in figure VII.3, was very small, in an interval of ± 0.2 dB (among the values in the frequencies around 3 GHz). This first result indicated that, in fact, almost no shielding effectiveness effect could be observed at low frequencies, between 100 kHz and 3 GHz.

Diff_INES_B_SCALA1DB_AIR_7.8mm_senza_domopack
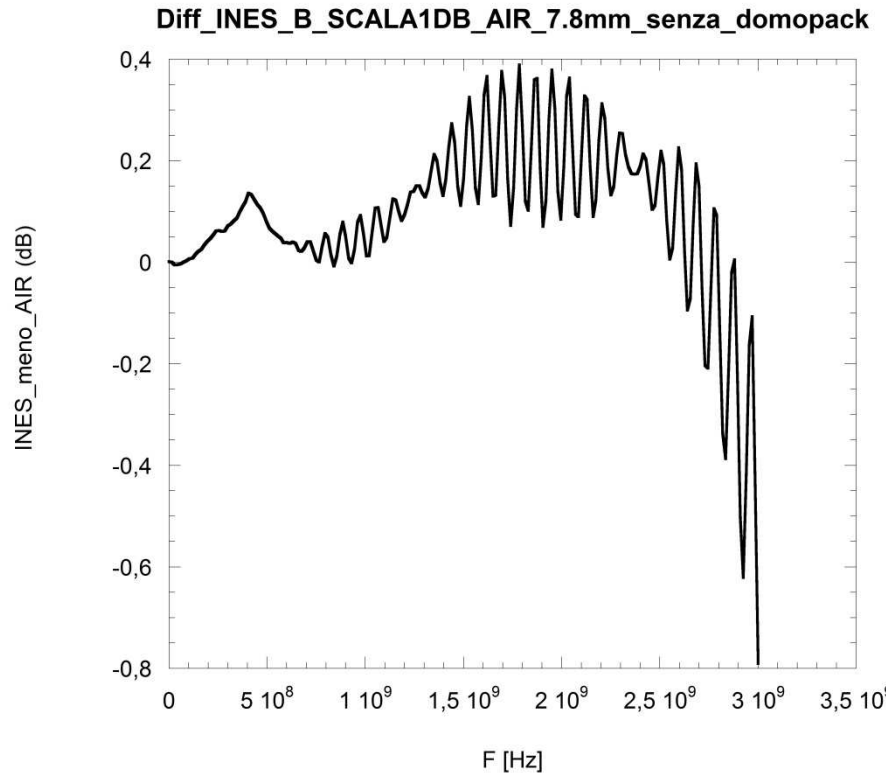
Figure VII.3: Superposition of the collected data to the zero setting curve

Conclusions and further investigations:

- The material is interesting for lightweight properties. Similar foam granules have already proven to constitute a good base for composite structures fulfilling insulating functions, as referred in the literature (Apkar'yan, *et al.*, 2008; Shu *et al.*, 2012).

- Lower frequency shielding effectiveness is however still to investigate with a new technique. Indeed, with the increase applications of electronic equipment, the electromagnetic interfering problem becomes more and more serious. Also, with the increasing use of electrical power, magnetic fields of low frequency are often encountered in our environment. These high field strengths may cause disturbances on video display units, with interference occurring mainly as frame disturbances when the magnetic flux density is above 0.5-1 µT (Keshtkar *et al.*, 2011).

VII.2 Assessment of the stabilization of pollutants by cytotoxicity tests: further observations and perspectives

VII.2.1 Study of the cytotoxicity of foams

For the study of cytotoxicity, cell viability is evaluated mainly by mitochondrial activity. Indeed, mitochondria enzymes convert most of the energy released from the breakdown of nutrients into the synthesis of ATP, the common currency for most energy-requiring reactions in ells. This efficient mitochondrial system uses molecular oxygen to complete the oxidation of fats, proteins, and sugars to carbon dioxide and water. A less efficient glycolytic system in the cytoplasm extracts energy from the partial breakdown of glucose to make ATP. Mitochondria cluster near sites of ATP utilization, such as sperm tails, membranes engaged in active transport, nerve terminals, and the contractile apparatus of muscle cells. Mitochondria have also a key role in

cellular responses to toxic stimuli from the environment. In response to drugs such as many that are used in cancer chemotherapy, mitochondria release into the cytoplasm a toxic cocktail of enzymes and other proteins that brings about the death of the cell. Defects in this form of cellular suicide, known as apoptosis, lead to autoimmune disorder, cancer and some degenerative diseases. Mitochondria form in a fundamentally different way from the ER, Golgi apparatus and lysosomes. Free ribosomes synthesize most mitochondrial proteins, which are released into the cytoplasm. Receptors on the surface of the mitochondria recognize and bind signal sequences on mitochondrial proteins. Energy-requiring process transports these proteins into the lumen of insert them into the outer or inner mitochondrial membranes (Pollard, 2008).

The Misapor commercial material was chosen as a porous reference for cytotoxicity study of foam samples (chapter V.5), as it presented an equivalent porosity to the compared sintered material (see part 1 of chapter VII).
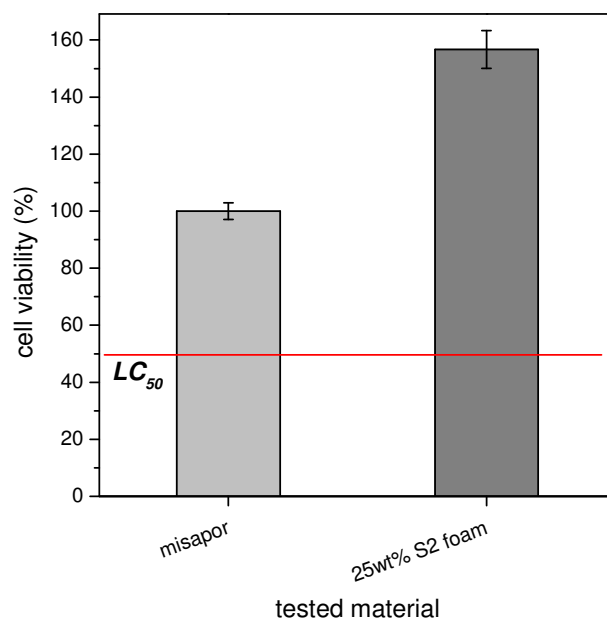
Figure VII.4: Cell viability after 24 hours direct study on porous samples

From figure VII.4, the porous reference Misapor presents a level of cell viability lower than that of the compared foam from formulation 25 wt% S2 (sintered at 900 °C for 5 min, presented in part VII.1). In fact, if the total porosity of both samples is equivalent, however, the open porosity is more important in the foam sample than in the Misapor reference. Cells, once seeded, could disperse inside the important network of pores and it is well-known that cellular activity is favored in pores interstices. The high cell viability (> 150 %) of foams can be explained by the important specific surface contact area (80% porosity) which enable to cell to attach also inside pores cavities. On another hand, the important Fe quantity in the foam may have interacted deeply in the cell viability. The high Fe amount in sample impacts positively on the results, promoting cell growth, as an important element in the cellular metabolism.

VII.2.2 Deepen study of the cytotoxicity regarding pre-stabilized MSWI ashes based sample

Pre-stabilized MSWI ashes "sintered glass-ceramic" is actually of porosity around 30%. Tested with TCLP method, which is usually used for the evaluation of toxicity of a waste, pre-stabilized MSWI ashes ceramic leachate corresponded to the level "inert waste", but this test did not give

insurance of its use as a final product. The cytotoxicity comparative tests enabled to evaluate the environmental impact of pre-stabilized MSWI ashes ceramic as a final product for building applications, with window glass as most relevant comparison reference. Direct method and indirect method showed different results.

Direct method was giving interesting information about the development of cells. Pre-stabilized MSWI ashes crystalline composition as showed in figure V.15a was mainly constituted of Wollastonite ($CaSiO_3$), several forms of silica SiO_2, Albite KSiAlO and Anorthite (Ca,Na) ($Al_4Si_2O_8$). The solubility of those crystals was not known, but it could be reasonably deduced that the cells culture in direct method was mainly associated to the concentration of the element present in these crystals: Ca, Si, O, Al, K and Na. According to Dufrane *et al*, (2003) pseudowollastonite is able to induce several changes, as pH increase, release of calcium (Ca^{2+}) and silicate (SiO^{3-}) ions, in the environment leading to the papthite –like layer formation. These changes could potentially lead to cellular toxicity. Wollastonite being comparable to pseudowollastonite, we could deduce that the percentage of wollastonite in glass-ceramics was prior to that of heavy elements susceptible to impact on samples toxicity, during this time period. In other papers concerning the toxicity of waste products, the cytotoxicity was determined in percentages, with 20% set as the maximum level for the definition of non-toxicity. (Huang *et al*., 2010). This result was supported by the following two facts: (1) wollastonite is one of two major crystalline phases of Apathite/Wollastonite glass ceramic that has excellent biocompatibility and bioactivity (Cannillo *et al*., 2009); and (2) wollastonite ceramic itself, owing to its relevant bioactivity, is usually regarded as a potential candidate for artificial bone (Liu et al., 2008). In indirect method, cells proliferation was not visible, but could be estimated quantitatively. After 3 days of leaching, it decreased, meaning probably that certain ions had reached threshold concentrations, from which the effect on cells culture became negative. The leachate in table V.9 (TCLP, 24 hours) showed an important presence of Cl, Ca, K, Br, S and Zn which may be detectable again in the cell culture medium of the indirect method. Except for Br and S, all those elements are convenient for cell culture.

As a conclusion, the correlation between TCLP, XRD and cytotoxicity measurements enables to assess the non-toxicity of waste based samples, thanks to the possibility to cross the various information given by each measure. X-ray diffraction indicates the main phases susceptible to interact with the external environment; TCLP identifies the ions susceptible to be rapidly leached in a liquid and cytotoxicity illustrates the responses of living organisms to the material. By comparison with biocompatible glasses, the first chemical interactions between the material and cells can be determined.

VII.3 Conclusions

Many types of wastes have been successfully converted into dense or porous glass-ceramics. We can summarize our experiences in the following points:

- We fulfilled the "GlaCERCo" targets of valorization and vitrification of waste, since: i) we focused on glass-based engineering products with high commercial value such as lightweight tiles or panels for ventilated façades and foams for thermal and acoustic insulation foams, or with unconventional functional properties (e.g. magnetic properties) for new applications (e.g. panels subjected to induction heating); ii) many products were obtained by direct sintering of glass/waste mixtures, with satisfactory stabilization of pollutants in the matrix provided by simple viscous flow sintering; iii) vitrification (corresponding to the melting of mixtures of wastes) was applied with "sustainability" constraints, i.e. the costs of the process could be minimized using waste glasses as raw materials for glazes to be applied on products from direct sintering (the minimization of costs is due to the reduction of volumes; we keep exploiting, however, the high chemical stability of waste glasses and glass-ceramics, when properly formulated, in the glazes);

- The direct sintering of glass/waste mixtures is advantageous for the minimization of costs, but also for the stabilization of specific waste. In fact, some waste (such as F-containing waste) may decompose upon vitrification, with release of hazardous gasses. The products from direct sintering can be treated as glass-ceramics, although not developed by crystallization of a homogenous glass, for the observed glass/waste interactions, leading to new crystal phases;

- The glass/waste interaction is particularly interesting with iron-rich waste, since it may be associated to the reduction of Fe_2O_3 into FeO and Fe_3O_4. The reduction implies the release of oxygen gas, that can lead to highly porous foams even in the absence of other (expensive) foaming additives; in addition, the possible formation of magnetite (Fe_3O_4) is interesting for the ferrimagnetic behavior of waste-derived glass-ceramics;

- The low costs associated to direct sintering and the high chemical stability of glass-ceramics can be effectively coupled in the manufacturing of novel layered glass-ceramics, with a core from direct sintering, and a glaze from sinter-crystallization of waste-derived glasses; the products match the properties of specific valuable ceramic materials (porous stoneware ceramics) for application in ventilated façades;

- A particular innovation concerns the development of new procedure for the assessment of the safety of waste-derived glass-ceramic products. In fact, conventional leaching tests were coupled with cytotoxicity tests. The new tests are thought to be particularly useful for the removal of the "social stigma" on waste-derived materials.

References

Apkar'yan A.S. Khristyukov V.G. Smirnov G.V. (2008) Granulated foam glass ceramic – a promising heat-insulation material, Glass and Ceramic, translated from Steklo I Keramika, 3, 10-12.

Cannillo V. Pierli F. Sampath S. Siligardi C. (2009) Thermal and physical characterization of apatite/wollastonite bioactive glass–ceramics, J. Eur. Ceram. Soc., 29, 611-619.

Citu, T.M. Oulahna D. Hemati M. (2011) Wet granulation in laboratory scale high shear mixers: Effect of binder properties, Powder Technol., 206 (1-2), 25-33.

Desideri D. Cavallin T. Maschio A. (2014) Development of an improved version of sample holder for measuring the shielding effectiveness of planar films, Int. J. Appl. Electromag. Mech., 45, 273-278.

Drinovsky J. Kejik Z. (2009) Electromagnetic shielding efficiency measurement of composite materials, Measur. Sci. Rev., 9 (4), 109-112.

Huango W.J. Tang H.C. Lin K.L. Liao M.H. (2010) An emerging pollutant contributing to the cytotoxicity of MSWI ash wastes: Strontium, J. Haz. Mat., 173, 5797-604.

Keshtkar A. Maghoul A. Kalantarnia A (2011) Magnetic shielding effectiveness in low frequency, Int. J. Comput. Electr. Eng., 3(4), 507-513.

Liu X. Morra M. Carpi A. Li B. (2008) Bioactive calcium silicate ceramics and coatings, Biomed. Pharmacother., 62 (8), 526-529.

Migliaccio M. Ferrara G. Gifuni A. Sorrentino A. Colangelo F. Ferone C. Cioffi R. Messina F. (2013) Shielding effectiveness tests of low-cost civil engineering materials in a reverberating chamber, Prog. Electromag. Res. B, 54, 227-243.

Shu Z. Garcia-Ten J. Amoros J.L. Zhou J. Wang Y.X. (2012) Cleaner production of porcelain tile powders. Granule and green compact characterization, Ceram. Int., 38, 517-526.

Xin R. Zhang Q. Gao J. (2010) Identification of the wollastonite phase in sintered 45S5 bioglass and its effect on in vitro bioactivity, J. Non-Cryst. Sol., 356, 1180-1184.

Chapter VIII

Publications

VIII.1 List of papers

Papers in peer-reviewed journals, published

Ponsot I., Bernardo E., Boccaccini A.R., Chinnam R.K., Detsch R., Bontempi E., *Recycling of Pre-stabilized Municipal Waste Incinerator Fly Ash and Soda-Lime Glass into Sintered Glass-ceramics*, J. Cleaner Prod. (2015) 89, 224-230.

Ponsot I., Dal Mas G., Bernardo E., Dal Maschio R., Sglavo V. M., *Double strengthening by ion exchange of sintered nepheline glass-ceramics: a new simplified method*, J. Ceram. Proc. Res., (2014), 15 [6], 411-417.

Ponsot I., Pontikes Y., Baldi G., Chinnam R.K., Detsch R., Boccaccini A.R., Bernardo E., *Magnetic glass ceramics by sintering of borosilicate glass and inorganic waste* (2014) Materials, 7 (8), pp. 5565-5580.

Bernardo E., Ponsot I., Colombo P., Grasso S., Porwal H., Reece M.J., *Polymer-derived SiC ceramics from polycarbosilane/boron mixtures densified by SPS* (2014) Ceram. Int., 40 (9 PART A), pp. 14493-14500.

Marangoni M., Ponsot I., Kuusik R., Bernardo E., *Strong and chemically inert sinter crystallised glass ceramics based on Estonian oil shale ash*, Adv. Appl. Ceram. (2014) 113 [2], 120-128.

Ponsot I., Falcone R., Bernardo E., *Stabilization of Fluorine-containing Industrial Waste by Production of Sintered Glass-ceramics*, Ceram. Int. (2013) 39 [6], 6907-6915.

Ponsot I., Bernardo E., *Self-glazed glass ceramic foams from metallurgical slag and recycled glass*, .J Cleaner Prod. (2013) 59 [15], 245-250.

Papers in peer-reviewed journals, submitted

Marangoni M., Ponsot I., Cicek B.,Bernardo E., *Double Layer Waste-derived Glass-Ceramics Prepared by Low Temperature Sintering/Sinter-crystallization*, J. Cleaner Prod., (submitted in 2014).

Ponsot I., Detsch R., Boccaccini A.R., Bernardo E., *Waste-derived Glass Ceramic Composites Prepared by Low Temperature Sintering/Sinter-crystallization*, Adv. Appl. Ceram. Special issue: Glass and Ceramic Composites for high Technology Applications, (submitted in 2015)

Papers in conference proceedings

Ponsot I., Bernardo E., *Obtainment of glass-ceramic composites based on clay, recycled glass and fluorine-containing industrial waste*, Proc. 13th Eur Inter-Reg Conf Ceram (CIEC), Barcelona, Spain, 12-14 September 2012.

VIII.2 List of oral and poster presentations

VIII.2.1 Oral presentations (I. Ponsot as presenting author)

Ponsot I., Bernardo E., *Dense and porous functional glass-ceramics from metallurgical slags and recycled glasses*, 12th ESG conference Parma, 21-24 September 2014.

Ponsot I., Marangoni M., Bernardo E., *Mixture of metallurgical slags and recycled glasses converted into functional glass-ceramics: thermally insulating foams and magnetic monoliths for induction heating*, 13th CIMTEC Montecatini Terme, 08-13 June 2014.

Ponsot I, Bernardo E., *New lightweight glass-ceramics from the sintering of recycled glasses and inorganic waste*, 13th ECERS Limoges, 23-27 June 2013.

Ponsot I., Marangoni M., Bernardo E., *Glass-ceramics from low-temperature sintering of glass and industrial wastes*, 23rd ICG Prague, 1-5 July 2013.

Varila L., Lenger J., Cozzika T., Teplovana M., Ponsot I., *Justifying the immobilization of nuclear waste in a glassy matrix*, 23rd ICG Prague, 1-5 July 2013.

1st, 2nd, 3rd and 4th GlaCERCo workshops: research progress

VIII.2.2 Contribution to other oral presentations

Bernardo E., Ponsot I., Çetin S., *Novel glass-ceramic construction materials from inorganic waste and recycled glasses*, 12th ESG conference Parma, 21-24 September 2014.

Marangoni M., Ponsot I., Bernardo E., Colombo P., *Glass and glass-ceramics from natural and waste raw materials*, 13th CIMTEC Montecatini Terme, 08-13 June 2014.

VIII.2.3 Poster presentations

Ponsot I., Bernardo E., *Obtainment of glass-ceramic composite based on clay, recycled glass and fluorine-containing industrial waste*, 13th Eur Inter-reg Conf Ceram, Barcelone, October 2012.

Ponsot I., Bernardo E., *Iron slag and recycled glass for foam panels*, 3rd Int Slag Valorisation Symp, Leuven, April 2013.

Chapter IX

Appendices

IX.1 Sinter-crystallization: case study #1. Sintered Nepheline Glass-ceramics

Note: This part is a participation to a work mainly conducted by Enrico Bernardo and his master student G. Dal Mas at the University of Padova, with the collaboration of R. Dal Maschio and V.M. Sglavo from the University of Trento. My contribution concerned paper editing, data analysis and plotting [related paper: Strengthening by Controlled Na/K Ion Exchange of Sintered Nepheline Glass-ceramics by I. Ponsot, G. Dal Mas, E. Bernardo, R. Dal Maschio, V. M. Sglavo, Journal of Ceramic Processing Research, 15 (6), 411-417].

The possibility of achieving very high compressive stresses at the surface of nepheline glass-ceramics, owing to the transformation of main crystal phase into kalsilite, was discovered more than 40 years ago, but the very long processing times associated to conventional glass-ceramic manufacturing prevented extensive applications.

The feasibility of nepheline-containing glass-ceramics by a rapid sintering of fine glass powders was achieved. On the other hand, to renew interest on strengthening by ion exchange induced transformation, for a selected glass-ceramic, developed using glass cullet as main raw material and sintered at very low temperature (840 °C), ion exchange treatments were found to be effective especially in increasing the reliability of samples (e.g. Weibull's modulus exceeding 18).

IX.1.1 Introduction

Nepheline, i.e. $NaAlSiO_4$ or $Na_2O \cdot Al_2O_3.2SiO_2$, is known to be quite particular among the crystals developed upon controlled glass devitrification. Like in other feldspars and feldspathoïds, Al^{3+} ions occur in tetrahedral coordination that is surrounded by four oxygen atoms. More precisely, the crystal is virtually identical to that of trydimite (form of crystalline silica), with part of $[SiO_4]$ units being replaced by $[AlO_4]$ units. Since the ions for the compensation of the charge neutrality are located in the interstitial sites, nepheline may be seen as a "stuffed derivative of silica" (Höland and Beall, 2002). Within certain limits, sodium ions can be replaced by other "stuffing species", such as potassium and calcium ions, thus forming nepheline solid solutions (with general formula represented by $K_xNa_yCa_z\square_{8-(x+y+z)}Al_{x+y+2z}Si_{6-(x+y+2z)}O_{32}$), where $\square$ represents a vacant cation site) (Duke *et al.*, 1967).

The pioneering paper by Duke *et al.* (1967) revealed the possibility of exploiting the structure of nepheline for a remarkable chemical strengthening effect, based on the exchange of Na^+ with K^+, applied to glass-ceramics. Unlike glasses, the high compressive stress at the surfaces is not simply due

to the difference in ionic radius between sodium and potassium, but it is associated to a specific change in the crystal structure. As previously mentioned, potassium solubility in nepheline is limited, so that the progressive replacement of Na^+ with K^+ ions causes the transformation of nepheline into kalsilite ($K_2O \cdot Al_2O_3 \cdot 2SiO_2$) with volumetric expansion. The compressive stress generated by the transformation is so high that bending strength of nepheline glass-ceramic rods after treatment can exceed the impressive level of 200.000 psi, i.e. ~ 1.4 GPa. The major issue concerns the composition of the starting glass: it was observed that glasses with a relatively high potassium content lead to the most remarkable strengthening. The incorporation of potassium into a nepheline solid solution likely led to a somewhat more "spaced" crystal lattice compared to pure sodium-based nepheline, thus favoring ionic diffusion.

The investigation presented here was conceived in order to renew the interest towards nepheline glass-ceramics transformed by ionic exchange, checking the conditions for: i) simplified glass-ceramic manufacturing, based on sintering; ii) modified strengthening, with effects on the reliability rather than on the strength of glass-ceramics. In fact, glass-ceramics with only nepheline as crystalline phase were developed by extremely slow conventional nucleation/growth treatments (4 hours at ~ 850 °C + 4 h at 1100 °C), aided by high content (>7 wt-%) of TiO_2 in the starting glasses, acting as nucleating agent (Duke *et al.*, 1967). The nepheline glass-ceramics here discussed refer to a much simplified process, i.e. sintering of fine glass powders. According to recent experiences, this approach may lead to very fast crystallization, even in the absence of nucleating agents (Bernardo *et al.*, 2009). The feasibility of sintering or, better, "sinter-crystallization", could promote the manufacturing of components with complex geometries, including highly porous foams (e.g. obtained by the replica method, already successfully applied to sintered glass-ceramics (Bernardo, 2007)).

The second challenge concerns the refinement of the chemical strengthening process. The usual treatment on glass, e.g. with potassium replacing sodium ions, provides high compressive stresses with maximum intensity just at sample surface. Surface cracks can propagate at higher applied loads (i.e. tensile stresses actually tend to expand the cracks only if exceeding the pre-compression), but the variability of crack length causes variability of strength like in an untreated material. In the presence of an "engineered stress profile", that is maximizing compressive stress at a certain depth beneath the surface, the reliability of glass can be impressively enhanced (cracks from the surface experience an increasing resistance to their propagation) (Green *et al.*, 1999; Sglavo and Bonafini, 2000; Sglavo, 2001; Sglavo and Green, 2001; Sglavo *et al.*, 2001 and 2004). The feasibility of a double chemical treatment on glass-ceramics with reversible nepheline-kalsilite transformation, to the authors' knowledge, is discussed for the first time here; double treatments, in fact, have been applied only to leucite-based glass-ceramics used for dental applications and obtained by a much more complex treatment than simple pressure-less viscous flow sintering, and with different transformation mechanism (Fisher and Marx, 2001 and 2003).

IX.1.2 Experimental Methods

In the present work we referred to three glass compositions (E, F and Centura® in table IX.1) known to yield nepheline-based glass-ceramics. E and F glasses correspond to the most effective compositions reported by Duke *et al.* (1967), whereas Centura® is a commercial glass-ceramic manufactured by Corning (Höland and Beall, 2002). The composition of a panel glass from dismantled cathode ray tubes (CRTs), nominally recyclable, but practically unused, due to the limited production of new CRTs, is reported in Table IX.1. The glass can be effectively treated as a "waste glass", to be

considered only for products substantially different from CRTs ("closed loop recycling"); in fact, this specific type of glass has been already considered for glass foams or in the formulation of glasses to be converted into glass-ceramics (Bernardo, 2007; Bernardo and Albertini, 2006; Andreola *et al.*, 2005; Bernardo *et al.*, 2005).

Oxides	Contents (wt%)			
	E	F	Centura®	Panel glass from dismantled CRTs
SiO$_2$	41.4	40.8	43.3	62.0
Al$_2$O$_3$	31.2	31.2	29.8	3.2
Na$_2$O	11.7	10.4	14.0	8.4
K$_2$O	7.5	9.5	–	6.3
MgO	–	–	–	1.1
CaO	–	–	–	1.8
BaO	–	–	5.5	12.6
SrO	–	–	–	4.7
As$_2$O$_3$	0.7	0.7	0.9	–
TiO$_2$	7.4	7.4	6.5	–

Table IX.1. Chemical composition of three reference glasses (Höland and Beall, 2002; Duke et al., 1967) for the production of nepheline-based glass-ceramics and of a reference waste glass

Oxides	Content (wt-%)		
	N1	N2	N3
SiO$_2$	45.1	44.4	48.7
Al$_2$O$_3$	34.0	33.9	20.0
Na$_2$O	12.7	11.3	9.4
K$_2$O	8.2	10.4	9.0
MgO	–	–	0.7
CaO	–	–	1.1
BaO	–	–	8.1
SrO	–	–	3.0
Formulation	Oxides and carbonates	Oxides and carbonates	64% CRT panel glass 9% SiO$_2$ 18% Al$_2$O$_3$ 4% Na$_2$CO$_3$ 5% K$_2$CO$_3$
T$_g$	760 ºC	730 ºC	600 ºC
T$_C$	980 ºC	1080 ºC	840 ºC

Table IX.2. Chemical composition, formulation and characteristic temperatures of the investigated glasses

As previously specified, a primary goal of the present work was a simplified processing, especially concerning the crystallization, based on sintering. This led us to consider E and F compositions, tailored to promote crystallization by conventional nucleation and growth, without TiO$_2$ (nucleating agent). In addition, since glass frits (powders) are used, the fining of glass is not needed; this means that also As$_2$O$_3$ (fining agent) can be avoided. The compositions N1 and N2, reported in Table IX.2, effectively feature the same weight balance of characteristic oxides (SiO$_2$, Al$_2$O$_3$, Na$_2$O, K$_2$O) present in E and F glasses, respectively, without other oxides. N3 was inspired by Centura®, but with

significant changes: again, TiO_2 was avoided in the glass formulation and, although the overall molar content of alkali oxides is almost the same, N3 features potassium oxide, absent in Centura®. While N1 and N2 glasses were produced from pure oxides and carbonates, N3 was mostly derived from the CRT panel glass (64 wt-%). N1 and N2 glasses were prepared by melting the raw materials at 1600 °C for 2 h in alumina crucibles; the two glasses, after rapid cooling by direct extraction from the furnace, were separated from the refractory crucible by cutting after the complete solidification. N3 glass was prepared by melting the raw materials at 1550 °C for 2 h in a Pt crucible; very rapid cooling was performed by pouring the glass melt in water.

A portion of the small beams from the bending test were treated in molten salts, i.e. in melted KNO_3 and Na_2SO_4, at 590 °C. The samples and the salts were poured in a Pt crucible and heated with a rate of 10 °C/min; after a holding stage at 590 °C of variable duration, the crucible was subjected to natural cooling to room temperature and the samples were separated by washing in hot water. Selected samples were subjected to bending strength measurements after ionic exchange treatment. Also in this case, at least ten samples were considered for each condition.

IX.1.3 Results and Discussion

Glass transition (T_g) and crystallization (T_C) temperatures of the three glasses are reported in Table IX.2. Figure IX.1 shows the evolution of bulk density as a function of the sintering treatment for N1 glass. The maximum density level is very close to that of the glass-ceramics prepared by Duke et al. (1967), but it corresponds to a quite particular sintering condition, i.e. direct heating (DH) at high temperature. Sintering at the crystallization temperature, 980 °C, with a conventional heating rate of 10 °C/min (CH), determined visibly porous bodies, whereas quite smooth and brilliant surfaces were achieved at 1180 °C (T_C+200 °C). The remarkable difference is likely due to intensive crystallization during conventional heating at temperatures below 980 °C; the formation of a number of rigid inclusions, corresponding to nepheline crystals, reasonably "froze" the viscous flow of the residual glass. Diffraction patterns shown in figure IX.2a confirm this hypothesis: the sample is substantially crystallized even for a very short holding time (30 min) at 980 °C, after conventional heating. The large specific surface of the fine glass powder evidently promotes the crystallization, even in the absence of nucleating agents, as observed for waste-derived glasses (Bernardo *et al*., 2005; Bernardo, 2007; Bernardo *et al*., 2009).

Direct heating at temperatures well exceeding T_C improves densification by changing the balance among viscous flow sintering and crystallization (Bernardo et al., 2009): the glass, far above the transition temperature, experiences an enhanced viscous flow; the consequent reduction of free glass surfaces reduces the crystallization (see the limited intensity of the peaks in the pattern recorded on sample N1 treated at T_C+200 °C for 1 h, pattern DH in figure IX.2a). The enhanced densification of samples "directly" sintered at 1180 °C, combined with partial crystallization, is evident in figure IX.3a, showing isolated pores in a micro-crystalline matrix. Such evolution was accompanied by good mechanical properties, with the bending strength slightly exceeding 100 MPa, as reported in table IX.3.
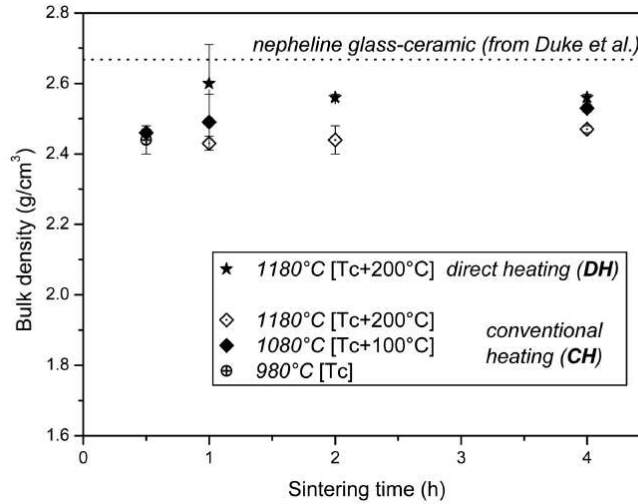
Figure IX.1: Evolution of density with sintering treatments for N1 glass

As demonstrated by the very close matching of powder diffraction peaks and reference lines in figure IX.2a, the developed crystal phase always corresponds to nepheline solid solution, $Na_3K(Si_{0.56}Al_{0.44})_8O_{16}$ (PDF#76-2465). The chemical composition is associated to substantial potassium incorporation (potassium and sodium ions being in the proportion 1:3), but also suggests the presence of vacancies (Si/Al ratio is higher than 1, thus determining an excess of positive charge, to be compensated by the "stuffing species").

Figure IX.2: a) phase evolution of N1 glass in different sintering conditions (powder diffraction – CH: conventional heating, DH: direct heating); b) glancing incidence x-ray diffraction pattern of N1 glass-ceramic after ion exchange treatment

Quite unexpectedly, the probable presence of vacancies did not help the transformation of nepheline into kalsilite upon the ion exchange treatment as reported by Duke *et al.* (1967). Glass-ceramics samples, prepared with the best sintering conditions (direct heating at 1180 °C, holding time = 1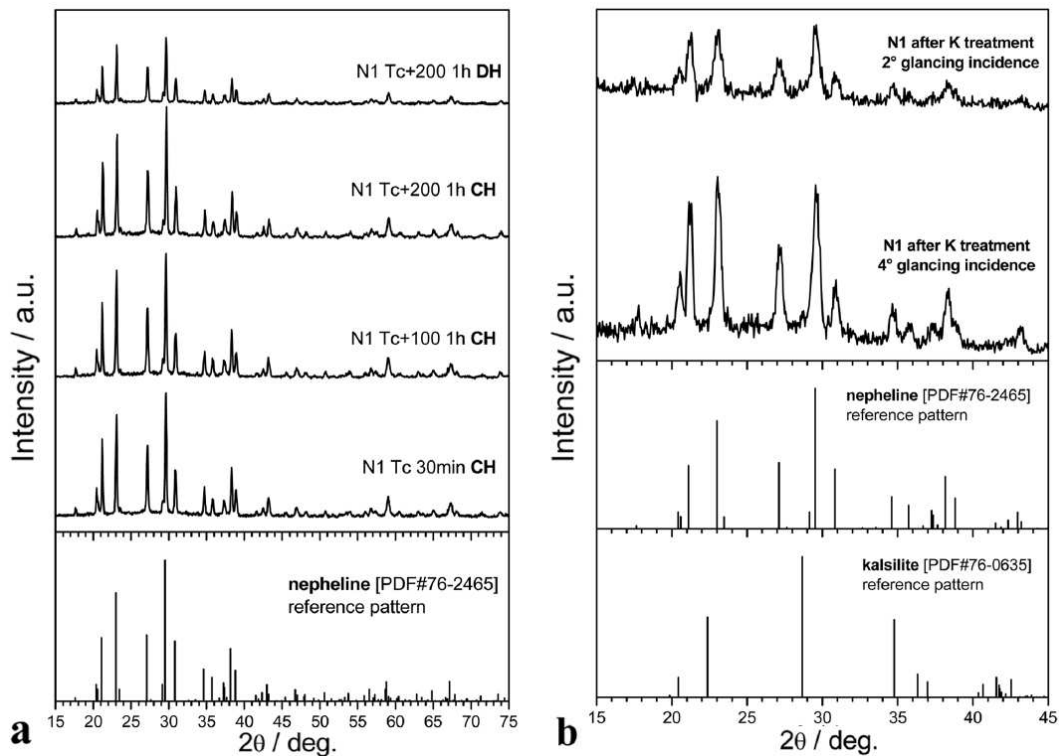 h), broke into fragments during the treatment, initially scheduled to last 8 h (Duke *et al.*, 1967). After a series of try-and-error tests, it was inferred that glass-ceramics from N1 glass could withstand a maximum of 2 h treatment in molten potassium nitrate.

The limited duration of the ion exchange treatment did not cause any appreciable change in the phase distribution on the surface, as shown by the glancing incidence diffraction analysis. Operating with a relatively high glancing incidence angle (4°, bottom pattern in figure IX.2b), i.e. collecting signals from the surface and from layers slightly below it (it is well known that patterns obtained at large glancing angles more bulk sensitive than those obtained at small glancing-angles) (Begg *et al.*, 2001), the diffraction pattern reveals the same crystal phase found with powder analysis; operating with a lower angle (2°, top pattern in Figure IX.2b), i.e. maximizing the contribution from the surface, the signals are obviously weaker, but with no practical change in the position of peaks. An effective transformation of nepheline should be accompanied by the shift of some main peaks (e.g. those at ~23° and ~30°) and the disappearance of others (e.g. that at ~27°). The absence of surface changes is further confirmed by the strength values, which remain similar to those of as prepared N1 glass-ceramic (Table IX.3).

A quite different behavior was found for N2 glass. Based on a different balance among constituents, N2 glass features higher crystallization temperature (1080 °C) than N1 glass, but shows good densification at the same temperature (porosity slightly exceeding 2%) by direct sintering (see figure IX.3b). The previously presented nepheline solid solution, $Na_3K(Si_{0.56}Al_{0.44})_8O_{16}$, is confirmed as the characteristic crystal phase, as shown by figure IX.4. However, the glass-ceramic from N2 glass is weaker that the one from N1 glass (see table IX.3), and exhibits a higher sensitivity to ion exchange. More precisely, glass-ceramic from N2, sintered at 1080 °C (for 1 h), was able to withstand the treatment in potassium nitrate for 3 h and undergo to some transformation, as shown in figure IX.4b. The peaks corresponding to the main crystal phase, nepheline, are almost negligible compared to those corresponding to K-rich phases, such as kalsilite ($KAlSiO_4$ or $K_2O \cdot Al_2O_3 \cdot 2SiO_2$, PDF#76-0635) and leucite ($KAlSi_2O_6$ or $K_2O \cdot Al_2O_3 \cdot 4SiO_2$, PDF#85-1421).

The occurrence of the expected transformation of nepheline into kalsilite did not determine any strength improvement; conversely, as reported in table IX.3, the bending strength decreased substantially (almost 40%). Figure IX.3c and d show the changes occurring on the surface after ion exchange treatment; the surface, originally smooth (after cutting from larger specimens and polishing), become rougher after the treatment. In our opinion the results from the ion exchange treatment of glass-ceramics from both N1 and N2 glasses differs only in terms of intensity. The expected volume increase, associated to the insertion of K^+ within the nepheline structure and its transformation into kalsilite, effectively occurred but it was not sustainable at the interface with the unmodified material. The mutual constraint of transformed crystals forced them to develop a significant interfacial stress, likely enhanced by the residual micropores (acting as stress concentrators). In other words, the strengthening observed by Duke *et al.* (1967) is probably possible only with pore-free materials, difficult to be obtained by pressureless sintering.
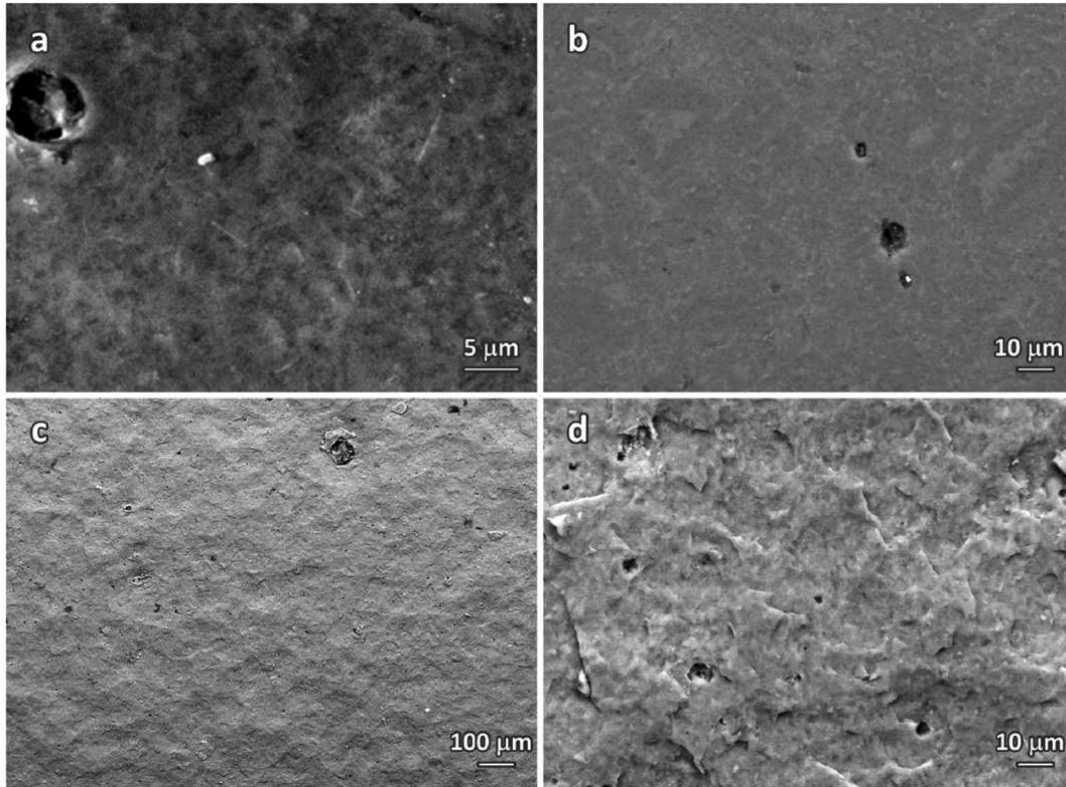
Figure IX.3: Details of the surface of nepheline-based sintered glass-ceramics:
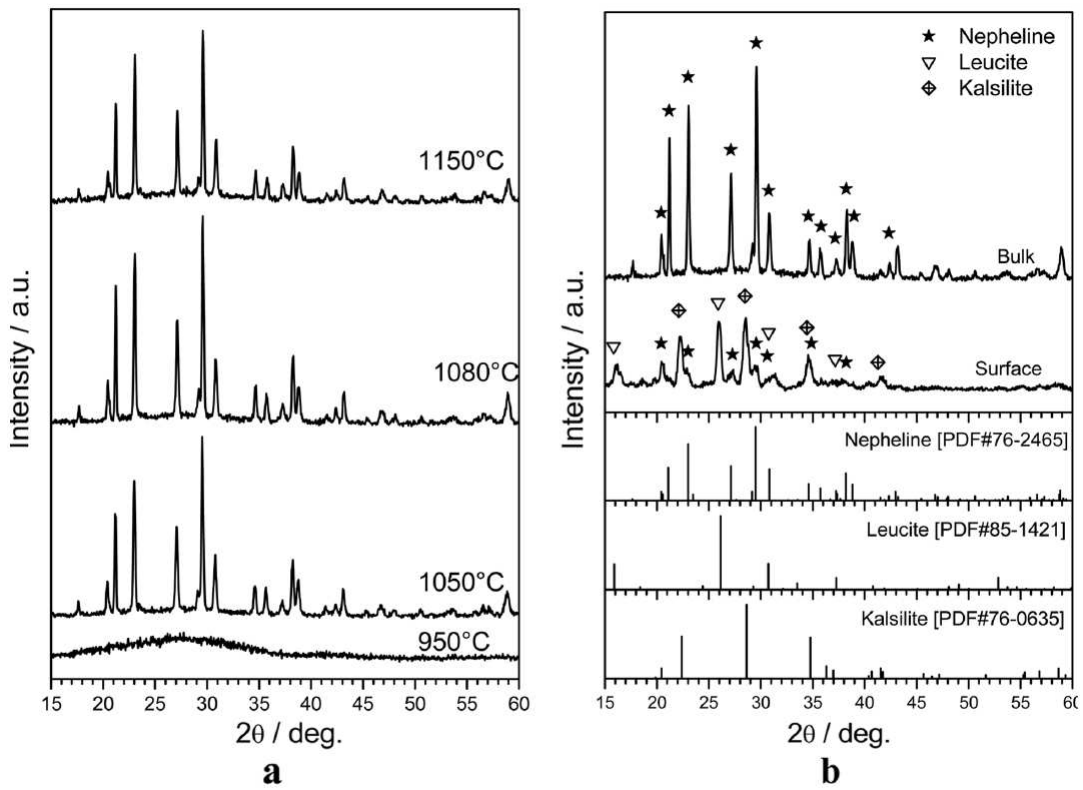*a) N1; b) N2; c,d) N2 after ion exchange treatment*

Figure IX.4: a) phase evolution of N2 glass at different sintering temperatures (powder diffraction; holding time=1h); b) comparison between powder diffraction pattern (1080 °C, 1h) and glancing incidence pattern after ionic exchange treatment (3°)

The third glass, N3, was considered with the main aim of limiting nepheline formation. In fact, a reduction in the content of the crystal phase undergoing transformation was thought to "dilute" the stresses arising from the ion exchange treatment and to maintain the integrity of the samples. Figure IX.5a clearly shows that leucite (PDF#85-1419) is formed together with nepheline after sinter-crystallization at 840 °C (1 h). The new formulation allowed a much lower processing temperature, without direct heating: the enhanced content of network modifiers (e.g. BaO and SrO), not to be incorporated in the crystal structure, favor viscous flow even at relatively low temperatures; crystallization can be coupled with a satisfactory densification (residual porosity of about 3.5%) even with finite heating rate (20 °C/min). The semi-quantitative phase analysis provided by the Match! program package suggests a 60/40 nepheline/leucite weight proportion; considering the composition of N3 glass, this would be associated to an approximate crystallization degree of 65%.

As reported in table XI.3, the strength of nepheline-leucite glass-ceramics from N3 glass (approximately 70 MPa) is far below that of nepheline glass-ceramics from N1 and N2, but it increases sensibly after the ion exchange treatment in molten potassium nitrate without any degradation of the sample surface, as shown by figure IX.5a.
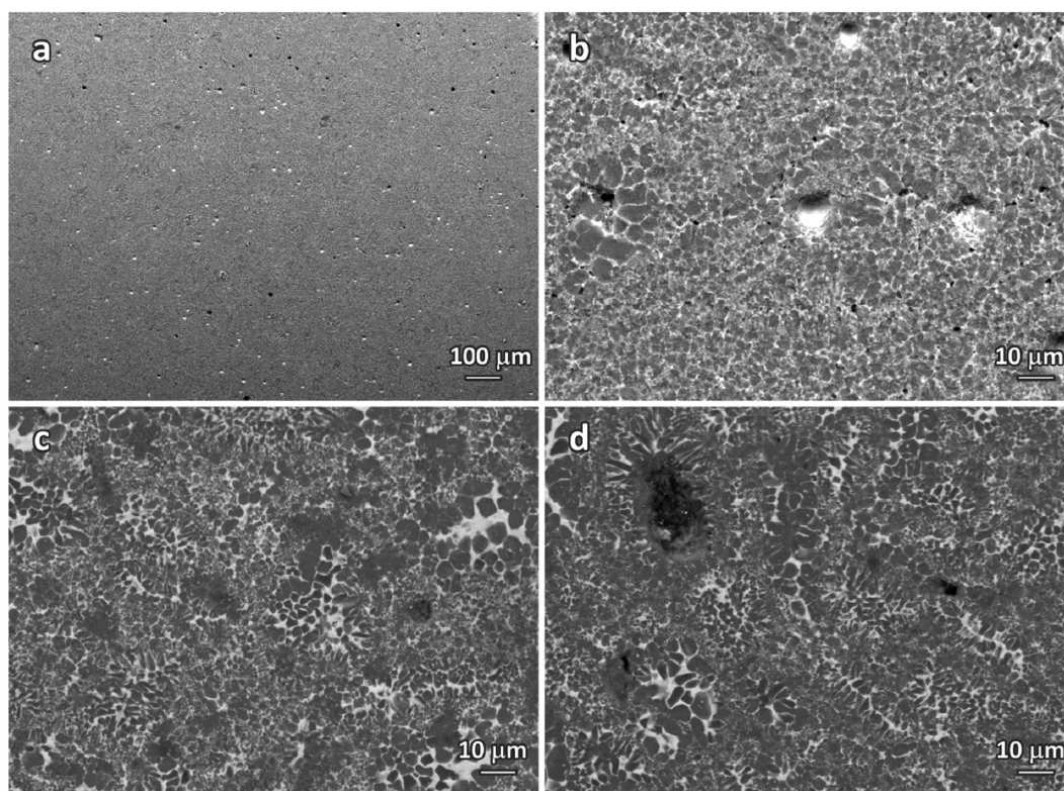
Figure IX.5: Details of the surface of sintered glass-ceramics from N3 glass: a,b) after sintering; c) after first treatment, in molten K-nitrate; d) after second treatment, in molten Na-sulphate

The glancing incidence diffraction patterns of figure IX.6 show the occurrence of nepheline-to-kalsilite transformation, in N3 glass-ceramic, after 8 h in K-nitrate, and its reversibility, after additional 4 h in Na-sulphate. Nepheline, not recognizable in the pattern after the first treatment, is found again after the second treatment, along with leucite and kalsilite, according to sodium diffusion.

The partial restoration of nepheline is testified by the distribution of potassium and sodium (determined by energy-dispersive x-ray spectroscopy (EDS) analysis) along the thickness of samples, as shown in figure IX.7.

Figure IX.5 also testifies that glass-ceramics from N3 glass were subjected to a sort of "recrystallization" during ion exchange treatments. In fact, crystals change from a quite uniform distribution in untreated sample (Figure IX.5b) to an almost bimodal distribution, with larger crystals (diameter of about 5 μm) surrounded by smaller ones, in treated samples (Figure IX.5c and d); the amorphous phase, clearly recognizable from the light coloration in backscattered images (associated to heavier elements, such as Ba and Sr), is also modified, being more concentrated in some points. This suggests an "active" role of the residual glass phase during the crystallization; a glass network with relatively larger free volume, due to large ions (again, Ba and Sr), likely promotes the diffusion of alkali ions.

The presence of a point of maximum potassium concentration below the surface (20-25 μm) (Figure IX.7) can be correlated to a maximum compressive stress at that depth, as reported for an "engineered stress profile" (ESP) (Green *et al.*, 1999; Sglavo *et al.*, 2001; Sglavo *et al.*, 2004). Like in ESP glass (Sglavo *et al.*, 2001; Sglavo *et al.*, 2004), the main effect does not concern the level of strength (reduced at approximately 100 MPa), but the scatter of the data. As reported in table IX.3 the standard deviation of strength is well below 10% of the average level, and Weibull modulus exceeds 18.
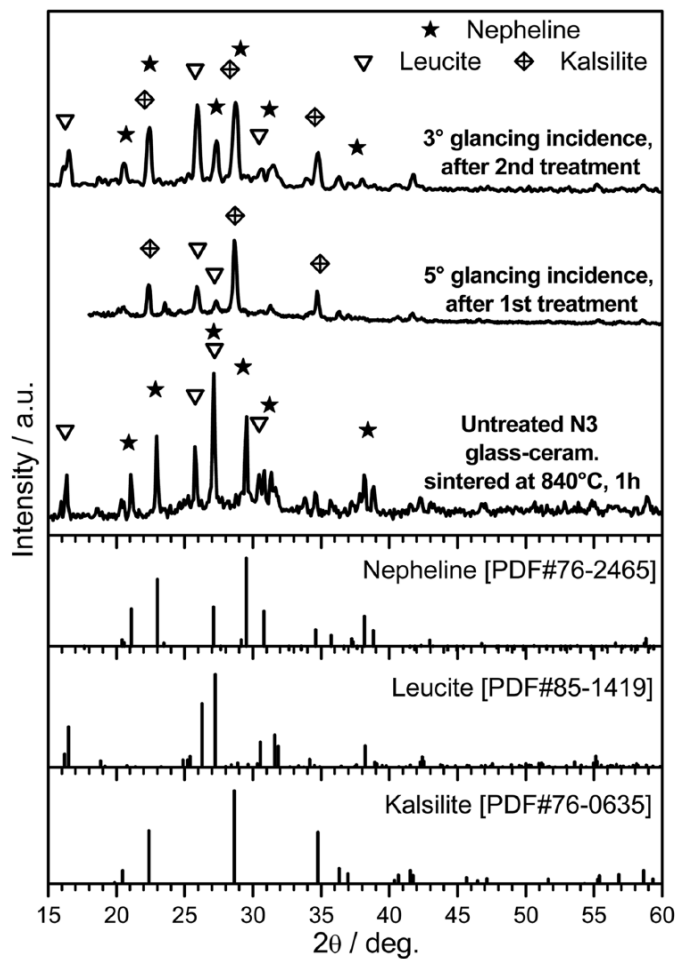

Figure IX.6: Diffraction patterns of glass-ceramics form N3 glass, before ion exchange (powder analysis) and after ion exchange treatments (glancing incidence)

A final remark concerns the possible impact of the proposed approach. To the authors' opinion the strengthening and the dramatic decrease of dispersion of strength data could be an opportunity for glass-ceramic components loaded in bending, especially thinking at porous materials. As well discussed by Gibson and Ashby (2005), the strength of open-celled foams is conditioned by the bending strength of the cell edges ("bending-dominated" behavior); improvements in the bending strength of the solid phase could lead to an impressive strengthening of foams, to be variously exploited (construction of lightweight cores for sandwich structures, impact absorbers, filters etc.) (Gibson and Ashby, 2005). The possibility to apply a sintering approach would greatly simplify the manufacturing of highly porous foams, as previously mentioned (Bernardo, 2007). Finally, it should be observed that nepheline may be found as one of the main phases in waste-derived glass-ceramics (Bernardo *et al.*, 2005; Leroy *et al.*, 2001; Zhang *et al.*, 2007): the fabrication of high strength foams, after sintering and ionic exchange treatment, could allow high value applications for waste glasses.
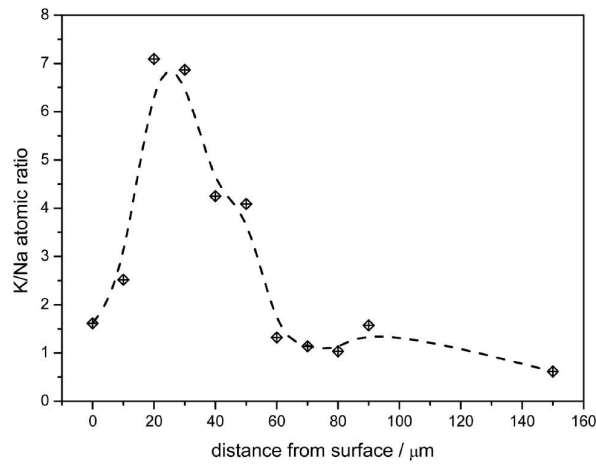
Figure IX.7: Trend of K/Na ratio with increasing distance from the surface of a sample subjected to double ion exchange treatment

		N1	N2	N3
Optimal sintering temperature (°C)		1140	1080	840
Heating mode		Direct	Direct	20 °C/min
Density (g · cm^{-3})		2.60 ± 0.11	2.56 ± 0.02	2.77 ± 0.1
Porosity (%)		2.1 ± 0.5	2.3 ± 0.8	3.4 ± 0.7
Bending strength	Mean value ± Std. Dev. (MPa)	102.7 ± 12.8	88.5 ± 11.6	73.0 ± 15.9
	Weibull parameters: σ_0 (MPa) m			79.8 4.9
Soaking time in molten K salt		2 h	3 h	8 h
Bending strength, after ion exchange (K)	Mean value ± Std. Dev. (MPa)	93.6 ± 35.0	56.5 ± 20.8	140.2 ± 12.4
	Weibull parameters: σ_0 (MPa) m			146.3 12.2
Soaking time in molten Na salt		–	–	4 h
Bending strength, after 2nd ion exchange (K, Na)	Mean value ± Std. Dev. (MPa)			99.4 ± 5.40
	Weibull parameters: σ_0 (MPa) m			102.0 18.4

Table IX.3 – Sintering conditions, porosity and mechanical properties, before and after ion exchange treatments, of sintered glass-ceramics from the investigated glasses

IX.1.4 Conclusions

Ion exchange-induced nepheline-kalsilite transformation has been observed in glass-ceramics produced by sintering sodium-potassium alumino-silicate glasses. The transformation could not be exploited for glass-ceramics with only nepheline as crystalline phase; the intense stresses developed upon ion exchange, combined with a limited but not negligible residual porosity, led to the rupture of samples upon the chemical treatment. Successful treatments were applied to nepheline-leucite glass-ceramics, obtained by re-using a significant content of waste glass. The reversibility of nepheline-kalsilite transformation was found to be suitable, more than for strengthening, for an impressive reduction of the scatter of strength data. This fact could find applications in the manufacturing of (especially porous) reliable glass-ceramics.

IX.2 Sinter-crystallization: case study #2. Oil shale ash-derived glass-ceramics

Note: work mainly conducted by Enrico Bernardo and Mauro Marangoni, at the University of Padova, and R. Kuusik, (University of Tallinn). My contribution concerned paper editing, data analysis and plotting [related paper: Strong and chemically inert sinter crystallized glass ceramics based on Estonian oil shale ash, by Marangoni M., Ponsot I., Kuusik R., Bernardo E, Adv Appl Ceram (2014) 113 [2], 120-128].

IX.2.1 Introduction

Oil shale is a fine-grained sedimentary rock containing organic matter. The organic matter is divided in a soluble fraction, bitumen, and an insoluble fraction which is named kerogen. Upon suitable thermal treatments, kerogen releases crude oil or natural gas that are used as fossil fuels (Yen, 1976). Oil shales deposits are distributed all over the world and range from small occurrences to those of enormous size that contain many billions of barrels of potentially extractable shale oil. Total world resources of shale oil are conservatively estimated at 2.8 trillion barrels. Today, shale oil is more expensive to produce than crude oil because of the further costs of mining and processing, the deposits being extensively exploited are only in Brazil, China, Estonia, Germany and Israel (World Energy Council, 2010). However, owing to the increasing cost of petroleum-based products and the decline of petroleum supplies, economical interest in oil shale resources is arising, as testified by the intensive research on novel mining techniques (e.g. "fracking")(Howard *et al*., 2011).

A major issue of oil shale processing is the relatively low combustible fraction, 35-46 wt.% of the starting mass, compared to the amount of ashes generated and needing some stabilization, owing to the significant traces of heavy metals (mostly Cd, Pb, Cr, Zn, Tl, As and Ni)(Aunela-Tapola *et al*., 1998; Adamson *et al*., 2010; Blinova *et al*., 2012). Management of ashes is particularly important in Estonia, where oil shale is processed in an amount of 14.6 million tons/year (2005), 75% being used for electricity generation, 5% for heat generation and 20% for production of shale oil and coke production (World Energy Council, 2007; Ots, 2006).

Oil shale ash has been object of valuable studies concerning its stabilization and valorization in glass-ceramics to be applied as building materials (Gorokhovsky *et al.*, 2001, 2002a and 2002b; Luan *et al.*, 2010), basically because of the composition, suitable for the preparation of glasses of the $CaO-Al_2O_3-SiO_2$ system, a well-recognized reference for waste-derived glasses (Höland and Beall, 2006; Hreglich and Cioffi, 2009; Fernandes *et al.*, 2009; Vasilopoulos et al., 2009; Bernardo *et al.*, 2012). The present paper aims at evidencing the feasibility of a sintering approach for the production of strong and chemically stable glass-ceramics, based on glass frits. More precisely, the cost of overall glass-ceramic manufacturing can be significantly lowered, comparing to a conventional nucleation and growth process, if we consider that no refining of the parent glass is required for glass frits. Furthermore surface crystallization, operating on fine glass powders, may lead to substantial crystallization by application of very short sintering treatments (fast heating – 40 °C/min – and limited holding stage), so that nucleating agents to promote crystallization are not needed (Bernardo, 2008; Gutzow et al., 1998; Karamanov, 2009).

IX.2.2 Characterization of the raw materials

	ESP 1	ESP 2	Rhyolite	Soda lime glass	Borosilicate glass	ASH 1 glass	ASH 2 glass
Chemical composition							
Oxide content/wt-%							
SiO_2	34·7	31·9	73·4	71·9	72	52·3	52·0
Al_2O_3	9·4	9·1	15·2	1·2	7	11·0	10·7
B_2O_3					12		
Na_2O	0·2	0·3	1·7	14·3	6	2·2	2·6
K_2O	4·2	7·4	4	0·4	2	4·2	6·5
BaO					<0·1		
MgO	5·9	3·4	0·3	4		4·9	3·1
CaO	27·6	27·7	0·5	7·5	1	21·4	21·4
Fe_2O_3	4·4	3·8	1·5	0·3		3·7	3·2
MoO_3			0·1			0·0	0·0
TiO_2	0·5	0·5	0·1	0·1		0·4	0·4
MnO_2	1·5	1·1					
L.O.I.	11·6	14·8	4·8	0·3			
Metal traces*/mg kg^{-1}							
As	38·6	21·5					
Cd	0·6	0·15					
Cr	46·5	48·5					
Cu	16·3	17·7					
Pb	153·2	71·36					
Zn	112·5	56·2					
Formulation							
Glass	Balance/wt-%						
ASH 1 glass	67		23	10			
ASH 2 glass		65	23	12			

Tab. IX.4: Chemical composition of the starting raw materials and formulation of the investigated glasses
* Average of the heavy metals concentration reported by Bilinova et al. for oil-shale fly ashes obtained by pulverized firing (ESP 1) and circulating fluidized bed (ESP 2).

The raw materials employed mainly consisted of fly ash residues, collected from electrostatic precipitator, formed after combustion of Estonian oil shale at Estonian Power Plant (Estonia), in two distinct conditions, causing some differences in the overall chemical compositions (Table IX.4). ESP1 is formed operating with pulverized oil shale, at temperatures 1200 °C to 1400 °C, whereas ESP2 derives from circulating fluidized bed combustion of lumpy oil shale, at temperatures 750 °C to 830° (Kuusik *et al.*, 2005). The ashes were mixed with secondary components such as rhyolite, i.e.an inexpensive alumino-silicate volcanic rock (abundant, but with limited use in the ceramic industry), provided by Ce.Ri.Col. (Centro Ricerche Colorobbia, Vinci, Italy) and recovered soda lime cullet (Sail SPA, Biella, Italy). Recovered soda lime glass corresponds to the fraction of recycled material which is hardly reused, after color selection and removal of metallic and polymeric residues, for the preparation of new glass articles, owing to the presence of ceramic contaminations. The chemical composition of the raw materials, according to X-ray (Philips XRF Sequential Spectrometer PW 2400, Eindhoven, The Netherlands) fluorescence analysis, is reported in table IX.4.

The choice of the thermal treatment was accomplished by selecting the materials with the highest crystallization and densification degrees. Indeed, a high degree of crystallization guarantees an improvement of the mechanical properties (i.e. by crack deflection) whereas a high densification improves the strength of the material by reducing the porosity. The evaluation of the density degree, δ, was estimated from the density of a sample, determined by means of the Archimedes' method, divided by the maximum value in the whole set of density data. The evaluation of the crystallization degree was performed using a semi-quantitative approach. In fact, Rietveld refinements of multiphase glass-ceramics require crystallographic data, for each phase,

associated to a well-defined stoichiometry; these data are difficult to be collected due to the formation of many solid solutions. It is well known, however, that the intensity of diffraction peaks is proportional to the quantity of a given phase. For comparison purposes, for each phase "i", we identified a single characteristic diffraction peak. For a given sintering condition, the evaluation of the degree of crystallization, α_i, was estimated by dividing the total counts associated to the distinctive peak by the maximum counts associated to the same peak in the whole set of samples.

Since densification (by viscous flow) and crystallization occur simultaneously, in sinter-crystallized material, for each sample we considered an index, Σ, arbitrarily set as:

$$\Sigma = \frac{1}{2} \cdot \delta + \frac{1}{2n} \sum_i \alpha_i \text{ , where } n \text{ is the number of the crystal phases.}$$
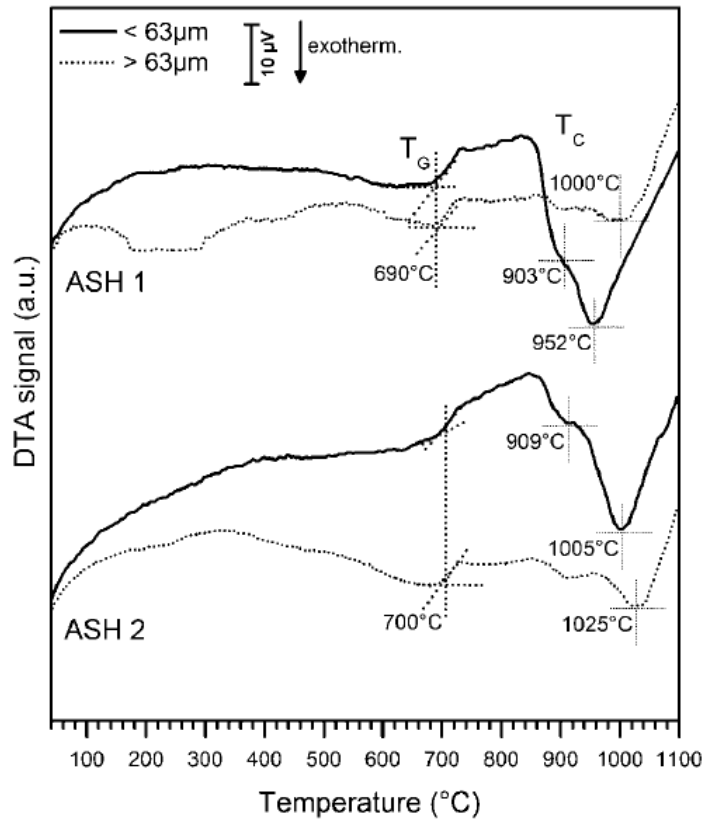
Fig. IX.8: DTA plots for fine and coarse glass powders

IX.2.3 Results and discussion

For the investigated waste glasses the thermal analysis, as illustrated by figure IX.8, featured several effects. More precisely, ASH1 glass exhibited glass transition (T_g) at 690 °C and exothermic peaks, reasonably associated to crystallization of different phases, at about 890, 950 and 1000 °C. The slight variations in the chemical formulation, for ASH2 glass, determined a variation of the T_g, located at 700 °C, and the shift of the exothermic peaks at about 910, 1005 and 1025 °C.

For both glasses, some peaks were more pronounced and shifted to slightly lower temperatures for fine powders (<63 μm) than for coarse ones (>63 μm), as an evidence of surface mechanism of

crystallization (Bernardo and Scarinci, 2008; Bernardo, 2008; Bernardo et al., 2009). The exothermic peaks appearing at higher temperatures were less sensitive to the size of glass powders, and they were interpreted as an evidence of bulk crystallization which was determined at 1000 °C for ASH1 and 1025 °C for ASH2.
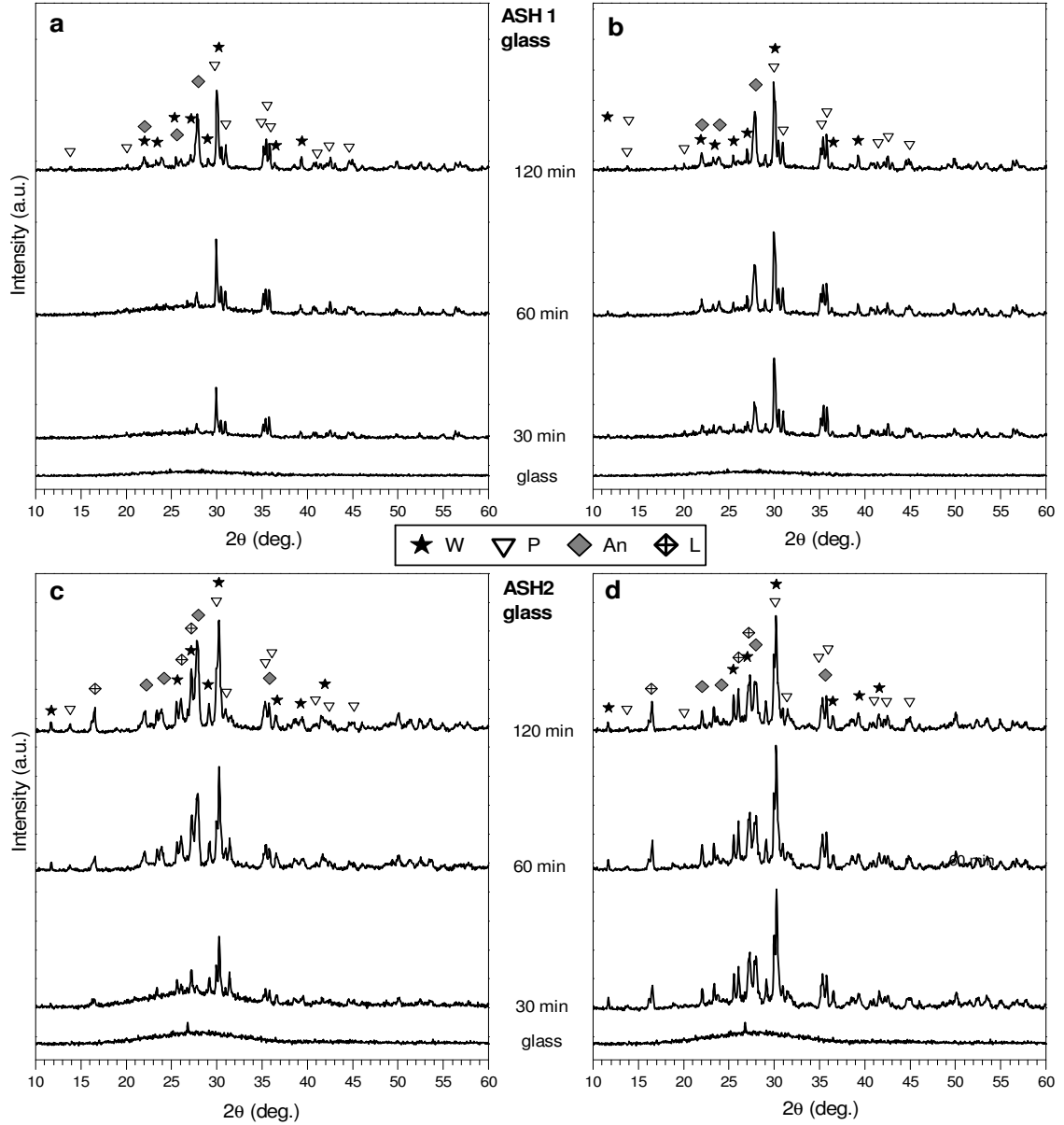
Fig. IX.9: Diffraction patterns of glass-ceramics from direct sintering of ASH 1: a) 900 °C; b) 950 °C and ASH 2: c) 900 °C; d) 1000 °C

The temperatures associated to surface crystallization were taken as references for sintering treatments. As a consequence ASH1 glass was processed at 900 and 950 °C, whereas ASH2 glass was treated at 900 and 1000 °C. The second exothermic effect, for fine ASH2 powders, almost overlapped with the pick attributed to bulk crystallization and a high crystallization degree was expected.
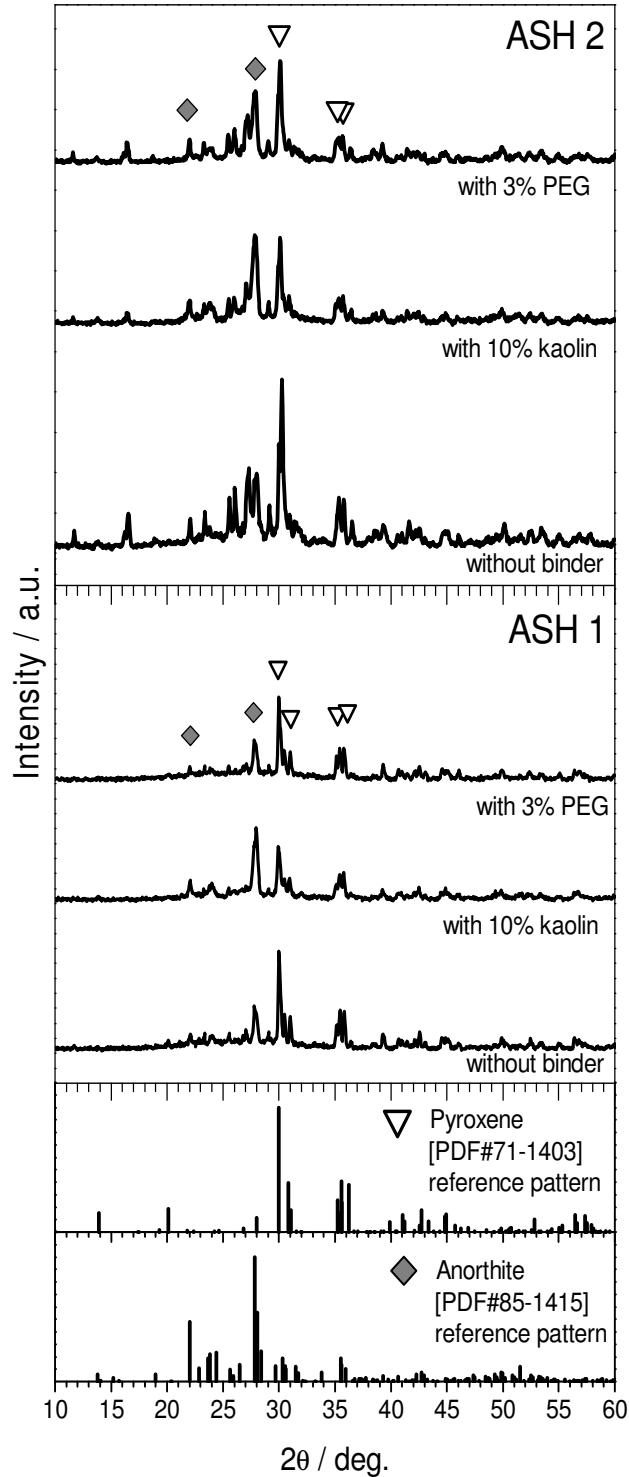
Figure IX.10: Diffraction patterns of glass-ceramics from optimized sintering treatments (at 950 °C for ASH1, at 1000 °C for ASH2)

Sintering treatments of ASH1 glass, as illustrated by figure IX.9a (900 °C) and figure IX.9b (950 °C), led to the separation of different phases, in form of a Ca-Fe rich pyroxene (omphacite, $Fe_{0.52}Al_{0.48}Ca_{0.47}Na_{0.53}Si_2O_6$, PDF#71-1403), a Ca-Na feldspar (sodium exchanged anorthite, $Na_{0.45}Ca_{0.55}Al_{1.55}Si_{2.45}O_8$, PDF#85-1415) and β-wollastonite ($CaSiO_3$, PDF#72-2284). Omphacite traces are visible even at low temperature, for short holding times, whereas wollastonite and

feldspar formed at higher temperature or for long sintering treatments (900 °C 120 min holding time). ASH2 glass, as illustrated by figure IX.9c (900 °C) and figure IX.9d (1000 °C), led to a more complex phase assemblage, based on the previously identified crystal phases with further formation of akermanite ($(Ca_{1.53}Na_{0.51})(Mg_{0.39}Al_{0.41}Fe_{0.16})(Si_2O_7)$, PDF#72-2127), a K-rich feldspathoid (leucite, $K(AlSi_2O_6)$, PDF#851626). Akermanite phase was observed especially at low temperature and for short treatments; at higher temperature or for longer holding times akermanite practically disappeared, replaced by the other phases.

Glass (sintering *T*/°C)	Holding time/min	Apparent density/g cm^{-3}	Σ
ASH1 (900)	30	2·75 ± 0·02	0·62
	60	2·76 ± 0·01	0·66
	120	2·74 ± 0·03	0·87
ASH1 (950)	30	2·75 ± 0·02	0·76
	60	2·72 ± 0·02	0·94
	120	2·71 ± 0·01	0·95
ASH 2 (900)	30	2·64 ± 0·02	0·66
	60	2·68 ± 0·02	0·78
	120	2·65 ± 0·01	0·85
ASH 2 (1000)	30	2·66 ± 0·02	0·96
	60	2·64 ± 0·01	0·98
	120	2·60 ± 0·01	0·98

Table IX.5: Results from preliminary densification/crystallization evaluation

The weighted index conceived in order to consider both crystallization and densification, as shown by table IX.5, allowed a rough but rapid selection of optimum sintering conditions. 30 min at 950 °C, for ASH1 glass, and 30 min at 1000 °C, for ASH2, were sufficient to yield high indices, not significantly increased with longer treatments. Sinter-crystallization is confirmed as an extremely efficient process for glass-ceramic manufacturing, for very short (and consequently cost effective) thermal treatments.

The manufacturing of larger sintered glass-ceramic samples was associated to some refinements, concerning the impact of binders. In fact, kaolin performs two important functions in ceramic bodies. The first function is due to the adhesion forces among kaolin and powders mixed with it (Ring, 1996), the second is related to the reactions occurring upon firing. Kaolin is subjected to dehydration into metakaolinite at about 550 °C, in turn decomposing at about 925 °C into fine-grained mullite and silica (Shackelford and Doremus, 2010; Ring, 1996). From the XRD patterns we can note that for kaolin-containing mixtures mullite did not form; however, it is also evident that anorthite peaks become more significant compared to those associated to wollastonite. This is interpreted as a further evidence of the reaction between CaO and metakaolinite, already observed in mixtures including a Ca-rich waste glass and clay (Bernardo *et al.*, 2010).

The introduction of PEG, as expected, did not modify substantially the phase assemblage, compared to the one without binders, because of its organic nature (PEG burn out was performed at about 300 °C, according to Han *et al.* (1997), much below the transition temperature of the two glasses, i.e. much before any possibility of viscous flow). However, slight differences in the peaks intensity are visible, especially for ASH2 glass, between the sample without any binder and the one with PEG. This could be associated to the different heating conditions, since the sample without binder was sintered by direct insertion at 1000 °C. In these conditions crystallization could be somewhat enhanced (the peak associated to wollastonite is higher) by the availability of a remarkable amount of free glass surfaces. On the contrary, the sample with binder, heated at 40

°C/min, could experience some sintering before starting to crystallize; consequently the reduction of the specific surface inhibits the nucleation of crystal phases.

Glass	Binder	E/GPa	ρ/g cm^{-3}	Total porosity/%	Measured strength σ_4/MPa	Weibull parameters σ_0/MPa	m	Estimated strength σ_{eq}/MPa	H_V/GPa
ASH 1	PEG	92±6	2·62±0·04	7	87±20	95	4·6	16·4	6·3±0·3
	Kaolin clay	79±2	2·52±0·02	7	90±19	98	3·9	14·8	6·8±0·2
ASH 2	PEG	67±6	2·44±0·08	6	94±10	99	10·7	48·0	6·1±0·4
	Kaolin clay	67±8	2·49±0·06	8	99±17	107	6·2	29·5	5·9±0·4
ASH 2+BSG	PEG	59±4	2·27±0·03	7	72±11	77	6·7	25·0	6·0±0·8

Table IX.6: Mechanical properties of optimized sintered glass-ceramics

Figure IX.11: SEM backscattered electron image of glass-ceramics from ASH1 glass: a,b) glass with Kaolin; c,d) glass mixed with PEG

The values of bending strength, Young's modulus and Vickers microhardness compare favorably with other waste-based glass-ceramics (Bernardo *et al.*, 2010). The bending strength, in particular, is quite high if we consider an amount of total porosity estimated not to be lower than 6% (reasonable owing to the gas release from PEG or kaolin residues, upon firing), from image analysis of polished surfaces.

The weakening effect of residual porosity was likely well compensated by intensive crack deflection at glass/crystal interfaces, similarly to the case of dental glass-ceramics (Chen et al.,

2011). The fracture surfaces of figure IX.11a and figure IX.11c, for glass-ceramics from ASH1 glass, as well as figure IX.12a and figure IX.12c, for glass-ceramics from ASH2 glass, on one hand confirm the internal porosity, on the other they feature a remarkable roughness, especially for the stronger sample, that from ASH2 glass powders bound with PEG (applying Weibull's statistic approach, the characteristic strength of 99 MPa is related to a remarkable Weibull's modulus (m), exceeding 10).

The difference in strength could be due to different microstructures. Samples containing kaolin clay (figure IX.11b and figure IX.12b) feature quite small and poorly interconnected crystals, as well as some amorphous areas (see "Am" in ASH1 glass). On the contrary, samples processed with PEG addition, exhibit long interlocking fibrous microcrystals (figure IX.11d and figure IX.12d). The lower strength of glass-ceramic samples from ASH1 glass, compared to those from ASH2 glass is not yet clear; we can observe, however, that the pores in samples form ASH1 glass are less homogenous (big pores, like that at the top of figure IX.11d could provide a more intensive stress concentration) and the crystals are slightly thinner.
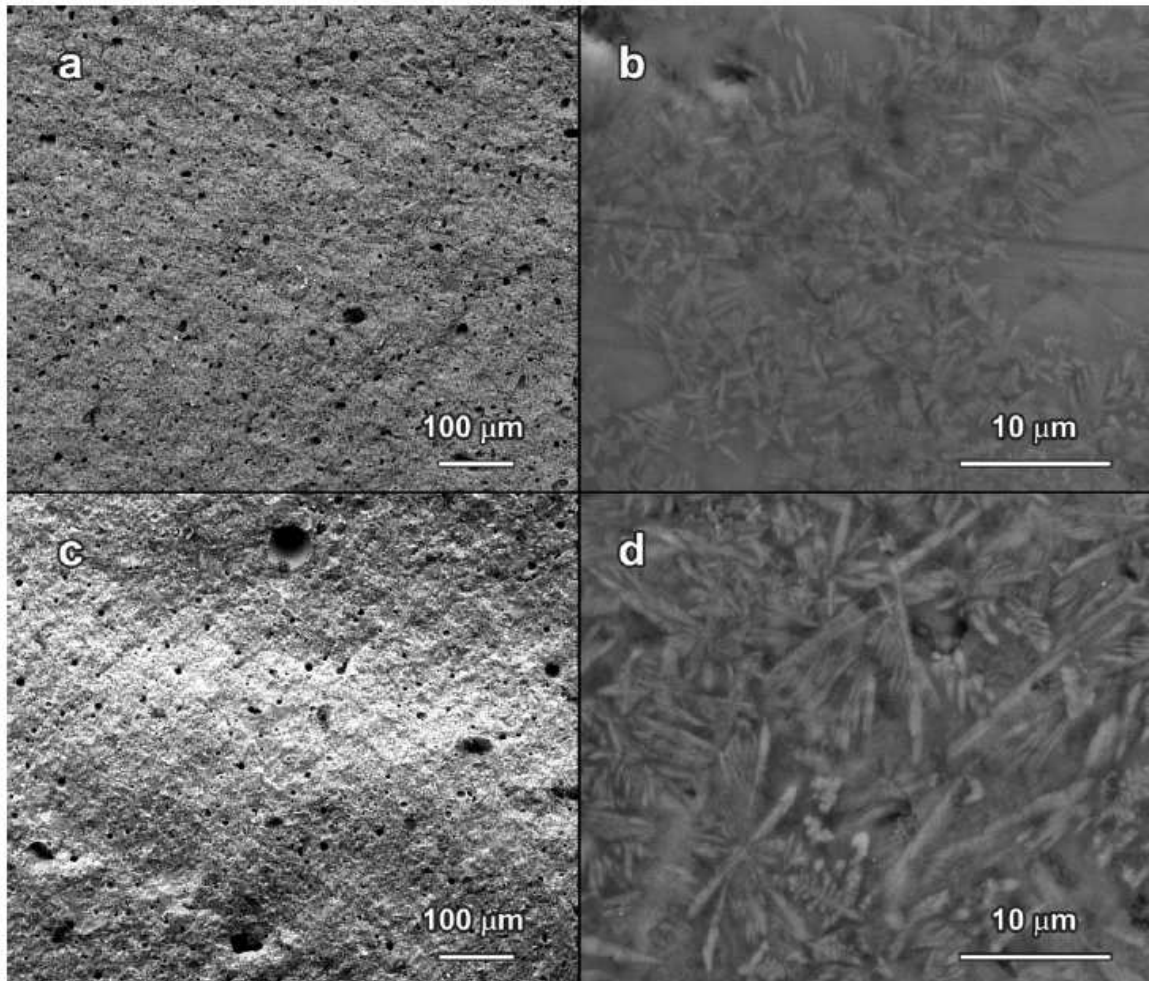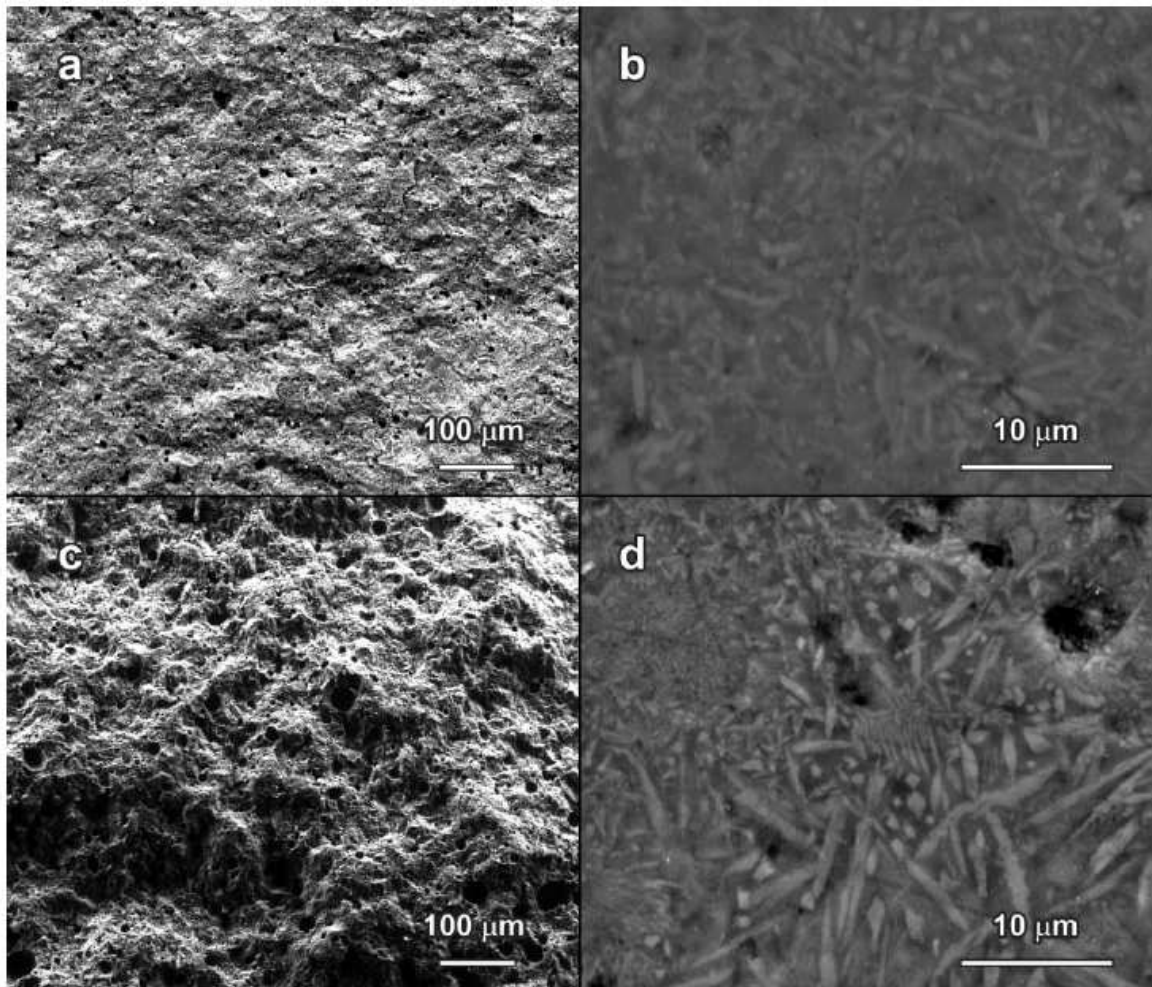

Figure IX.12: SEM backscattered electron image of glass-ceramics from ASH2 glass: a,b) glass with Kaolin; c,d) glass mixed with PEG

Because of the high m value, a limited degradation of strength, for the sample from ASH2 glass, is expected when passing to the scale of conventional floor tiles, i.e. panels with dimensions of $300 \times 300 \times 8$ mm.

In the hypothesis of flaws occurring with a volume distribution, such as residual pores, and following the scaling equations provided by Quinn (2003), the bending strength data measured on small bars subjected to 4 point bending were analyzed thus to predict an "equivalent" bending strength, for panels (σ_{eq}), well exceeding the limit (35 MPa) for the best tiles for building applications (BIa group, ISO 10545-4).

Mechanical strength is not the only key issue for a waste-derived material to be effectively employed in building applications. In fact, any waste-derived material should be chemical stable, i.e. provide a permanent immobilization of pollutants. Table IX.7 reports the results from leaching test: the best material (ASH2 with PEG binder) features limited release of ions, but cannot be considered as inert, according to current Italian standards (D.M., 2010). An interesting strategy for stabilization, according to recent studies (Bernardo and Dal Maschio, 2011), is not associated to the reformulation of waste-derived glasses, but to the sintering with a secondary glass. Considering the high percentage of fly ash employed (65-67 wt%), the amount of heavy metals present in the parent glass is not negligible.

Element	Limits for non-hazardous materials/ppm	Limits for inert materials/ppm	Leachate from ASH 2 [+PEG]/ppm	Leachate from ASH 2-borosilicate [+PEG]/ppm
As	0·2	0·05	0·0212	0·0115
Ba	10	2	0·0761	0·019
Cd	0·1	0·004	0·003	0·0014
Cr	1	0·05	0·0234	0·0072
Cu	5	0·2	0·5049	0·0154
Hg	0·02	0·001	<0·0004	<0·0004
Mo	1	0·05	<0·0033	<0·0033
Pb	1	0·05	0·1023	0·0047
Sb	0·07	0·006	<0·0099	<0·0099
Se	0·05	0·01	<0·0122	<0·0122
Zn	5	0·4	0·2114	0·2322

Table IX.7: Results from leaching tests of selected sintered glass-ceramics
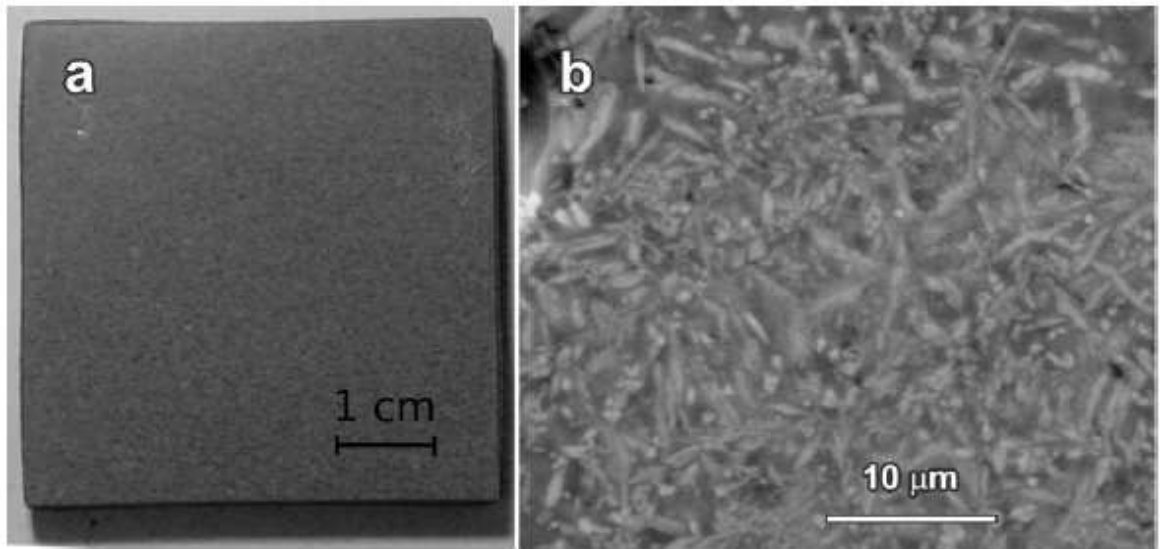
Figure IX.13: Details of sintered glass-ceramics from the mixing of ASH2 glass with borosilicate glass: a) visual appearance; b) high magnification SEM image (backscattered electrons)

Hence after firing a part of the metal ions participate to the formation of crystal phases and part of them are stabilized by the amorphous phase; consequently under leaching conditions the heavy metals may be released both from the crystallites and the amorphous phase. The increased chemical stabilization achieved by adding an inert secondary glass to the waste derived glass may

be due to the further dilution and embedding of both the crystallites and the heavy metals present in a chemically inert glass-ceramic. In other words, it is possible to improve the chemical stability not only *before* vitrification, but even *after* it by adding a more stable glass to a waste derived glass-ceramic. In the present case, ASH2 glass was mixed with recycled pharmaceutical glass (composition shown in table IX.4, in the proportion 7:3, and processed with PEG binder, leading to the glass-ceramic sample shown in figure IX.13a. Although related to a lower content of ASH2 glass, the mechanical properties of the new sample (after sintering at 1000 °C for 30 min), remain substantial, as testified by table IX.6. Despite a lower degree of crystallization, evident from the comparison with the glass-ceramic from ASH2 glass alone, shown in figure IX.14 (see the lower intensity of peaks), the strength could be reasonably enhanced by the fine distribution of crystals, as illustrated by figure IX.13b. As reported in table IX.7, the new formulation caused the leaching of pollutants to be well below the limits for a material to be considered as inert.
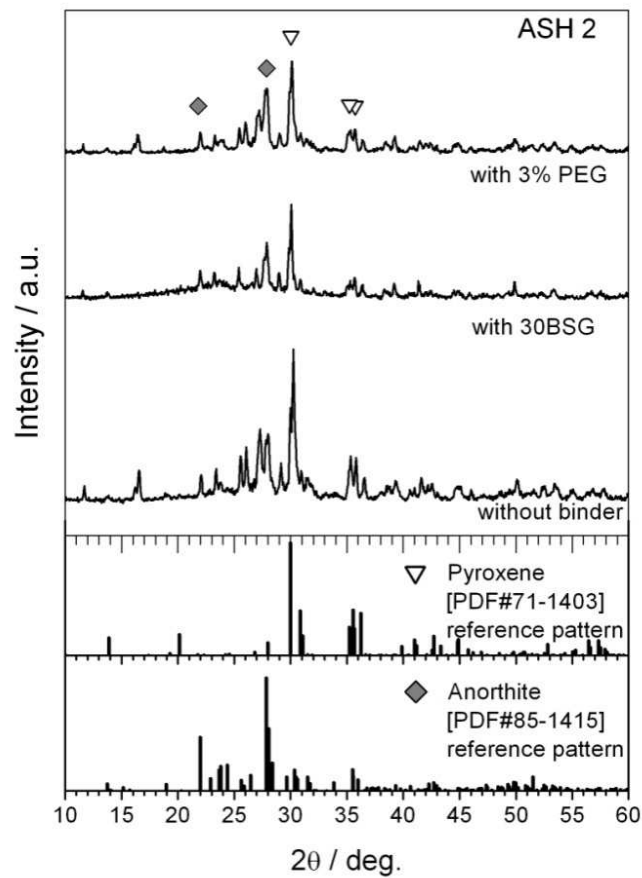
Figure IX.14: Comparison of x-ray diffraction patterns of optimized glass-ceramics from ASH2 glass

Further studies will certainly dedicated to extending the present approach, in terms of compositions to be tested and manufacturing procedures. It would be interesting, as an example, to evaluate samples from double-pressing operations, in which a strong core based on ASH2 glass would be accompanied by a chemically resistant top layer, acting as a glaze, based on a mixture of ASH2 glass and borosilicate glass.

IX.2.4 Conclusions

We may conclude that:

- Selected kinds of Estonian oil shale ash may be employed as the main raw material (being used in an amount exceeding 60 wt.%) in the formulation of waste-derived glasses, to be converted into glass-ceramics;

- Sinter-crystallization, found to be active for the investigated compositions, allowed the obtainment of glass-ceramics by very fast and cost effective firing treatments (sintering at temperatures not exceeding 1000 °C, holding time of 30 min, fast heating);

- Optimized formulations, in terms of composition and selection of binders, led to strong glass-ceramics, with a high reliability (Weibull's modulus exceeding 10);

- The chemical stability of the sintered glass-ceramics may be improved by mixing waste-derived glass with recycled borosilicate glass.

IX.3 Polymer-derived SiC-boron carbide composites

Note: work mainly conducted by Enrico Bernardo and Salvatore Grasso, at the University of Padova, and Nanoforce, (Queen Marie College, London). My contribution concerned the pyrolysis of polycarbosilane-based mixtures and the mechanical characterization, by indentation (related paper: Polymer-derived SiC ceramics from polycarbosilane/boron mixtures densified by SPS, by E. Bernardo, I. Ponsot, P. Colombo, S. Grasso, H. Porwal, M.J. Reece), Ceram Int, 40 (2014) 14493-14500)

Spark plasma sintering (SPS) is considered as an efficient method for densification of advanced ceramics. Since commercially available prepyrolized polycarbosilane could not be densified by SPS even at 2050 °C, the addition of amorphous boron was investigated. Aiming to control dispersion of boron in the powder mixture, the preceramic polymer was mixed either before or after pyrolysis. Boron worked as sintering additive resulting in dense monoliths with good combination of Vickers hardness and indentation fracture toughness. Toughening mechanisms were mainly attributed crack deflection of finely distributed boron carbide phase. The mixing before pyrolysis was found to provide a more homogenous distribution of the second phase.

IX.3.1 Introduction

Our work aims to investigate the manufacture bulk dense advanced ceramics derived from a polymer precursor. Effect of sintering additives as boron was also investigated.

The SPS invention in the 1930s led to the elaboration of reinforced ceramics, thanks to its ability to heat fast and at very high temperatures. A wide range of innovative products in fields such as cutting tools and hard materials, biomaterials, materials for nuclear energy applications, and materials with low coefficient of thermal expansion have been elaborated using this process (Suarez *et al.*, 2013; Grasso *et al.*, 2009 and 2013; Vasylkiv *et al.*, 2012). By applying SPS after pyrolysis of pre-ceramic polymers in reducing atmosphere, it is possible to consolidate the obtained ceramics and give them high hardness, density and fracture toughness.

Some investigations on the impurities in silicon carbide have demonstrated the positive effect on the fracture toughness, especially considering B_4C; the role of boron, however, is examined for percentages well below 5 wt% (Kazumori *et al*, 2008; Maître *et al*., 2008). This study is focused on weight percentages of boron even exceeding 5%. In fact, we will refer to composites with a boron content of 5% and 10%. Composite compositions in traditional studies (Zhang *et al.,* 2013), present a ratio of B to Si superior or equal to 1. Few percentages like those presented here are not frequently described.

The addition of a secondary component in SiC is supposed to decrease both the sintering temperature necessary for full densification, which is known to be problematic, and mechanical properties. In this study, by taking into account the fact that sintering of B_4C by SPS shows excellent mechanical properties (Moshtaghioun *et al.*, 2013), composite formulations allowing both fast SPS process and relevant mechanical properties were elaborated. Then, mechanical properties were expected to be equivalently good to those of B_4C and SiC.

A second novelty of the present investigation concerns the origin of SiC, i.e. a commercial polycarbosilane. This specific type of preceramic polymer is a well-known precursor for silicon

carbide, especially when considering the manufacturing of fibers (with the commercial names of "Nicalon" and "Tyranno") (Colombo *et al.*, 2010). General advantages of preceramic polymers are the low processing temperatures and, above all, the possibility of using polymer processing techniques, like fiber spinning. However, heating of preceramic polymers generally leads to the formation of cracks and pores in the ceramic products, if not thin-walled (i.e. if not in form of fibers, microcellular foams, thin films), due to the release of a great amount of gases (mainly hydrocarbons) (Wild and Buhler, 1991; Renlund *et al.*, 1991) during the polymer-to-ceramic conversion (at T > ~500 °C), which results also in a significant volume contraction of up to 60%. Monoliths can be produced only by applying hot pressing to pre-ceramized materials, or including fillers, which can either react with the preceramic precursor (reaction with the main ceramic residue, with gaseous by-products or with the atmosphere) or remain inert during firing. Densification of polymer-derived ceramics by SPS has been seldom applied (Gash *et al.*, 2001; Wan *et al.*, 2003; Duan *et al.*, 2004; Sandua *et al.*, 2012; An *et al.*, 2014).

The introduction of fillers takes advantage of the features of the preceramic polymers: in fact, fillers can be easily and homogeneously dispersed in liquids, obtained from the melting or from the dissolution in solvents of polymer precursors (Colombo *et al*., 2013b). In the present case, boron can react with the different components of the ceramic residue from the pyrolysis of the preceramic polymer, i.e. free carbon, oxygen (present as a contamination in polycarbosilanes) and possibly even silicon.

IX.3.2 Experimental Procedure

A commercial polycarbosilane (PCS, Nipusi® type S, Nippon Carbon Co., Ltd.) was used as SiC precursor. Boron was provided in the form of micro-sized particles (< 1 μm, supplied by Sigma Aldrich with purity>95%) and mixed with the SiC precursor in two different ways. In the first case, B powders ("B pwd") were dry mixed with pre-pyrolyzed PCS by means of a rotary mill (ball milled at 350 rpm using QM planetary ball mill (Nanjing University Instrument Plant) and zirconia balls (diameter-10 mm) for 4 h with a powder-to-ball weight ratio of 1:20.). In the second case ("B sol") B powders were cast in solutions of PCS in acetone (50 ml of solvent for 10 g of PCS), under magnetic stirring. The B-containing dispersions were dried at 60 °C overnight and the resulting solid residues were first ground into fine powders and then subjected to pre-pyrolysis.

Pre-pyrolysis treatments, for both pure PCS and PCS/B mixtures, consisted of a heating stage at 1000 °C for 1 h in nitrogen (2 °C/min heating rate, natural cooling). B was added in an amount of 5 and 10 wt%; when considering PCS/B mixtures, the weight proportions of polymer and filler were adjusted on the basis of the ceramic yield of the polymer (68 wt%) (Li *et al.*, 2008).

The polymer-derived powder mixtures were sintered using a SPS furnace (FCT HP D 20; FCT Systeme GmbH, Rauenstein, Germany) under vacuum (5 Pa). The samples were heated up to the sintering temperature at a rate of 100 °C/min. The samples were kept at the sintering temperature for 5 or 10 minutes. The pressure was held constant to 16 MPa up to the sintering temperature, afterwards the pressure was raised up to 50 MPa in 5 minutes. The initial low pressure allowed for the complete degasification during SPS heating.

The apparent density of the SiC-based ceramics obtained by SPS was measured by means of the Archimedes' principle. X-ray diffraction analyses (Bruker D8 Advance, Karlsruhe, Germany) were performed directly on disc samples, employing CuKα radiation (0.15418 nm), in the interval

2θ=15-65°. Phase identification was achieved by means of the Match! program package (Crystal Impact GbR, Bonn, Germany), supported by data from PDF-2 database (ICDD-International Centre for Diffraction Data, Newtown Square, PA).

Polished samples were employed for Vickers indentation tests, which yielded the hardness (H$_v$) and the indentation fracture toughness (K$_C$) of the investigated materials. The fracture toughness was calculated by measuring the length of the cracks emanating from the corners of the Vickers indents. At low load (10 N, Palmqvist crack system), we considered the empirical simplified equation (see eq. 1) provided by Niihara *et al.* (1982) and already applied to SiC ceramics (Zhang *et al.*, 2012a):

$$K_C = 0.036 \cdot \left(P \cdot H_v / L \right)^{0.5} \tag{1}$$

where P is the applied load, H$_v$ is the Vickers hardness, L is the length of emanated Palmqvist-type cracks.

At high load (20 N), for the densest samples, we used the well-known equation (eq. [2]) provided by Anstis *et al.*, (1981) as follows:

$$K_C = \xi \cdot \left(E/H_v \right)^{0.5} \cdot \left(P/c^{1.5} \right) \tag{2}$$

where c is the length of emanated half-penny cracks and ξ is a calibration factor (ξ=0.016±0.004). E is the elastic modulus of the material, supposed to be equal to that of SiC (430 GPa).

IX.3.3 Results and Discussion

Table IX.8 summarizes the processing conditions applied to the investigated SiC-based ceramics, together with some measured properties.

Precursor	Boron content (wt%)	Mixing mode	SPS treatment, 50 MPa at …/for…	Archimedes' density (g/cm^3)	Vickers Hardness, H_V (GPa)	Indentation Fracture Toughness, K_{IC} (MPa m$^{0.5}$)
PCS	0	–	1900 °C/10 min	2.12 ± 0.01	–	–
			2050 °C/10 min	2.44 ± 0.04	22.4 ± 4.2	4.2 ± 0.8[a]
PCS/Boron series#1	5	Pre-pyrolized PCS powders [B$_{pwd}$]	2050 °C/10 min	2.70 ± 0.01	19.9 ± 2.1	4.1 ± 0.7[a]
	10		2050 °C/5 min	2.96 ± 0.01	22.3 ± 1.7	5.8 ± 0.8[a]
			2050 °C/10 min	2.97 ± 0.01	19.6 ± 4.1	5.8 ± 1.3[a]
PCS/Boron series#2	5	PCS solution [B$_{sol}$]	2050 °C/10 min	3.03 ± 0.01	20.6 ± 1.1	4.5 ± 0.5[b]
	10		2050 °C/10 min	2.99 ± 0.02	25.8 ± 2.7	4.7 ± 0.2[b]

[a]According to the equation by Niihara et al.
[b]According to the equation by Anstis et al.

Table IX.8: Summary of processing conditions and properties of polymer-derived SiC-based ceramics

The first system to be processed with SPS was that of pure SiC, from powders of pre-pyrolized PCS, without additives. Due to the low pre-pyrolysis temperature, the precursor powders were X-ray amorphous and contained some oxygen contaminations and some residual H as well, (Li *et al.*, 2001; Sorarù *et al.*, 1990) i.e. they were expected to undergo further transformations during SPS treatment, as effectively found observing the variations in the SPS chamber pressure, with gas release, shown in figure IX.15a.
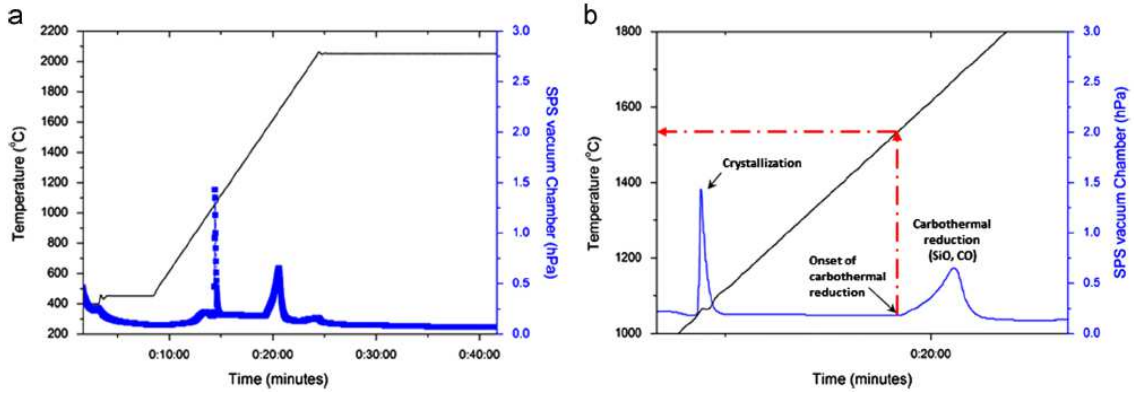
Fig.IX.15: SPS Temperature profiles for pure pre-pyrolized PCS: a) overall plot;
b) high magnification detail

In particular, the pressure peak at approximately 1050 °C was likely due to crystallization, in turn associated to H_2 release (from decomposition of residual –CH_2– units in the polymer backbone) (Sorarù et al., 1990; Bouillon et al., 1991), or to carbothermal reduction reaction occurring between boron oxide and C (Corradetti *et al.*, 2013). The second pressure peak (less intense), at about 1600 °C, could be ascribed to carbothermal reactions involving the oxygen contamination, generally found in the ceramic residue of polycarbosilanes. Carbothermal reactions imply the release of both CO and SiO, and usually take place starting from 1450 °C (Kim *et al.*, 2008). This is consistent with the high magnification detail of SPS chamber pressure plot in figure IX.15b, showing that the second gas evolution actually started at about 1500 °C.
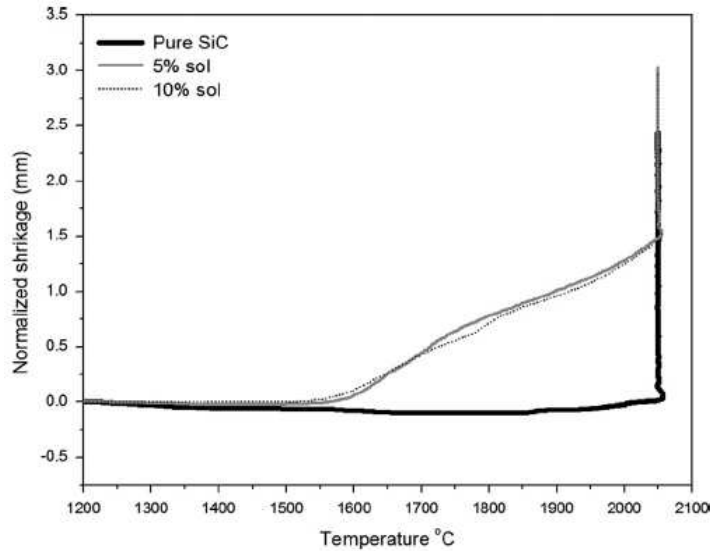
Figure IX.16: Shrinkage plots for different polymer-derived SiC-based ceramics processed by SPS

The boron addition had a remarkable impact on SPS processing, as highlighted by the density data reported in table IX.8. The values for samples from pure pre-pyrolized PCS were quite far from the theoretical density for SiC (~3.21 g/cm³ for all polytypes) (Harris, 1995). This fact is confirmed by the relative shrinkage plots in figure IX.16: some densification of pure pre-pyrolized PCS started only at the end of the heating stage, when the maximum SPS temperature (set at 2050 °C) was reached. Sintering experiments with maximum temperature at 1900 °C were consequently

inadequate. At 2050 °C, nearly one half of the holding time was necessary to achieve a relative shrinkage of only 2 %. On the contrary, B-containing samples exhibited some shrinkage already during the heating stage, i.e. starting from 1600 °C; at 2050 °C, the shrinkage was well above 2 %. The expected higher homogeneity of B distribution, using the "B sol" mixing approach, was associated to an improvement of the shrinkage, from 3.5-4 % to 4.5-5 %.
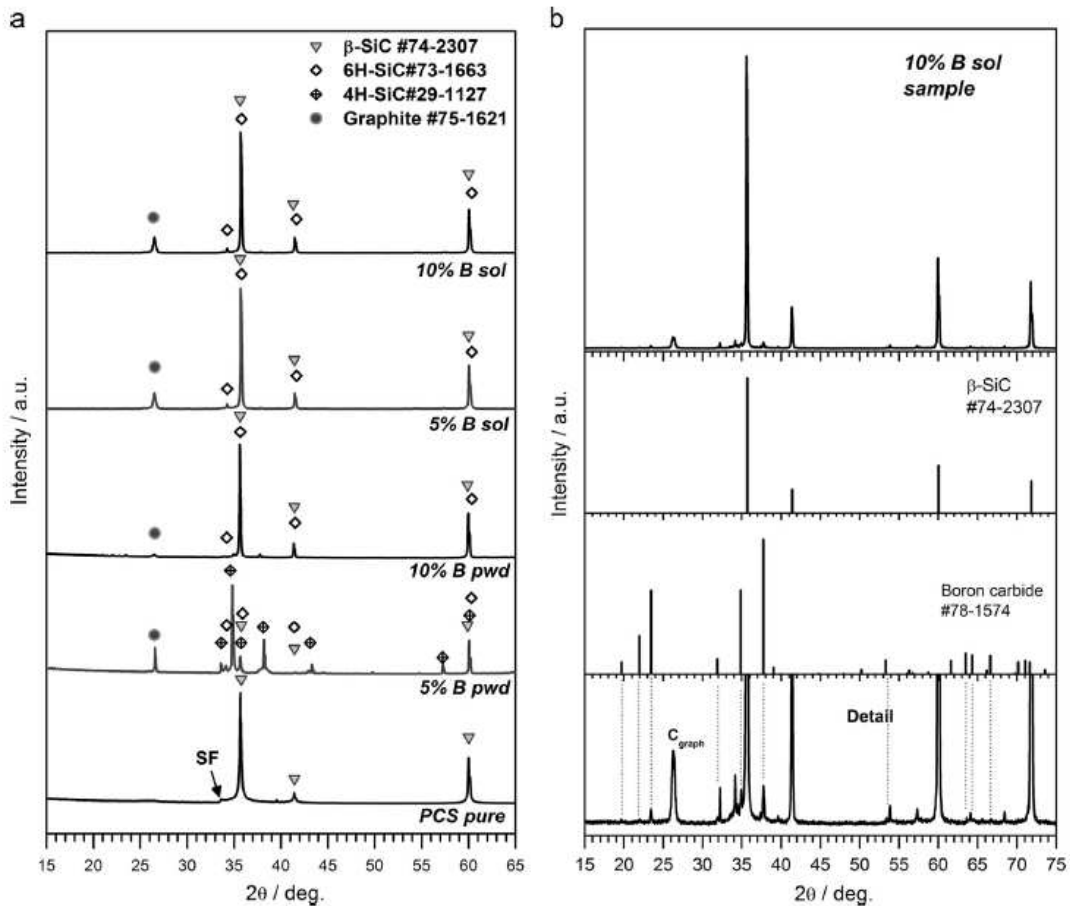

Figure IX.17: X-ray diffraction patterns: a) comparison of samples with different boron addition (SPS at 2050°C, for 10 min); b) refined analysis for the 10% B sol sample

From the X-ray diffraction patterns in figure IX.17a we can note some differences among the ceramic from pure PCS and the ceramics developed with B addition, sintered at 2050 °C, also in terms of phase composition. Pure PCS led to practically phase pure cubic SiC (β-SiC, PDF#74-2307). The additional shoulder located at 2θ~34° is attributable to stacking faults (Kurtenbach *et al.*, 1998). B-doped SiC, with 5% B, developed by powder mixing [B pwd] is significantly different from the other B-doped ceramics: while the first one features traces of hexagonal SiC (α-SiC, PDF#29-1127) and, above all, boron carbide ($B_{6.5}C$ or $B_{13}C_2$, PDF#78-1574), the other ones feature traces of hexagonal SiC in a second polymorphic variant (α-SiC, PDF#73-1663) and graphitic carbon (PDF#75-1621). The peaks attributable to boron carbide were particularly weak, as highlighted also by the higher resolution detail reported in figure IX.17b (see the dotted lines, corresponding to the most intense peaks of $B_{6.5}C$). Except for the sample with 5% B [P pwd], boron likely concentrated in a well-distributed nano-crystalline boron carbide phase.
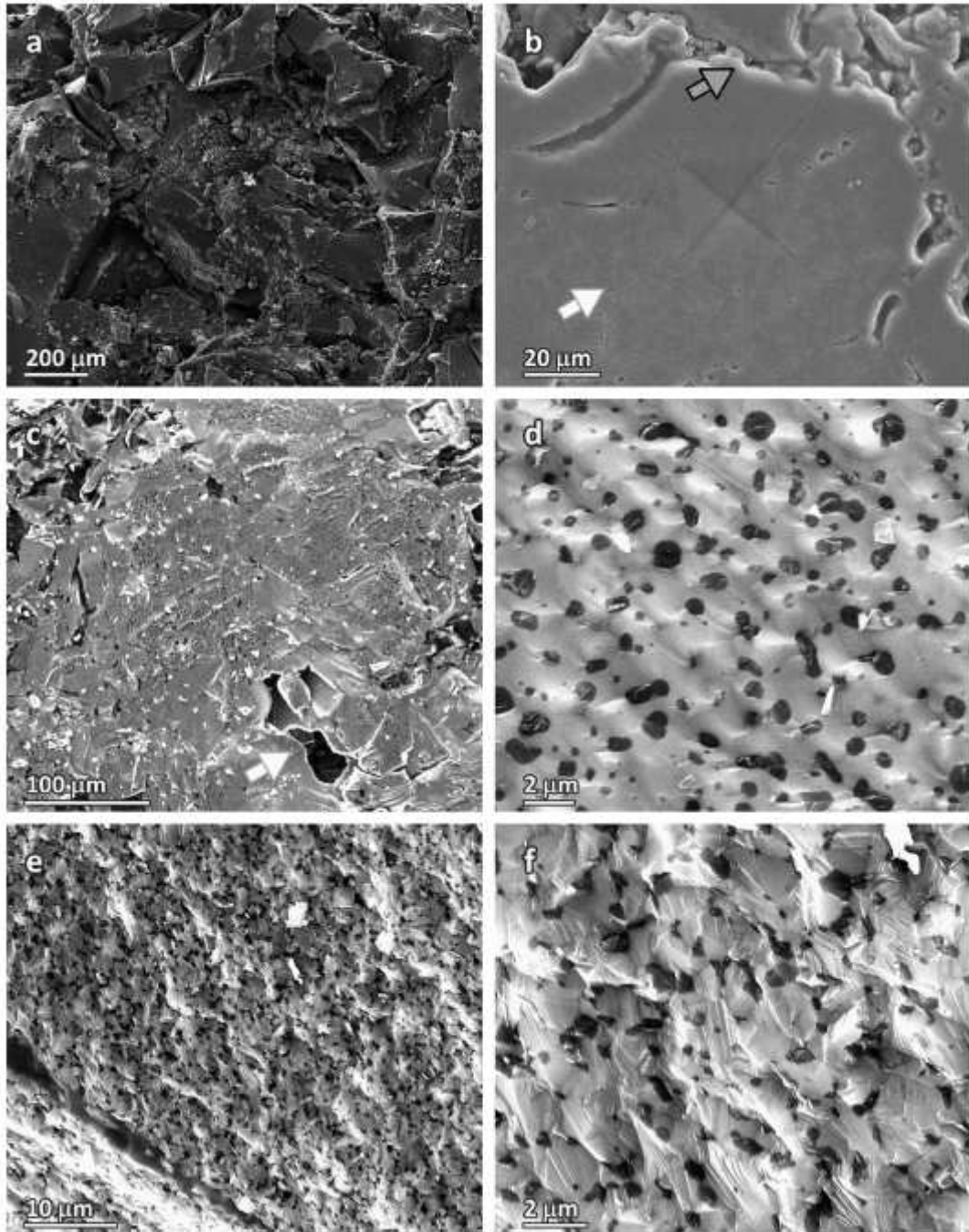
Figure IX.18: SEM micrographs of SiC-based ceramics processed by SPS: a,b) pure PCS; c,d) 5% pwd; e,f) 10% B pwd

The poor densification of samples from pure PCS is further testified by the micrographs in figure IX.18. The fracture surface of the sample from pure PCS, in figure IX.18a, reveals the presence a number of distinct dense granules, partially joined at the interface. These granules most probably correspond to the former particles of pre-pyrolized PCS, transformed into dense agglomerates of SiC crystals. The transformation was confirmed by the indentation analysis applied on the same densified zones, after polishing, as illustrated in figure IX.18b; both hardness and fracture toughness values match well those of SiC ceramics (Noviyanto *et al.*, 2013). The poor

densification could be explained on the basis of an analogy with frit-derived glass-ceramics, where the viscous flow of fine glass powder may be inhibited by a substantial surface crystallization, according to the remarkable viscosity increase provided by the same crystal inclusions (A.R. Boccaccini, 1998). In the present case, the crystallization of SiC hindered any viscous flow of the amorphous residue from PCS.

The samples from PCS and B, with boron added to pre-pyrolized PCS powders [B pwd], were much denser, but still had a quite heterogeneous microstructure. More precisely, figure IX.18c shows the sample with 5% B, exhibiting quite large irregular voids (in particular, see the voids at the bottom), uniform grey zones and zones with a multitude of darker micro-sized spots. The voids are attributed to a limited packing of former particles of pre-pyrolized PCS, while the uniform grey zone correspond to agglomerates of SiC crystals. The zones with dark grey micro-spots are particularly interesting: the spots, according to EDS analysis, actually correspond to a secondary, boron rich phase, surrounded by the main SiC phase. In our opinion, the bi-phasic zones originated upon interaction between the surface of granules of pre-pyrolized PCS with B particles; the chemical interaction between B and the oxygen contaminations provided a borate liquid phase, that helped the densification by a dissolution and precipitation mechanism, and later converted into a boron carbide phase, by carbothermal reduction occurring already at around 1000 °C (Corradetti, *et al*., 2013).

A higher boron content led to a more homogenous biphasic structure, shown in figure IX.18e and f. Figure IX.18e (bottom part) shows the persistent presence of relatively large defects; figure IX.18f illustrates the particular fracture surface, comprising a lot of steps (more pronounced than in the case of 5% B). These steps are probably caused by crack deflection in SiC crystals (zones with a lighter colour), around boron carbide phase, favored by the thermo-elastic mismatch between the two phases. Figure IX.19a, referring to the polished surface of a B sol 5% sample, clearly shows light grey boundaries between adjacent former granules of pre-pyrolized material; high magnification details, see figure IX.19b, highlight the formation of a number of SiC microcrystals (light grey), surrounded by a multitude of darker spots, attributed to both the segregation of a boron rich phase and micropores; some larger pores and irregularly shaped dark grey areas are also visible. figure IX.19c and d clarify that these dark zones do not represent voids, but a further phase.

The structure of the matrix around the dark inclusion, attributed to graphitic carbon, in figure IX.19d, is quite similar to that of B pwd samples, but on a much finer scale (very rough surface, from multiple crack deflections around microcrystals and dark spots). figure IX.19e, referring to a sample with higher B content (B sol 10%), confirms this situation. Finally, the crack deflection occurring around the microcrystals is further testified by the image of the crack path on a polished surface (see figure IX.19f , details of a crack emanating from a Vickers indent). Further proofs of the optimum dispersion of B-rich secondary phase and of the multiple deflections of cracks are reported in figure IX.20.
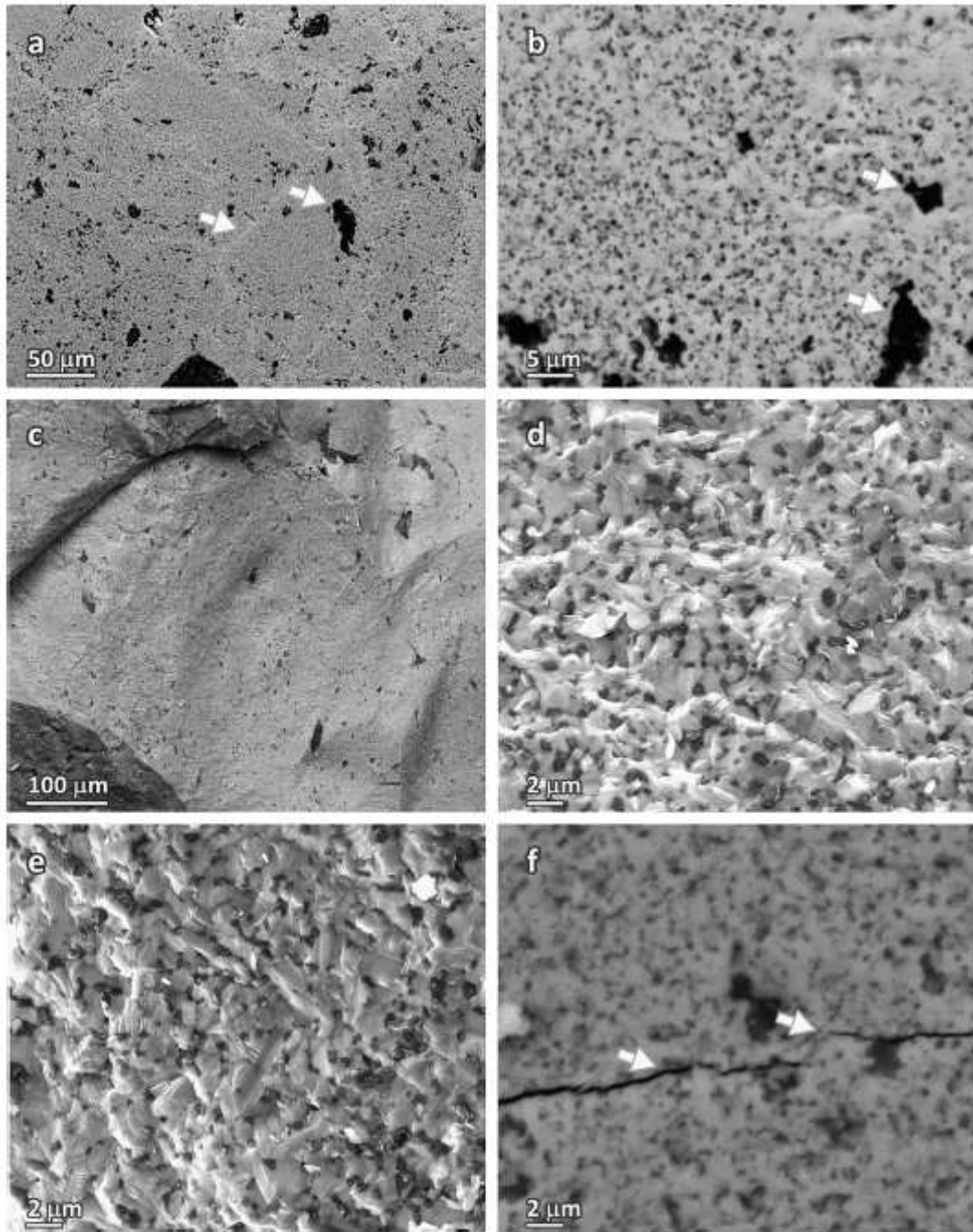
Figure IX 19: SEM micrographs of SiC-based ceramics processed by SPS: a-d) 5% B sol ; e,f) 10% B sol

The differences in hardness between samples with the same B content, but different mixing procedures, are reputed to be insignificant; in fact, the measurements on B sol samples were made considering much wider indents, i.e. the properties were averaged on a much wider volume, including the above described micro-pores. In any case, even considering the lowest values, the mechanical properties of the B-containing samples, reported in table IX.8 compare favorably with those of SiC monoliths (Noviyanto *et al.*, 2013). The good values of hardness derive however from the influence of the entire microstructure of the samples; if the presence of micropores would give a decrease in hardness, this is increased by the presence of boron carbide sub-micron inclusions ($B_{13}C_2$ is in fact classified as a super-hard phase). (Zhang *et al.*, 2012b)

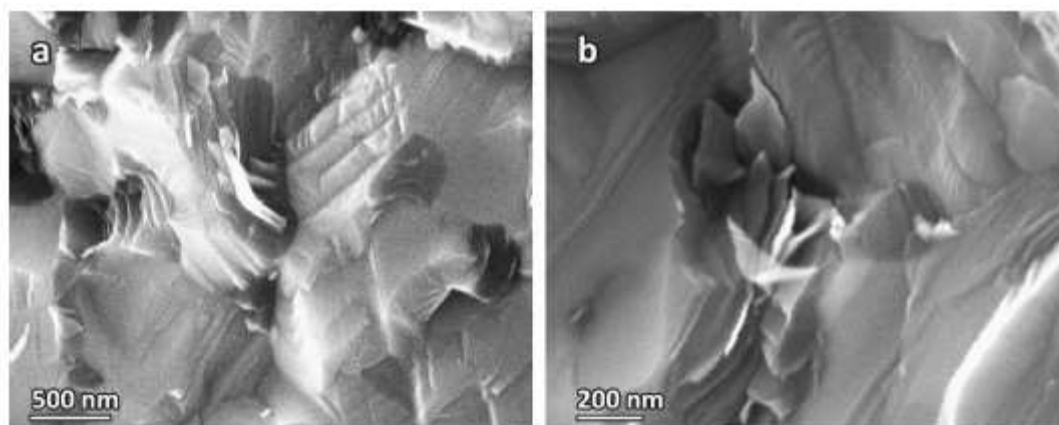*Figure IX.20: a) high magnification details of multiple crack deflections in sample 10% B sol; b) evidence of sub-micrometric B-rich secondary phase*

The prepared SiC-based composites for structural components, to the authors' opinion, have some potential for structural components. However, further efforts will be needed to verify the feasibility of much larger samples, essential for the effective assessment of any toughening effect provided by the boron carbide phase (e.g. by measurement of the bending of chevron-notched bars).

IX.3.4 Conclusions

The main findings of this study may be summarized as follows:

- Spark plasma sintering (SPS) can provide dense SiC-based ceramic composites, starting from a commercial polycarbosilane (PCS); the presence of a boron filler is essential for the effective densification since the crystallization of SiC hinders any viscous flow of the ceramic residue of the preceramic polymer;

- The incorporation of B can be achieved both by operating with the ceramic residue of PCS (mixing of powders after pyrolysis of PCS) and by operating with the starting polymer (B added as a filler);

- The two types of mixing lead to similar microstructures, comprising fine boron-carbide crystals in a SiC matrix; the addition of B in the polymer leads to a more homogeneous distribution of secondary phase.

IX.4 Short Life Cycle Analysis of a glass-ceramic tile from waste recycling

IX.4.1 Introduction

The construction field, which is in constant evolution, is experiencing a singular revolution, in which sustainability plays in important role. A lot of building materials nowadays are submitted to the evaluation of environmental impact. Buildings manufacturing may require an optimized LCA (Ramesh *et al*., 2010), particularly when considering external insulation and means employed for the optimization of energy recovery in a "passive system" (Mora, *et al.*, 2011; Stazi *et al*., 2012; Radhi *et al*., 2013; Stephan *et al*., 2013), and sometimes focusing specifically on the façades (Blom *et al*., 2010; Kim, 2011; Taborianski *et al*., 2012). Some LCA in the construction field focus on the type of materials used (Blengini, *et al*., 2010; Chau *et al*., 2012). Very often, new alternative materials appear, that are partly or totally made by recycling inorganic waste. The Life Cycle Analysis (LCA) tool is able to give an overview of the economic as well as environmental impact of such alternatives, generally on a comparison basis. The possibility of producing waste-based panels assessed by LCA would enable to ensure public opinion of the validity of the process in the sustainable aspect. To consider the specific life-cycle of a waste as secondary raw material instead of an End-of-use substance, recently LCA methods for waste management systems (Alexis *et al*., 2014) are available. The environmental impact of construction materials concerns also waste based materials (Garcia *et al*., 2007; Coelho *et al.*, 2012). Glass and ceramics have been the subject of environmental studies, particularly regarding the end-of-life stage, the carbon footprint and the energy consumption (Vellini *et al*., 2009; Quinteiro *et al.*, 2012a and 2012b). This review has for objective to summarize the LCA analysis comparing waste based innovative materials to traditional ones, in the construction field. Materials considered are among: i) Glass foams for lightweight concretes from recycled glass (Blengini *et al*., 2012); ii) Lightweight glass-ceramics for ventilated façades. According to Cabeza *et al*. (2014), in a study of LCA in the building sector, construction materials such as concrete and steel can account for most of the materials –related environmental impacts, and use-phase energy consumption can account for 50% of total life-cycle impacts. For this reason, it would be interesting to improve the manufacturing of the construction materials in a way to decrease their environmental impact. In this idea, LCA has already been done on glass foam aggregate from waste glass (Blengini *et al.*, 2012). Beyond enhancing energy saving during the operational phase of buildings, such products are expected to increase recyclability of the building as a whole. A recent study of LCA (de Gracia *et al.,* 2014) on ventilated façades, a target application of lightweight waste-based ceramics, is an ideal support to this study. The raw material chosen corresponds to the type of waste investigated in chapter V.2. The LCA methodology followed here corresponds to ISO 14040 (2006) and ISO14044 (2006), in the purpose to answer an environmental issue on the aspects of physical good: by designing new product and comparing improvements in competing products and service, through the greening of the building industry. The analysis is presented in two particular ways: the first one sets the functional unit as a quantity of produced material in kg whereas in the second one, a superficial area in m² is considered.

IX.4.2 Goal and scope definition

IX.4.2.a Objective of the study

Manufacturing of waste based ceramic tile relative to that of composite plastic tile (comparative LCA, see table IX.9. The purpose is also to determine if the introduction of waste in the raw materials composition gives lower potential environmental impacts. The results will be used by the company to take decision on whether to launch a parallel production using this process and how to equip the production site.

	Life span façade systems			Building life span	Façade area covered
	Plastic composite panels	*Waste Ceramic tiles*	*Metal frame (supporting structure)*		
Baseline LCA	10 years	20 years	40 years	40 years	4 x 5m²

Table IX.9: comparison between various materials for this application

IX.4.2.b Function (wall system) and functional unit

According to ISO 14040, the functional unit is a quantified description of product systems' performances. The adopted function is covering a wall surface of 1000 m². The product is supposed to have a thickness of around 10 mm and volume mass of 2 kg/m^3 so this surface is equivalent to **2 T (FU)**. The second opportunity is to consider a **façade area of 4 x 5 m², 40 years service, life span 10 years and 20 years.**

IX.4.2.c Product systems: cradle to the grave (pre-use, use, post-use).

All the processes involved in the production, distributed and disposal of the tile in Italy.

IX.4.3 Inventory- first analysis

In the first analysis, an appropriate inventory would be described as following (see figure IX.22).
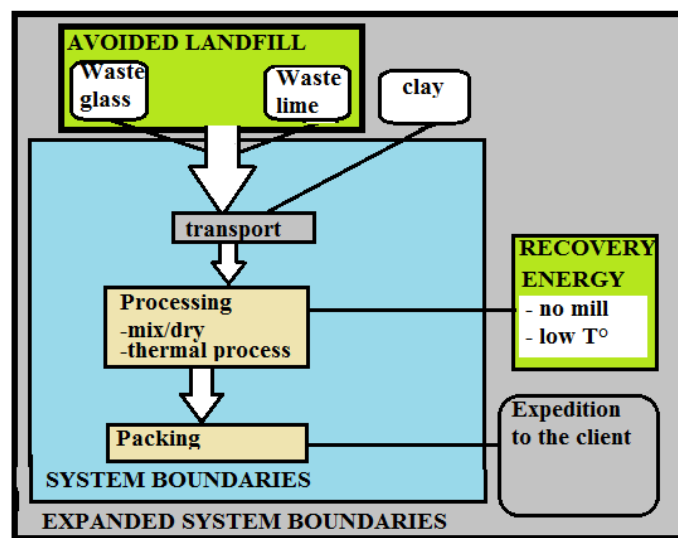

Figure IX.22: input and output data of the tile waste-to-production chain

The waste glass and waste lime, instead of going to landfill storage, are recovered as raw materials for the production, together with clay. The glass-ceramic process may proceed by a fast process, such as sinter-crystallization or direct sintering, for a short holding time and at temperatures lower than 1100 °C due to the low softening temperature of the mixture, as presented in the bibliography (Bernardo, 2008; Bernardo and Scarinci, 2008; Bernardo *et al.*, 2009; Bernardo *et al.*, 2010; Ponsot *et al.*, 2012) and in chapter V.1. This may bring a recovery of energy, from the fact that the waste material may be already partially ground, and so the milling process would be reduced, and from the optimized thermal treatment. The delta input – output waste is positive, which means that there is a decrease of the waste production in this cycle (table IX.10).

Wastes input	*Waste output*
1.8 T as raw material	
Mixing with reused waste from pressing 0.1 T	Pressing 0.1 T
	Thermal process : used filters and dusts from abatement fume system (0.1 T)
	Delivery and client use :
Total : 1.9 T	Total : 0.3 T

Table IX.10: quantity of input and output waste

IX.4.3.a Suppliers

The raw materials suppliers chosen in the study correspond to companies that are susceptible to produce regularly the waste glass, waste lime and clay by direct or indirect ways. The glass manufacturing company, to provide the waste glass, in amounts estimated of $1.8 \times 70\% = 1.26$ T/year, may produce an estimated average of waste production by producing 100 T/year glass pieces, among them 1 % scrap. The ceramic plant, to provide waste lime, may dispose of furnaces zones, with a regular use of exhausted lime in its fume abatement system. The supplied quantity obtained by calculation may be of $1.8 \times 20 \% = 0.36$ T/year. Regarding clay, the quantity imported would come from an extraction plant of which impact on price depend on plants geographic position (see table IX.11).

Materials	*Proportion [wt%]*	*Supply*	*Emissions*	*Energy consumption*
Waste glass	70	Glass manufacturing company	Gas, CO_2, non-dangerous waste glass. (part of the emission are taken as raw materials) quantity 5%	
waste lime	20	from fume abatement system : glass and pigments plant		
clay	10	extraction plant	H_2O, CO_2 (emissions into air), waste kaolin (emissions into soil). quantity 5%	Extracting process

Table IX.11: repartition of the emissions and energy consumption per material supplied

IX.4.3.b Transport

If the transport is made by road (or boat), the energy consumptions depend on oil or fuel consumption parameters. The quantity supplied by road set at 0.36 T/year waste lime on 500 km and 1,26 T/year waste glass on 100 km (in the case where the production plant is located near to a glass manufacturer, for example). During the delivery to the client and the transportation to landfill, 2

T/year new panel and 2 T/year waste panel is supposed to be transported on a distance of about 500 km. We deduce an estimation of the emissions, into air, in CO_2, gas, PF and hydro carbides.

IX.4.3.c Manufacturing

In the manufacturing processes, most of the various emissions and energy consumption comes from the thermal treatment at 900 °C. The other steps of the process are non-negligible, particularly because of the heat and fine particles emissions, but solutions exist to recover the dissipated heat and to act on a reduction of the particles emissions places.

IX.4.3.d Use

The final use corresponds to the installation of 2 T panels covering the surfaces of non-residential and residential buildings. The waste and dusts emitted should not be more than a 5% quality target (see table IX.12).

Process	Energy consumption	Emissions into air	Emissions into water and soil
Raw materials mixing in 50 wt% water (tanks) - important water usage here	electricity for rotors	H_2O vapor, CO_2, gas, heat (emissions into air), waste and (indirectly from electricity production CO_2, H_2O)	liquid waste mixture
Drying (spray drying)	gas or electricity or both – constant T° around 150 °C	H_2O vapor, CO_2, gas, heat	waste
Pressing	gas or electricity or both – pressure of around 400 bars	CO_2, gas, dusts (emissions into air, and soil indirectly)	waste
Drying and thermal treatment Other: maintenance	gas or electricity or both – constant T° around (here not taken into consideration, but maybe relevant)	CO_2, gas, heat, (major contribution) Oil, grease, metallic scrap, plastic…	waste final product (discharge)
Packaging: 1 Palette and 1 T paper boxes, glue	electricity or gas for the packing machine	CO_2, heat	into water: dusts from and cleaning process before packing into soil: waste paper, waste final product, waste glue (resin)

Table IX.12: repartition of the impacts on a Ceramic plant for the manufacturing of tiles

IX.4.3.e Disposal

Depending on acceptance conditions, the building waste (coming from panels dismantlement or replacement) after certification of non-hazard, can be recycled in road construction (emissions into water and soil) and aggregates for concrete if properties are certified according to the related rules and regulations. The other part is sent to landfill storage for non-dangerous waste. The emissions into water and soil may be present.

Note:

Data source: see IX.4.7 and bibliography;

Reference process and technology: traditional ceramic process and technology; Geographical area: Italy;

Monitoring details and measurement method (specific unit of measurement, method for calculating average values, variance and irregularities in the measurements): to be determined.

IX.4.4 Inventory - second analysis

In the second analysis, the inventory may focus merely on separate the product cycle in 3 stages: pre-use, use and post-use, as presented on figure IX.23.
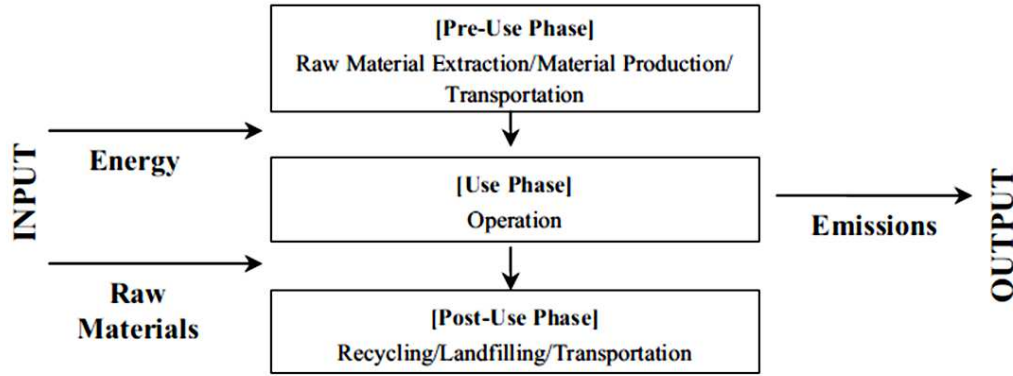

Figure IX.23: flow diagram and system boundary (Kim, 2011)

Components	Plastic composite			Glass waste		
	Mass (kg)	5% wastage	Total	Mass (kg)	5% wastage	total
PMMA (acrylic)	876	49				
Biofiber composite	185	9				
Epoxy	4	0				
Aluminum	53	3		164	8	
Silicon (rubbers)	52	3		49	3	
Waste glass				1899	95	
Total input (kg)		64	1234			2217

Table IX.13: materials for the generation of ventilated façade panels (Kim, 2011)

		Energy	Green house gas (GHG) emissions			
		Embodied energy (MJ)	CO_2 (kg)	CH_4 (kg)	CF_4 (kg)	C_2F_6 (kg)
Pre-use phase	PMMA (1 kg)	135	6.85E+00	2.44E−02	0.00E+00	0.00E+00
	Cardboard (1 kg)	10	7.09E−01	8.92E−04	0.00E+00	0.00E+00
	Epoxy (1 kg)	235	1.10E+00	0.00E+00	0.00E+00	0.00E+00
	Steel (1 kg)	30	9.00E−01	1.63E−04	1.69E−09	2.11E−10
	Aluminum (1 kg)	169	9.96E+00	2.24E−02	3.60E−04	4.20E−05
	Silicone (1 kg)	44	1.16E+00	7.85E−03	0.00E+00	0.00E+00
	EPDM (1 kg)	89	2.96E+00	9.94E−03	8.28E−08	9.20E−08
	Float glass (1 kg)	14	9.68E−01	2.32E−03	1.69E−07	1.88E−08
	Transportation (1 km)	3	2.28E−01	2.77E−04	0.00E+00	0.00E+00
Use phase	Electricity (1 MJ)	3.72	2.98E−01	6.49E−03	0.00E+00	0.00E+00
	Natural gas (1 MJ)	1.15	5.58E−02	1.60E−04	0.00E+00	0.00E+00
Post-use phase	Construction waste (1 kg) landfilled	0.008	5.32E−04	7.37E−07	1.07E−11	1.19E−12
	PMMA (1 kg) recycled	−43	−3.37E−01	8.28E−05	0.00E+00	0.00E+00
	Cardboard (1 kg) recycled	−1.25	−5.55E−01	1.31E−03	−6.88E−09	−7.64E−10
	Glass (1 kg) recycled	−3.15	−3.76E−01	−4.44E−06	0.00E+00	0.00E+00
	Aluminum (1 kg) recycled	−104	−9.33E+00	−1.57E−02	−2.52E−04	−2.80E−05

Table IX.14: list of the embodied energy (MJ) and gas for the consumption of each material (Kim, 2011)

Supporting metallic structures are made of Al and Silicon. The other components of the panels are either PMMA, biofibers, epoxy resin, or waste glass. For each component, the equation (1) is applied using data from table IX.14. Results are described in histogram views (figure IX.24).
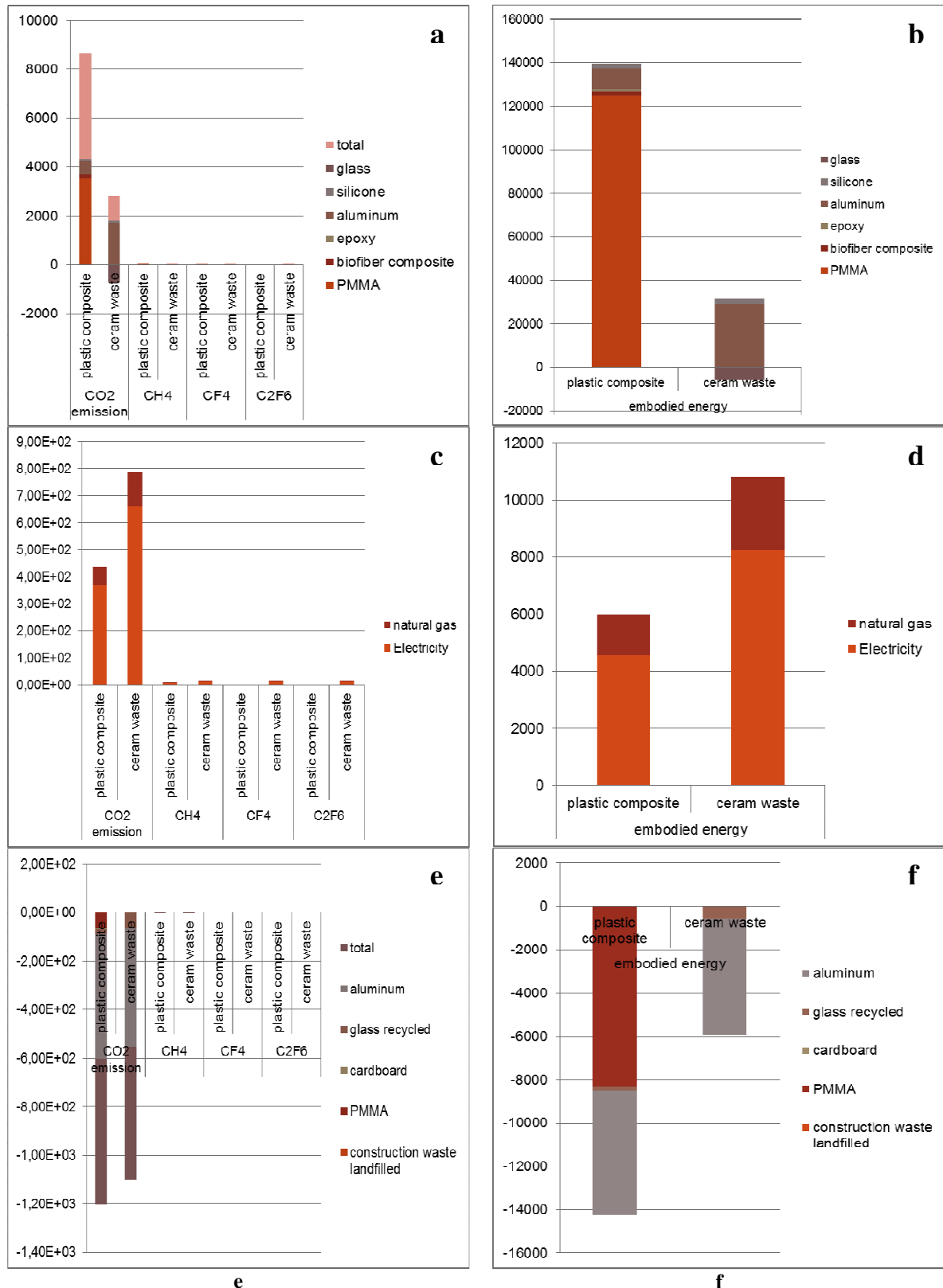
Figure IX.24: histogram representations of gas (left part) and energy consumption (right part) in the "Pre-use" (a;b), "use"(c;d) and "post-use"(e;f) systems

IX.4.5 Impact assessment

IX.4.5.a Classification

In table IX.14 are summarized the various impact levels.

Environment	Impact
Global	Greenhouse effect (CO_2, H_2O), ozone layer (other gases and fumes), consuming nonrenewable resources, (kaolin clay, gas) trouble to human health (dusts, heat)
Regional	Soil acidification, eutrophication, chronical toxicity (if present in incoming waste), poor water resources (water use)
Local	Human health (breath), soil degradation, biodiversity

Table IX.14: how does the system affect the environment?

IX.4.5.b Characterization

The quantitative characterization of the emitted product EP is based on the following equation, with Q, the quantity and EQ $(j)_i$ the substance contribution level:

$$EP\ (j)_i = Q \times EQ\ (j)_i, \tag{1}$$

As an example, the total emission of CO_2 during the whole process, EP (CO_2), is reparsed among each step involved in CO_2 emission: transport, supply, manufacturing, packaging, use and finally disposal, which is written:

$$EP\ (CO_2) = Q_1 \times EQ(CO_2)\ _{transport} + Q_2\ EQ\ (CO_2)\ _{supply} + Q_3\ EQ\ (CO_2)\ _{manufacturing} + Q_4\ EQ\ (CO_2)\ _{packaging} + Q_5\ EQ\ (CO_2)\ _{use} + Q_6\ EQ\ (CO_2)\ _{disposal}$$

Free softwares (such as Gemis www.oeko.de/service/gemis/, Eiolca www.eiolca.net or CMLCA http://www.leidenuniv.nl/interfac/cml/ssp/software/cmlca/) enable to extend and quantify the analysis with non-theory values. Excel, as used here, enable to make a pre-estimation of the interest to pursuit such study, to get a general overview and also to point out eventual particularities.

IX.4.6 Discussion of results

IX.4.6.a Results from inventory analysis and impact assessment

The results presented in the second estimation show three stages of energy consumption. Pre use, use, and post use. In the pre-use stage, waste based ceramic is preferable to plastic. Indeed, the production of plastic itself is energy consuming. In the use and post-use stages, plastic is preferable. One explanation is firstly by considering the shaping energy, which is quite high in the case of ceramics, as they require a thermal treatment, at least up to. Even if nowadays, energy consumption of furnaces is very well optimized, in the case of plastic, we go only to a maximum of 600 °C. Another explanation for this would be that the manipulation energy would depend on materials weight, it could be seen that some ceramic from waste can have the same mechanical properties as those of plastic composites (lightweight and strong). In the post use stage, dismantlement would effectively be energy consuming as well as landfill disposal. Nowadays, plastic, once used, is easily recycled and then there

is an environmental benefit for using it. However, plastic material is easier degraded than ceramic and then it is expected to be replaced after 10 years use instead of 20 years in the case of ceramics.

IX.4.6.b Conclusions and recommendations

At pre use and use stages, the sub-process that should be improved first would be the filtration of fumes and dusts, and the energy recovery by heat redistribution (heat from furnace can be redistributed to spray dryer for example). At use and post use stages, the mechanical and thermal properties of the ceramic can be improved to increase the performance of the building. Working on the feasibility of such waste based ceramic materials would enable to improve the parameters that favor the use of plastic. The reason is not that plastic is not good, but plastic could be used in another application where it would not degrade easily.

IX.4.6.c Limitations

LCA cannot address local impacts. The European law does not authorize easily the thermal treatment of waste, particularly when they are classified dangerous. It requires specific installation that can be a heavy additional cost. It says nothing on social aspects. LCA does not include the environmental impact that was induced to the LCA of the owner of incoming waste.

References

Adamson J. Irha N. Adamson K. Steinnes E. U. Kirso (2010) Effect of oil shale ash application on leaching behavior of arable soils: an experimental study, Oil shale 27 250-257.

Andreola L. Xu W. Rajagopalan S. Wang C. H. Wang, Y. Fan, L. Zhang, D. Jiang, J. Kapat, L. Chow, B. Guo, J. Liang, R. Vaidyanathan (2004) Carbon-nanotube-reinforced polymer-derived ceramic composites, Adv. Mater. 16 2036-2040.

Andreola F. Barbieri L. Corradi A. Lancellotti I. Falcone R., Hreglich S. (2005) Glass-ceramics obtained by the recycling of end of life cathode ray tubes glasses, Waste Manag. 25 183-189.

Anstis G.R. Chantikul P. Lawn B.R. Marshall D.B. (1981) A critical evaluation of indentation techniques for measuring fracture toughness: I, direct crack measurement, J. Am. Ceram. Soc. 64 (9) 533-538.

Aunela-Tapola L.A. Frandsen F.J. Hasanen E.K. (1998) Trace metal emissions from the Estonian oil shale fired power plant, Fuel Process. Technol. 57 1-4.

Barsoum M.W. (2003) Fundamentals of Ceramics, Institute of Physics London.

Begg B.D. Hess N.J. McCready D.E. Thevuthasan S. Weber W.J. (2001) 'Heavy-ion irradiation effects in $Gd_2(Ti_2-xZr_x)O_7$ pyrochlores, Nucl. Mat. 289 188-193.

Bernardo E. Andreola F. Barbieri L. Lancellotti I. (2005) Sintered glass-ceramics and glass-ceramic matrix composites from CRT panel glass, J. Am. Ceram. Soc. 88 1886-1891.

Bernardo E. Albertini F. (2006) Glass foams from dismantled cathode ray tubes, Ceram. Int. 32 603-608.

Bernardo E. (2007) Micro- and Macro-cellular Sintered Glass-ceramics from Wastes, J. Eur. Ceram. Soc. 27 2415-2422.

Bernardo E. Scarinci G. (2008) Fast sinter crystallization of waste glasses, Adv. Appl. Ceram. 107 344–349.

Bernardo E. (2008) Fast sinter-crystallization of a glass from waste materials, J. Non-Cryst. Sol. 354 3486-3490.

Bernardo E. Scarinci G. Edme E. Michon U. Planty N. (2009) Fast-sintered gehlenite glass–ceramics from plasma-vitrified municipal solid waste incinerator fly ashes, J. Am. Ceram. Soc. 92 528-530.

Bernardo E. Bonomo E. Dattioli A. (2010) Optimization of sintered glass–ceramics from an industrial waste glass, Ceram. Internat. 36 1675–1680.

Bernardo E. Dal Maschio R. (2011) Glass-ceramics from vitrified sewage sludge pyrolysis residues and recycled glasses, 31 2245-2252.

Bernardo E. Pontikes Y. Angelopoulos G.N. (2012) , Adv. Appl. Ceram. 108 472-478.

Blengini G.A. Di Carlo T. (2010) Changing role of life cycle phases, subsystems and materials in the LCA of low energy buildings, Ener. Build. 42 869-880.

Blengini G.A. M. Busto M. Fantoni D. Fino (2012) Eco-efficient waste glass recycling: Integrated waste management and green product development through LCA, Waste manag. 32 1000-1008.

Blinova I. Bityukov I. Kasemet K. Ivask A. A. Käkinen, I. Kurvet, O. Bondarenko, L. Kanarbik, M. Sihtmäe, V. Aruoja, H. Schvede, A. Kahru (2012) Environmental hazard of oil shale combustion fly ash, J. Haz. Mat. 229-230 192-200.

Blom I. Itard L. Meijer A. (2010) Environmental impact of dwellings in use: maintenance of façade components, Build. Env. 45 2526-2538.

Boccaccini A.R. (1998) On the viscosity of glass composites containing rigid inclusions, Mat. Lett. 34 285-289.

Bouillon E. Langlais F. Pailler R. Naslain R. F. Cruege, P. V. Huong, J. C. Sarthou, A. Delpuech, C. Laffon, P. Lagarde, M. Monthioux, A. Oberlin (1991) Conversion mechanisms of a polycarbosilane precursor into an SiC-based ceramic material, J. Mat. Sci. 26 (5) 1333-1345.

Cabeza L.F. Rincon L. Vilariño V. Perez G. Castell A. (2014) Life cycle assessment (LCA) and energy analysis (LCEA) of buildings and the building sector: a review, Renew. Sustain. Ener. Rev. 29 394-416.

Chau C.K. Hui W.K. Ng W.Y. Powell G. (2012) Assessment of CO_2 emissions reduction in high-rise concrete office buildings using different material use options, Res. Cons. Recycl. 61 22-34.

Chen X. Chadwick T.C. Wilson R.M. Hill R.G. M.J. Cattell (2011) Crystallization and flexural strength optimization of fine-grained leucite glass-ceramics for dentistry, Dent. Mater. 27 1153-1161.

Coelho A. de Brito J. (2012) Influence of construction and demolition waste management on the environmental impact of buildings, Waste manag. 32 532-541.

Colombo P. Bernardo E. Parcianello G. (2013a) Multifunctional advanced ceramics from preceramic polymers and nano-sized active fillers, J. Eur. Ceram. Soc. 33 (3) 453-469.

Colombo P. Mera G. Riedel R. Sorarù G.D. (2013b) Polymer-Derived Ceramics: 40 Years of Research and Innovation in Advanced Ceramics, J. Am. Ceram. Soc. 93 (7) 1805-1837.

Corradetti S. Carturan S. Biasetto L. Andrighetto A. P.Colombo (2013) Boron carbide as a target for the SPES project, J. Nuclear Mat. 432 (1-2) 212-221.

D.M. (2010) Criteria for acceptance of waste at landfills according to Italian regulation.

de Gracia A. Navarro L. Castell A. Boer D. Cabeza L.F (2014) Life cycle assessment of a ventilated façade with PCM in its air chamber, Solar Energy 104 115-123.

Duan R.G. Kuntz J.D. Garay J.E. Mukherjee A.K. (2004) Metal-like electrical conductivity in ceramic nano-composite, Scripta Materialia 50 1309–1313.

Duke D.A. MacDowell J.F. Karstetter B.R. (1967) Crystallization and Chemical Strengthening of Nepheline Glass-Ceramics, J. Am. Ceram. Soc. 50 67-74.

Fernandes H.R. Tulyaga D.U. Ferreira J.M.F. (2009) , Adv. Appl. Ceram. 108 9-13.

Ferreira T. Rasband W. (1997-2012) ImageJ User Guide, U. S. National Institutes of Health, Bethesda, Maryland, USA IJ 1.46 R http://rsbweb.nih.gov/ij/.

Fisher H. Marx R. (2001) Improvement of Strength Parameters of a Leucite-reinforced Glass Ceramic by Dual-ion Exchange, J. Dent. Res. 80 336-339.

Fisher H. Marx R. (2003) Suppression of subcritical crack growth in a leucite-reinforced dental glass by ion exchange, J. Biomed. Mat. Res. Part A 66A 885-889.

Garcia N Irusta R. A. Y. Nuñez Moral (2007) Environmental performance of waste based construction materials. LCA study., CARTIF Foundation Boecillo, Valladolid Spain claisse.info/supplementaryabstracts.htm.

Gasch M.J. Mukherjee A.K. (2001) Preparation of a Si_3N_4/SiC nanocomposite by high-pressure sintering of polymer precursor derived powders, Scripta Materialia 45 1063–1068.

Gibson L.J. Ashby M.F. (eds.) (1999) Cellular Solids, Structure and Properties, Cambridge University Press Cambridge, UK.

Gorokhovsky A.V. Gorokhovsky V.A. Mescheryakov D.V. Mendez-Nonell J. J.I. Escalante-Garcia, M.I. Pech-Canul, and G. Vargas-Gutierrez (2001) Inorganic wastes in manufacturing of glass-ceramics: slurry of phosphorous fertilizer production and oil shale ash, Mater. Lett. 51 281–284.

Gorokhovsky A.V. Escalante-Garcia J.I. Mendez-Nonell J. Gorokhovsky V.A. D.V. Mescher (2002a) Foamed glass-ceramic materials based on oil shale by-products, Glass Sci. Technol. 75 259-262.

Gorokhovsky A.V. Gorokhovsky V.A. Mescheryakov D.V. Kopchekchi A.A. (2002b) Glass-ceramics based on oil shale ash, Glass Ceram. 59 191–193.

Grasso S. Sakka Y. Maizza G. (2009) Electric current activated/assisted sintering (ECAS): a review of patents 1906–2008, Sci. Technol. Adv. Mat. 10 (5) 053001 (24 pages).

Grasso S. Chinnam R.K. Porwal H. Boccaccini A.R. M.J. Reece (2013) Low temperature spark plasma sintering of 45S5 Bioglass®, J. Non-Cryst. Solids 362 25-29.

Green D.J. Tandon R. Sglavo V.M. (1999) Crack Arrest and Multiple Cracking in Glass Using Designed Residual Stress Profiles, Science 283 1295-1297.

Gutzow I. Pascova R. Karamanov A. Schmelzer J. (1998) The kinetics of surface induced sinter-crystallization and the formation of glass-ceramic materials, J. Mater. Sci. 33 5265-5273.

Han S. Kim C. Kwon D. (1997) Thermal/oxidative degradation and stabilization of polyethylene glycol, Polymer. 38 317–323.

Harris G.L.(ed.) (1995) Properties of Silicon Carbide, INSPEC, Institution of Electrical Engineers London.

Höland W. Beall G.(eds.) (2002) Glass-ceramic technology, The American Ceramic Society, 2002 Westerville OH.

Howarth R.W. Ingraffea A. Engelder T. (2011) Natural gas: Should fracking stop?, Nature 477 271–273.

Hreglich S. Cioffi F. (2008) Adv. Appl. Ceram. 108 22-26.

Karamanov A. (2009) Adv. Appl. Ceram. 108 14-21.

Kim Y.W. Eom J.H. Wang C. Park C.B. (2008) Processing of Porous Silicon Carbide Ceramics from Carbon-Filled Polysiloxane by Extrusion and Carbothermal Reduction, J. Am. Ceram. Soc. 91 (4) 1361-1364.

Kim K.H. (2011) A comparative life cycle assessment of a transparent composite façade system and a glass curtain wall system, Ener. Build. 43 3436-3445.

Koga K. et al. (1978) Method of producing dense sintered silicon carbide body from polycarbosilanes, US Patent 4 105 455 106/44.

Kurtenbach D. Martin H.P. Müller E. Roewer G. A. Hoell (1998) Crystallization of polymer derived silicon carbide materials, J. Eur. Ceram. Soc. 18 (13) 1885-1891.

Kuusik R. Uibu M. Kirsimäe K. (2005) Characterization of oil shale ashes formed at industrial-scale CFBC boilers, Oil Shale 22 407-419.

Laurent AL Clavreul J. Bernstad A. Bakas I. Niero M. Gentil E. Christensen T.H. Hauschild M.Z. (2014) Review of LCA studies of solid waste management systems - part II: methodological guidance for a better practice, Waste manag. 34 589-606.

Leroy C. Ferro M.C. Monteiro R.C.C. Fernandes M.H.V. (2001) Production of glass-ceramics from coal ashes', J. Eur. Ceram. Soc. 21 195-202.

Li H. Zhang L. Cheng L. Wang Y. Z. Yu, M. Huang, H. Tu, H. Xia (2008) Effect of the polycarbosilane structure on its final ceramic yield, J. Eur. Ceram. Soc. 28 (4) 887–891.

Luan J. Li A. Su T. Cui X. (2010) Synthesis of nucleated glass-ceramics using oil shale fly ash, J. Hazard. Mater. 173 427–432.

Ly H.Q. Taylor R. Day R.J. Heathey F. (2001) Conversion of polycarbosilane (PCS) to SiC-based ceramic Part I Characterization of PCS and curing products, Part II Pyrolysis and characterization, J. Mat. Sci. 36 (16) 4037-4057.

Maître A. Vande Put A. Laval J.P. Valette S. G. Trolliard (2008) Role of boron on the Spark Plasma Sintering of an α-SiC powder, J. Eur. Ceram. Soc. 28 (9) 1881-1890.

Mora R. Bitsuamlak G. Horvat M. (2011) Integrated life-cycle design of building enclosures, Build. Env. 46 1469-1479.

Moshtaghioun B.M. Cumbrera-Hernández F. L. Gómez-García D. de Bernardi-Martín S.A. Domínguez-Rodríguez, A. Monshi, M. Hasan Abbasi (2013) Effect of spark plasma sintering parameters on microstructure and room-temperature hardness and toughness of fine-grained boron carbide (B4C), J. Eur. Ceram. Soc. 33 (2) 361-369.

Nijhara K. Morena R. Hasselman D.P.H. (1982) Evaluation of KIC of brittle solids by the indentation method with low crack-to-indent ratios, J. Mat. Sc. Letters 1 (1) 13-16.

Noviyanto A. Han S.W. Yu H.W. Yoon D.H. (2013) Rare-earth nitrate additives for the sintering of silicon carbide, J. Eur. Ceram. Soc. 33 (15-16) 2915-2923.

Ots A. (2006) Oil shale as a power fuel, Oil Shale 22 367-368.

Ponsot I. Falcone R. Bernardo E. (2013) Stabilization of fluorine-containing industrial waste by production of sintered glass-ceramics, Ceram Int 39 6907-6915.

Quinn G.D. (2003) Weibull Strength Scaling for Standardized Rectangular Flexure Specimens, J. Am. Ceram. Soc. 86 508-510.

Quinteiro P. Araujo A. Oliveira B. Dias A.C. Arroja L. (2012a) Allocation of energy consumption and greenhouse gas emissions in the production of earthenware ceramic pieces, J. Cleaner Prod. 31 14-21.

Quinteiro P. Araujo A. Oliveira B. Dias A.C. Arroja L. (2012b) Carbon footprint and energy consumption of commercially produced earthenware ceramic piece, J. Eur. Ceram. Soc. 32 2087-2094.

Radhi H. Sharples S. (2013) Global warming implications of facade parameters: LCA of residential buildings in Bahrain, Env. Impact Assess. Rev. 38 99-108.

Ramesh T. Prakash R. Shukla K.K. (2010) life cycle energy analysis of buildings: An overview, Ener. Build. 42 1592-1600.

Renlund G.M. Prochazka S. Doremus R.H. (1991) Silicon Oxycarbide Glasses: Part I. Preparation and Chemistry, Part II. Structure and Properties, J. Mat. Res. 6 2716-2734.

Ring T.A. (1996) Fundamentals of Ceramic Powder Processing and Synthesis, Academic Press.

Sandu V. Cimpoiasu E. Aldica G. Popa S. E. Sandu, B. St. Vasile, N. Hurduc, I. Nor (2012) Use of preceramic polymers for magnesium diboride composites, Physica C: Superconductivity 480 102–107.

Sglavo V.M. Bonafini M. (2000) Design and Production of High Reliability Soda-Lime Silicate Glass, Ceramics - Processing, Reliability, Tribology and Wear (ed. G. Müller)Weinheim, Germany, Wiley-VCH 353-358.

Sglavo V.M. (2001) ESP (Engineering Stress Profile) Glass: a Novel Approach to Obtain Improved Mechanical Performance, Riv. Stn. Sper. Vetro 6 49 (written in italian).

Sglavo V.M. Prezzi A. Zandonella T. (2004) ESP (Engineered Stress Profile) silicate glass, High strength material, insensitive to surface defects and fatigue, Adv. Eng. Mater. 6 344-349.

Sglavo V.M. Larentis L. Green D.J. (2001a) Flaw Insensitive Ion-Exchanged Glass: I, Theoretical Aspects, J. Am. Ceram. Soc. 84 1827-1831.

Sglavo V.M. Green D.J. (2001b) Flaw Insensitive Ion-Exchanged Glass: II, Production and Mechanical Performance, J. Am. Ceram. Soc. 84 1832-1838.

Shackelford J.F. Doremus R.H. (2010) Ceramic and Glass Materials, Springer.

Sorarù G.D. Babonneau F. Mackenzie J.D. (1990) Structural evolutions from polycarbosilane to SiC ceramic, J. Mat. Sci. 25 (9) 3886-3896.

Stazi F. Mastrucci A. Munafo P. (2012) Lycle cycle assessment approach for the optimization of sustainable building envelopes: an application on solar wall systems, Build. Env. 58 278-288.

Stephan A. Crawford R.H. de Mytternaere K.K. (2013) A comprehensive assessment of the Life-cycle energy of passive houses, Appl. Ener. 112 23-34.

Suárez M. Fernández A. Menéndez J.L Torrecillas R. H. U. Kessel, J. Hennicke, R. Kirchner and T. Kessel (2013) Chapter 13: Challenges and Opportunities for Spark Plasma Sintering: A Key Technology for a New Generation of Materials, Sintering Applications, Sintering Applications (ed. Burcu Ertug) ISBN: 978-953-51-0974-7, Pub. InTech, DOI: 10.5772/53706.

Taborianski V.M. Prado R.T.A. (2012) Methodology of CO2 emission evaluation in the life cycle of office building façades, Env. Impact Assess. Rev. 33 41-47.

Vasilopoulos K.C. Tulyaganov D. U. Agathopoulos S. Karakassides M. A. M. Ribeiro, J. M. F. Ferreira and D. Tsipas (2009) , Adv. Appl. Ceram. 108 27-32.

Vasylkiv O. Borodianska H. Badica P. Grasso S. Y. Sakka, A. Tok, L. Su, M. Bosman, J. Ma (2012) High Hardness BaCb-(BxOy/BN) Composites with 3D Mesh-Like Fine Grain-Boundary Structure by Reactive Spark Plasma Sintering, J. Nanosci. Nanotechno. 12 959-965.

Vellini M. Savioli M. (2009) Energy and environmental analysis of glass container production and recycling, Ener. 34 2137-2143.

Wan J. Gasch M.J. Mukherjee A.K. (2003) Silicon Nitride–Silicon Carbide Nancocomposites Fabricated by Electric-Field-Assisted Sintering, J. Am. Ceram. Soc. 86 (3) 526–528.

Wild M.J. Buhler P. (1998) On the phase composition of polymethylsiloxane derived ceramics, J. Mat. Sci. 33 5441-5444.

World Energy Council (2007) Survey of energy resources executive summary, URL http://www.worldenergy.org/.

World Energy Council (2010) Survey of energy resources executive summary, ISBN 978 0 946121 021 URL http://www.worldenergy.org/.

www.crystalimpact.com/.

Yen T.F. (1976) Oil Shale , Developments in Petroleum Science 5 Elsevier, Amsterdam ISBN 9780444414083.

Zhang J. Dong W. Li J. Qiao L. Kheng J. and Sheng J. (2007) Utilization of coal fly ash in the glass–ceramic production, J. Haz. Mat. 149 523-526.

Zhang Z. Du X. Wang W. Fu Z. H. Wang (2013) Preparation of B4C–SiC composite ceramics through hot pressing assisted by mechanical alloying, Int. J. Refract. Met. H. 41 270-275.

Zhang H. Lopez-Honorato E. Javed A. Shapiro I. P. Xiao (2012a) A study of the microstructure and Vickers indentation fracture toughness of silicon carbide coatings on TRISO fuel particles, J. Am. Ceram. Soc. 95 (3) 1086-1092.

Zhang S. Lu W. Shen Q. Zhang L. (2012b) Synthesis and characterization of B13C2 boron carbide ceramic by pulsed electric current sintering, Ceram. Int. 38 (2) 895-900.